

University of Southampton Research Repository ePrints Soton

Copyright © and Moral Rights for this thesis are retained by the author and/or other copyright owners. A copy can be downloaded for personal non-commercial research or study, without prior permission or charge. This thesis cannot be reproduced or quoted extensively from without first obtaining permission in writing from the copyright holder/s. The content must not be changed in any way or sold commercially in any format or medium without the formal permission of the copyright holders.

When referring to this work, full bibliographic details including the author, title, awarding institution and date of the thesis must be given e.g.

AUTHOR (year of submission) "Full thesis title", University of Southampton, name of the University School or Department, PhD Thesis, pagination

UNIVERSITY OF SOUTHAMPTON

FACULTY OF PHYSICAL SCIENCES AND ENGINEERING

Physics and Astronomy

Nanoparticle-DNA Conjugates For Biomedical Applications

by

Amelie Heuer-Jungemann

Thesis for the degree of Doctor of Philosophy

December 2014

UNIVERSITY OF SOUTHAMPTON

ABSTRACT

FACULTY OF PHYSCIAL SCIENCES AND ENGINEERING

Physics and Astronomy

Thesis for the degree of Doctor of Philosophy

NANOPARTICLE-DNA CONJUGATES FOR BIOMEDICAL APPLICATIONS

by

Amelie Heuer-Jungemann

In recent years biomolecules have been used to infer specific functionality to nanomaterials. Advances in conjugation techniques have allowed for the development of a vast range of hybrid bio-nano materials. Their applications range from biosensing and targeted therapy to metamaterials. In particular the conjugation of nanomaterials to functional oligonucleotides has been a thriving area of scientific research.

In this project the main aim was to explore the uses of gold nanoparticle-DNA conjugates for biomedical applications. Probes for the real-time intracellular detection of mRNA were synthesized. These probes showed great target specificity, excellent biocompatibility and good cellular uptake. Importantly, unlike free nucleic acids, they displayed no susceptibility to degradation by nuclease enzymes. The ability to detect mRNAs in a live cell, in real time has tremendous diagnostic applications.

Furthermore, multifunctional probes were designed. In addition to live cell mRNA detection, we developed probes with the ability to deliver a cytotoxic drug. Utilizing their inherent high specificity for target mRNAs, we demonstrated that cell-type specific targeted drug delivery was possible. In the absence of the target mRNA, the drug remained tightly bound within the probe.

With a view of developing advanced materials, capable of performing multiple roles simultaneously, we investigated the use of nanoparticle assemblies for biomedical applications. In order to create highly stable nanoconstructs, a novel tool for the programmed assembly of DNA-nanomaterials was demonstrated. The use of copper-free click chemistry resulted in nano-assemblies connected by ssDNA. The employment of this novel tool proved to produce assemblies with covalently linked particles. Moreover, it was shown that gold nanoparticle dimers displayed excellent stability with respect to a variety of conditions commonly met within a biological environment.

Additionally, the formation of heterogeneous nanoassemblies was demonstrated. Dimers of optical and either semi-conductor or magnetic nanocrystals were assembled representing examples of multi-role probes with exciting potential for applications in biomedicine.

Table of Contents

Abstract

Table of conte	ents	I
List of figures	3	VIII
List of tables_		XII
List of equation	ons	XII
List of scheme	es	XII
List of accom	panying materials	XIV
Declaration of	f authorship	XV
Acknowledge	ments	XVII
Abbreviations	S	- XVIII
1. Introduction	on	1
2. Backgroun	nd	5
2.1. Synthes	sis of spherical gold nanoparticles	5
2.1.1.	Synthesis of gold nanospheres using the citrate reduction metho	d6
2.1.2. red	Synthesis of small gold nanospheres using sodium borohydride ucing agent	
2.1.3.	Comparison between citrate and sodium borohydride reduction methods	11
2.1.4.	Surface stabilisation of gold nanoparticles	12
2.2. Optical	properties of gold nanoparticles	14
2.3. Synthes	is and properties of oligonucleotides	16
2.4. Modific	ation of nanomaterials with oligonucleotides	18
2.4.1.	Oligonucleotide modification of gold nanoparticles	18
2.4.2.	Oligonucleotide modification of nanomaterials of different cher	
con	npositions	21

	2.5. Interacti	ions of gold nanoparticles with cells	23
	2.5.1.	DNA-AuNP conjugates for live cell mRNA detection	25
	2.5.1	.1. Epithelial to mesenchymal transition	28
	2.5.2.	DNA-AuNP conjugates for targeted drug delivery	29
	2.5.3.	Gold nanoparticle assemblies for intracellular applications	31
	2.6. Program	nmed assembly of DNA-nanomaterial conjugates	32
	2.6.1.	Click chemistry	35
	2.7. Referen	ces	36
3.	Experimen	ital procedures	63
	3.1. Synthes	is of spherical gold nanoparticles	63
	3.1.1.	Gold nanoparticles (13 ± 1 nm)	63
	3.1.2.	Gold nanoparticles (5 ± 2 nm)	64
	3.2. Surface	modification of nanomaterials with oligonucleotides	65
	3.2.1.	DNA attachment to 5nm AuNPs	65
	3.2.2.	DNA attachment to 13 nm AuNPs	67
	3.2.3.	DNA attachment to Cu _{2-x} Se NPs and Fe ₃ O ₄ NCs	69
	3.2.4.	DNA attachment to graphene oxide	70
	3.3. AuNP-I	ONA conjugates for biomedical applications	70
	3.3.1.	Design of oligonucleotides for nano-probes	71
	3.3.2.	Nano-probe synthesis	72
	3.4. Program	nmed ligation of DNA-nanomaterials	72
	3.4.1.	Formation of 5 nm AuNP dimers	72
	3.4.2.	Formation of 13nm AuNP dimers and trimers	73
	3.4.3.	Formation of Fe ₃ O ₄ NC dimers	74
	3.4.4.	Formation of heterodimers	74
	3.4.5.	Formation of GO/AuNP hybrid nanostructures	75
	3.5. Oligonu	cleotide and nanomaterials characterisation techniques	76

	3.5.1. Gel electrophoresis.	76
	3.5.1.1. Agarose gel electrophoresis	76
	3.5.1.2. Polyacrylamide gel electrophoresis	
	3.5.2. Spectroscopy	78
	3.5.2.1. UV-visible spectroscopy	_78
	3.5.2.1.1. Oligonucleotide UV melting	78
	3.5.2.1.2. Determination of oligonucleotide loading on AuNPs	- <i>-</i> 79
	3.5.2.2. Fluorescence spectroscopy	79
	3.5.2.2.1. Oligonucleotide fluorescence melting	79
	3.5.2.2.2. Determination of target specificity	80
	3.5.2.2.3. Glutathione assay	-80
	3.5.2.2.4. Nuclease assays	81
	3.5.2.2.5. Cell culture media stability assays	81
	3.5.2.2.6. Determination of doxorubicin loading	82
	3.5.3. Transmission electron microscopy	82
	3.5.4. ζ-potential measurements	82
	3.6. Cell culturing	82
	3.7. Cell culture studies characterization techniques	83
	3.7.1. Viability assay	83
	3.7.2. Microscopy	84
	3.7.2.1. Transmission electron microscopy	-84
	3.7.2.2. Confocal microscopy	- 85
	3.7.2.2.1. Immunofluorescent labelling	-85
	3.7.2.2.2. Cells incubation with AuNPs	86
	3.8. References	86
4.	Results and discussion on synthesis and surface functionalization of nanomaterials.	92

	4.1. Spheric	al gold nanoparticles	93
	4.1.1.	Gold nanospheres (13 ± 1 nm)	93
	4.1.2.	Gold nanospheres (5 ± 2 nm)	94
	4.2. Surface	modification of nanomaterials with oligonucleotides	95
	4.2.1.	Mono-functionalization of 5nm AuNPs	96
	4.2.2.	AuNPs coated with a dense shell of oligonucleotides	98
	4.2.3.	DNA attachment to Cu _{2-x} Se NPs and Fe ₃ O ₄ nanocubes <i>via</i> ED	C
	cou	upling	101
	4.2.4.	DNA Attachment to graphene oxide via EDC coupling	103
	4.3. Referen	nces	106
5.	Results an	d discussion on biomedical applications of DNA-gold	
	nanopartic	ele conjugates	113
	5.1. Formati	ion, physicochemical characterization, stability and specificity te	sts of
	nano-pi	obes	113
	5.1.1.	Formation and physicochemical characterisation of nano-prob	es114
	5.1.2.	Stability tests of nano-probes	116
	5.1.2	2.1. Glutathione assay	116
	5.1.2	2.2. Nuclease assays	117
	5.1.2	2.3. Cell culture media stability assays	123
	5.1.3.	Specificity assays	124
	5.2. Interact	ions of nano-probes with cell culture	126
	5.2.1.	Immunofluorescent labelling of cells	127
	5.2.2.	Live cell mRNA detection	129
	5.2.3.	Transmission electron microscopy of cells incubated with nan	Ю-
	pro	bes	134

	5.2.4.	Viability assays for cells incubated with nano-probes	137
	5.3. Nano-pi	robes for targeted drug delivery	138
	5.3.1.	Physicochemical characterisation and stability assays of drug-lo	oaded
	Vin	nentin nano-probes	139
	5.3.2.	Interactions of drug-loaded Vimentin nano-probes with cell	
	cult	ture	143
	5.3.2	.1. Viability assays of cells incubated with drug-loaded Vime	entin
		nano-probes	145
	5.4. Referen	ces	146
6.	Results and	d discussion on programmed ligation of DNA-functiona	lized
	nanomater	ials	156
	6.1. Analysi	s of oligonucleotides	157
	6.1.1.	Oligonucleotide UV melting	
	6.1.2.	Denaturing polyacrylamide gel electrophoresis.	
	6.2. Program	nmed ligation of DNA-nanomaterials	161
	6.2.1.	Formation of 5 nm AuNP dimers	162
	6.2.2.	Formation of 13 nm AuNP dimers and trimers	166
	6.2.3.	Formation of Fe ₃ O ₄ NC dimers	169
	6.2.4.	Formation of heterodimers	170
	6.2.5.	Formation of GO/AuNP hybrid structures	173
	6.3. Gold na	noparticle dimers for intracellular applications	178
	6.3.1.	Stability assays of dimers	179
	6.3.1	.1. Cell culture media stability assays of dimers	179
	6.3.1	.2. Nuclease assays of dimers	180
	6.3.2.	Interactions of dimers with cell culture	181

	6.3.2.1. Viability assays of cells incubated with dimers	181
	6.3.2.2. Transmission electron microscopy of cells incubated with	
	dimers	182
	6.4. References	184
7.	Summary and outlook	190
	7.1. Summary of results	190
	7.2. Outlook to future work	193
	7.3. References	195
Αį	opendix I	i
	AI.1 List of reagent suppliers	
	AI.2 Formulations of cell culture media	
Αį	opendix II	
	AII.1 Sample calculation for the determination of the concentration of a colle	
go	ld solution	
	AII.2 Synthesis of oligonucleotides	vi
	AII.3Synthesis and water transfer of Cu _{2-x} Se NPs	yiii
	AII.3.1 Synthesis of Cu _{2-X} Se NPs	. <u>.</u> . <u>.</u>
	AII.3.2 Water transfer of Cu _{2-X} Se NPs	ix
	AII.4 Synthesis and water transfer of Fe ₃ O ₄ NCs	ix
	AII.4.1 Synthesis of Fe ₃ O ₄ NCs	ix
	AII.4.2 Water transfer of Fe ₃ O ₄ NCs	X
	AII.5 Synthesis of graphene oxide	xi
	AII.6 Determination of oligonucleotide loading on a gold nanoparticle	xii
	AII.7 Quantification of duplexes on nano-probes	xiii
	AII.8 Additional confocal microscopy images for chapter 5	XV

All.9 Determination of Doxorubicin loadingxv
AII.10 Additional TEM images for chapter 6xvi
AII.10.1 5 nm AuNP dimersxvi
AII.10.2 13 nm AuNP dimers and trimersxvii
AII.10.3 GO/AuNP hybrid assembliesxviii
AII.12 Gel analysis using Image Jxviii
AII.13 Referencesxix

List of figures

Figure 2.1 Chemical structures of the four naturally occurring DNA bases and the structure of a DNA strand with the sequence TCGA	-17
Figure 2.2 Illustration of the formation of DNA base-pairing showing hydrogen bonding (dashed lines)	-17
Figure 2.3 Chemical structure of doxorubicin	_30
Figure 3.1 Chemical structures of trisodium citrate (1) and BSPP (2)	64
Figure 3.2 Details of chemical modifications on oligonucleotides used	-67
Figure 3.3 Chemical structure of glutathione	.80
Figure 4.1 Transmission electron micrograph A), corresponding size distribution histogram B) and normalized UV-vis spectrum C) of 13 nm AuNPs	. 93
Figure 4.2 Transmission electron micrograph A) and corresponding size distribution histogram B) as well as a normalized UV-vis spectrum of 5 nm AuNPs	-95
Figure 4.3 Agarose gel for the separation of 5 nm AuNP mono- and diconjugates	98
Figure 4.4 A) Normalized UV-vis spectra of BSPP- (black) and DNA-coated (red) AuNPs. B) Corresponding ζ-potential measurements of BSPP-coated AuNPs (green) and DNA-AuNPs (red). C) Agarose gel of BSPP-coated AuNPs (lane 2) and DNA-AuNPs (lane 1). D) TEM micrograph of DNA-AuNPs-	99
Figure 4.5 TEM micrographs of Fe ₂ O ₃ nanocubes A) and Cu2-xSe NPs D) before and after DNA conjugation B) and E). Corresoponding ζ-potential measurements of Fe ₃ O ₄ nanocubes C) and Cu2-xSe NPs F) before (red) and after DNA conjugation (green)1	103
Figure 4.6 A) Normalized UV-visible spectra of graphene oxide (black), graphene oxide and EDC/sulfo-NHS (red), graphene oxide mixed with DNA (non-covalent) (blue) and graphene oxide with covalently attached DNA after EDC coupling (pink) B) UV-vis spectra of GO (black) and GO@DNA (red). C) ζ-potential graphs of GO (red) and GO@DNA (green)1	104
Figure 5.1 Fluorescence melting curves of A) Vimentin nano-probes and B) total mRNA nano-probes (both modified with Cy5) and C) Desmocollin nano-probes and D) Krt8 nano-probes (both modified with Cy3)	115
Figure 5.2 Fluorescence spectra of total mRNA detecting nano-probes incubated with GSH and free Cy3-DNA after particle dissolution1	116
Figure 5.3 Graphs showing the fluorescence of the sense and flare strands for A) Vimentin and total mRNA NFs (Sense: Cy3, Flare: Cy5) and B) Desmocollin and Cytokeratin 8 NFs (Sense: Cy5, Flare: Cy3). For comparison the fluorescence of free sense DNA after particle dissolution (at constant probe concentrations) is shown in green1	117

Figure 5.4 A) Spectrum showing the fluorescence of the Vimentin sense strand (black) and for comparison the fluorescence of free sense DNA after particle dissolution (red). B) Native polyacrylamide gel displaying a reference dye in lane 1, the degradation of a 'free' DNA duplex (Vimentin dsDNA) in lane 2, and the still intact duplex in lane 3
Figure 5.5 Fluorescence monitoring of Vimentin probe sense strand fluorescence (Cy3) after washing with CaCl ₂ and treatment with DNAse I120
Figure 5.6 Fluorescence monitoring of A) Vimentin and total mRNA nano-probes (Sense strand: Cy3, Flare strand: Cy5) incubated with DNAse II and B) Desmocollin and Krt8 nano-probes (Sense strand: Cy5, Flare strand: Cy3) incubated with DNAse II121
Figure 5.7 Data showing the fluorescence of the Vimentin sense strand (black) upon incubation with DNAse II and for comparison the fluorescence of free sense DNA after particle dissolution (red)122
Figure 5.8 Fluorescence spectra of total mRNA nano-probes (A) flare strand Cy5 and B) sense strand Cy3 fluorescence) incubated in different cell culture media. C) UV-vis spectrum of nano-probes before (black) and after (red) incubation with cell culture media123
Figure 5.9 Fluorescence spectra of nano-probes incubated with their respective mRNA targets124
Figure 5.10 Fluorescence spectra of nano-probes incubated with matched and mismatched targets
Figure 5.11 Fluorescence emissions of flare strands in response to increasing target concentrations126
Figure 5.12 Immunofluorescent labelling of 16HBE (1) and fibroblasts (2) with Vimentin (A), Desmocollin (B) and Cytokeratin 8 (C). Nuclei are stained with DAPI128
Figure 5.13 Confocal microscopy images showing the successful detection of total mRNA in A) epithelial cells (16HBE) and B) fibroblasts (MRC-5). Nuclei are stained with Hoechst 33342 (Invitrogen)130
Figure 5.14 Confocal microscopy images of live cells (1) 16HBE epithelial cells, 2) MRC-5 fibroblasts) incubated with mRNA detection probes. A) Vimentin detection Cy5, blue, B) Desmocollin detection, Cy3, pink and C) Cytokeratin 8 detection, Cy3, pink. Nuclei are stained with Hoechst 33342 (Invitrogen)
Figure 5.15 Confocal cross-section image of Vimentin nano-probes in MRC-5. The cross-hairs mark the point of interest; X and Y sections are shown on the right hand side and the bottom of the image. Nuclei are stained with Hoechst 33342 (Invitrogen)133
Figure 5.16 Fluorescence time-lapse study on epithelial cells incubated with Desmocollin nano-probes (Cy3 fluorescence)
Figure 5.17 Transmission electron micrographs of cells incubation with nano-probes. Scale bars are 100nm. Red arrows indicate NPs in the cytosol. Green arrows indicate endosomal barriers. RER = rough endoplasmatic reticulum; MVB = multivesicular body; E = endosome, M = mitochondrion

Figure 5.18 Viability assay for cells incubated with different nano-probes. ($n=3$, *** $p < 0.01$ for a one-tailed t test)138
Figure 5.19 Fluorescence melting curves of Vimentin nano-flares and Doxorubicin-loaded Vimentin nano-flares140
Figure 5.20 Fluorescence time-course measuring the potential leaking of doxorubicin from the Vimentin nano-flares (black graph). For comparison, fully released doxorubicin at the same concentration was measured also (red graph)141
Figure 5.21 A) Fluorescence calibration curve for concentration-dependent doxorubicin fluorescence. B) Varying DOX fluorescence (concentration) with varying flare strand amounts142
Figure 5.22 Confocal microscopy images of A) 16HBE epithelial cells and B) fetal lung fibroblasts (MRC-5) after 18h incubation with doxorubicin-loaded Vimentin nano-flares. The large images show doxorubicin fluorescence only (green) while the small inset images show the full image with stained nuclei (yellow) and flare fluorescence (cyan), see Appendix II for larger images. Nuclei were stained with Hoechst 33342 (Invitrogen). Scale bars are 30 μm ———————————————————————————————————
Figure 5.23 Viability assay of 16HBE and MRC-5 cells incubated with Doxorubicin only (400 pmol) as well as Vimentin nano-probes (1 pmol) with varying amounts of drugloading. Mean SEM, $n=3$, ***p < 0.001, **p < 0.01, **p < 0.1 for a one-tailed t test145
Figure 6.1 A) UV melting curve of S1 + S2 . No duplex is formed due to a lack of complementarity. B) Melting curve for S1 + S3 showing duplex melting. C) Melting curve for S1 + S2 + S3 showing duplex melting between all three strands. D) Melting curve for S2 + S3 showing duplex melting.
Figure 6.2 Denaturing polyacrylamide gel of free DNA. Lane 1: Reference dye, Lane 2: S1 (27 mer), Lane 3: S2 (31 mer), Lane 4: S3 (52 mer), Lane 5: S1 + S2 ; Lane 6: Clicked DNA (58 mer)160
Figure 6.3 Agarose gel electrophoresis showing distinct bands for unreacted monoconjugates and dimers in dimer systems. A faint band in the middle corresponds to monoconjugates hybridized to S3 without having formed dimers162
Figure 6.4 Agarose gel electrophoresis demonstrates the success of the 'click' reaction. Lane 1: Monoconjugate as reference; Lane 2: 'nicked' dimers, connected via splint strand S3; Lane 3: 'clicked' dimers, hybridized to S3; Lane 4: 'nicked' dimers treated with splint complement S4; Lane 5: 'clicked' dimers treated with S4163
Figure 6.5 TEM images of A) clicked 5nm AuNP dimers connected via a continuous single strand of ssDNA B) TEM images of the control experiment. As DNA cannot click, the dimer breaks apart and mostly monoconjugates can be found165
Figure 6.6 Agarose gel showing the different mobilities of AuNPs, dimers and trimers167
Figure 6.7 TEM micrographs and corresponding grouping charts of A) 13 nm AuNP dimers and B) trimers. Scale bars are 50 nm. For statistical analyses more than 200 particles from at least three different experiments were counted168
Figure 6.8 TEM micrograph and corresponding grouping chart of Fe ₃ O ₄ NC dimers170

Figure 6.9 A) TEM micrographs of Fe ₃ O ₄ -Au heterodimers and B) corresponding grouping chart171
Figure 6.10 A) TEM micrographs of Cu _{2-x} Se-Au heterodimers and B) corresponding grouping chart
Figure 6.11 Purification of unconjugated AuNPs from GO/AuNP hybrid structures <i>via</i> agarose gel electrophoresis173
Figure 6.12 Normalized UV-vis spectra of GO (red) and GO/AuNP hybrid assemblies (black)
Figure 6.13 Representative TEM images for GO/AuNP hybrid assemblies175
Figure 6.14 A) Agarose gel purification of covalently linked GO-AuNP assemblies (lane 1) and assemblies formed simply by DNA hybridisation (lane 2) after treatment with S4. B) The corresponding, recovered products of lanes 1 and 2 176
Figure 6.15 Normalized UV-vis spectra of clicked GO/AuNP hybrid assemblies and 'control' assemblies after treatment with S4 and agarose gel purification177
Figure 6.16 TEM micrographs of ligated (A) and control AuNP/GO assemblies after treatment with S4 177
Figure 6.17 Agarose gel electrophoresis of AuNP dimers after incubation in cell culture medium (lane 2). Lane 1: dimers as reference 179
Figure 6.18 Agarose gel electrophoresis of AuNP dimers after incubation with A) DNAse I and B) DNAse IL
Figure 6.19 Viability assay of MRC-5 fibroblasts incubated with AuNP dimers. Mean SEM, $n=3$, *** $p < 0.01$ for a one-tailed t-test182
Figure 6.20 TEM micrographs of cells incubated with AuNP dimers. Scale bars are 100nm. V= vesicle, EX = exosome, MVB = multivesicular body
Figure AII.1 Calibration curves of the relative fluorescence of Desmocollin, Cytokeratin 8, Vimentin and total mRNA flare strandsxiii
Figure AII.2 Additional magnified confocal microscopy images of epithelial cells incubated with total mRNA detection nano-probes. Mitochondrial association of flare strands can be clearly observedxv
Figure AII.3 Additional TEM images for 5 nm AuNP dimers connected via single strand of clicked ssDNAxvi
Figure AII.4 Additional TEM images of 13 nm AuNP dimersxvii
Figure AII.5 Additional TEM images of 13 nm AuNP trimersxvii
Figure AII.6 TEM images of AuNP/GO hybrid assembliesxviii
Figure AII.7 Image J analysis of the agarose gel depicting the success of the 'click' reaction (cf. Figure 6.4)xviii

List of tables

Table 3.1 Oligonucleotide sequences and modifications used in chapter 5	66
Table 3.2 Oligonucleotide sequences used for biomedical applications in chapter 6.	- 68
Table AI.1 Formulation of Minimum Essential Medium (MEM)	ii
Table AI.2 Formulation of Dulbecco's Modified Minimum Essential Medium (DMEM)	i ii
Table AI.2 Formulation of Roswell Park Memorial Medium (RPMI)	iv
Table AII.1 Determination of DNA-loading on AuNPs	Xii
Table AII.2 Quantification of sense-flare duplexes on AuNPs	xiv
Table AII.3 Determination of Doxorubicin loading	- xvi
List of equations	
Equation 2.1 Calculation of the total extinction cross-section for metal nanoparticles	15
Equation 3.1 Beer-Lambert Law rearranged for the determination of concentrations of colloidal gold and oligonucleotides in solution	78
Equation AII.1 Sample calculation for the determination of the concentration of a gold nanoparticle solution	
List of schemes	
Scheme 2.1 Reaction mechanisms of the reduction of gold precursors by citrate	6
Scheme 2.2 Schematic illustration of a gold nanoparticle core stabilized by citrate anions	8
Scheme 2.3 Influence of the pH on the formation of gold nanoparticles with respect to citrate protonation A) and gold precursor speciation B)	9
Scheme 2.4 Reduction mechanism of gold salt by sodium borohydride	10
Scheme 2.5 Illustration of the surface stabilisation of AuNPs synthesised by sodium borohydride reduction	11
Scheme 2.6 Schematic illustration of the growth of gold nanospheres	11
Scheme 2.7 Illustration of the surface stabilisation of gold nanoparticles by BSPP	12
Scheme 2.8 Schematic illustration of the surface plasmon resonance on metal nanoparticles depicting the displacement of the conduction band electron cloud relative to the nanoparticle core	

Scheme 2.9 A) Method of conjugating multiple oligonucleotides to citrate-capped gold nanoparticles, creating a DNA corona. B) Method of conjugating a discrete number of oligonucleotides to BSPP-coated gold nanoparticles
Scheme 2.10 Schematic illustration of the EDC/ sulfo-NHS coupling reaction23
Scheme 2.11 Illustration of the process of epithelial to mesenchymal transition
Scheme 2.12 Mechanism of the ring-strain promoted, copper-free azide-alkyne
cycloaddition36
Scheme 3.1 Reaction mechanism for the disulfide bond reduction by BSPP66
Scheme 4.1 RedOx reactions leading to the dissolution of gold100
Scheme 5.1 Schematic illustration of the nano-probes. A) Desmocollin and Cytokeratin 8 nano-probes display Cy3-modified flare strands and Cy5-modified sense strands. B) Vimentin and total mRNA nano-probes display Cy5-modified flare strands and Cy3-modified sense strands
Scheme 5.2 Schematic illustration of the nano-probe. Arrows indicate outermost parts of oligonucleotides, accessible by DNAse I
Scheme 5.3 Schematic illustration of the nano-probe for live cell mRNA detection based on DNA-AuNP conjugates
Scheme 5.4 Illustration of the multi-functional nano-probe capable of mRNA detection and simultaneous targeted drug delivery
Scheme 6.1 Illustration of the DNA click ligation process. Azide (S1) and alkyne (S2) oligonucleotides are brought together <i>via</i> a complementary splint strand (S3). The click reaction then takes place resulting in a ligated strand157
Scheme 6.2 Illustration of dimer formation using the method of DNA- click chemistry. 3'-azide (S1) and 5'-alkyne (S2) DNA-AuNP conjugates are brought into close proximity through a templating splint strand (S3) with non-complementary overhangs (<i>orange</i>). 'Clicking' occurs immediately after hybridisation. Addition of a single DNA strand (S4), fully complementary to S3, results in the removal of S3 through competitive hybridisation, leaving a nanoparticle dimer system connected via a single continuous DNA strand161
Scheme 6.3 Schematic representation of the gold nanoparticle assembly using 'nicked' DNA. Due to the lack of an azide group on C1 , dimer formation is only possible in the presence of the splint strand S3. Upon treatment with S4 the system breaks apart into mono-conjugates as the DNA strands were unable to undergo the click reaction
Scheme 6.4 Schematic illustration of the formation of 13 nm AuNP dimers using DNA click ligation166
Scheme 6.5 Schematic illustration of the formation of 13 nm AuNP trimers using DNA click ligation166
Scheme 6.6 Schematic illustration of the control experiment. C1 modified AuNPs and AmS2-modified GO are brought together <i>via</i> S3. Upon treatment with S4, assemblies

for ease of visualisation. However, in the reality both materials are modified with a number of DNA strands
Scheme 6.7 Schematic illustration of a multiplexed nano-probe based on a dimer of gold nanoparticles
Scheme 7.1 Schematic illustration of the different applications of DNA-AuNP conjugates. Single conjugates were developed into live cell mRNA detection probes and drug delivery vehicles. Interactions of AuNP dimers with cells were investigated190
Scheme 7.2 Schematic illustration of the surface modifications of different nanomaterials with oligonucleotides in order to create building blocks for self-assembly. Assembled structures shown are AuNP dimers (13 nm and 5 nm) and trimers (13 nm), $Cu_{2-x}Se$ -AuNP heterodimers, Fe_3O_4 -AuNP heterodimers, Fe_3O_4 dimers, GO-AuNP hybrid assemblies191
List of accompanying materials
Appendix I – Supplementary material for chapter 3i
Appendix II – Supplementary material for chapters 4-6vi

DECLARATION OF AUTHORSHIP

I, Amelie Heuer-Jungemann

declare that this thesis and the work presented in it are my own and has been generated by me as the result of my own original research.

Nanoparticle-DNA Conjugates for Biomedical Applications

I confirm that:

- 1. This work was done wholly or mainly while in candidature for a research degree at this University;
- 2. Where any part of this thesis has previously been submitted for a degree or any other qualification at this University or any other institution, this has been clearly stated;
- 3. Where I have consulted the published work of others, this is always clearly attributed;
- 4. Where I have quoted from the work of others, the source is always given. With the exception of such quotations, this thesis is entirely my own work;
- 5. I have acknowledged all main sources of help;
- 6. Where the thesis is based on work done by myself jointly with others, I have made clear exactly what was done by others and what I have contributed myself;
- 7. Parts of this work have been published as:

Articles in academic press:

- 1. <u>Heuer-Jungemann, A.</u>; Kirkwood, R.; El-Sagheer, A.; Brown, T.; Kanaras, A. G. "Copper-free Click Chemistry as an Emerging Tool for the Programmed Ligation of DNA-functionalised Gold Nanoparticles" *Nanoscale*, **2013**, 5 (16), 7209-7212.
- 2. <u>Heuer-Jungemann, A.</u>; Harimech, P.; Brown, T.; Kanaras, A. G. "Gold Nanoparticles and Fluorescently-Labelled DNA as a Platform for Biological Sensing" *Nanoscale*, **2013**,5, 9503–9510.
- 3. <u>Heuer-Jungemann, A.</u>; Kiessling, L.; Kymakis, E.; Stratakis, E.; Brown, T.; El-Sagheer, A.E.; Kanaras, A.G. "Covalent linking of Gold Nanoparticles to Graphene Oxide Sheets via DNA Click- Chemistry" (in preparation).

Other publications:

Fernandes, R.F.; Smyth, N.R.; Muskens, O.L.; Ardern-Jones, M.; <u>Heuer-Jungemann</u>, <u>A.</u>; Kanaras, A.G. "Interactions of Skin with Gold Nanoparticles of Different Surface Charge, Shape and Functionality" *Small*, **2014**, in press – doi: 10.1002/smll.201401913.

- 5. <u>Heuer-Jungemann, A.</u>; Howarth, N.M.; Ja'Afaru, S.C.; Rosair, G.M. "Development of a convenient route for the preparation of the N^2 -Cbz-protected guaninyl synthon required for Boc-mediated PNA synthesis" *Tetrahedron Letters*, **2013**, 54 (46), 6275 6278.
- 6. <u>Heuer-Jungemann, A.</u>; McLaren, R.G.; Hadfield, M.S.; Lee, A.L. "Gold(I)-catalysed iodoalkoxylation of allenes" *Tetrahedron*, **2011**, 67 (9), 1609 1616.

Abstracts, Posters or Presentations at Conferences:

- 1. NANAX5 (May 2012, Fuengirola, Spain)
- 2. E-mrs Spring Meeting (May 2012, Strasbourg, France)
- 3. COST TD1003 Meeting (April 2013, Bratislava, Slovakia)
- 4. NanoFar Autumn School (October 2013, Santiago de Compostela, Spain)
- 5. COST TD1003Meeting (April 2014, Catania, Italy)
- 6. E-mrs Spring Meeting (May 2014, Lille, France)
- 7. UK Colloids (July 2014, London, UK)
- 8. Faraday Discussion FD175 (September 2014, Bristol, UK)

Awards:

- 1. Silver medal at the SET for Britain 2014 event in Biological and Biomedical Sciences.
- 2. EPSRC-funded Fellowship 'Doctoral Prize' for 2015.

Signed:		
<i>6</i> · · · · · · · · · · · · · · · · · · ·		
Date:		

Acknowledgements

Firstly, I would like to thank my supervisor Dr Antonios Kanaras for enabling me to carry out such an amazing research project, for his advice, for giving me opportunities to present my work at international conferences and for helping me to develop as a scientist. During the past three years he has given me the opportunity to develop a great toolkit of skills such as the preparation of academic journals and grant applications (and writing these with a good flow!). I would also like to thank my second supervisor Prof. Tom Brown for his guidance and advice on DNA chemistry as well as for many interesting discussions. Thanks also to Dr Peter Lackie for help and advice on the biological side of the project and for the supply of cells. Furthermore I'd like to thank everyone at the Biomedical Imaging Unit (Dr Anton Page, Dr David Johnston, Dr Elizabeth Angus, Dr Suzanne Brooks, Mrs. Patricia Goggin, Mrs. Janice Coles and Mr. James Thompson) for their advice on microscopy and cell biology, but also for their constant support and supply of sweets and tea. I would also like to thank Dr Afaf El-Sagheer for synthesis of oligonucleotides and for continued encouragement, advice and friendship. Furthermore I have to thank ATD Bio for synthesis of oligonucleotides as well as PrimerDesign for help with DNA sequence design. I must also thank Prof. Liberato Manna, Dr Teresa Pellegrino and their respective research groups for supplying the iron oxide and copper selenide nanoparticles as well as Dr Emmanuel Stratakis and Dr Emmanul Kymakis for providing the graphene oxide.

A big thank you also to members of my research group (past and present): Dr Rute Fernandes, Johanna Midelet, Erika Conca, Pascal Harimech, Patrick Vilela, Paulino Alonso Cristobal, Rob Kirkwood and Dr André Utgenannt, who have become much more than just my colleagues in the past years. With their constant support, encouragement, laughter and distractions on Friday evenings, they have made the past three years some of the most enjoyable in my life (despite the PhD stress!). For this I also have to thank my dear friends Andy Turnbull, Suzie Plumb and Dr Sari Giering.

I would also like to thank Johanna Midelet, Patrick Vilela, Alex Greenwood and Adam Johnson for proof-reading parts of this thesis.

Furthermore I have to thank everyone at 5 Khartoum Road (past and present). This house was the best thing that happened to me when I moved to Southampton.

Finally I would like to thank my parents Anke and Helmut Heuer-Jungemann, my brother Steffen Heuer-Jungemann and my boyfriend Adam Johnson for their constant encouragement, support, advice, enlightening discussions and most importantly for their love. I could not have done it without them.

Abbreviations

 \mathbf{A} – Adenine

Abs – absorbance

AmS1 – oligonucleotide with alkyne modification (X1):

5' - (NH₂)AAAAAAAACGAGTGCTAAGGATCCGAAX₁

AmS2 – oligonucleotide with azide modification (X2):

3' - (NH₂) AAAAAAAGCTTACCTATAGACGTCACTTX₂

AuNP – Gold nanoparticle

AuNR - Gold nanorod

BLAST – Basig Local Alignment Search Tool

BSA – Bovine Serum Albumin

BSPP – bis(p-sulfonatophenyl)phenyl phosphine dehydrate dipotassium salt

C – Cytosine

C1 – oligonucleotide: 5' – (C₆H₁₂S)AAAAAAAACGAGTGCTAAGGATCCGAA

cm - centimetre

Ct - citrate

CuAAC – Copper-catalysed azide-alkyne cycloaddition

D – dilution

DMEM – Dulbecco's Modified Minimum Essential Medium

DNA – deoxyribonucleic acid

DNAse - deoxyribonuclease

DOX - Doxorubicin

DTT - dithiothreitol

EDC – 1-(3-(dimethylamino)propyl)-3-ethyl-carbodiimidemethiodide

EDTA – ethylenediaminetetraacetic acid

FBS – fetal bovine serum

FDA - Food and Drug Administration

g – gram

G - Guanine

GA-PEG – Gallic Polyethylene glycol

GO – Graphene oxide

h - hour

HBSS – Hank's balanced salt solution

L – litre

 $n - nano (10^{-9})$

NC - nano cube

NF – nano-probe

nm – nanometre

NIR - near-infrared

NP – nanoparticle

NPs – nanoparticles

 $\mu - \text{micro} (10^{-6})$

 μm – micrometre

 $\mathbf{m} - \text{milli } (10^{-3})$

M - molar

max – maximum

MEM – Minimum Essential Medium

MET – Mesenchymal to epitelial transition

min – minutes

mRNA – messenger RNA

MW – molecular weight

O.D. – optical density

 $\mathbf{p} - \text{pico} (10^{-12})$

PAE – programmable atom equivalent

PAGE – Polyacrylamide gel electrophoresis

PBS – phosphate buffered saline

PIPES – piperazine-1,4-bis(2-ethanesulfonic acid)

ppm – parts per million

PSMA – prostate-specific membrane antigen

QDs – quantum dots

RedOx – reduction-oxidation

RNA – ribonucleic acid

rpm – rotation per minute

RPMI – Roswell Park Memorial Institute Medium

RT-PCR – reverse transcriptase polymerase chain reaction

s – seconds

S1 – oligonucleotide with alkyne modification (X1):

5' – (C₆H₁₂S)AAAAAAAACGAGTGCTAAGGATCCGAAX₁

S2 - oligonucleotide with azide modification (X2):

 $3'-(C_6H_{12}S) \ AAAAAAAAGCTTACCTATAGACGTCACTTX_2\\$

S3 – oligonucleotide:

5'-ACACCGAATGGATATCTGCAGTGAATTCGGATCCTTAGCACTCGACACAC

S4 – oligonucleotide:

5' - GTGTGTCGAGTGCTAAGGATCCGAATTCACTGCAGATATCCATTCGGTGTGT

SAXS – Small Angle X-ray Scattering

SERS – Surface Enhanced Raman Spectroscopy

s-NHS – N-hydroxysulfosuccinimide

SPION – Superparamagnetic iron oxide nanoparticle

SPR – surface plasmon resonance

T-Thymine

TBE – Tris borate EDTA buffer

TEM – transmission electron microscopy

UV-vis – ultra-violet-visible

V - volts

W – watt

XANES – X-ray Absorption Near Edge Structure

 ξ – zeta

°C – degrees Celsius

CHAPTER 1

-Introduction-

The scientific interplay between nanotechnology and biology has resulted in a fast-moving research area of a highly interdisciplinary nature. Bionanotechnology involves the use of advanced nanomaterials for applications in biology. In particular the utilization of inorganic nanomaterials for implementations in biomedicine has been an area of high impact research. The unique properties of inorganic nanoparticles have resulted in many novel applications ranging from imaging and sensing to therapy. In many cases a distinct superiority of these nanomaterials compared to conventional imaging or therapeutic agents has been demonstrated.

In the past two decades, great efforts have been focussed on the conjugation of biomolecules to inorganic nanomaterials. These biomolecules include proteins, peptides and nucleic acids. Making use of the inherent specific properties of aforementioned biomolecules, scientists have developed a great range of novel hybrid nanomaterials. For example, proteins, peptides as well as nucleic acids have been used to guide nanoparticle assembly into pre-defined structures [1-7]. It has been shown that resulting assemblies show potential for implementations in materials science [8, 9] and biomedicine [10-12]. Moreover, the conjugation of peptides or nucleic acids to nanomaterials has been utilized to target their delivery to biologically relevant sites (e.g. tumours or intracellular compartments) [13, 14].

These two examples demonstrate the range of potential applications for bionanotechnological materials developed so far within this young and thriving scientific field. The work presented hereafter aims to display further developments in this area.

The main theme of this thesis was focussed on the use of synthetic nucleic acids (oligonucleotides) for nanoparticle assembly and biosensing applications.

In **Chapter 4**, the surface functionalization of different nanomaterials with oligonucleotides is discussed. The additional functionality inferred to the nanomaterials by the DNA ligand gives rise to a variety of applications. On the one hand, DNA-nanomaterial conjugates can have important implementations in biomedicine. On the other hand they can form building blocks for the programmed organization of 2D assemblies.

Chapter 5 presents results on DNA-gold nanoparticle conjugates for intracellular applications. Probes for the intracellular detection of mRNA in live cells are introduced. These probes consist of gold nanoparticles conjugated to fluorophore-tagged oligonucleotides. The sequence of these oligonucleotides can be designed to detect any chosen mRNA. We furthermore incorporated a chemotherapeutic drug into the probe design. Cell-type specific targeted drug delivery will be demonstrated.

Chapter 6 discusses the use of click chemistry for the programmed ligation of DNA-coated nanomaterials with a view of creating advanced biomedical probes. This method enables the facile fabrication of nano-sized assemblies, connected by single-stranded DNA. The broad applicability of the proposed method is demonstrated by the formation of heterogeneous systems. These can include either two nanoparticles or the 2D nanomaterial graphene oxide. Resulting assemblies will be of interest for applications in biomedicine and -sensing as well as materials science. Additionally, the interactions of gold nanoparticle dimers with cells will be discussed. We expect that gold nanoparticle dimers have the potential of being developed into multi-role theranostic nano-probes.

1.1 References

- 1. Kostiainen, M.A., et al., Electrostatic assembly of binary nanoparticle superlattices using protein cages. Nat Nano, 2013. **8**(1): p. 52-56.
- 2. Fan, C., DNA Nanotechnology: From Structure to Function. 2013: Springer.
- 3. Loweth, C.J., et al., *DNA-based assembly of gold nanocrystals*. Angewandte Chemie-International Edition, 1999. **38**(12): p. 1808-1812.
- 4. Kanaras, A.G., et al., *Towards multistep nanostructure synthesis: Programmed enzymatic self-assembly of DNA/gold systems*. Angewandte Chemie-International Edition, 2003. **42**(2): p. 191-194.
- 5. Sonnichsen, C., et al., A molecular ruler based on plasmon coupling of single gold and silver nanoparticles. Nat Biotechnol, 2005. **23**(6): p. 741-5.
- 6. Nykypanchuk, D., et al., *DNA-guided crystallization of colloidal nanoparticles*.

 Nature, 2008. **451**(7178): p. 549-52.
- 7. Park, S.Y., et al., *DNA-programmable nanoparticle crystallization*. Nature, 2008. **451**(7178): p. 553-6.
- 8. Kuzyk, A., et al., *DNA-based self-assembly of chiral plasmonic nanostructures* with tailored optical response. Nature, 2012. **483**(7389): p. 311-4.
- 9. Yan, W.J., et al., Self-Assembly of Chiral Nanoparticle Pyramids with Strong R/S Optical Activity. J Am Chem Soc, 2012. **134**(36): p. 15114-15121.
- Xu, L.G., et al., Regiospecific Plasmonic Assemblies for in Situ Raman Spectroscopy in Live Cells. Journal of the American Chemical Society, 2012.
 134(3): p. 1699-1709.
- Chou, L.Y.T., K. Zagorovsky, and W.C.W. Chan, DNA assembly of nanoparticle superstructures for controlled biological delivery and elimination.
 Nature Nanotechnology, 2014. 9(2): p. 148-155.

CHAPTER 1 - Introduction

- 12. Liu, G.L., et al., A nanoplasmonic molecular ruler for measuring nuclease activity and DNA footprinting. Nat Nanotechnol, 2006. **1**(1): p. 47-52.
- Juliano, R.L., et al., Cell-targeting and cell-penetrating peptides for delivery of therapeutic and imaging agents. Wiley Interdisciplinary Reviews: Nanomedicine and Nanobiotechnology, 2009. 1(3): p. 324-335.
- 14. Bagalkot, V., et al., Quantum dot Aptamer conjugates for synchronous cancer imaging, therapy, and sensing of drug delivery based on Bi-fluorescence resonance energy transfer. Nano Letters, 2007. **7**(10): p. 3065-3070.

CHAPTER 2

-Background-

In this thesis, nanoparticle-DNA conjugates were employed for biomedical applications such as live cell mRNA detection [1-6] and targeted drug delivery (see **chapter 5**). They were furthermore employed as building blocks for programmed assembly of advanced nanomaterials for potential biomedical applications (see **chapter 6**).

This chapter will introduce relevant background information on the individual building blocks used in this project. **Section 2.1** will discuss different syntheses of gold nanoparticles. The optical properties of gold nanospheres will be elucidated in **section 2.2**. Oligonucleotide synthesis and modification of nanomaterials with oligonucleotides will be discussed in **sections 2.3** and **2.4**. The concept of using DNA-AuNP conjugates as probes for live cell mRNA detection and targeted drug delivery will be introduced in **section 2.5**. Finally, with a view of creating advanced nanostructures for multiplexed biomedical applications, the programmed assembly of nanomaterial-DNA conjugates will be discussed (**section 2.6**).

Parts of this chapter were published in: <u>Heuer-Jungemann</u>, A.; Harimech, P. K.; Brown, T.; Kanaras, A. G. "Gold nanoparticles and fluorescently-labelled DNA as a platform for biological sensing", *Nanoscale*, **2013**, 5 (20), 9503-9510.

2.1 Synthesis and surface stabilisation of spherical gold nanoparticles.

The use of colloidal gold dates back to ancient times, where they found use in the staining of glass [7, 8]. An example for this is the famous 'Lycurgus Cup' [9] dating back to the 4th century AD. However, it was not until the 19th century, when the first reported study on the synthesis and properties of gold nanoparticles was published by Faraday [10]. Initial refinements of the synthesis were reported by Turkevich [11, 12] and later by Frens [13]. The synthesis of colloidal gold is based on the reduction of gold salts in the presence of a capping agent. In the following paragraphs, different methods for the synthesis of gold nanospheres with an average size of 13 nm (see **section 2.1.1**) or 5 nm (see **section 2.1.2**) will be discussed.

2.1.1 Synthesis of gold nanospheres using the citrate reduction method.

The most commonly applied method for the synthesis of monodisperse gold nanospheres with an average diameter of 13 nm, is the citrate reduction method. First reported by Turkevich [11, 12] and Frens [13], it has been the subject of many scientific publications [14-21].

In this method, an aqueous solution of tetrachloroauric acid (or sodium tetrachloroaurate) is reduced by an aqueous solution of trisodium citrate at boiling (see section 3.1 for synthetic protocol). The size of the resulting colloids can be tuned by adjusting the molar ratio of gold precursor to citrate [13]. Although seemingly simple, the reaction mechanisms behind the formation of colloidal gold are rather complex (see scheme 2.1).

A) RedOx reaction between citrate and gold precursor

AuCl₃ + 2e ---

B) Complexation of gold chloride and acetone dicarboxylate anion

C) Decomposition of acetone dicarboxylate

D) RedOx reaction between acetone and AuCl₃

O
$$+ \text{AuCl}_3$$
 \longrightarrow AuCl $+ 2\text{Cl}^- + \text{CH}_3\text{COOH} + \text{HCOOH}$

E) Disproportionation of AuCl into Au⁰

F) Nanoparticle formation

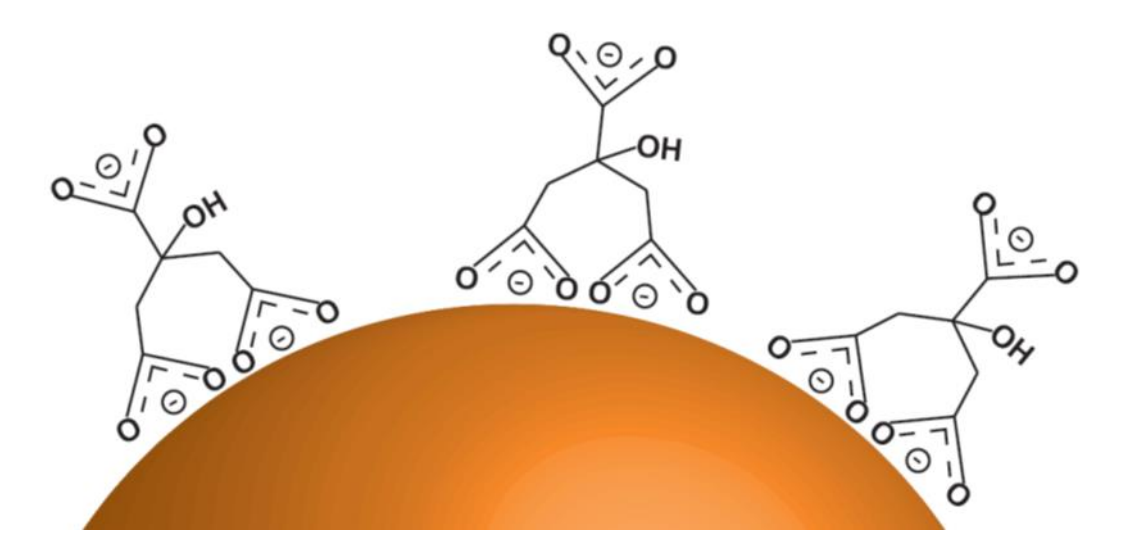
$$n Au^0 \xrightarrow{\text{nucleation}} AuNPs$$

Scheme 2.1 Reaction mechanisms of the reduction of gold precursors by citrate. Adapted from ref. [22].

The first steps in reaction \mathbf{A} involve the oxidation of citrate into acetone dicarboxylate and the simultaneous reduction of gold (III) precursor to form gold (I) chloride. In the second reaction \mathbf{B} , dicarboxylate anions form larger complexes with gold (I) chloride. These complexes then coagulate into precursors and form gold nuclei (Au⁰) by the disproportionation of gold chloride (reaction \mathbf{E}). This is followed by nanoparticle growth \mathbf{F} .

It has been shown by Privman *et al.* that monodispersity in the colloidal gold sample is crucially dependent on a rapid coagulation [23]. Thus Xia and co-workers concluded that a rapid formation of acetone dicarboxylate promoted rapid coagulation and hence a more uniform particle size [17, 22]. However, as outlined in reaction **C**, acetone dicarboxylate can be subject to decomposition into acetone. As discussed by Privman and co-workers, decomposition is favoured at elevated temperature and high pH [24]. Reaction **D** shows that acetone can reduce gold (III) precursors [25]. This results in further nucleation processes. The occurrence of nucleation events at different time points causes an increasingly broad size distribution of the resulting nanoparticles.

Although not immediately obvious, the role of citrate in this reaction is three-fold, as reported by Peng *et al.* [19]. It firstly acts as a reducing agent inducing the formation Au⁺ from Au³⁺. Secondly it acts as a capping agent (see **scheme 2.2**), and thirdly it serves as a pH buffer during the reaction, influencing the reaction kinetics [19, 21].



Scheme 2.2 Schematic illustration of a gold nanoparticle core stabilized by citrate anions.

A reduction in pH may lead to the protonation of citrate, which in turn influences the electrostatic stabilisation of AuNPs (scheme 2.3 A). It furthermore influences the active gold precursor species (see scheme 2.3 B) and thus the reactivity and rate of nucleation [21].

A) Protonation of citrate

$$C_6H_5O_7^{3-} + H_2O$$
 \longrightarrow $C_6H_6O_7^{2-} + OH^ pKa = 6.4$ $C_6H_6O_7^{2-} + H_2O$ \longrightarrow $C_6H_7O_7^{-} + OH^ pKa = 4.76$ $C_6H_7O_7^{-} + H_2O$ \longrightarrow $C_6H_8O_7$ $+ OH^ pKa = 3.13$

B) Gold precursor species

Scheme 2.3 Influence of the pH on the formation of gold nanoparticles with respect to citrate protonation **A**) and gold precursor speciation **B**). Adapted from ref [21], pKa values were obtained from ref. [26].

Many studies have tried to shed light onto the growth mechanism of gold nanospheres [27-30], however due to conflicting results, no conclusive mechanistic pathway has been agreed on to date.

2.1.2 Synthesis of small gold nanospheres using sodium borohydride as reducing agent.

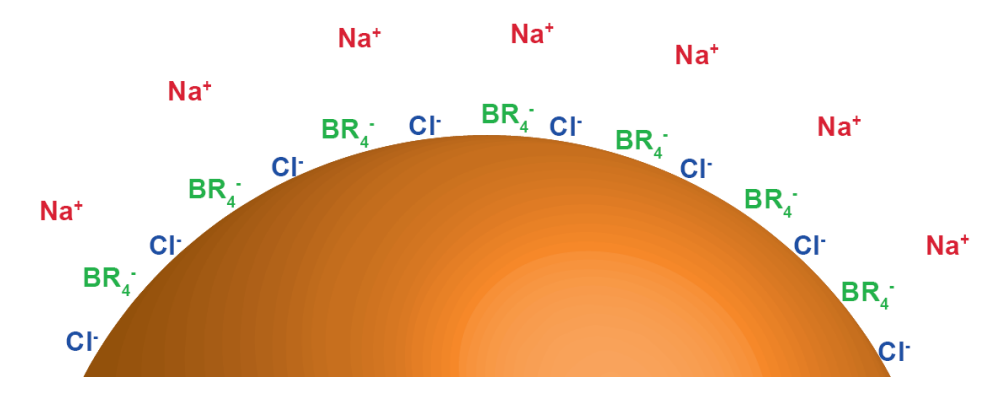
The synthesis of small gold nanoparticles with good size distributions has been achieved using various methods. The most popular is the Brust-Schiffrin method [31]. In the synthetic procedure, small gold nanospheres are produced in organic solvents. Reduction of gold precursor is achieved with the strong reducing agent sodium borohydride (NaBH₄). In this method alkanethiols are used as capping agents.

The sizes of produced particles can be controlled in a range of 1-3 nm and 2-5 nm by varying the concentration of thiol [31, 32]. A potential disadvantage of this method is the use of thiols, such as dodecanethiol, as capping agents. Due to the strength of the thiol-gold bond, ligand exchange reactions do not always result in stable particles [33, 34]. Alternative synthetic protocols for the synthesis of small gold nanoparticles without covalent ligand stabilisation have been reported [34-36]. For example, in water, sodium borohydride can also be used as a reducing agent (see scheme 2.4). The gold precursor is quickly reduced into Au⁰, initiating nucleation.

$$2NaAuCl_4 + 18H_2O + 6NaBH_4 \longrightarrow 2Au^0 + 8NaCl + 21H_2 + 6B(OH)_3$$

Scheme 2.4 Reduction mechanism of gold salt by sodium borohydride. Adapted from ref.[37].

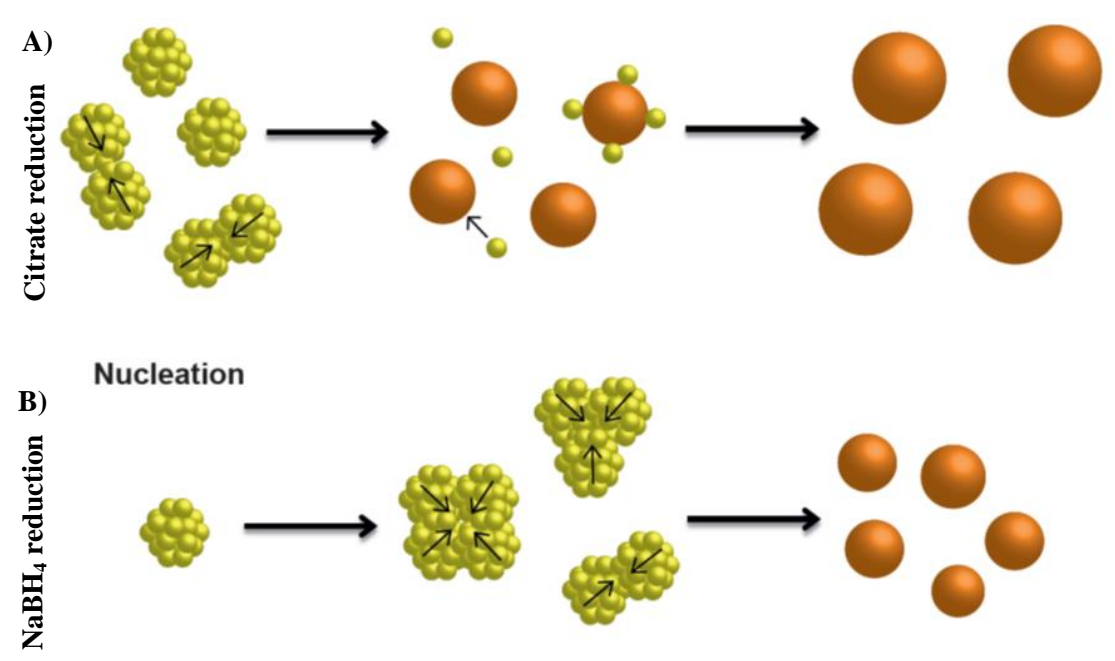
Deraedt *et al.* recently showed that in this reaction, sodium borohydride can act as both reducing and capping agent (see **scheme 2.5**), analogous to the role of citrate in the Turkevich method [38] (cf. **section 2.1.1**).



Scheme 2.5 Illustration of the surface stabilisation of AuNPs synthesised by sodium borohydride reduction. Adapted from ref.[38], where $\mathbf{R} = \mathbf{H}$ or \mathbf{OH} . N.B.: Deraedt *et al.* further suggested potential surface stabilisation by hydride ions not shown here.

2.1.3 Comparison between citrate and sodium borohydride reduction methods

Recently Polte *et al.* studied the growth mechanisms of AuNPs synthesised by citrate or NaBH₄ reduction using *in situ* SAXS and XANES [39]. They reported that nanoparticle growth by citrate reduction occurred in three separate phases (see **scheme 2.6 A**). On the other hand, growth by NaBH₄ reduction occurred in only two steps.



Scheme 2.6 Schematic illustration of the growth of gold nanospheres. Adapted from ref [39].

In this case nuclei were formed within 100 ms. Subsequently, particles were grown via coalescence (see **scheme 2.6 B**). The fast nucleation resulted in a slightly smaller particle size compared to particles formed utilizing the citrate reduction method. Furthermore, Polte and co-workers observed polydispersity in particles grown by sodium borohydride reduction. To some degree this can be counteracted by slowing down the reaction kinetics (e.g. by a slight increase in pH [19] through addition of a weak base such as K_2CO_3 and/or low temperature [40]).

2.1.4 Surface stabilisation of gold nanoparticles.

Following the synthetic methods discussed earlier, the surface of gold nanoparticles is stabilized by either citrate or borohydride anions (see schemes 2.2 and **2.5**). Stabilization is generally achieved through electrostatic effects or weak van der Waal's forces [41, 42]. These electrostatically stabilized colloids are stable in water. However, a disadvantage is their inherent susceptibility to irreversible aggregation induced by high salt concentrations and pH changes [41-44]. On the other hand, the weak electrostatic stabilisation facilitates ligand exchange reactions with covalently bound molecules. Proposed agents include amines, phosphines or thiols [45]. For example, the bulky phosphine ligand bis(p-sulfonatophenyl)phenyl) phosphine dehydrate (BSPP), introduced by Schmidt et al. [46], has been used extensively for the stabilisation of gold nanospheres [47] (see scheme 2.7). An advantage of using BSPP as a capping agent is the ability to reversibly aggregate particles using salt. This allows for concentration of a nanoparticle solution by centrifugation. Obtaining a highly concentrated solution of nanoparticles is important for many applications, especially for those in biomedicine. However, for biomedical applications stronger stabilizing agents often are required. For this reason, thiol-gold chemistry is routinely employed. The high



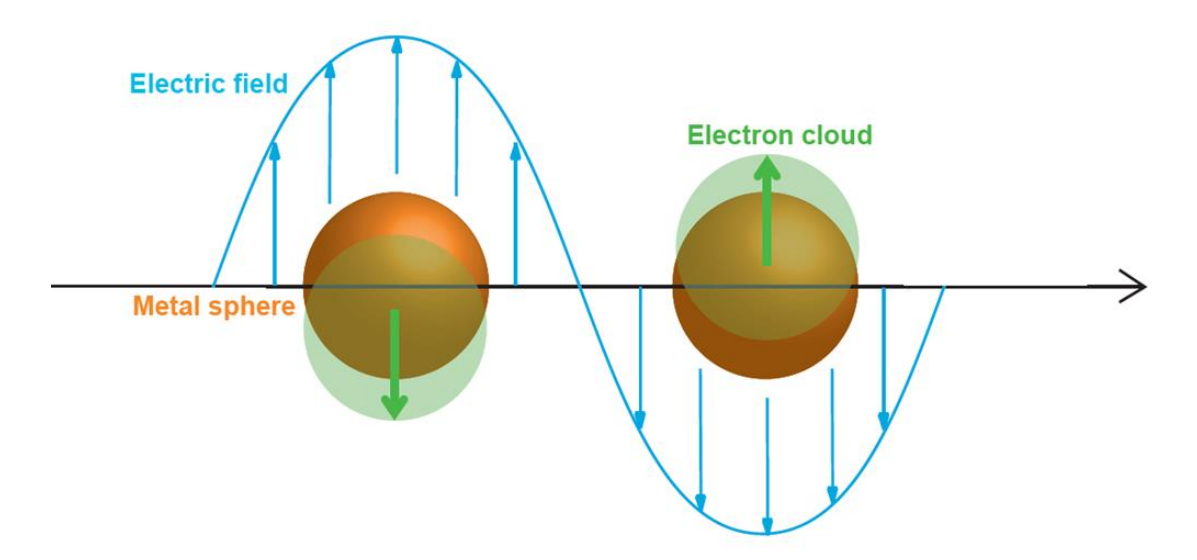
Scheme 2.7 Illustration of the surface stabilisation of gold nanoparticles by BSPP.

affinity of gold surfaces for thiols facilitates ligand exchange reactions with more labile ligands (e.g. citrate or BSPP) [45, 48]. The strength of the resulting gold-thiol covalent bond is similar to that of a gold-gold bond [48, 49]. Stabilisation of colloidal gold by thiols is therefore an advantageous approach to prepare highly stable nanoparticles [42, 46, 50-55]. Additionally, in many cases thiolated capping agents also infer additional functionality. For example, thiolated polyethylene glycols [56-59] are commonly used as 'stealth' ligands for biomedical applications [60-62]. Gold nanoparticles functionalised with thiolated peptides have found applications in cellular targeting and sensing [63-70]. The use of thiolated oligonucleotides [71-76] for the functionalization of gold nanoparticles has resulted in wide-spread applications ranging from biomedicine [77] to programmable self-assembly [78].

The use of functional oligonucleotides for the surface capping of a variety of different nanomaterials forms the main theme of this work and will be further discussed in **section 2.4**.

2.2. Optical properties of gold nanoparticles.

The striking colours of noble metal nanoparticles have attracted the attention of mankind for centuries [8]. Their distinct optical properties, which are significantly different from those found in the bulk material, arise from their unique interactions with light [79]. As such, metal nanoparticles can show optical responses ranging from the visible to the near infrared range. These optical properties derive from the coherent oscillation of free conduction band electrons caused by interactions with an electromagnetic field [8, 79]. They are mostly observed in gold, silver and copper as these possess free conduction band electrons [9]. These electrons form an electron cloud around the particle core, according to the Drude-Sommerfeld model [79]. Upon interactions with electromagnetic radiation, the electron cloud is displaced relative to the nanoparticle core, creating a dipole [9]. The electron cloud displacement induces a restoring force based on attractive Coulomb interactions between electrons and the particle core [8]. This results in the coherent oscillation of the electron cloud [9]. The collective oscillation of conduction band electrons (see scheme 2.8) is referred to as the



Scheme 2.8 Schematic illustration of the surface plasmon resonance on metal nanoparticles depicting the displacement of the conduction band electron cloud relative to the nanoparticle core. Adapted from ref. [8].

surface plasmon resonance (SPR)

The first quantitative description of the SPR was reported by Mie in 1908 [80]. Mie solved Maxwell's equations using boundary conditions appropriate for spherical particles. In his theorem, the electric field around a particle that is smaller than the wavelength of light can be assumed to be constant [8]. If the free conduction band electrons are excited to oscillate by an externally applied electric field, their return to the ground state can be either radiative or non-radiative (absorption or scattering). The extinction cross-section can be expressed as the sum of the absorption and the scattering cross-section [79].

For particles smaller than 25 nm, the scattering cross-section becomes negligible. Thus the Mie theory for the extinction cross-section can be written as the following relationship (quasistatic or dipole approximation) [79].

$$\sigma_{ext} = \frac{9V\epsilon_m^{3/2}}{c} \times \frac{\omega\epsilon_2(\omega)}{[\epsilon_1(\omega) + 2\epsilon_m]^2 + \epsilon_2(\omega)^2}$$

Equation 2.1 Calculation of the total extinction cross-section for metal nanoparticles. V = particle volume, c = speed of light, $\omega =$ angular frequency of exciting radiation, $\epsilon_m =$ dielectric constant of the surrounding medium, $\epsilon_1(\omega)$ and $\epsilon_2(\omega)$ are the real and imaginary parts of the dielectric constant of the particle material $(\epsilon(\omega) = \epsilon_1(\omega) + i\epsilon_2(\omega))$. Adapted from ref. [79].

From **Eq. 2.1**, one can see that a resonance (i.e. the SPR) only occurs if $\epsilon_1(\omega) \approx -2\epsilon_m$, supposing that ϵ_2 is small or only weakly dependent on ω [79]. Furthermore, as reported by Kreibig *et al.*, the width and height of the surface plasmon resonance peak is approximately determined by $\epsilon_2(\omega)$ [81].

Although V is dependent on the particle size ($V = 4\pi/3$ R³) [82], and therefore influences the peak intensity, the dipole approximation does not predict the position of the SPR as a function of particle size [79]. However, experimental results have shown that the SPR blue- or red-shifts for smaller or larger particles respectively [18]. Therefore a modification to the dipole approximation was adapted, so that the dielectric constant ϵ became size-dependent ($\epsilon = (\omega, R)$) - (intrinsic size effect) [79].

Furthermore one can see from **Eq. 2.1** that the SPR is dependent on the dielectric constant of the surrounding medium. This property can be used to explain shifts in the SPR as a result of changes in the medium to which nanoparticles are exposed [82, 83] and is the basis of the use of metal nanoparticles in sensing applications [84-88].

2.3. Synthesis and properties of oligonucleotides.

Deoxyribonucleic acid (DNA) is a biological polymeric macromolecule, essential for life. It is made up of nucleotide monomers [89]. These nucleotides consist of a pentose sugar, a phosphate group and a base [89]. The nature of the base determines the nucleotide, as the other two building blocks remain constant. In DNA there are four naturally occurring bases: The purines Guanine (G) and Adenine (A), and the pyrimidines Cytosine (C) and Thymine (T) [89] (see **Figure 2.1**). Nucleotides linked by phosphodiester linkages (phosphate backbone), make up a DNA strand (see **Figure 2.1**). At physiological pH phosphate groups are negatively charged, resulting in DNA being a highly charged anionic polymer.

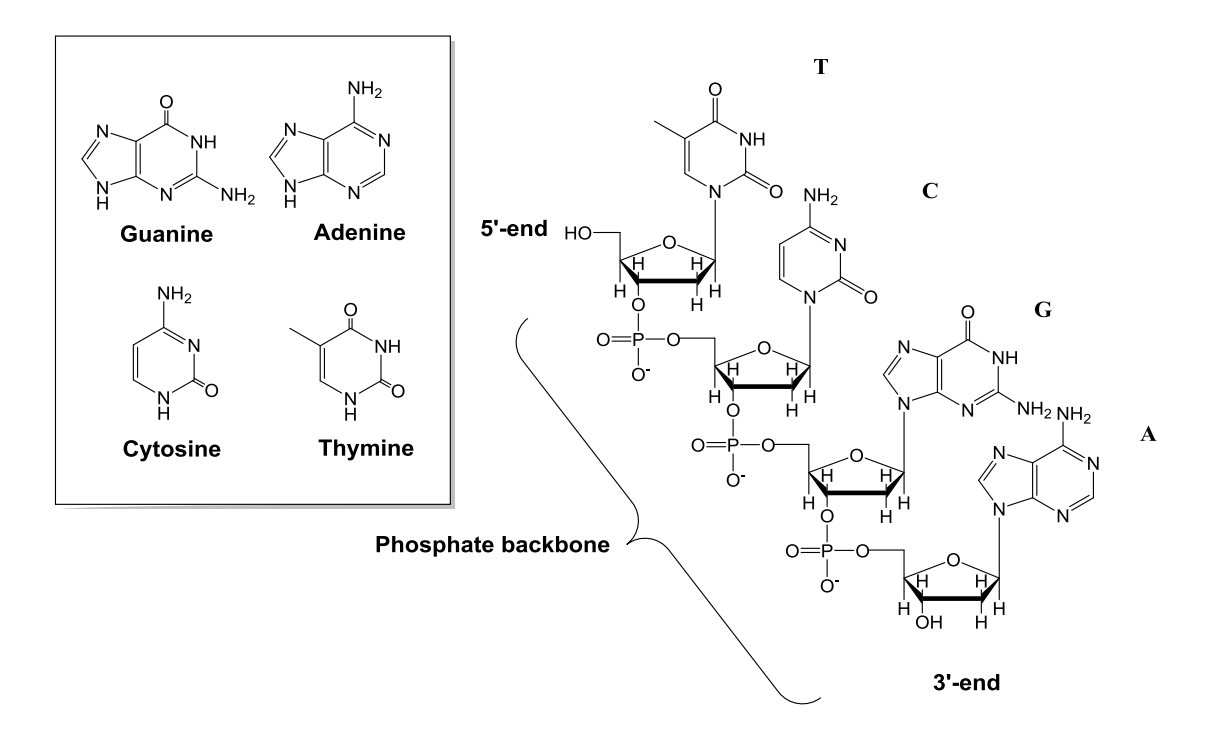


Figure 2.1 Chemical structures of the four naturally occurring DNA bases and the structure of a DNA strand with the sequence TCGA.

In 1953, Watson and Crick showed that in solution, DNA strands form a duplex. It was found that base pairing was highly specific as **A** would only pair with **T** and **G** would only pair with **C** [90] (see **Figure 2.2**). The duplex is stabilised by hydrogen bonding and hydrophobic base stacking. The latter is based on π -stacking interactions – attractive van der Waals forces [89]. The strength of these interactions is dependent on the aromaticity and the dipole moments of the individual bases [91].

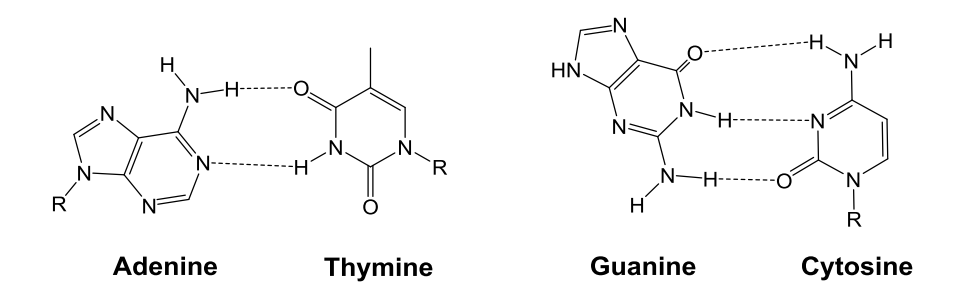


Figure 2.2 Illustration of the formation of DNA base-pairing showing hydrogen bonding (dashed lines).

Oligonucleotides are synthetic DNA strands produced by automated solid phase phosphoramidite synthesis [92-94]. The sequence of individual oligonucleotide strands can be designed and pre-programmed. Furthermore it is possible to functionalize designer oligonucleotides with a wide range of functional groups such as for example fluorescent dyes [95] or moieties enabling further chemical reactions [96]. These can be either incorporated *via* a functionalized column used for solid phase synthesis (for 3' modifications only) or by utilization of pre-modified nucleoside phosphoramidite monomers [97]. Additionally oligonucleotides can be synthesised with amino alkyl linkers for post-synthetic modifications.

Due to their ease of synthesis and functionalization as well as their inherent accurate addressability, oligonucleotides have found wide-spread applications in biomedicine and materials nanotechnology [1-3, 97-103]. Especially their use as a scaffold for the programmed self-assembly (see **section 2.6**) of nanomaterials has become a hot topic [47, 64, 104-111].

2.4 Modification of nanomaterials with oligonucleotides.

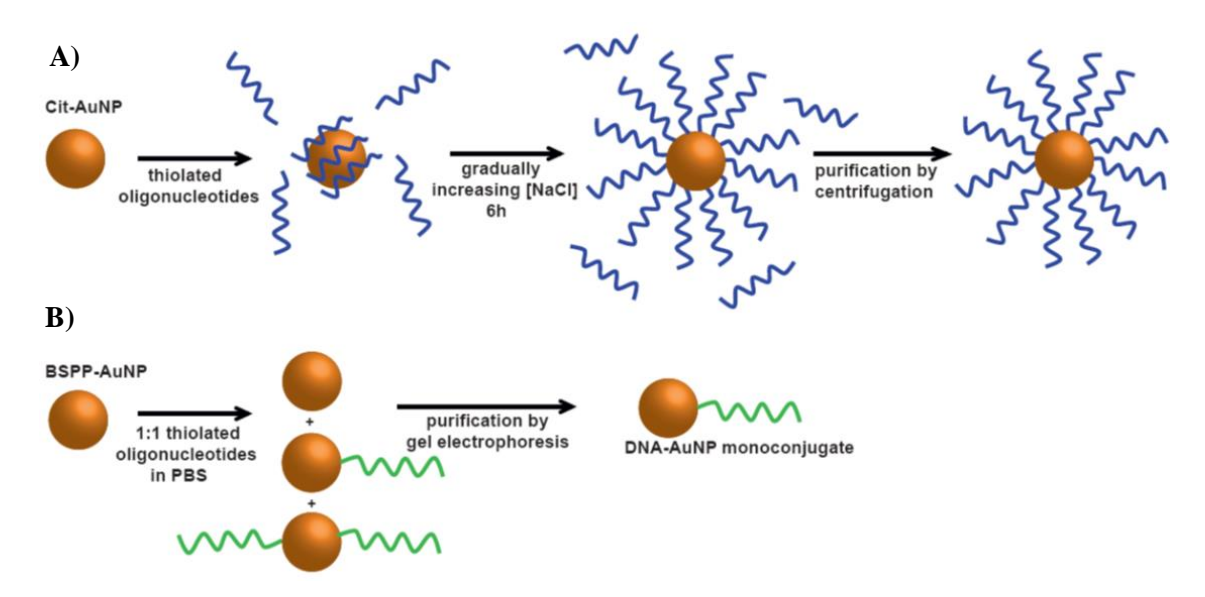
2.4.1 Oligonucleotide modification of gold nanoparticles.

Pioneering work by research groups lead by Alivisatos [72] and Mirkin [71] in 1996 showed that it was feasible to attach DNA to gold nanoparticles. While Mirkin and co-workers demonstrated that gold nanoparticles can be modified with a dense DNA corona [71], Alivisatos and co-workers showed that it was equally possible to produce AuNPs conjugated to a discrete number of oligonucleotides [72].

DNA modification endows the nanoparticle with functional properties inherent to the DNA ligand. These include accurate addressability and high target specificity, which can be encoded in the oligonucleotide sequence [104, 108, 112, 113]. Thus,

DNA-gold nanostructures have become increasingly important units for applications in sensing and nanomedicine [1, 2, 4, 5, 114-116], metamaterials [117, 118], nano-optics and nanoelectronics [119, 120].

Due to well established gold-thiol chemistry, the conjugation of thiolated oligonucleotides to AuNPs is straightforward. **Scheme 2.9** shows two commonly used approaches.



Scheme 2.9 A) Method of conjugating multiple oligonucleotides to citrate-capped gold nanoparticles, creating a DNA corona. Adapted from ref. [105] **B)** Method of conjugating a discrete number of oligonucleotides to BSPP-coated gold nanoparticles.

The first one shows the conjugation of a large number of oligonucleotides onto a citrate-coated gold nanosphere (**Scheme 2.9 A**). In this 'salt ageing' procedure, the concentration of sodium chloride is gradually increased over time. In order to achieve a high surface loading, it is imperative to screen the repulsive charges between the gold nanoparticle surface and the negatively charged phosphate backbone on the DNA, as well as the charges between individual DNA strands [121]. This, eventually, results in a dense layer of oligonucleotides on the gold nanoparticle surface [77].

As shown by Kanaras *et al.* a similar result can be obtained using a vacuum centrifugation method in which the ionic strength and concentrations of oligonucleotides and AuNPs are gradually increased as a result of an overall decreasing reaction volume [122]. Further studies showed that the final oligonucleotide surface-loading is dependent on the surface curvature of particles and can be finely tuned by means of adjusting the final sodium ion concentration [99, 121, 123]. Additionally, Hurst *et al.* reported that sonication during DNA conjugation resulted in a substantial increase in surface loading [124]. Recently Zhang and co-workers reported on a novel instantaneous and quantitative DNA conjugation method using a pH-assisted route [125]. They reported that quantitative DNA adsorption was achieved within 3 min using a citrate buffer at pH 3.

Densely-functionalized DNA-nanoparticle conjugates have been widely employed for biomedical studies [1, 3-6, 99, 101, 126-128]. In this thesis densely-functionalized DNA-AuNP conjugates were employed for live cell mRNA detection and targeted drug delivery (see section 2.5 and chapter 5). They were further used as building blocks for the programmed assembly of AuNP dimers and trimers with views of creating advanced nanoconstructs for biomedical applications (see section 2.6 and chapter 6).

In order to program the organization of nanoparticles into well-defined assemblies, it is often advantageous to only conjugate one or few DNA strands to the nanoparticle surface [129-131]. To control the number of DNA strands per nanoparticle, it is important to regulate the stoichiometry of DNA to AuNPs in the experimental protocol [130]. However, as illustrated in **Scheme 2.9 B**, when a stoichiometry of 1:1 is used, a population of mono- and diconjugates (AuNPs conjugated to one or two DNA strands) as well as 'bare' AuNPs are produced, despite stoichiometric mixing [75, 132]. Purification is the key to obtaining discrete DNA-AuNP conjugates [74, 108, 129, 133].

Strategies for purification of mono- and diconjugates include anion-exchange high performance liquid chromatography [129], density gradient centrifugation [133] and agarose gel electrophoresis. Of these, purification by agarose gel electrophoresis is most commonly used [73, 74, 130]. The agarose gel consists of a porous matrix. The average pore size can be controlled by the weight/volume percentage [75]. During electrophoresis, molecules are separated according to their size and charge. However, Pellegrino et al. reported that for DNA-AuNP conjugates the effective increase in size, inferred by DNA conjugation, was the determining factor for separation of mono- and diconjugates [76]. Furthermore, Zanchet et al. reported that a ratio of AuNP size to DNA length of at least 1:10 must be achieved for efficient separation in the agarose gel matrix [73]. Recently Busson and co-workers suggested that 'lengthening strands' may be used for more efficient separation [134]. In this method, oligonucleotides conjugated to the AuNP surface are hybridised with a longer complementary DNA strand, which in turn could be hybridised to yet another strand. They reported that using this technique, even large AuNPs (30 nm) conjugated to one short oligonucleotide strand could be efficiently separated from 'bare' AuNPs and diconjugates using agarose gel electrophoresis [134].

2.4.2 Oligonucleotide modification of nanomaterials of different chemical composition.

In order to create a library of different functional nanomaterials for the programmed DNA-mediated assembly of advanced nanostructures, a variety of building blocks are required. As discussed in **section 2.4.1** the conjugation of oligonucleotides to AuNPs is straightforward owing to well-established thiol-gold chemistry. For

nanomaterials of different chemical compositions, protocols for DNA conjugation have been adapted [135-143].

In many cases, inorganic nanoparticles are stabilized by polymers [144, 145] containing variable functional end-groups such as hydroxyl, carboxyl, amine, alkyne, azide or aldehydes for further modifications [136, 146]. Cutler and co-workers showed that azide-functionalized superparamagnetic iron oxide nanoparticles (SPIONs) could be modified with a dense layer of alkyne functionalized oligonucleotides using Cu (I)catalysed click chemistry [137]. Whilst Wang et al. suggested using azidefunctionalized graphene oxide (GO) sheets for the covalent conjugation of alkenemodified DNA [147]. Zhang et al. recently showed that by using an azide-bearing amphiphilic polymer to cap nanoparticles, DNA could be coupled to nanomaterials of different compositions via azide-alkyne cycloaddition chemistry [136]. conjugation of amine-modified DNA to CdSe-ZnS core-shell quantum dots, coated with a carboxyl-terminated polymer shell, Sun et al. suggested the use of well-established 1ethyl-3-(3-dimethylaminopropyl)carbodiimide (EDC)/sulfo-NHS coupling [138]. EDC is a commonly used cross-linking reagent employed for the coupling of a primary amine with a carboxylic group [148]. The general reaction mechanism is outlined in scheme **2.10**. In the first step, EDC reacts with a carboxylic group on the nanomaterial to form an unstable intermediate. In order to avoid hydrolysis and subsequent re-formation of the carboxylic group, the o-acylisourea ester intermediate is reacted with sulfo-NHS to give a semi-stable amine-reactive NHS-ester. The reaction with amine-terminated DNA results in the formation of a stable amide bond between nanomaterial and DNA. Using this method, Liu and co-workers showed that amine-terminated DNA could also

be conjugated to the surface of graphene oxide [149] by making use of the

Scheme 2.10 Schematic illustration of the EDC/ sulfo-NHS coupling reaction. Adapted from ref. [148].

abundance of carboxylic groups on the GO surface [147]. Following these reports, carboxyl-functionalized nanomaterials employed in studies within this project (Fe_3O_4 , $Cu_{2-x}Se$ and graphene oxide) were conjugated to amine-terminated DNA using EDC coupling [63, 148] (see **chapter 4** for results).

2.5 Interactions of gold nanoparticle-DNA conjugates with cells.

It has been shown that DNA-AuNP conjugates are taken up by cells in large numbers [150] without the aid of a co-carrier [77, 150]. It was furthermore shown that the oligonucleotide loading played an important role in DNA-AuNP uptake. For surface loadings of more than 18 pmol/cm², cellular internalisation of a very high number of DNA-AuNPs per cell was possible [77, 150].

Since this discovery, studies on the uptake mechanism of DNA-AuNP conjugates have received significant attention. However, to date fully conclusive results have not been reported. It was shown that within the cellular environment, the

hydrodynamic radius of DNA-AuNPs was greatly increased and a change in charge could be observed [150]. One hypothesis is that these changes were caused by the adsorption of cellular proteins, which assisted internalization [150]. However, further investigations demonstrated that adsorption of common cellular proteins such as bovine serum albumin (BSA) and transferrin resulted in reduced cellular uptake, which contradicted previous observations [151]. Latest studies suggested that scavenger receptors - receptors involved in the recognition and uptake of anionic macromolecules [152] - mediated the uptake of oligonucleotide-functionalized gold nanoparticles. It was further discussed that oligonucleotides mimic the complex structure of Poly I, a wellknown binding ligand for scavenger receptors, resulting in internalization. Recently Mirkin and co-workers showed that class A scavenger receptors as well as lipid-rafts were involved in the endocytosis mechanism of gold nanoparticle-DNA conjugates [153]. An additional question remaining to be answered is the mechanism of endosomal escape. In order for DNA-AuNP conjugates to deliver their cargo (e.g. antisense DNA) or interact with specific intracellular molecules (e.g. mRNA), they must escape endosomal compartmentalization. Mirkin and co-workers reported that the majority of DNA-AuNP conjugates were located in late endosomes. However, few particles could be found outside endosomes, in the cells' cytoplasm [154]. This was shown by transmission electron microscopy thin sectioning. Different pathways leading to endosomal escape have been reported. These include pore formation in the endosomal membrane, pH-buffering or fusion into the endosomal membrane [155]. Brust and coworkers discussed that peptide-coated AuNPs were capable of disrupting the endosomal membrane, resulting in endosomal escape [156]. However, for the case of AuNP-DNA conjugates no conclusive explanation for the endosomal escape mechanism has been reported to date.

2.5.1 DNA-AuNP conjugates for live cell mRNA detection.

The cell is one of the most complex biological environments containing a vast number of different biomolecules with multiple biological roles. Being able to detect these biomolecules with great selectivity is of high importance in order to understand biological processes, disease progression and to formulate and monitor specific treatments. Common sensing methods for the detection of biologically important molecules [157-161] are frequently based on platforms of nucleic acids due to their inherent property to selectively bind a complementary target [162-171]. However, downfalls of these methods are their inability of detecting targets within the cellular environment in real time or susceptibility to nuclease digestion [77]. Furthermore, in order to assist nucleic acid-based probes to enter cells, the use of co-carriers is required [172, 173]. These can exhibit significant cytotoxicity [174-176]. On account of the aforementioned problems with conventional detection systems, the urgent need for new types of stable and highly sensitive endocellular sensors has become apparent. In response to this requirement, scientists have developed a novel detection system based on fluorescent DNA attached to gold nanoparticles [1-5, 102, 177-179].

The general concept of fluorophore-tagged nucleic acid-gold nanoparticle conjugates as biological sensors relies on the quenching ability of gold nanoparticles. A fluorophore placed within a few nanometres of a metal nanoparticle exhibiting a strong plasmon field, experiences enhancement or quenching effects due to its interactions with the plasmonic field [180]. The degree of enhancing or quenching depends on many factors such as a) the emission wavelength of the fluorophore, b) the orientation of the fluorophore relative to the surface of the particle, c) the distance from the nanoparticle surface as well as d) the morphological characteristics of the particle (which define its plasmonic properties) [179-182]. Libchaber and co-workers were

among the first groups to extensively study the quenching efficiency of 1.4 nm gold nanoparticles with respect to different dyes (Rhodamine 6G, Fluorescein, Texas Red, Cy5) [178]. A stem-loop oligonucleotide anchored to the gold nanoparticle was functionalized with a fluorophore, which, due to the close proximity to the gold nanoparticle was completely quenched [180, 181]. Upon target binding, the loop would open and fluorescence would be restored due to the increase in the distance of the fluorophore from the gold nanoparticle. In their studies it was found that all dyes were quenched more efficiently than when DABCYL, a quencher often used in conventional molecular beacons, was used [178]. Maxwell et al. employed a similar strategy using 2.5 nm AuNPs [179]. Due to their excellent quenching abilities, small particles are often used for these purposes [179]. However, if a detection system, based on a similar model was to be adopted for *in vitro* applications, small gold nanoparticles may not be suitable because they have shown to exhibit significant cytotoxicity [183]. On the contrary, larger particles (up to 50 nm) have shown good cellular uptake and negligible cytotoxicity [184, 185]. Due to the ease of synthesis and low cytotoxicity, 13-15 nm AuNPs are most widely employed in cellular applications, but in some cases larger (up to 20 nm) AuNPs are used due to a higher oligonucleotide loading capability [150, 186, 187]. Based on this hypothesis, Mirkin and co-workers developed a sensor for mRNA detection in living cells [1], which was also used as a model system in studies carried out within this project (see chapter 5). Their so-called 'nano-flare' sensor consists of oligonucleotide-functionalized gold nanoparticles hybridised to a flare/reporter strand-a short oligonucleotide strand functionalised with a fluorophore.

Due to the quenching ability of the gold nanoparticle, detectable fluorescence from the reporter strand is negligible. Upon target binding, the reporter strand is released through competitive hybridisation and a fluorescence signal correlating directly with the relative amounts of target can be observed [1].

Following these initial results, the sensor was advanced further for simultaneous mRNA detection and regulation of protein expression [3, 4]. Li *et al.* adapted this approach and developed a multiplexed probe capable of detecting up to three different mRNA targets simultaneously [5]. These multiplexed probes were shown to be especially useful in the field of cancer diagnosis [4, 5].

Cancer related oligonucleotide sequences have been investigated especially in the context of nano-flare type probes as this technology is a promising candidate for cancer diagnosis and treatment [5, 101, 188, 189]. For example, Gu and co-workers developed a sensor for the detection of the STAT5B transcript, an important protein involved in tumour proliferation and metastasis [102]. Their approach, as opposed to the one proposed by Mirkin and co-workers, did not involve a separate reporter strand, but rather a 'two in one' system in which the fluorophore was attached to a hairpin oligonucleotide. Upon target binding the hairpin would open and a fluorescence signal could be observed.

Likewise, Tu et al. created a system for the detection of microRNA [190]. The potential advantage of this strategy is the localised signal, as the fluorophore is still anchored to the gold nanoparticle instead of being released into the cell's cytoplasm. In this way Gu et al. showed that when their sensors were incubated with MCF-7 human breast cancer and C6 mouse glioma cell lines, only the human STATB5 expressing MCF-7 cells showed a high fluorescent signal. The authors showed that their probe made it possible to visualize STAT5B gene expression in real time, which allowed rapid identification of tumour progression stages as well as evaluation of anti-cancer

treatment outcomes [102]. Similarly, Tang and co-workers developed probes to monitor different mRNA targets associated with tumour progression [5, 101].

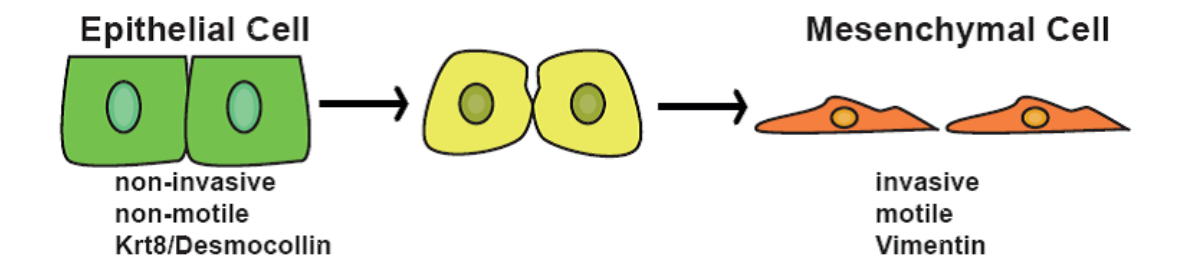
In this project the initial concept developed by Mirkin and co-workers was adapted for the detection of total mRNA as well as cell-type specific mRNAs Vimentin, Desmocollin or Cytokeratin 8 (see **section 3.3.1** for design of oligonucleotides. Also see **chapter 5** for the relevant results). Especially Vimentin and Desmocollin have shown to be markers of invasive epithelial cell-based lung cancer in conjunction with epithelial to mesenchymal transition (see **section 2.5.1.1**).

2.5.1.1 Epithelial to mesenchymal transition.

Epithelial cells are uniformly-shaped, non-motile, stationary cells, often forming sheets (epithelia) [191]. Mesenchymal cells, on the other hand, display no uniform shape, nor tight adhesion with other cells. They are highly motile and move individually [191].

The biological process of epithelial to mesenchymal transition (EMT) occurs naturally during embryonic development, wound healing and tissue regeneration [192]. However, it has also been found to play a major role in fibrosis and cancer progression [193]. To account for differences in EMT, it has been classed into three separate types [194]. Types 1 and 2 are involved in natural processes such as wound healing and generally results in cells either undergoing mesenchymal to epithelial transition (MET) upon completion of their task, or apoptosis [192]. However, type 3 EMT describes invasive cells involved in cancer metastasis. In this process cancerous epithelial cells migrate away from the primary tumour site to form a secondary tumour in a different location. During EMT, epithelial cells undergo several biochemical changes, which allow them to adopt mesenchymal characteristics [194]. These include increased

motility, enhanced elasticity, invasive behaviour, enhanced production of extracellular matrix components and increased resistance towards apoptosis [195] see **scheme 2.11**.



Scheme 2.11 Illustration of the process of epithelial to mesenchymal transition.

Once EMT is completed, formerly stationary epithelial cells are capable of migrating away from the original epithelial layer. The biochemical changes have been found to be dependent on the up- or downregulation of certain proteins. A protein strongly up-regulated is the intermediate filament protein and mesenchymal cell marker Vimentin [196-199].

On the other hand epithelial cell markers such as desmocollin and cytokeratin 8 are strongly down-regulated [191]. Therefore these three biomarkers were chosen as targets. Human bronchial epithelial cells (16HBE) and fetal lung fibroblasts (MRC-5) were used as model epithelial and mesenchymal cells (see **chapter 5**).

As demonstrated in **section 5.2**, cell specific mRNA detection with high fluorescence signal in both cell types tested was made possible using the nano-probes.

2.5.2 DNA-AuNP conjugates for targeted drug delivery.

Due to their excellent biostability, biocompatibility and cellular uptake, gold nanoparticle-DNA conjugates have resulted in applications for targeted drug delivery [200-208]. Dhar *et al.* showed that platinum (IV)-based drugs could be delivered

efficiently to cancer cells by using DNA-AuNPs as carriers [200]. They reported that in several cases the activity and cytotoxicity of the delivered drugs exceeded those of cisplatin, suggesting a more efficient drug delivery. In another study, Zhang and coworkers constructed Paclitaxel-DNA-AuNPs as a strategy to deliver hydrophobic drugs and overcoming drug efflux [201]. On the other hand, Xiao and co-workers showed that the FDA-approved chemotherapeutic drug doxoroubicin (see **Figure 2.3**) can be loaded into double-stranded DNA-gold nanorod (AuNR) conjugates [202]. Drug-release could be tightly controlled *via* DNA melting by irradiation with near-infrared (NIR) light, making use of the photon to thermal response of AuNRs [209-211].

Figure 2.3 Chemical structure of doxorubicin.

In 2010 Kim *et al.* proposed a multi-functional DNA-AuNP conjugate for combined computed tomography imaging and therapy of prostate cancer [206]. Here a prostate-specific membrane antigen (PSMA) RNA aptamer conjugated to a gold nanoparticle was used to target prostate cancer cells. Additional incorporation of doxorubicin resulted in a multi-functional probe. The use of PSMA aptamers for the targeted delivery of doxorubicin had previously been demonstrated by Bagalkot and co-

workers [212, 213]. Using the AS1411 aptamer immobilized on a gold nanoparticle, Latorre and co-workers were able to deliver doxorubicin or AZD8055 to breast cancer and uveal melanoma cells [207].

Recently Tang *et al.* demonstrated the capability of molecular beacon-AuNP conjugates as multiplexed live cell mRNA detection and combined targeted drug delivery probes [189]. Their system was based on the use of hairpin oligonucleotide-AuNP conjugates, as previously discussed in **section 2.5.1**.

Several studies by Alexander and co-workers reported on the use of DNA-AuNP conjugates for the delivery of the anti-cancer drugs doxorubicin and actinomycin [203-205]. They recently showed that by combining conjugation of folic acid and a thermoresponsive polymer, targeted and controlled drug delivery to neuroblastoma cells was possible [205].

In this project nano-probes for the detection of Vimentin mRNA (see **section 2.5.1**) were designed to selectively deliver doxorubicin to Vimentin-expressing cells. The relevant results are discussed in **chapter 5.**

2.5.3 Gold nanoparticle assemblies for intracellular applications

Nanoparticle assemblies present potent candidates for applications in biomedicine. However, detailed studies investigating the interactions of such assemblies with cells are limited. For example Xu *et al.* demonstrated the DNA-mediated assembly of gold nanoparticle – gold nanorod satellite structures [214]. They showed that by combining properties of AuNRs and AuNPs in one probe, effective *in situ* Raman spectroscopy in live cells was possible. Moreover, Chan and co-workers recently demonstrated that complex AuNP satellite structures, assembled by DNA hybridisation, were taken up by cells [78]. Chou *et al.* further found that after being uptaken by macrophages,

assemblies were slowly degraded. However, in order to use nanoparticle assemblies for biomedical applications such as biosensing, it is important that assemblies do not dissociate when exposed to conditions met within a biological environment.

The formation of robust assemblies for potential biomedical applications is discussed in **chapter 6**. Concepts for assembly formation are discussed in the following section (**section 2.6**).

2.6 Programmed assembly of DNA-nanomaterial conjugates.

The ability to assemble nanomaterials into pre-defined 2 and 3D structures has enabled the fabrication of novel nanomaterials with distinct properties. These unique properties result from the precise organization of individual nanomaterial building blocks within the assembled structure [215]. Such assembled nanostructures have found potential applications in fields ranging from biotechnology [78] and biomedicine [78, 214] to catalysis [216] and materials science [217]. As a result, great efforts have been made to design novel strategies to control and program the organization of nanomaterials. Resulting procedures are either based on top-down or the bottom-up approaches. Top-down methods involve the fabrication of micro-or nano-sized materials from a bulk material. This process often utilizes lithographic techniques. Using this method allows the formation of assemblies with high degrees of precision. However, at present, top-down methods have not yet reached a level that allows the fabrications of materials with molecular or atomic precision [218].

Contrastingly, bottom-up methods start from the nano-sized building blocks and employ molecular chemistry/biology techniques to create hierarchically ordered nanostructures [219]. Nature has many examples of such perfectly ordered, naturally occurring (nano-) structures. For example the complex 3D structure of proteins,

assembled from various subunits or the helical arrangement of DNA into duplexes and triplexes. Therefore it was not surprising when first reports emerged (in the late 20th century) utilizing biomolecules for the programmed organization of nanoparticles [71]. In particular, the use of DNA as a scaffold for the evolution of inorganic nanoparticles into complex functional materials has been explored extensively [128, 220-222]. Thus Mirkin and co-workers recently introduced the term 'programmable atom equivalents' (PAE) [215]. These PAEs are building blocks made up of DNA-nanoparticle conjugates. It has been demonstrated that PAEs can be built into highly order structures by means of DNA hybridisation. Types of inorganic nanoparticles that have evolved as PAEs include Gold, Silver and Palladium as well as oxides like Fe_xO_y, SiO₂ or TiO₂ and semi-conductor nanoparticles such as CdSe, CdS and PbS [215]. Macfarlane et al. suggested that these PAEs could be used to create a 'new periodic table'. Assemblies would hence be equivalents of molecules, held together by oligonucleotides that act as the 'molecular glue' [215]. Accordingly many research groups have demonstrated that nanoparticle dimers, trimers or even pyramids can be assembled by DNA hybridisation [47, 64, 78, 112, 117, 223-228]. Due to their distinct optical properties, many studies have focussed on the assembly of plasmonic nanoparticles - in particular gold nanoparticles. Resulting structures have shown interesting properties such as the creation of 'hot spots' in a dimer of plasmonic nanoparticles. For example, these can be employed as enhancers for surface enhanced Raman scattering (SERS). Other applications of plasmonic nanoparticle dimers or trimers include their employments as molecular rulers, biosensors or optical metamaterials [134, 229]. Most of these studies were centred on homogeneous systems utilizing only one type of nanomaterial. Recently more diverse studies on the fabrication of heterogeneous nanoassemblies have emerged. These assemblies display interesting novel properties arising from the

combined properties of the different nanomaterials employed. For example, Maye *et al.* fabricated CdSe/ZnS quantum dot-AuNP heterodimers using DNA hybridisation [230]. These dimers resulted in a significant enhancement of the QD fluorescence arising from interactions with the gold nanoparticle. Similarly Alivisatos and co-workers demonstrated the assembly of Au-Ag heterodimers in order to study arising bonding and antibonding plasmon modes. These occurred due to a break in symmetry in the heterodimeric structure [231]. Recently research groups of Mirkin and Gang advanced the field even further. Using different PAEs, both groups demonstrated that DNA can be used to create nanoparticle superlattices [109, 138, 232]. Depending on the types of PAEs and DNA linker length used, more than 100 different crystal lattices were produced [109].

In this project both homo- and heterogeneous assemblies (Au-Au, Fe₃O₄- Fe₃O₄, Au-Cu_{2-x}Se, Au-Fe₃O₄ and GO-Au) were formed so as to create advanced nanostructures for potential biomedical applications. The combined properties of two or more different nanomaterials within one probe could result in highly advanced, multirole biomedical probes. For example, Liu *et al.* showed that heterodimers of Cu_{2-x}Se and gold, formed by direct growth, could pose potent contrast agents for deep tissue imaging [233]. Zhu *et al.* demonstrated the synthesis by direct growth of heterodimers composed of an optical (Au) and a magnetic (Fe₃O₄) nanomaterial [234]. They furthermore elucidated their great potential for *in vivo* computed tomography and magnetic resonance dual model imaging.

In this project a novel, universally applicable approach was employed to create highly stable assemblies. The method used was based on DNA-click chemistry (see section 2.6.1).

2.6.1 Click chemistry.

In recent years, copper(I)-catalyzed click chemistry (CuAAC) has become an established method for the facile, fast and versatile linking of molecules, without the need for specific reaction conditions [235] Given its simplicity, CuAAC has been employed in many research areas such as DNA (nano-) technology [236-238] and nanoparticle ligand modifications [239, 240]. Unfortunately, one of the downfalls of this method is the requirement of a copper (I) complex to catalyse the click reaction by bringing together the reactants at an intermediate structure [235, 241]. This process is often not straightforward; especially in aqueous solutions where copper (I) can be converted into an inactive copper (II) complex. Additionally, the cytotoxicity of copper becomes an issue when developing biocompatible protocols [242]. Copper-free click chemistry is a tool employed very widely nowadays in many areas of chemistry, but especially in DNA chemistry [96, 243]. Similar to the CuAAC, this reaction relies on an azide-alkyne Huisgen cycloaddition which results in a highly stable triazole moiety. Whilst the Cu-catalysed variant can be carried out with a wide variety of alkenes, the Cu-free version requires alkynes set in a highly strained environment. Due to the lack of a catalyst in the Cu-free version, a different driving force is required; in this case it is strain. Introducing the alkyne as a highly strained and hence a highly reactive cyclooctyne enables the alkyne-azide [3+2] cycloaddition reaction [96, 244] to proceed without a metal catalyst (see scheme 2.12).

The results presented in **chapter 6** show that copper-free click chemistry is an excellent new tool for the programmed ligation of DNA-nanomaterials.

Scheme 2.12 Mechanism of the ring-strain promoted, copper-free azide-alkyne cycloaddition. Adapted from ref. [244].

2.7 References

- 1. Seferos, D.S., et al., *Nano-flares: Probes for transfection and mRNA detection in living cells.* J Am Chem Soc, 2007. **129**(50): p. 15477-15479.
- Zheng, D., et al., Aptamer Nano-flares for Molecular Detection in Living Cells.
 Nano Letters, 2009. 9(9): p. 3258-3261.
- 3. Prigodich, A.E., et al., *Nano-flares for mRNA Regulation and Detection*. ACS Nano, 2009. **3**(8): p. 2147-2152.
- 4. Prigodich, A.E., et al., *Multiplexed nanoflares: mRNA detection in live cells*.

 Anal Chem, 2012. **84**(4): p. 2062-6.
- 5. Li, N., et al., A Multicolor Nanoprobe for Detection and Imaging of Tumor-Related mRNAs in Living Cells. Angewandte Chemie-International Edition, 2012. **51**(30): p. 7426-7430.
- 6. Heuer-Jungemann, A., et al., Gold nanoparticles and fluorescently-labelled DNA as a platform for biological sensing. Nanoscale, 2013. **5**(20): p. 9503-9510.
- 7. Mulvaney, P., Surface Plasmon Spectroscopy of Nanosized Metal Particles.

 Langmuir, 1996. 12(3): p. 788-800.

- 8. Kelly, K.L., et al., *The Optical Properties of Metal Nanoparticles: The Influence of Size, Shape, and Dielectric Environment.* The Journal of Physical Chemistry B, 2002. **107**(3): p. 668-677.
- Liz-Marzan, L.M., Nanometals formation and color. Materials Today, 2004.
 7(2): p. 26-31.
- Faraday, M., The Bakerian Lecture: Experimental Relations of Gold (and Other Metals) to Light. Philosophical Transactions of the Royal Society of London, 1857. 147: p. 145-181.
- 11. Turkevich, J., P.C. Stevenson, and J. Hillier, *A study of the nucleation and growth processes in the synthesis of colloidal gold.* Discussions of the Faraday Society, 1951. **11**(0): p. 55-75.
- 12. Turkevich, J., P.C. Stevenson, and J. Hillier, *The Formation of Colloidal Gold*. The Journal of Physical Chemistry, 1953. **57**(7): p. 670-673.
- 13. Frens, G., Controlled Nucleation for Regulation of Particle-Size in Monodisperse Gold Suspensions. Nature-Physical Science, 1973. **241**(105): p. 20-22.
- 14. Enustun, B.V. and J. Turkevich, *Coagulation of Colloidal Gold*. Journal of the American Chemical Society, 1963. **85**(21): p. 3317-3328.
- 15. Turkevich, J., *Colloidal gold. Part I.* Gold Bulletin, 1985. **18**(3): p. 86-91.
- 16. Turkevich, J., *Colloidal gold. Part II.* Gold Bulletin, 1985. **18**(4): p. 125-131.
- 17. Kimling, J., et al., *Turkevich Method for Gold Nanoparticle Synthesis Revisited*.The Journal of Physical Chemistry B, 2006. 110(32): p. 15700-15707.
- 18. Bastus, N.G., J. Comenge, and V. Puntes, *Kinetically Controlled Seeded Growth Synthesis of Citrate-Stabilized Gold Nanoparticles of up to 200 nm: Size Focusing versus Ostwald Ripening*. Langmuir, 2011. **27**(17): p. 11098-11105.

- 19. Ji, X., et al., Size Control of Gold Nanocrystals in Citrate Reduction: The Third Role of Citrate. Journal of the American Chemical Society, 2007. **129**(45): p. 13939-13948.
- 20. Wu, H., et al., Shape evolution of citrate capped gold nanoparticles in seeding approach. Colloids and Surfaces A: Physicochemical and Engineering Aspects, 2012. **415**(0): p. 174-179.
- 21. Schulz, F., et al., Little Adjustments Significantly Improve the Turkevich Synthesis of Gold Nanoparticles. Langmuir, 2014. **30**(35): p. 10779-10784.
- 22. Xia, H., et al., Synthesis of Monodisperse Quasi-Spherical Gold Nanoparticles in Water via Silver(I)-Assisted Citrate Reduction. Langmuir, 2009. **26**(5): p. 3585-3589.
- 23. Privman, V., et al., *Mechanism of formation of monodispersed colloids by aggregation of nanosize precursors*. Journal of Colloid and Interface Science, 1999. **213**(1): p. 36-45.
- 24. Wiig, E.O., Carbon Dioxide Cleavage from Acetone Dicarboxylic Acid. The Journal of Physical Chemistry, 1927. **32**(7): p. 961-981.
- 25. Li, G., et al., Spherical and Planar Gold(0) Nanoparticles with a Rigid Gold(I)-Anion or a Fluid Gold(0)-Acetone Surface†. Langmuir, 2003. **19**(16): p. 6483-6491.
- 26. Silberberg, M., *Principles of General Chemistry*. 2009: McGraw-Hill Companies, Incorporated.
- 27. Mariscal, M.M., J.J. Velazquez-Salazar, and M.J. Yacaman, *Growth mechanism of nanoparticles: theoretical calculations and experimental results*.

 CrystEngComm, 2012. **14**(2): p. 544-549.

- 28. Jörg, P., et al., New insights of the nucleation and growth process of gold nanoparticles via in situ coupling of SAXS and XANES. Journal of Physics: Conference Series, 2010. **247**(1): p. 012051.
- 29. Zhou, Y., et al., Quantitative nucleation and growth kinetics of gold nanoparticles via model-assisted dynamic spectroscopic approach. Journal of Colloid and Interface Science, 2013. **407**(0): p. 8-16.
- 30. Polte, J., et al., Mechanism of Gold Nanoparticle Formation in the Classical Citrate Synthesis Method Derived from Coupled In Situ XANES and SAXS Evaluation. Journal of the American Chemical Society, 2010. **132**(4): p. 1296-1301.
- 31. Brust, M., et al., *SYNTHESIS OF THIOL-DERIVATIZED GOLD NANOPARTICLES IN A 2-PHASE LIQUID-LIQUID SYSTEM*. Journal of the Chemical Society-Chemical Communications, 1994(7): p. 801-802.
- 32. Hostetler, M.J., et al., Alkanethiolate gold cluster molecules with core diameters from 1.5 to 5.2 nm: Core and monolayer properties as a function of core size. Langmuir, 1998. **14**(1): p. 17-30.
- 33. Changsheng, S., et al., Size-controlled synthesis of monodispersed gold nanoparticles stabilized by polyelectrolyte-functionalized ionic liquid.

 Nanotechnology, 2008. 19(28): p. 285601.
- 34. Young, J.K., et al., Size-controlled synthesis of monodispersed gold nanoparticles via carbon monoxide gas reduction. Nanoscale Research Letters, 2011. 6.
- 35. Sivaraman, S.K., S. Kumar, and V. Santhanam, *Monodisperse sub-10 nm gold* nanoparticles by reversing the order of addition in Turkevich method The role

- of chloroauric acid. Journal of Colloid and Interface Science, 2011. **361**(2): p. 543-547.
- 36. Sivaraman, S., S. Kumar, and V. Santhanam, *Room-temperature synthesis of gold nanoparticles Size-control by slow addition*. Gold Bulletin, 2010. **43**(4): p. 275-286.
- 37. Alsawafta, M., et al., The effect of hydrogen nanobubbles on the morphology of gold-gelatin bionanocomposite films and their optical properties.

 Nanotechnology, 2012. 23(6).
- 38. Deraedt, C., et al., Sodium Borohydride Stabilizes Very Active Gold Nanoparticle Catalyst. Chemical Communications, 2014.
- 39. Polte, J., et al., New insights of the nucleation and growth process of gold nanoparticles via in situ coupling of SAXS and XANES. Xiv International Conference on Small-Angle Scattering (Sas09), 2010. **247**.
- 40. Zhang, T., et al., A new strategy improves assembly efficiency of DNA monomodified gold nanoparticles. Chemical Communications, 2011. **47**(20): p. 5774-5776.
- 41. Mohr, F. and H. Schmidbaur, *Gold Chemistry: Applications and Future Directions in the Life Sciences*. 2009: John Wiley & Sons.
- 42. Rurack, K. and R. Martinez-Manez, *The Supramolecular Chemistry of Organic-Inorganic Hybrid Materials*. 2010: Wiley.
- 43. Wang, A., et al., *Gold Nanoparticles: Synthesis, Stability Test, and Application* for the Rice Growth. Journal of Nanomaterials, 2014. **2014**: p. 6.
- 44. Lin, J.-H. and W.-L. Tseng, *Ultrasensitive detection of target analyte-induced aggregation of gold nanoparticles using laser-induced nanoparticle Rayleigh scattering*. Talanta, 2015. **132**(0): p. 44-51.

- 45. Geddes, C.D., *Reviews in Plasmonics 2010*. 2011: Springer.
- 46. Schmid, G. and A. Lehnert, *The Complexation of Gold Colloids*. Angewandte Chemie-International Edition in English, 1989. **28**(6): p. 780-781.
- 47. Loweth, C.J., et al., *DNA-based assembly of gold nanocrystals*. Angewandte Chemie-International Edition, 1999. **38**(12): p. 1808-1812.
- 48. Hakkinen, H., *The gold-sulfur interface at the nanoscale*. Nat Chem, 2012. **4**(6): p. 443-455.
- 49. Pakiari, A.H. and Z. Jamshidi, *Nature and Strength of M-S Bonds (M = Au, Ag, and Cu) in Binary Alloy Gold Clusters*. The Journal of Physical Chemistry A, 2010. **114**(34): p. 9212-9221.
- 50. Murphy, C.J., et al., *Chemical sensing and imaging with metallic nanorods*. Chemical Communications, 2008(5): p. 544-557.
- 51. Daniel, M.-C. and D. Astruc, *Gold Nanoparticles: Assembly, Supramolecular Chemistry, Quantum-Size-Related Properties, and Applications toward Biology, Catalysis, and Nanotechnology.* Chemical Reviews, 2003. **104**(1): p. 293-346.
- 52. Sardar, R., et al., Gold Nanoparticles: Past, Present, and Future†. Langmuir, 2009. 25(24): p. 13840-13851.
- Jin, R., Quantum sized, thiolate-protected gold nanoclusters. Nanoscale, 2010.2(3): p. 343-362.
- 54. Won Ho, K., et al., Cationic Lipid-coated Gold Nanoparticles as Efficient and Non-cytotoxic Intracellular siRNA Delivery Vehicles. Pharmaceutical Research, 2012. **29**(2): p. 362-74.
- 55. Badia, A., et al., Gold-sulfur interactions in alkylthiol self-assembled monolayers formed on gold nanoparticles studied by solid-state NMR. Journal of the American Chemical Society, 1997. **119**(45): p. 11104-11105.

- 56. Kanaras, A.G., et al., *Thioalkylated tetraethylene glycol: a new ligand for water soluble monolayer protected gold clusters.* Chemical Communications, 2002(20): p. 2294-2295.
- 57. Oh, E., et al., Colloidal Stability of Gold Nanoparticles Coated with Multithiol-Poly(ethylene glycol) Ligands: Importance of Structural Constraints of the Sulfur Anchoring Groups. The Journal of Physical Chemistry C, 2013. 117(37): p. 18947-18956.
- 58. Cho, W.-S., et al., Size-dependent tissue kinetics of PEG-coated gold nanoparticles. Toxicology and Applied Pharmacology, 2010. **245**(1): p. 116-123.
- Manson, J., et al., Polyethylene glycol functionalized gold nanoparticles: the influence of capping density on stability in various media. Gold Bulletin, 2011.44(2): p. 99-105.
- 60. Larson, T.A., P.P. Joshi, and K. Sokolov, *Preventing Protein Adsorption and Macrophage Uptake of Gold Nanoparticles via a Hydrophobic Shield.* ACS Nano, 2012. **6**(10): p. 9182-9190.
- 61. Kawano, T., et al., 213. PEG-Modified Cationic Gold Nanoparticles and Their Abilities of In Vivo Gene Delivery. Mol Ther, 2005. 11(S1): p. S84-S84.
- 62. Das, S., Microbial Biodegradation and Bioremediation. 2014: Elsevier Science.
- 63. Bartczak, D. and A.G. Kanaras, *Preparation of Peptide-Functionalized Gold Nanoparticles Using One Pot EDC/Sulfo-NHS Coupling*. Langmuir, 2011. **27**(16): p. 10119-10123.
- 64. Coomber, D., et al., *Programmed assembly of peptide-functionalized gold nanoparticles on DNA templates.* Langmuir, 2010. **26**(17): p. 13760-2.

- 65. Tiwari, P.M., et al., Enhanced intracellular translocation and biodistribution of gold nanoparticles functionalized with a cell-penetrating peptide (VG-21) from vesicular stomatitis virus. Biomaterials, 2014. **35**(35): p. 9484-94.
- 66. Levy, R., et al., Rational and combinatorial design of peptide capping Ligands for gold nanoparticles. Journal of the American Chemical Society, 2004. **126**(32): p. 10076-10084.
- 67. Chandrawati, R. and M.M. Stevens, Controlled assembly of peptidefunctionalized gold nanoparticles for label-free detection of blood coagulation Factor XIII activity. Chemical Communications, 2014. **50**(41): p. 5431-5434.
- 68. Bartczak, D., et al., Manipulation of in Vitro Angiogenesis Using Peptide-Coated Gold Nanoparticles. Acs Nano, 2013. **7**(6): p. 5628-5636.
- 69. Kumar, A., et al., Gold nanoparticles functionalized with therapeutic and targeted peptides for cancer treatment. Biomaterials, 2012. **33**(4): p. 1180-1189.
- 70. Fernandes, R., et al., *Interactions of Skin with Gold Nanoparticles of Different Surface Charge, Shape, and Functionality*. Small, 2014: p. n/a-n/a.
- 71. Mirkin, C.A., et al., *A DNA-based method for rationally assembling nanoparticles into macroscopic materials*. Nature, 1996. **382**(6592): p. 607-609.
- 72. Alivisatos, A.P., et al., *Organization of 'nanocrystal molecules' using DNA*.

 Nature, 1996. **382**(6592): p. 609-611.
- 73. Zanchet, D., et al., *Electrophoretic isolation of discrete Au nanocrystal/DNA conjugates*. Nano Letters, 2001. **1**(1): p. 32-35.
- 74. Parak, W.J., et al., Conformation of oligonucleotides attached to gold nanocrystals probed by gel electrophoresis. Nano Letters, 2003. **3**(1): p. 33-36.
- 75. Parak, W.J., et al., *Biological applications of colloidal nanocrystals*.

 Nanotechnology, 2003. **14**(7): p. R15-R27.

- 76. Pellegrino, T., et al., *Gel electrophoresis of gold-DNA nanoconjugates*. Journal of Biomedicine and Biotechnology, 2007.
- 77. Giljohann, D.A., et al., *Gold nanoparticles for biology and medicine*. Angew Chem Int Ed Engl, 2010. **49**(19): p. 3280-94.
- 78. Chou, L.Y.T., K. Zagorovsky, and W.C.W. Chan, *DNA assembly of nanoparticle superstructures for controlled biological delivery and elimination*.

 Nature Nanotechnology, 2014. **9**(2): p. 148-155.
- 79. Link, S. and M.A. El-Sayed, Size and temperature dependence of the plasmon absorption of colloidal gold nanoparticles. Journal of Physical Chemistry B, 1999. **103**(21): p. 4212-4217.
- 80. Mie, G., Beiträge zur Optik trüber Medien, speziell Kolloidaler Metallösungen.
 Annalen der Physik, 1908. **25**(4): p. 377-445.
- 81. Kreibig, U.V., M., *Optical Properties of Metal Clusters*. Vol. 25. 1995: Springer: Berlin.
- 82. Ghosh, S.K. and T. Pal, *Interparticle coupling effect on the surface plasmon resonance of gold nanoparticles: From theory to applications.* Chemical Reviews, 2007. **107**(11): p. 4797-4862.
- 83. Jensen, T.R., et al., Nanosphere Lithography: Effect of the External Dielectric Medium on the Surface Plasmon Resonance Spectrum of a Periodic Array of Silver Nanoparticles. The Journal of Physical Chemistry B, 1999. **103**(45): p. 9846-9853.
- 84. Li, X., et al., Localized surface plasmon resonance (LSPR) of polyelectrolyte-functionalized gold-nanoparticles for bio-sensing. Colloids and Surfaces A: Physicochemical and Engineering Aspects, 2009. **332**(2–3): p. 172-179.

- 85. Bolduc, O.R. and J.-F. Masson, Advances in Surface Plasmon Resonance Sensing with Nanoparticles and Thin Films: Nanomaterials, Surface Chemistry, and Hybrid Plasmonic Techniques. Analytical Chemistry, 2011. **83**(21): p. 8057-8062.
- 86. Daisuke, T., et al., *High-sensitivity surface plasmon resonance sensors utilizing high-refractive-index silver nanoparticle sheets*. Japanese Journal of Applied Physics, 2014. **53**(1S): p. 01AF01.
- 87. Messersmith, R.E., G.J. Nusz, and S.M. Reed, *Using the Localized Surface Plasmon Resonance of Gold Nanoparticles To Monitor Lipid Membrane Assembly and Protein Binding.* The Journal of Physical Chemistry C, 2013. **117**(50): p. 26725-26733.
- 88. Da, P., et al., Surface Plasmon Resonance Enhanced Real-Time Photoelectrochemical Protein Sensing by Gold Nanoparticle-Decorated TiO2 Nanowires. Analytical Chemistry, 2014. **86**(13): p. 6633-6639.
- 89. Berg, J.M.T., J.L.; Streyer, L., *Biochemistry*. 7 ed. 2011: W.H. Freeman.
- 90. Watson, J.D. and F.H. Crick, *Molecular structure of nucleic acids; a structure* for deoxyribose nucleic acid. Nature, 1953. **171**(4356): p. 737-8.
- 91. Blackburn, G.M., *Nucleic Acids in Chemistry and Biology*. 2006, Cambridge: Royal Society of Chemistry.
- 92. Pon, R.T., N. Usman, and K.K. Ogilvie, *DERIVATIZATION OF CONTROLLED PORE GLASS-BEADS FOR SOLID-PHASE OLIGONUCLEOTIDE SYNTHESIS*.

 Biotechniques, 1988. **6**(8): p. 768-775.
- 93. Damha, M.J., P.A. Giannaris, and S.V. Zabarylo, *AN IMPROVED PROCEDURE FOR DERIVATIZATION OF CONTROLLED-PORE GLASS-*

- BEADS FOR SOLID-PHASE OLIGONUCLEOTIDE SYNTHESIS. Nucleic Acids Research, 1990. 18(13): p. 3813-3821.
- 94. Caruthers, M.H., Gene Synthesis Machines: DNA Chemistry and its Uses. Science, 1985. 230(4723): p. 281-285.
- 95. Hall, L.M., M. Gerowska, and T. Brown, A highly fluorescent DNA toolkit: synthesis and properties of oligonucleotides containing new Cy3, Cy5 and Cy3B monomers. Nucleic Acids Research, 2012. **40**(14).
- 96. Shelbourne, M., et al., Fast copper-free click DNA ligation by the ring-strain promoted alkyne-azide cycloaddition reaction. Chemical Communications, 2011. 47(22): p. 6257-6259.
- 97. Herdewijn, P., *Oligonucleotide Synthesis: Methods and Applications*. 2005: Humana Press.
- 98. Nitin, N., et al., Peptide-linked molecular beacons for efficient delivery and rapid mRNA detection in living cells. Nucleic Acids Research, 2004. **32**(6).
- 99. Rosi, N.L., et al., Oligonucleotide-modified gold nanoparticles for intracellular gene regulation. Science, 2006. **312**(5776): p. 1027-1030.
- 100. Chen, T., et al., *DNA Micelle Flares for Intracellular mRNA Imaging and Gene Therapy*. Angewandte Chemie-International Edition, 2013. **52**(7): p. 2012-2016.
- 101. Pan, W., et al., Multiplexed Detection and Imaging of Intracellular mRNAs

 Using a Four-Color Nanoprobe. Analytical Chemistry, 2013. **85**(21): p. 1058110588.
- 102. Xue, J.P., et al., Visual detection of STAT5B gene expression in living cell using the hairpin DNA modified gold nanoparticle beacon. Biosensors & Bioelectronics, 2013. **41**: p. 71-77.

- 103. Banga, R.J., et al., *Liposomal Spherical Nucleic Acids*. Journal of the American Chemical Society, 2014. **136**(28): p. 9866-9869.
- 104. Claridge, S.A., et al., Enzymatic ligation creates discrete multinanoparticle building blocks for self-assembly. J Am Chem Soc, 2008. **130**(29): p. 9598-9605.
- Nykypanchuk, D., et al., DNA-guided crystallization of colloidal nanoparticles.Nature, 2008. 451(7178): p. 549-52.
- 106. Park, S.Y., et al., *DNA-programmable nanoparticle crystallization*. Nature, 2008. **451**(7178): p. 553-6.
- 107. Gu, H., et al., *A proximity-based programmable DNA nanoscale assembly line*.

 Nature, 2010. **465**(7295): p. 202-5.
- 108. Kim, J.W., J.H. Kim, and R. Deaton, *DNA-linked nanoparticle building blocks* for programmable matter. Angew Chem Int Ed Engl, 2011. **50**(39): p. 9185-90.
- 109. Macfarlane, R.J., et al., *Nanoparticle superlattice engineering with DNA*. Science, 2011. **334**(6053): p. 204-8.
- 110. Tang, L.H., et al., DNA-Directed Self-Assembly of Graphene Oxide with Applications to Ultrasensitive Oligonucleotide Assay. Acs Nano, 2011. **5**(5): p. 3817-3822.
- 111. Premkumar, T. and K.E. Geckeler, *Graphene-DNA hybrid materials: Assembly, applications, and prospects.* Progress in Polymer Science, 2012. **37**(4): p. 515-529.
- 112. Heuer-Jungemann, A., et al., Copper-free click chemistry as an emerging tool for the programmed ligation of DNA-functionalised gold nanoparticles.

 Nanoscale, 2013. 5(16): p. 7209-7212.
- 113. Tan, S.J., Campolongo, M. J., Luo, D., Cheng, W., *Building plasmonic nanostructures with DNA*. Nature Nanotechnology, 2011. **6**: p. 268 276.

- 114. Deng, H., et al., Gold nanoparticles with asymmetric polymerase chain reaction for colorimetric detection of DNA sequence. Anal Chem, 2012. **84**(3): p. 1253-8.
- 115. Dineva, M.A., et al., Simultaneous visual detection of multiple viral amplicons by dipstick assay. J Clin Microbiol, 2005. **43**(8): p. 4015-21.
- 116. Perlette, J. and W.H. Tan, *Real-time monitoring of intracellular mRNA hybridization inside single living cells*. Anal Chem, 2001. **73**(22): p. 5544-5550.
- 117. Kuzyk, A., et al., *DNA-based self-assembly of chiral plasmonic nanostructures* with tailored optical response. Nature, 2012. **483**(7389): p. 311-4.
- 118. Yan, W.J., et al., Self-Assembly of Chiral Nanoparticle Pyramids with Strong R/S Optical Activity. J Am Chem Soc, 2012. **134**(36): p. 15114-15121.
- 119. Liu, J.F., et al., Metallization of Branched DNA Origami for Nanoelectronic Circuit Fabrication. ACS Nano, 2011. **5**(3): p. 2240-2247.
- 120. Huschka, R., et al., *Light-induced release of DNA from gold nanoparticles:* nanoshells and nanorods. J Am Chem Soc, 2011. **133**(31): p. 12247-55.
- 121. Demers, L.M., et al., A fluorescence-based method for determining the surface coverage and hybridization efficiency of thiol-capped oligonucleotides bound to gold thin films and nanoparticles. Analytical Chemistry, 2000. **72**(22): p. 5535-5541.
- 122. Kanaras, A.G., et al., *Towards multistep nanostructure synthesis: Programmed enzymatic self-assembly of DNA/gold systems*. Angewandte Chemie-International Edition, 2003. **42**(2): p. 191-194.
- 123. Hill, H.D., et al., *The role radius of curvature plays in thiolated oligonucleotide loading on gold nanoparticles.* ACS Nano, 2009. **3**(2): p. 418-24.

- 124. Hurst, S.J., A.K.R. Lytton-Jean, and C.A. Mirkin, *Maximizing DNA loading on a range of gold nanoparticle sizes*. Analytical Chemistry, 2006. **78**(24): p. 8313-8318.
- 125. Zhang, X., M.R. Servos, and J. Liu, *Instantaneous and Quantitative Functionalization of Gold Nanoparticles with Thiolated DNA Using a pH-Assisted and Surfactant-Free Route*. Journal of the American Chemical Society, 2012. **134**(17): p. 7266-7269.
- 126. Massich, M.D., et al., Regulating Immune Response Using Polyvalent Nucleic Acid-Gold Nanoparticle Conjugates. Molecular Pharmaceutics, 2009. **6**(6): p. 1934-1940.
- 127. Hao, L., et al., Nucleic acid-gold nanoparticle conjugates as mimics of microRNA. Small, 2011. **7**(22): p. 3158-62.
- 128. Cutler, J.I., E. Auyeung, and C.A. Mirkin, *Spherical nucleic acids*. J Am Chem Soc, 2012. **134**(3): p. 1376-91.
- 129. Claridge, S.A., et al., *Isolation of discrete nanoparticle DNA conjugates for plasmonic applications*. Nano Letters, 2008. **8**(4): p. 1202-1206.
- 130. Qin, W.J. and L.Y.L. Yung, Nanoparticle-DNA conjugates bearing a specific number of short DNA strands by enzymatic manipulation of nanoparticle-bound DNA. Langmuir, 2005. **21**(24): p. 11330-11334.
- 131. Kim, J.W., J.H. Kim, and R. Deaton, *DNA-Linked Nanoparticle Building Blocks for Programmable Matter*. Angewandte Chemie-International Edition, 2011.
 50(39): p. 9185-9190.
- 132. Wen, Y., et al., Stable Gold Nanoparticle Conjugation to Internal DNA Positions: Facile Generation of Discrete Gold Nanoparticle—DNA Assemblies.

 Bioconjugate Chemistry, 2010. **21**(8): p. 1413-1416.

- 133. Yan, W.J., et al., Self-Assembly of Chiral Nanoparticle Pyramids with Strong R/S Optical Activity. Journal of the American Chemical Society, 2012. **134**(36): p. 15114-15121.
- 134. Busson, M.P., et al., Optical and Topological Characterization of Gold Nanoparticle Dimers Linked by a Single DNA Double Strand. Nano Letters, 2011. 11(11): p. 5060-5065.
- Mitchell, G.P., C.A. Mirkin, and R.L. Letsinger, *Programmed Assembly of DNA Functionalized Quantum Dots*. Journal of the American Chemical Society, 1999.
 121(35): p. 8122-8123.
- 136. Zhang, C., et al., A general approach to DNA-programmable atom equivalents.

 Nat Mater, 2013. **12**(8): p. 741-746.
- 137. Cutler, J.I., et al., *Polyvalent Oligonucleotide Iron Oxide Nanoparticle "Click"*Conjugates. Nano Letters, 2010. **10**(4): p. 1477-1480.
- 138. Sun, D. and O. Gang, *Binary Heterogeneous Superlattices Assembled from Quantum Dots and Gold Nanoparticles with DNA*. Journal of the American Chemical Society, 2011. **133**(14): p. 5252-5254.
- 139. Su, X., et al., Mild Two-Step Method to Construct DNA-Conjugated Silicon Nanoparticles: Scaffolds for the Detection of MicroRNA-21. Bioconjugate Chemistry, 2014.
- Zhang, X., M.R. Servos, and J.W. Liu, Fast pH-assisted functionalization of silver nanoparticles with monothiolated DNA. Chemical Communications, 2012.
 48(81): p. 10114-10116.
- 141. Li, L.-L., et al., An Exceptionally Simple Strategy for DNA-Functionalized Up-Conversion Nanoparticles as Biocompatible Agents for Nanoassembly, DNA

- Delivery, and Imaging. Journal of the American Chemical Society, 2013. **135**(7): p. 2411-2414.
- 142. Sitharaman, B., Nanobiomaterials Handbook. 2011: Taylor & Francis.
- 143. Parak, W.J., et al., Conjugation of DNA to silanized colloidal semiconductor nanocrystalline quantum dots. Chemistry of Materials, 2002. **14**(5): p. 2113-2119.
- 144. Lin, C.-A.J., et al., *Design of an Amphiphilic Polymer for Nanoparticle Coating and Functionalization*. Small, 2008. **4**(3): p. 334-341.
- 145. Quarta, A., et al., Polymer coated inorganic nanoparticles: tailoring the nanocrystal surface for designing nanoprobes with biological implications.

 Nanoscale, 2012. 4(11): p. 3319-3334.
- 146. Wu, W., Q.G. He, and C.Z. Jiang, *Magnetic Iron Oxide Nanoparticles:*Synthesis and Surface Functionalization Strategies. Nanoscale Research Letters,
 2008. **3**(11): p. 397-415.
- 147. Wang, Z.H., et al., *Polyvalent DNA-graphene nanosheets "click" conjugates*. Nanoscale, 2012. **4**(2): p. 394-399.
- 148. Hermanson, G.T., Bioconjugate Techniques. 2010: Elsevier Science.
- 149. Liu, F., J.Y. Choi, and T.S. Seo, *Graphene oxide arrays for detecting specific DNA hybridization by fluorescence resonance energy transfer.* Biosensors & Bioelectronics, 2010. **25**(10): p. 2361-2365.
- 150. Giljohann, D.A., et al., Oligonucleotide loading determines cellular uptake of DNA-modified gold nanoparticles. Nano Letters, 2007. **7**(12): p. 3818-3821.
- Patel, P.C., et al., Scavenger Receptors Mediate Cellular Uptake of Polyvalent
 Oligonucleotide-Functionalized Gold Nanoparticles. Bioconjug Chem, 2010.
 21(12): p. 2250-2256.

- 152. Greaves, D.R. and S. Gordon, *Recent insights into the biology of macrophage scavenger receptors*. Journal of Lipid Research, 2005. **46**(1): p. 11-20.
- 153. Choi, C.H.J., et al., *Mechanism for the endocytosis of spherical nucleic acid nanoparticle conjugates*. Proceedings of the National Academy of Sciences, 2013. **110**(19): p. 7625-7630.
- 154. Wu, X.C.A., et al., *Intracellular Fate of Spherical Nucleic Acid Nanoparticle Conjugates*. Journal of the American Chemical Society, 2014. **136**(21): p. 7726-7733.
- 155. Varkouhi, A.K., et al., *Endosomal escape pathways for delivery of biologicals*.

 Journal of Controlled Release, 2011. **151**(3): p. 220-228.
- 156. Nativo, P., I.A. Prior, and M. Brust, *Uptake and intracellular fate of surface-modified gold nanoparticles*. Acs Nano, 2008. **2**(8): p. 1639-1644.
- 157. Cole, S.P.C., et al., Overexpression of a Transporter Gene in a Multidrug-Resistant Human Lung-Cancer Cell-Line. Science, 1992. **258**(5088): p. 1650-1654.
- 158. Lu, J., et al., *MicroRNA expression profiles classify human cancers*. Nature, 2005. **435**(7043): p. 834-838.
- 159. Calin, G.A. and C.M. Croce, *MicroRNA signatures in human cancers*. Nature Reviews Cancer, 2006. **6**(11): p. 857-866.
- 160. Esquela-Kerscher, A. and F.J. Slack, *Oncomirs microRNAs with a role in cancer*. Nature Reviews Cancer, 2006. **6**(4): p. 259-269.
- 161. Ottem, E.N., et al., Differential expression and regulation of brain-derived neurotrophic factor (BDNF) mRNA isoforms in androgen-sensitive motoneurons of the rat lumbar spinal cord. Molecular and Cellular Endocrinology, 2010.

 328(1-2): p. 40-46.

- 162. Nolan, T., R.E. Hands, and S.A. Bustin, *Quantification of mRNA using real-time RT-PCR*. Nature Protocols, 2006. **1**(3): p. 1559-1582.
- 163. VanGuilder, H.D., K.E. Vrana, and W.M. Freeman, *Twenty-five years of quantitative PCR for gene expression analysis*. Biotechniques, 2008. **44**(5): p. 619-626.
- 164. Bustin, S.A., Absolute quantification of mRNA using real-time reverse transcription polymerase chain reaction assays. Journal of Molecular Endocrinology, 2000. **25**(2): p. 169-193.
- 165. Gibson, U.E.M., C.A. Heid, and P.M. Williams, *A novel method for real time quantitative RT PCR*. Genome Research, 1996. **6**(10): p. 995-1001.
- 166. Wong, M.L. and J.F. Medrano, *Real-time PCR for mRNA quantitation*. Biotechniques, 2005. **39**(1): p. 75-85.
- 167. Brown, P.O. and D. Botstein, *Exploring the new world of the genome with DNA microarrays*. Nature Genetics, 1999. **21**: p. 33-37.
- 168. Chen, J.J., Key aspects of analyzing microarray gene-expression data.

 Pharmacogenomics, 2007. **8**(5): p. 473-482.
- 169. Kane, M.D., et al., Assessment of the sensitivity and specificity of oligonucleotide (50mer) microarrays. Nucleic Acids Research, 2000. **28**(22): p. 4552-4557.
- 170. Bassell, G.J., et al., Single Messenger-Rnas Visualized by Ultrastructural in-Situ Hybridization Are Principally Localized at Actin Filament Intersections in Fibroblasts. Journal of Cell Biology, 1994. **126**(4): p. 863-876.
- Bishop, J.M., *The Molecular-Genetics of Cancer*. Science, 1987. **235**(4786): p. 305-311.

- 172. Boussif, O., et al., A Versatile Vector for Gene and Oligonucleotide Transfer into Cells in Culture and in-Vivo Polyethylenimine. Proceedings of the National Academy of Sciences of the United States of America, 1995. **92**(16): p. 7297-7301.
- 173. Haensler, J. and F.C. Szoka, *Polyamidoamine Cascade Polymers Mediate Efficient Transfection of Cells in Culture*. Bioconjug Chem, 1993. **4**(5): p. 372-379.
- 174. Filion, M.C. and N.C. Phillips, *Toxicity and immunomodulatory activity of liposomal vectors formulated with cationic lipids toward immune effector cells.*Biochimica Et Biophysica Acta-Biomembranes, 1997. **1329**(2): p. 345-356.
- 175. Lv, H.T., et al., *Toxicity of cationic lipids and cationic polymers in gene delivery*.

 Journal of Controlled Release, 2006. **114**(1): p. 100-109.
- 176. Soenen, S.J.H., A.R. Brisson, and M. De Cuyper, *Addressing the problem of cationic lipid-mediated toxicity: The magnetoliposome model*. Biomaterials, 2009. **30**(22): p. 3691-3701.
- 177. Chung, C.H., et al., Nuclease-resistant DNA aptamer on gold nanoparticles for the simultaneous detection of Pb2+ and Hg2+ in human serum. Biosensors & Bioelectronics, 2013. **41**: p. 827-832.
- 178. Dubertret, B., M. Calame, and A.J. Libchaber, *Single-mismatch detection using gold-quenched fluorescent oligonucleotides*. Nat Biotechnol, 2001. **19**(4): p. 365-370.
- 179. Maxwell, D.J., J.R. Taylor, and S.M. Nie, *Self-assembled nanoparticle probes* for recognition and detection of biomolecules. J Am Chem Soc, 2002. **124**(32): p. 9606-9612.

- 180. Kang, K.A., et al., Fluorescence Manipulation by Gold Nanoparticles: From Complete Quenching to Extensive Enhancement. Journal of Nanobiotechnology, 2011. 9(1): p. 16.
- 181. Dulkeith, E., et al., Fluorescence Quenching of Dye Molecules near Gold Nanoparticles: Radiative and Nonradiative Effects. Physical Review Letters, 2002. **89**(20): p. 203002.
- 182. Dulkeith, E., et al., Gold nanoparticles quench fluorescence by phase induced radiative rate suppression. Nano Letters, 2005. **5**(4): p. 585-589.
- 183. Pan, Y., et al., Size-Dependent Cytotoxicity of Gold Nanoparticles. Small, 2007.

 3(11): p. 1941-1949.
- 184. Chithrani, B.D., A.A. Ghazani, and W.C.W. Chan, *Determining the size and shape dependence of gold nanoparticle uptake into mammalian cells*. Nano Letters, 2006. **6**(4): p. 662-668.
- 185. Alkilany, A.M. and C.J. Murphy, *Toxicity and cellular uptake of gold nanoparticles: what we have learned so far?* Journal of Nanoparticle Research, 2010. **12**(7): p. 2313-2333.
- 186. Hill, H.D., et al., The Role Radius of Curvature Plays in Thiolated Oligonucleotide Loading on Gold Nanoparticles. ACS Nano, 2009. **3**(2): p. 418-424.
- 187. Cederquist, K.B. and C.D. Keating, *Curvature Effects in DNA:Au Nanoparticle Conjugates*. ACS Nano, 2009. **3**(2): p. 256-260.
- 188. Altieri, D.C., Survivin, versatile modulation of cell division and apoptosis in cancer. Oncogene, 2003. **22**(53): p. 8581-8589.
- 189. Li, N., et al., A tumour mRNA-triggered nanocarrier for multimodal cancer cell imaging and therapy. Chemical Communications, 2014. **50**(56): p. 7473-7476.

- 190. Tu, Y., et al., Fluorescence quenching of gold nanoparticles integrating with a conformation-switched hairpin oligonucleotide probe for microRNA detection.

 Chemical Communications, 2012. **48**(87): p. 10718-10720.
- 191. Lee, J.M., et al., *The epithelial–mesenchymal transition: new insights in signaling, development, and disease.* The Journal of Cell Biology, 2006. **172**(7): p. 973-981.
- 192. Kalluri, R., *EMT: When epithelial cells decide to become mesenchymal-like cells.*The Journal of Clinical Investigation, 2009. **119**(6): p. 1417-1419.
- 193. Lamouille, S., J. Xu, and R. Derynck, *Molecular mechanisms of epithelial—mesenchymal transition*. Nat Rev Mol Cell Biol, 2014. **15**(3): p. 178-196.
- 194. Kalluri, R. and R.A. Weinberg, *The basics of epithelial-mesenchymal transition*.

 The Journal of Clinical Investigation, 2009. **119**(6): p. 1420-1428.
- 195. Zeisberg, M. and E.G. Neilson, *Biomarkers for epithelial-mesenchymal transitions*. The Journal of Clinical Investigation, 2009. **119**(6): p. 1429-1437.
- 196. Katsumoto, T., A. Mitsushima, and T. Kurimura, *The role of the vimentin intermediate filaments in rat 3Y1 cells elucidated by immunoelectron microscopy and computer-graphic reconstruction*. Biology of the Cell, 1990. **68**(2): p. 139-146.
- 197. Ivaska, J., et al., *Novel functions of vimentin in cell adhesion, migration, and signaling*. Experimental Cell Research, 2007. **313**(10): p. 2050-2062.
- 198. Satelli, A. and S. Li, *Vimentin in cancer and its potential as a molecular target* for cancer therapy. Cellular and Molecular Life Sciences, 2011. **68**(18): p. 3033-3046.
- 199. Dauphin, M., et al., Vimentin expression predicts the occurrence of metastases in non small cell lung carcinomas. Lung Cancer, 2013. **81**(1): p. 117-122.

- 200. Dhar, S., et al., *Polyvalent Oligonucleotide Gold Nanoparticle Conjugates as*Delivery Vehicles for Platinum(IV) Warheads. Journal of the American

 Chemical Society, 2009. **131**(41): p. 14652-14653.
- 201. Zhang, X.-Q., et al., Strategy for Increasing Drug Solubility and Efficacy through Covalent Attachment to Polyvalent DNA–Nanoparticle Conjugates. ACS Nano, 2011. 5(9): p. 6962-6970.
- 202. Xiao, Z., et al., DNA Self-Assembly of Targeted Near-Infrared-Responsive Gold Nanoparticles for Cancer Thermo-Chemotherapy. Angewandte Chemie International Edition, 2012. 51(47): p. 11853-11857.
- 203. Alexander, C.M., M.M. Maye, and J.C. Dabrowiak, DNA-capped nanoparticles designed for doxorubicin drug delivery. Chemical Communications, 2011.
 47(12): p. 3418-3420.
- 204. Alexander, C.M., J.C. Dabrowiak, and M.M. Maye, Investigation of the Drug Binding Properties and Cytotoxicity of DNA-Capped Nanoparticles Designed as Delivery Vehicles for the Anticancer Agents Doxorubicin and Actinomycin D. Bioconjugate Chemistry, 2012. 23(10): p. 2061-2070.
- 205. Alexander, C.M., et al., *Multifunctional DNA-Gold Nanoparticles for Targeted Doxorubicin Delivery*. Bioconjugate Chemistry, 2014. **25**(7): p. 1261-1271.
- 206. Kim, D., Y.Y. Jeong, and S. Jon, A Drug-Loaded Aptamer—Gold Nanoparticle Bioconjugate for Combined CT Imaging and Therapy of Prostate Cancer. ACS Nano, 2010. 4(7): p. 3689-3696.
- 207. Latorre, A., et al., DNA and aptamer stabilized gold nanoparticles for targeted delivery of anticancer therapeutics. Nanoscale, 2014. **6**(13): p. 7436-7442.

- Zheng, J., et al., A Spherical Nucleic Acid Platform Based on Self-Assembled
 DNA Biopolymer for High-Performance Cancer Therapy. ACS Nano, 2013.
 7(8): p. 6545-6554.
- 209. Jo, W., et al., *Photon to thermal response of a single patterned gold nanorod cluster under near-infrared laser irradiation*. Biofabrication, 2011. **3**(1).
- 210. Mackey, M.A., et al., *The Most Effective Gold Nanorod Size for Plasmonic Photothermal Therapy: Theory and In Vitro Experiments.* The Journal of Physical Chemistry B, 2014. **118**(5): p. 1319-1326.
- 211. Huang, X., et al., Cancer Cell Imaging and Photothermal Therapy in the Near-Infrared Region by Using Gold Nanorods. Journal of the American Chemical Society, 2006. **128**(6): p. 2115-2120.
- 212. Bagalkot, V., et al., *An Aptamer–Doxorubicin Physical Conjugate as a Novel Targeted Drug-Delivery Platform.* Angewandte Chemie, 2006. **118**(48): p. 8329-8332.
- 213. Bagalkot, V., et al., Quantum dot Aptamer conjugates for synchronous cancer imaging, therapy, and sensing of drug delivery based on Bi-fluorescence resonance energy transfer. Nano Letters, 2007. **7**(10): p. 3065-3070.
- 214. Xu, L., et al., Regiospecific plasmonic assemblies for in situ Raman spectroscopy in live cells. J Am Chem Soc, 2012. **134**(3): p. 1699-709.
- 215. Macfarlane, R.J., et al., *Nucleic Acid-Modified Nanostructures as*Programmable Atom Equivalents: Forging a New "Table of Elements".

 Angewandte Chemie International Edition, 2013. **52**(22): p. 5688-5698.
- 216. Maeda, Y., et al., *Nanoparticle arrangement by DNA-programmed self-assembly for catalyst applications*. Journal of Applied Physics, 2010. **108**(9): p. -.

- 217. Kim, T.H., et al., *Nanoparticle Assemblies as Memristors*. Nano Letters, 2009. **9**(6): p. 2229-2233.
- 218. Diaz Fernandez, Y.A., et al., *The conquest of middle-earth: combining top-down and bottom-up nanofabrication for constructing nanoparticle based devices*.

 Nanoscale, 2014.
- 219. Cunningham, A. and T. Bürgi, Bottom-up Organisation of Metallic Nanoparticles, in Amorphous Nanophotonics, C. Rockstuhl and T. Scharf, Editors. 2013, Springer Berlin Heidelberg. p. 1-37.
- 220. Wilner, O.I. and I. Willner, *Functionalized DNA nanostructures*. Chem Rev, 2012. **112**(4): p. 2528-56.
- 221. Crew, E., et al., *MicroRNA conjugated gold nanoparticles and cell transfection*.

 Anal Chem, 2012. **84**(1): p. 26-9.
- 222. Xiao, Z.Y., et al., DNA Self-Assembly of Targeted Near-Infrared-Responsive Gold Nanoparticles for Cancer Thermo-Chemotherapy. Angewandte Chemie-International Edition, 2012. 51(47): p. 11853-11857.
- 223. Dujardin, E., et al., *DNA-driven self-assembly of gold nanorods*. Chemical Communications, 2001(14): p. 1264-1265.
- 224. Maeda, Y., et al., *Nanoparticle arrangement by DNA-programmed self-assembly for catalyst applications*. Journal of Applied Physics, 2010. **108**(9): p. 094326.
- 225. Lee, J.-H., G.-H. Kim, and J.-M. Nam, *Directional Synthesis and Assembly of Bimetallic Nanosnowmen with DNA*. Journal of the American Chemical Society, 2012. **134**(12): p. 5456-5459.
- 226. Azizi, A., et al., Surface plasmon resonance coupled circular dichroism of DNA-gold nanorods assembly. Journal of Physics D-Applied Physics, 2014. **47**(31).

- 227. Tan, L.H., H. Xing, and Y. Lu, *DNA as a Powerful Tool for Morphology Control, Spatial Positioning, and Dynamic Assembly of Nanoparticles.* Accounts of Chemical Research, 2014. **47**(6): p. 1881-1890.
- 228. Lau, K.L., G.D. Hamblin, and H.F. Sleiman, *Gold Nanoparticle 3D-DNA Building Blocks: High Purity Preparation and Use for Modular Access to Nanoparticle Assemblies.* Small, 2014. **10**(4): p. 660-666.
- Watanabe-Tamaki, R., et al., DNA-Templating Mass Production of Gold Trimer
 Rings for Optical Metamaterials. Journal of Physical Chemistry C, 2012.
 116(28): p. 15028-15033.
- 230. Maye, M.M., O. Gang, and M. Cotlet, *Photoluminescence enhancement in CdSe/ZnS-DNA linked-Au nanoparticle heterodimers probed by single molecule spectroscopy*. Chemical Communications, 2010. **46**(33): p. 6111-6113.
- 231. Sheikholeslami, S., et al., Coupling of Optical Resonances in a Compositionally Asymmetric Plasmonic Nanoparticle Dimer. Nano Letters, 2010. **10**(7): p. 2655-2660.
- 232. Maye, M.M., et al., Switching binary states of nanoparticle superlattices and dimer clusters by DNA strands. Nat Nanotechnol, 2010. 5(2): p. 116-120.
- 233. Liu, X., et al., Au–Cu2–xSe Heterodimer Nanoparticles with Broad Localized Surface Plasmon Resonance as Contrast Agents for Deep Tissue Imaging. Nano Letters, 2013. **13**(9): p. 4333-4339.
- 234. Zhu, J., et al., Synthesis of Au-Fe3O4 heterostructured nanoparticles for in vivo computed tomography and magnetic resonance dual model imaging. Nanoscale, 2014. **6**(1): p. 199-202.

- 235. Kolb, H.C., M.G. Finn, and K.B. Sharpless, *Click chemistry: Diverse chemical function from a few good reactions*. Angewandte Chemie-International Edition, 2001. **40**(11): p. 2004-+.
- 236. El-Sagheer, A.H. and T. Brown, Click Nucleic Acid Ligation: Applications in Biology and Nanotechnology. Accounts of Chemical Research, 2012. 45(8): p. 1258-1267.
- 237. El-Sagheer, A.H. and T. Brown, *Click Nucleic Acid Ligation*. Nucleic Acid Therapeutics, 2011. **21**(5): p. A6-A6.
- 238. Gerrard, S.R., et al., A New Modular Approach to Nanoassembly: Stable and Addressable DNA Nanoconstructs via Orthogonal Click Chemistries. ACS Nano, 2012. 6(10): p. 9221-9228.
- 239. Li, N. and W.H. Binder, *Click-chemistry for nanoparticle-modification*. Journal of Materials Chemistry, 2011. **21**(42): p. 16717.
- 240. Brennan, J.L., et al., *Bionanoconjugation via click chemistry: The creation of functional hybrids of lipases and gold nanoparticles.* Bioconjug Chem, 2006. **17**(6): p. 1373-1375.
- 241. Tornoe, C.W., C. Christensen, and M. Meldal, *Peptidotriazoles on solid phase:* [1,2,3]-triazoles by regiospecific copper(I)-catalyzed 1,3-dipolar cycloadditions of terminal alkynes to azides. Journal of Organic Chemistry, 2002. **67**(9): p. 3057-3064.
- 242. Cortizo, M. and M. Lorenzo de Mele, *Cytotoxicity of copper ions released from metal*. Biological Trace Element Research, 2004. **102**(1-3): p. 129-141.
- 243. Stubinitzky, C., et al., 2 '-Deoxyuridine conjugated with a reactive monobenzocyclooctyne as a DNA building block for copper-free click-type

CHAPTER 2 -Background

postsynthetic modification of DNA. Chemical Communications, 2014. **50**(76): p. 11218-11221.

244. Gold, B., et al., Selective Transition State Stabilization via Hyperconjugative and Conjugative Assistance: Stereoelectronic Concept for Copper-Free Click Chemistry. The Journal of Organic Chemistry, 2011. 77(1): p. 75-89.

CHAPTER 3

-Experimental Procedures-

Procedures for the synthesis, surface modifications and further applications are presented in **sections 3.1-4**, whilst characterisation techniques for nanomaterials and cell culture studies will be shown in **sections 3.5-7**.

3.1 Synthesis of spherical gold nanoparticles.

Spherical gold nanoparticles of two different sizes (13 nm and 5 nm) were synthesised in aqueous solutions using well-established bottom-up approaches. Protocols can be found in **section 3.1** and characterisation methods in **section 3.5**.

3.1.1 Gold nanoparticles (13 \pm 1 nm).

Gold nanospheres were synthesised by the citrate reduction method, first established by Turkevich [1, 2] and subsequently optimised by Frens [3] (see **section 2.1** for background information and detailed reaction mechanism). In detail, an aqueous solution of sodium tetrachloroaurate (100 mL, 1 mM) was brought to the boil under stirring. Once boiling, a hot aqueous solution of trisodium citrate **1** (see **Figure 3.1**) (5 mL, 2% wt/V) was added to the gold solution. A colour change from yellow to colourless to finally deep red could be observed, indicating the formation of nanoparticles [1-3]. The solution was then stirred under boiling for an additional 15 min and subsequently allowed to cool to room temperature under stirring. To exchange the citrate ligand with bis(p-sulfonatophenyl)phenyl phosphine dihydrate dipotassium salt (BSPP) **2** (see **Figure 3.1**) 20 mg of BSPP were added to the solution [4-7]. After 4 h of stirring, brine was used to induce particle aggregation *via* charge screening. Particle

aggregation was indicated by a colour change from red to blue [6, 8-10]. Following two rounds of centrifugation (5000 rpm, 10 min), decantation/re-dispersion and sonication, particles were finally re-dispersed in Milli-Q water and purified by filtration (0.2 μm syringe filter, VWR). Particles were stored at 4 °C prior to further functionalization (see section 3.2.2).

Figure 3.1 Chemical structures of trisodium citrate (1) and BSPP (2).

3.1.2 Gold nanoparticles (5 \pm 2 nm).

5 \pm 2 nm AuNPs were synthesised in an aqueous solution according to a published literature procedure [11] (for background information see **section 2.1**). In detail, solutions of sodium tetrachloroaurate (375 μ L, 4% wt/V) and potassium carbonate (500 μ L, 0.2 M) in ice-cold water (100 mL) were stirred in an ice bath. To this solution, a freshly prepared solution of sodium borohydride in water (0.5 mg/mL) was added in 5 \times 1 mL aliquots with rapid stirring. A colour change from dark purple to reddish orange was observed indicating the formation of AuNPs. After stirring for a further 5 min, the solution was centrifuged (12000 rpm, 10 min) to remove larger particles [12]. The supernatant was collected and BSPP 2 (see Fig. 3.1) (20 mg) was added whilst stirring. After 15 h, NaCl was added to the solution until a colour change from wine red to light purple was observed indicating particle aggregation [6, 8-10]. Particles were then centrifuged (5000 rpm, 30 min) and re-suspended in Milli-Q water.

After filtration (0.2 µm syringe filter, VWR), the purified particles with final concentrations of about 600nM were stored at 4 °C prior to physicochemical characterisation (see **section 3.5**) and further surface modifications (see **section 3.2**).

3.2 Surface modification of nanomaterials with oligonucleotides.

Nanomaterials of different compositions and morphologies (AuNPs, Cu_{2-x}Se NPs, Fe₃O₄ NCs and graphene oxide) were modified with oligonucleotides for either self-assembly (see **section 3.4**) or biomedical purposes (see **section 3.3**). For conjugation, thiol or amine-terminated oligonucleotides were utilized. All oligonucleotides were synthesised by Dr Afaf El-Sagheer from the group of Prof. Tom Brown at the University of Oxford (formerly University of Southampton) (see **Appendix II** for synthetic protocol).

3.2.1 DNA attachment to 5 nm AuNPs.

AuNP-DNA monoconjugates (i.e. particles modified with one DNA strand) were prepared according to modified literature procedures [13] In detail, equimolar amounts (15 pmol) of 5 ± 2 nm BSPP-coated AuNPs (see **section 3.1.2**) and thiolated oligonucleotides bearing azide (**S1**) or alkyne (**S2**) moieties (see **table 3.2** for sequences) were incubated in PBS (20 mM phosphate, 6 mM NaCl). To this, an aqueous solution of BSPP **2** (1 mg/20 μ L, 1/10 of total reaction volume) was added to reduce the disulfide on the oligonculeotide to the reactive thiol form [13] (see **scheme 3.1**). After 1 h incubation, functionalised AuNPs were purified by agarose gel electrophoresis (3% agarose gel, 9 V/cm, 90 min) (see **section 3.5.1.1**). Respective bands in the gel were extracted, cut into small pieces and stored in 0.5 × TBE buffer at

OLIGO
$$\begin{picture}(200,0) \put(0,0){\line(1,0){100}} \put(0,0){\line(1$$

Scheme 3.1 Reaction mechanism for the disulfide bond reduction by BSPP.

37 °C with gentle shaking overnight to allow conjugates to diffuse out of the gel. The resulting solution was collected, purified by triple high speed centrifugation (16400rpm, 6 °C, 45 min), decantation/re-dispersion and sonication. Conjugates were finally re-dispersed in hybridisation buffer (5 mM phosphate, 80 mM NaCl). Fully characterised monoconjugates were stored at 4 °C prior to applications in self-assembly processes (see **section 3.4**).

Table 3.1 Oligonucleotide sequences and modifications used in chapter 6.

Abbreviation	DNA sequences and modifications
S1	5' – (C ₆ H ₁₂ S)AAAAAAACGAGTGCTAAGGATCCGAA <mark>X</mark> 1
AmS1	5' – (NH ₂)AAAAAAACGAGTGCTAAGGATCCGAA <mark>X</mark> 1
C1	5' – (C ₆ H ₁₂ S)AAAAAAAACGAGTGCTAAGGATCCGAA
S2	3' – (C ₆ H ₁₂ S) AAAAAAAGCTTACCTATAGACGTCACTT <mark>X</mark> ₂
AmS2	3' – (NH ₂) AAAAAAAGCTTACCTATAGACGTCACTT <mark>X</mark> 2
S3	5' - ACACACCGAATGGATATCTGCAGTGAATTCGGATCCTTAGCACTCGACACAC
S4	5' - GTGTGTCGAGTGCTAAGGATCCGAATTCACTGCAGATATCCATTCGGTGTGT

5'-OLIGO
$$O \stackrel{\stackrel{\bullet}{\stackrel{}_{\stackrel{\bullet}{\stackrel{}}}{\stackrel{}}}}{\stackrel{\circ}{\stackrel{}}} O \longrightarrow S_S \longrightarrow OH$$

Figure 3.2 Details of chemical modifications on oligonucleotides used.

3.2.2 DNA attachment to 13 nm AuNPs.

13 ± 1 nm AuNPs were modified with a shell of oligonucleotides according to two different literature procedures [14, 15]. Each procedure involved a slow 'salt ageing' process, required to screen repulsive negative charges between DNA phosphate backbones and the particle surface , thus ensuring a high oligonucleotide surface loading [16, 17]. For the first procedure, citrate-coated AuNPs (500 μL, 6 nM) in Milli-Q water were incubated with thiol-modified DNAs S1 or S2 (25 μL, 40 μM) overnight (see table 3.1 for oligonucleotide sequences). The reaction volume was then increased to 1 mL with final concentrations of NaCl and PBS of 0.05 M and 2 mM respectively. After 2 h the volume was then slowly reduced to 250 μL by vacuum centrifugation (Eppendorf Concentrator) at 35 °C, ensuring a slow gradual increase in ionic strength ([NaCl]_{final}: 0.2 M) and DNA/particle concentration. The resulting DNA-coated AuNPs were then purified by three subsequent centrifugation (16400 rpm, 10 min) and decantation/re-dispersion steps. Finally, full characterized conjugates (see section 3.5) were stored in hybridisation buffer (5 mM phosphate, 80 mM NaCl) at 4 °C prior to self-assembly experiments (see section 3.4 and chapter 6). DNA-AuNP conjugates

prepared by this method were found to have an oligonucleotide loading of 160 ± 4 DNA strands per particle (see **Appendix II**).

For the second procedure, BSPP-coated AuNPs (1 mL, 10 nM) were incubated with thiol modified DNA (3 nmol) overnight (see **table 3.2** for oligonucleotide sequences). BSPP (1 mg/20 μ L, 10 μ L), phosphate buffer (0.1 M, pH 7.4) and sodium dodecyl sulfate (SDS) (10 %) were then added to achieve final concentrations of 0.01 M phosphate and 1 % SDS respectively. The addition of BSPP resulted in the conversion of the disulfide terminus on the oligonucleotide strands into thiols (cf. **scheme 3.1**).

Table 3.2 Oligonucleotide sequences used for biomedical applications in chapter 5.

Name	DNA sequences and modifications
Vimentin Sense	5'-Cy3-CTT TGC TCG AAT GTG CGG ACT T (A) ₈ -(C ₆ H ₁₂ S) -3'
Vimentin Flare	5'-Cy5-AAG TCC GCA CA-3'
Vimentin perfect target	5'-AAG TCC GCA CAT TCG AGC AAA G-3'
Vimentin 1 mismatch target	5'-AAG TTC GCA CAT TCG AGC AAA G-3'
Vimentin 2 mismatch target	5'-AAG TTC GAC CAT TCG AGC AAA G-3'
Desmocollin Sense	5'-Cy5-TGA GTA AAA CTG TGC CAC TCC G (A) ₈ -(C ₆ H ₁₂ S) -3'
Desmocollin Flare	5'-Cy3- C GGA GTG GCA CA -3'
Desmocollin perfect target	5'-CGG AGT GGC ACA GTT TTA CTC A-3'
Desmocollin 1 mismatch target	5'-CGG AGT GTC ACA GTT TTA CTC A-3'
Desmocollin 2 mismatch target	5'-CGA AGT GTC ACA GTT TTA CTC A-3'
Krt8 Sense	5'-Cy5-GGT GGT CTT CGT ATG AAT AC(A) ₈ -(C ₆ H ₁₂ S) - 3'
Krt8 Flare	5'-Cy3-GTA TTC ATA CGA AG-3'
Krt8 perfect target	5'-GTA TTC ATA CGA AGA CCA CC-3'
Krt8 1 mismatch target	5'-GTA TTC ATA TGA AGA CCA CC-3'
Krt8 2 mismatch target	5'-GTA CTC ATA TGA AGA CCA CC-3'
total mRNA Sense	5'-(C ₆ H ₁₂ S)AAACGGGC(T) ₂₉ -Cy3-3'
total mRNA Flare	5'-(A) ₁₂ GCCC-Cy5-3'
total mRNA perfect target	5'-AAAAAAAAA3'

Six additions of a NaCl solution (2 M) over a period of 8 h were required to achieve a final salt concentration of 0.15 M. The resulting DNA-coated AuNPs were then purified by three subsequent centrifugation (16400 rpm, 10 min) and decantation/re-dispersion steps. Finally, full characterized conjugates were stored in PBS buffer at 4 °C prior to further functionalization for biomedical applications (see section 3.3 and chapter 5). DNA-AuNP conjugates prepared by this method were found to have an oligonucleotide loading of 120 ± 2 DNA strands per particle (see section 3.5.2.1.2).

3.2.3 DNA attachment to Cu_{2-x}Se NPs and Fe₃O₄ NCs.

PEG-COOH coated Cu_{2-x}Se NPs and Fe₃O₄ nanocubes (NCs) were obtained from Prof. Liberato Manna and Dr Teresa Pellegrino at the Italian Institute of Technology, Genova (Cu_{2-x}Se NPs were synthesised by Mr. Francesco De Donato, Fe₃O₄ NC synthesis was carried out by Mr. Giammarino Pugliese and water transfer for both particle types were carried out by Mr. Andreas Riedinger. For synthetic protocols see **Appendix II**).

Amine terminated DNA **Ams1** or **AmS2** (see **table 3.1** for oligonucleotide sequences) was conjugated to carboxyl-terminated Cu_{2-x}Se NPs or Fe₃O₄ NCs *via* well-established EDC/sulfo-NHS coupling following an adapted literature protocol [18] (see **section 2.10** for reaction mechanisms). Reactions were carried out using silanized vials (hydrophobic) in order to prevent adsorption of particles on the vial [19]. Briefly, Cu_{2-x}Se NPs or Fe₃O₄ NCs were dissolved in sodium borate buffer (1 mL, 0.01 M, pH 8.5,) to final concentrations of 8.8 nM or 1.5 nM respectively. To this, solutions of 1-(3-(dimethylamino)propyl)-3-ethyl-carbodiimidemethiodide (EDC, 10 μl, 0.3 M) and N-hydroxysulfosuccinimide (sulfo-NHS 20 μl, 0.3 M) were added. Quickly after, amino-

terminated DNA **AmS1** or **AmS2** was added (0.9 nmol). The reaction mixture was then shaken overnight. Conjugates were purified by triple centrifugation (16400 rpm, 30 min), decantation/re-dispersion and sonication. Fully characterised conjugates (see **section 3.5**) and were finally re-dispersed in PBS buffer and stored at 4 °C prior to self-assembly applications (see **section 3.4** and **chapter 6**).

3.2.4 DNA attachment to graphene oxide.

Graphene oxide was prepared by a modified Hummers method [20] by Dr Emmanuel Kymakis and Dr Emmanuel Stratakis groups at the Institute of Electronic Structure and Laser, Greece (see **Appendix II** for synthesis details).

For oligonucleotide conjugation, EDC/sulfo-NHS coupling was utilized [18], making use of the abundant carboxylic groups on the surface of GO sheets [21]. To an aqueous solution of graphene oxide (600 μ L, 0.2 mg/mL) was added EDC (0.8 mg in phosphate buffer, pH 7.2) and sulfo-NHS (1.8 mg in phosphate buffer, pH 7.2). Quickly after, amine-terminated DNA **AmS2** (3 nmol) was added (see **table 3.1** for oligonucleotide sequences). The mixture was left to incubate overnight with gentle shaking. Excess DNA was then removed by triple centrifugation/decantation (16400 rpm, 30 mins). Finally the resulting precipitate was re-dispersed in hybridisation buffer (600 μ L, 5 mM phosphate, 80 mM NaCl)for physiochemical characterisation (see **section 3.5**) and further utilization in self-assembly processes (see **section 3.4** and **chapter 6**).

3.3 AuNP-DNA conjugates for biomedical applications.

During the course of this project, various DNA-AuNP conjugates were utilized for the live cell detection of mRNA [22-25], as well as for targeted drug release (see

chapter 5). The oligonucleotide probe design will be outlined in **section 3.3.1**, whilst the probe synthesis and drug incorporation are introduced in **section 3.3.2**. Sequences were designed to target the mRNAs of Vimentin, Desmocollin (pan) and Cytokeratin 8 (see **section 2.5** for background information). Furthermore the physicochemical characterisations of each probe as well as their applications in cell culture will be outlined in **sections 3.5** and **3.7** respectively.

3.3.1 Design of oligonucleotides for nano-probes.

mRNA sequences for Vimentin, Desmocollin (pan) and Cytokeratin 8 were obtained from the NCBI database (http://www.ncbi.nlm.nih.gov/nucleotide/). Sequences were then analysed for alignments with other sequences (i.e. similarities) using the NCBI's Basic Local Alignment Search Tool (BLAST) (www.ncbi.nlm.nih.gov/BLAST.cgi). This tool is an algorithm constructed to compare sequence information such as amino acids, proteins or nucleotides using published databases [26]. Here the nucleotide-specific blastn was utilized. The following settings were applied: Database: RefSeq RNA; Entrez Query: all[filter] NOT predicted[title]; Species: Homo sapiens; Expect threshold: 10; Match/Mismatch scores: 2/-3. Appropriate sequence targets were then chosen with the following criteria: Length of sense strand: 20-23 bases, melting temperature ~60 °C, GC content < 50 % (in accordance with previous literature reports) [22, 24, 25, 27-29], E value < 0.05, E value of nearest match > 1. Accordingly the flare strand was designed complementary to the sense strand with the following criteria: Length of flare strand: 10-12 bases, melting temperature ~40 °C (see **table 3.2** for all relevant sequences).

3.3.2 Nano-probe synthesis.

BSPP-coated AuNPs (13 ± 1 nm) were functionalised with numerous strands of sense DNA following published procedures described in **section 3.2.2** [22]. As prepared conjugates in PBS were then mixed with the flare strand (60 equivalents) and heated to 70 °C for 5 min, followed by slow, gradual cooling to room temperature to allow for hybridisation to occur. Fully assembled nano-probes were then purified by triple centrifugation (16400 rpm, 15 min), decantation/re-dispersion and sonication. Characterised nano-probes (see **section 3.5**) were finally re-suspended in sterile PBS buffer and immediately used for cell culture experiments (see **section 3.7**).

For implementation of doxorubicin, Vimentin probes were incubated with an excess of doxorubicin (1 mg/4 mL, Sigma Aldrich) and varying amounts of flare strands (60, 80, 100, 120 equivalents, see **Appendix II** for calculations of duplexes formed). The mixture was then heated briefly to 70 °C and subsequently left to slowly and gradually cool to room temperature. Doxorubicin-loaded nano-probes were then purified at least three times (or until no Doxorubicin fluorescence (excitation at: 480 nm, emission scan: 500-800 nm) [30] could be observed in the supernatant) by centrifugation (16400 rpm, 20 min) and re-dispersion in sterile PBS. Assembled probes were then immediately used in further cell culture experiments (see **section 3.7**).

3.4 Programmed ligation of DNA-NPs.

3.4.1 Formation of 5 nm AuNP dimers.

Equimolar amounts of 5 nm AuNP-DNA monoconjugates (S1/C1 or S2) (15 pmol) (see section 3.2.1) respectively were incubated in hybridisation buffer (5 mM phosphate, 80 mM NaCl) [31]. Typical reaction volume (V_{total}): 200 μ L. A gradual increase in salt concentration with simultaneous reduction of V_{total} was achieved by

vacuum centrifugation (Eppendorf Concentrator). After ~2 h, V_{total} was reduced to 10 μL. S3 (15 pmol) was then added and the reaction incubated at 65 °C for 5 min followed by slow, gradual cooling over several hours to allow hybridisation to commence. Prepared assemblies were then purified by agarose gel electrophoresis (3 %, 10 V/cm, 50 min) (see section 3.5.1.1). The dimer band was extracted from the gel and pelleted through high-speed centrifugation (16400 rpm, 50 min, 6 °C). Purified dimers were subsequently incubated with a large excess of S4 at 70 °C for 5 min, followed by a further heating and gradual cooling cycle. This resulted in the removal of splint strand S3 *via* competitive hybridisation [13, 31], leaving behind two particles connected by a single strand of ssDNA (or two monoconjugates in the case of C1/S2 dimers, see section 6.2). Resulting assemblies were then fully characterized (see section 3.5) and stored in hybridisation buffer at 4 °C.

3.4.2 Formation of 13 nm AuNP dimers and trimers.

For these experiments, 13 ± 1 nm AuNPs were synthesized and functionalized with strands of S1 or S2 following previously established protocols (see sections 3.1.2 and 3.2.2) [32-36]. For dimer formation, equimolar amounts of splint strand S3, S1-and S2-modified AuNPs in hybridisation buffer (5 mM phosphate, 80 mM NaCl) were mixed. For trimer formation, one equivalent of S1-AuNPs was mixed with two equivalents of S3 and S2-AuNPs (see section 6.2 for schematic illustrations) [31]. After briefly heating to 70 °C, assemblies were left to slowly and gradually cool down to room temperature over several hours. An excess of splint complement S4 was then added to the assemblies in order to remove S3 *via* competitive hybridization [13]. After a further heating and gradual cooling cycle, assemblies were purified *via* agarose gel electrophoresis (1.75 %, 9 V/cm, 50 min) (see section 3.5.1.1). Respective dimer or

trimer bands were then recovered from the gel, fully characterized (see **section 3.5**) and stored in PBS buffer at 4°C prior to further utilization in biomedical applications (see **section 3.6** and **chapter 6**).

3.4.3 Formation of Fe₃O₄ NC dimers.

AmS1- and AmS2-modified Fe₃O₄ NCs (see section 3.2.3) were mixed equimolarly (1.5 pmol) with S3 in PBS buffer. After briefly heating to 70 °C, assemblies were left to slowly and gradually cool down to room temperature over several hours to allow for hybridization to occur. An excess of splint complement S4 was then added to the assemblies in order to remove S3 *via* competitive hybridization [13]. Assemblies were then purified from excess DNA *via* centrifugation (16400 rpm, 20 min) and redispersion in PBS buffer. Following physiochemical characterization (see section 3.5), assemblies were stored at 4 °C before being shipped to the Istituto Italiano di Tecnologia, for further studies.

3.4.4 Formation of heterodimers.

Oligonucleotides (amine-terminated **AmS1/AmS2** for all NPs, except gold, where the terminus was thiol (**S1/S2**)) were conjugated to NPs as described in **sections 3.2.1** and **3.2.3**. For heterodimer formation, equimolar amounts (1.5 pmol) of **S3** and **AmS1**-DNA modified NPs (Cu_{2-x}Se or Fe₃O₄) and **S2**-AuNP monoconjugates (5 nm AuNPs) in PBS buffer were mixed and briefly heated to 70 °C before being left to slowly and gradually cool down to room temperature over several hours. Assemblies were purified by triple centrifugation (16400 rpm, 20 min) and re-dispersion in PBS buffer. **S4** was then added to the assemblies in order to remove **S3** via competitive hybridization [13]. After a further heating and gradual cooling cycle, assemblies were

purified by centrifugation (16400 rpm, 20min) and re-dispersion in PBS buffer. Following physicochemical characterization (see **section 3.5**), assemblies were stored at 4 °C.

3.4.5 Formation of GO/AuNP hybrid nanostructures.

Amine-terminated DNA **AmS1** was conjugated to GO via EDC coupling as described previously (see **section 3.2.4** and **scheme 2.10**). For assembly formation, an as prepared sample of **AmS1**-functionalised GO (600 µL, 0.2 mg/mL) was added to a solution of 13nm **S2**-AuNPs (3 pmol) (see **section 3.2.2**) in PBS. Then splint strand **S3** (3 pmol) was added and the reaction mixture was briefly heated to 70 °C followed by slow, gradual cooling to room temperature over several hours. Assemblies were purified from unreacted nanoparticles via agarose gel electrophoresis (2 %, 9 V/cm, 10 min) (see **section 3.5.1.1**). Only the nanoparticles entered the gel, whilst GO assemblies, due to their large size remained in the wells as reported in the literature [37]. The gel was stopped for 10min and re-run again for a further 20 min in order to ensure that any nanoparticles trapped between assemblies were allowed to travel into the gel. This procedure was repeated until no more nanoparticles were observed entering the gel matrix. Assemblies were then carefully removed from the wells of the gel and purified by centrifugation (16400 rpm, 15 min) and re-dispersion in hybridization buffer (5 mM phosphate, 80 mM NaCl).

In order to prove that assemblies were ligated, **S4** was added, followed by a heating and gradual cooling cycle in order to remove **S3** as discussed previously (**sections 3.4.1-4**). Agarose gel electrophoresis was then again employed to remove any potentially non-conjugated AuNPs (see **section 6.2** for schematic illustration).

Following physiochemical characterization (see **section 3.5**), assemblies were stored at 4 °C before being shipped to the Institute for Electronic Structure and Laser, Greece for further experiments involving the incorporation into photovoltaic devices.

3.5 Oligonucleotide and nanomaterials characterisation techniques.

For the characterisation of oligonucleotides, nanomaterials and nanomaterial-DNA conjugates various complimentary techniques were employed. These included: Gel electrophoresis (section 3.5.1), UV-vis and fluorescence spectroscopy (section 3.5.2), transmission electron microscopy (section 3.5.3) and ζ -potential measurements (section 3.5.4).

3.5.1 Gel electrophoresis.

3.5.1.1 Agarose gel electrophoresis.

Agarose gels were prepared by dissolving agarose (1.75 or 3 % wt/V) in 0.5×10^{-5} TBE buffer, followed by microwave heating [38]. Once all agarose had dissolved and melted, the resulting gel was then cast into the gel construct and a comb was inserted to form wells. After setting for 1 h the gel was placed in the electrophoresis buffer chamber containing 0.5×10^{-5} TBE buffer. Samples were mixed with Ficoll solution (15 % in 3 × TBE) to increase the sample density and hence prevent floating [39] and were subsequently loaded into the wells of the gel. The loaded gel was then electrophoresed at 9 V/cm. If required, respective bands were extracted from the gel, cut into small pieces and stored in 0.5×10^{-5} TBE buffer overnight to allow particles to diffuse out of the gel. Recovered products were then purified by triple centrifugation (16000 rpm, 15 min) and re-dispersion in water or PBS buffer.

3.5.1.2 Polyacrylamide gel electrophoresis.

Samples were prepared at 100 µl. Volumes exceeding this amount were freeze dried and re-diluted to 100 µl. A 10 % polyacrylamide gel was prepared in 70 mL volume. A solution containing Urea (7 M), 10 % acrylamide monomer solution, and $1 \times$ TBE buffer, was made up to 70 mL with distilled water (22. 5mL). The polyacrylamide gel was formed by the additions of an initiator (560 µl amine persulfate) and a crosslinker (56 µl N,N,N',N'-tetramethylethylenediamine) [39]. Polyacrylamide was immediately syringed into the glass construct and a comb inserted to create wells. After leaving to set for at least 1h, the gel was placed in a bath of $1 \times TBE$ running buffer, the comb was removed and the wells were flushed with the same running buffer. Electrodes were connected and the gel was run at 10 W for 1 h to fill the gel matrix with TBE buffer. DNA samples (each 100 µl) were denatured with formamide (75 µL) [40] and placed in a heating block at 90 °C for 5 min to denature. After heating, DNA samples were immediately placed on ice, preventing duplex formation to occur. Samples were mixed with Ficoll solution (15 % in 3 × TBE) to increase the sample density and hence prevent floating [39] and were subsequently loaded into the wells of the gel. A control lane was loaded with 10µl PAGE dye, providing visible blue reference points (12 mer and 55 mer) for the progress of DNA (only visible in UV). The loaded gel was run at 10 W for 1.5 h. Afterwards, the glass gel cast was removed from the bath and the polyacrylamide gel wrapped in an acetate sheet and imaged on a white background in a Syngene G:BOX under UV illumination.

3.5.2 Spectroscopy.

3.5.2.1 UV-visible spectroscopy.

Samples were analysed using a black low volume quartz cuvette (1 cm path length, Hellma Analytics) on Cary 300 Bio UV-vis Spectrophotometer.

The concentrations of colloidal AuNP or oligonucleotide solutions were determined form the corresponding absorption spectra at the peak maxima (~520 nm for AuNPs and 260 nm for oligonucleotides) using the Beer-Lambert law (equation 3.1):

$$c = \frac{AD}{\varepsilon l}$$

Equation 3.1 Beer-Lambert law rearranged for the determination of concentrations of colloidal gold and oligonucleotides in solution, where c = concentration (mol/L), A = absorbance at the peak maximum (a.u.), $l = \text{path length of light (cm) and } \epsilon = \text{extinction coefficient (L mol^-l cm^-l)}$.

Extinction co-efficients for AuNPs are: 13 nm AuNPs: $2.27 \times 10^8 \, \text{L mol}^{-1} \, \text{cm}^{-1}$, 5 nm AuNPs: $9.696 \times 10^6 \, \text{L mol}^{-1} \, \text{cm}^{-1}$ [41]. Extinction co-efficients for oligonucleotides are sequence specific and were determined by Dr Afaf El-Sagheer using either the nearest neighbour or the base composition model [42-44] . See **Appendix II** for sample calculations.

3.5.2.1.1 Oligonucleotide UV melting.

For UV melting, equimolar amounts of **S1**, **S2** and **S3** (see **table 3.2** for oligonucleotide sequences) as well as other possible combinations (**S2+S1**, **S1+S3**, **S2+S3**) were incubated in PBS (1 mL). Samples were then gradually heated and cooled over three rapid and three slow cycles. UV-vis absorption at 260 nm was monitored on a Cary 300 Bio UV-vis Spectrophotometer.

3.5.2.1.2 Determination of oligonucleotide loading on AuNPs.

The number of oligonucleotides per AuNP were determined as follows: to a solution of DNA-coated AuNPs of a known concentration (200 μ L) was added a solution of KI/I₂ (ratio of I₂ to KI = 1:6, 300 μ L, 34 mM) (see **scheme 4.1** for reaction mechanism) [45]. A colour change from red to yellow indicated the dissolution of colloidal gold [1, 2, 46].

The solution was made up to 1 mL with water and subsequently loaded onto a NAP₁₀ desalting column. After the solution had entered the column, it was eluted with water (1.5 mL) and the product was collected. The oligonucleotide O.D. was determined (at 260 nm) on a Cary 300 Bio UV-vis Spectrophotometer. This data, together with the initial O.D. given on the accompanying oligonucleotide data sheet (prepared by Dr. Afaf El-Sagheer) allowed for the determination of the concentration and hence the number of moles of oligonucleotides in solution, form which the degree of oligonucleotide-loading was confirmed (see **Appendix II**).

3.5.2.2 Fluorescence spectroscopy.

Samples were analysed using a black low volume fluorescence quartz cuvette (Hellma Analytics) on a Cary Eclipse Fluorescence Spectrophotometer.

3.5.2.2.1 Oligonucleotide fluorescence melting.

Assembled nano-probes in PBS (150 μ L, 2.5 nM) (see **section 3.3**) were slowly heated at a rate of 0.1 °C/min and a temperature range from 20 °C – 80 °C. Readings were taken at a rate of 0.1 °C/min (excitation wavelengths: 543 nm (Cy3) or 635 nm (Cy5) and emissions wavelengths: 563 nm (Cy3) or 662 nm (Cy5)).

3.5.2.2.2 Determination of target specificity.

Assembled nano-probes in PBS (150 µL, 2.5 nM) (see **section 3.2**) were incubated at 37 °C. Target sequences (prefect target, 1 mismatch target or 2 mismatch target) were then added and fluorescence readings were taken immediately until a plateau was reached (see **table 3.5** for oligonucleotide sequences). Fluorescence spectra were recorded, exciting at 543 nm (Cy3) or 635 nm (Cy5) and scanning the emission over a range of 550-800 nm (Cy3) or 650-800 nm (Cy5).

3.5.2.2.3 Glutathione assay.

Assembled total mRNA nano-probes in PBS (150 μL, 2.5 nM) (see section 3.3) were incubated at 37 °C with glutathione 3 (5 mM) (see Figure 3.3, also see section 2.1 for background information on ligand exchange). Four samples were set up to be incubated for 1 h, 3 h, 6 h and 24 h respectively. Each sample was then purified after the appropriate time by centrifugation/decantation (16400 rpm, 15 min). The resulting supernatant was collected and analysed for fluorescence (excitation: 543 nm, emission: 563 nm (Cy3)).

Figure 3.3 Chemical structure of glutathione.

3.5.2.2.4 Nuclease assays.

For DNAse I nuclease assays, assembled nano-probes (150 μL, 2.5 nM) (see section 3.3) in phosphate buffer or PBS at pH 7.4 were incubated at 37 °C with Bovine Serum Albumin (BSA) (5 mg/L) and MgCl₂ (0.25 mM) (see section 5.1 for discussion on nucleases). DNAse I (from bovine pancreas, Sigma Aldrich) was then added (0.38 mg/L or 0.38 mg/mL) and fluorescence (Cy3 or Cy5 respectively) was monitored immediately for up to 48 h (excitations: 543 or 635 nm, emissions: 563 or 662 nm respectively) [47].

For DNAse II nuclease assays, assembled nano-probes (150 μ L, 2.5 nM) (see **section 3.3**) in PBS at pH 4.5 were incubated at 37 °C. DNAse II (from porcine spleen, Sigma Aldrich) was then added (5 U/rxn) and fluorescence (Cy3 or Cy5 respectively) was monitored immediately for up to 48 h [48].

In the case of 13 nm AuNP dimers (see **section 3.4**) (150 µL, 2.5 nM), these were incubated with DNAse I or DNAse II in phosphate buffer at appropriate pH (see above) for 24 h. Dimers were then pelleted by centrifugation (16400 rpm, 10 min) and subsequently analysed in an agarose gel (1.75 %, 9 V/cm, 30 min).

3.5.2.2.5 Cell culture media stability assays.

Assembled total mRNA nano-probes in PBS (see **section 3.3**) were diluted to final concentrations of 1.5 nM in different cell culture media (MEM, DMEM and RPMI, see **Appendix I** for formulations). Fluorescence of the nano-probes (Cy3 and Cy5) was measured over 18 h (excitations: 543 or 635 nm, emissions: 563 or 662 nm respectively).

In the case of 13 nm AuNP dimers (see **section 3.4**) (150 μ L, 2.5 nM), these were incubated in MEM buffer for 24 h. Dimers were then pelleted by centrifugation (16400 rpm, 10 min) and subsequently analysed in an agarose gel (1.75 %, 9 V/cm, 30 min).

3.5.2.2.6 Determination of doxorubicin loading.

Vimentin nano-probes (150 μ L, 2.5 nM), loaded with varying amounts of doxorubicin (see section 3.3) were heated to 75 °C for 5 min. Probes were subsequently centrifuged at 16400 rpm for 10 min. Doxorubicin fluorescence in the supernatant was then recorded (excitation: 480 nm, emission scan: 500-800 nm). The drug-loading of each probe was determined from an appropriate calibration curve of doxorubicin fluorescence at 590 nm. From this it was determined that the average DOX loading was: 39 ± 3 for $40 \times$ duplex; 57 ± 4 for $60 \times$ duplex and 73 ± 2 for $80 \times$ duplex (see **Appendix II** for calculations).

3.5.3 Transmission electron microscopy.

Nanomaterials were visualized by transmission electron microscopy (Hitachi H7000 TEM, bias voltage: 75kV). Sample droplets (in water) were air dried on a 400 mesh formvar-coated copper grid (SPI). Size distribution histograms were generated from statistical analyses of relevant representative images using the Image J software.

3.5.4 ζ-potential measurements.

Net charges of nanomaterials were measured on a Malvern Zetasizer Nano ZS. For consistency all materials were dispersed in Milli-Q water for ζ -potential measurements. Disposable capillary cells were used for all measurements. Average net charges were determined from at least three independent measurements.

3.6 Cell culturing.

Human bronchial epithelial cells (16HBE) and human fetal lung fibroblasts (MRC-5) were cultured in Corning cell culture flasks using Modified Eagle's Medium

(MEM, Gibco) (see **Appendix I** for formulation) supplemented with 1% penicillin/streptomycin (Gibco), 1 % L-glutamine (Gibco), 1 mL nystatin (Gibco) and 10% foetal bovine serum (FBS, Sigma Aldrich). Cells were kept at 37 °C, 5 % CO₂ atmosphere in a Sanyo CO₂ incubator (model MCO-17AI). Cells were grown to 90% confluency and then passaged once a week. In all experiments cells from passages < 30 were used. All cell culture stocks were received from Dr Peter Lackie, Southampton General Hospital.

For passaging, cells were incubated with Hank's Balanced Salt Solution (HBSS) (10 mL) for 5 min and subsequently detached using trypsin (5 mL, 0.25 % trypsin, 0.01 % EDTA solution). Trypsin was then inhibited by the addition of full serum growth medium (13 mL). The resulting cell suspension was pelleted by centrifugation (1000 rpm, 5 min). The supernatant was decanted off and the resulting cell pellet was resuspended in a small amount of media ($400 - 600 \,\mu$ L). A small portion of this ($100 \,\mu$ L) was then seeded into a new cell culture flask containing full serum MEM growth medium (13 mL). This formed the cell stock. The remainder of the cells was used in further experiments (see **section 3.7** and **chapter 5**).

3.7 Cell culture studies characterization techniques.

3.7.1 Viability assay.

Cells were seeded in 24-well plates and cultured at 37 °C, 5 % CO₂ atmosphere in MEM medium to ~90 % confluency. Cells were then incubated with respective nanoprobes (as well as drug-loaded nano-probes or dimers, 1.38 pmol per 100.000 cells) (see section 3.4 and 3.5) for 18 h. Cells were then washed with HBSS buffer (500 μ L) followed by incubation with trypsin (350 μ L) to detach cells (5 min, 37 °C). Trypsin was then inhibited with cell culture media containing 10 % fetal bovine serum. The cell

viability was assessed using a dye exclusion assay [49]. Staining in a 1:1 ratio with trypan blue resulted in apoptotic cells displaying a blue coloured cytoplasm, whilst healthy cells retained a clear cytoplasm. Cells were then counted using a Neubauer haemocytometer and cell viability was evaluated. All viability assays were obtained from triplicates (see **Appendix II**).

3.7.2 Microscopy.

3.7.2.1 Transmission electron microscopy.

To investigate the intracellular fate of nanoparticles, cells were embedded in resin, cut into ultrathin sections and visualised by transmission electron microscopy. Resin embedding ensures the preservation of cell structure and intracellular compartments and allows specimens to be viewed in small sections with highly detailed resolution [50]. For this purpose, cells were seeded on cellulose transwell inserts in 12well plates at cell concentrations of 1×10^5 cells/mL for 16HBE or 0.5×10^5 cells/mL for MRC-5 cells. Once cells had grown to ~90% confluency they were incubated with respective nano-probes (see sections 3.3 and 3.4.) for set amounts of time (1, 2, 4, 6 and 18h) after which they were fixed for 1 h in 3% glutaraldehyde / 4% formaldehyde in 0.1 M piperazine-1,4-bis(2ethanesulfonic acid (PIPES buffer 0.1 M, pH 7.2). Then three washing steps (10min each) with PIPES buffer followed. Cells were subsequently treated with osmium tetroxide (1% in PIPES buffer 0.1M, pH 7.2) for 1 h. After a further three washing steps with PIPES buffer and one brief 30 s wash with deionised water, cells were stained with a 2 % aqueous solution of uranyl acetate for 20 min. The sample was then dehydrated by treatment with increasing % ages of ethanol solutions (30, 50, 70, 90 %) for 10 min each. N.B.: After treatment with 50 % ethanol, transwell inserts were cut from the

plastic in order to avoid plastic dissolution in high % ethanol. From this point onwards transwell membranes were placed in a small glass vial. After treatment with 90 % ethanol, the sample was finally fully dehydrated by two consecutive washes in absolute ethanol (20 min each). In order to prepare for resin embedding, samples were then treated with acetonitrile for 10 min followed by 1:1 acetonitrile: SPURR resin overnight. The sample was subsequently fully emerged in pure SPURR resin for 6 h for complete infiltration in order to ensure the removal of acetonitrile. After 6 h the transwells were cut in half and each embedded in fresh SPURR resin in small embedding capsules and polymerised at 60 °C for 24 h. Resin blocks were then cut using a Leica RM 2255 ultramicrotome. Ultrathin (~100 nm) sections were collected on TEM grids (200 mesh) and stained with Reynold's lead stain [51] prior to imaging on a Hitachi H7000 transmission electron microscope (operating bias voltage of 75 kV).

3.7.2.2 Confocal microscopy.

3.7.2.2.1 Immunofluorescent labelling.

Cells (see **section 3.6**) were grown on square glass coverslips in 6-well plates. Once cells were ~90 % confluent, they were washed 3 × with PBS followed by fixation in ice cold methanol. Subsequently, cells were washed 3 × with phosphate buffer (0.1 M) followed by a 30 min blocking in phosphate buffer containing 1 % BSA. Afterwards cells were incubated with primary antibody (anti-Vimentin (mouse), anti-Desmocollin (mouse), anti-Cytokeratin 18 (mouse), all Invitrogen) for 45 min, followed by three washing steps with phosphate buffer containing 1 % BSA (5 min each). Cells were then incubated with secondary antibody (goat, anti-mouse, labelled with Alexa Fluor 568, Invitrogen) for 45 min, followed by an additional three washing steps with phosphate buffer (0.1 M). Cells were then incubated with DAPI for 15 min followed by three

washing steps with phosphate buffer (0.1 M). Coverslips were then mounted in Mowiol containing Citifluor on glass slides and stored at 4 $^{\circ}$ C. Imaging was carried out on a Leica SP8 confocal microscope at \times 63 magnification using an oil immersion lens.

3.7.2.2.2 Cells incubation with AuNPs.

Cells (see **section 3.6**) were grown on square glass coverslips in 6-well plates. Once cells were ~90 % confluent, media was exchanged with fresh media containing different types of nano-probes (see **section 3.3**) for 18 h. Afterwards cells were incubated with Hoechst 33342 (5 µL) for 1 h to stain DNA and nuclei. For imaging the glass coverslip was removed and washed with PBS. It was then mounted on a glass slide with a drop of PBS in order to keep cells alive. The edges around the coverslip were sealed using double-sided tape in order to create a small 'incubation chamber'. All imaging was carried out on a Leica SP8 confocal microscope at 37 °C.

3.8 References.

- 1. Turkevich, J., P.C. Stevenson, and J. Hillier, *The Formation of Colloidal Gold*.

 The Journal of Physical Chemistry, 1953. **57**(7): p. 670-673.
- 2. Turkevich, J., P.C. Stevenson, and J. Hillier, A study of the nucleation and growth processes in the synthesis of colloidal gold. Discussions of the Faraday Society, 1951. **11**(0): p. 55-75.
- 3. Frens, G., Controlled Nucleation for Regulation of Particle-Size in Monodisperse Gold Suspensions. Nature-Physical Science, 1973. **241**(105): p. 20-22.

- 4. Schmid, G. and A. Lehnert, *The Complexation of Gold Colloids*. Angewandte Chemie-International Edition in English, 1989. **28**(6): p. 780-781.
- 5. Yang, J., J.Y. Lee, and H.-P. Too, Size sorting of Au and Pt nanoparticles from arbitrary particle size distributions. Analytica Chimica Acta, 2005. **546**(2): p. 133-138.
- 6. Loweth, C.J., et al., *DNA-based assembly of gold nanocrystals*. Angewandte Chemie-International Edition, 1999. **38**(12): p. 1808-1812.
- 7. Mohr, F. and H. Schmidbaur, *Gold Chemistry: Applications and Future Directions in the Life Sciences*. 2009: John Wiley & Sons.
- 8. Jain, P.K., et al., Calculated absorption and scattering properties of gold nanoparticles of different size, shape, and composition: Applications in biological imaging and biomedicine. Journal of Physical Chemistry B, 2006.

 110(14): p. 7238-7248.
- 9. Kreibig, U.V., M., *Optical Properties of Metal Clusters*. Vol. 25. 1995: Springer: Berlin.
- Mie, G., Beiträge zur Optik trüber Medien, speziell kolloidaler Metallösungen.
 Annalen der Physik, 1908. 330(3): p. 377-445.
- Zhang, T., et al., A new strategy improves assembly efficiency of DNA monomodified gold nanoparticles. Chemical Communications, 2011. 47(20): p. 5774-5776.
- 12. Zhang, T., et al., A new strategy improves assembly efficiency of DNA monomodified gold nanoparticles. Chem Commun (Camb), 2011. 47(20): p. 5774-6.
- 13. Claridge, S.A., et al., *Enzymatic ligation creates discrete multinanoparticle building blocks for self-assembly*. J Am Chem Soc, 2008. **130**(29): p. 9598-9605.

- 14. Kanaras, A.G., et al., *Towards multistep nanostructure synthesis: Programmed enzymatic self-assembly of DNA/gold systems.* Angewandte Chemie-International Edition, 2003. **42**(2): p. 191-194.
- 15. Rosi, N.L., et al., Oligonucleotide-modified gold nanoparticles for intracellular gene regulation. Science, 2006. **312**(5776): p. 1027-1030.
- 16. Hill, H.D., et al., *The role radius of curvature plays in thiolated oligonucleotide loading on gold nanoparticles.* ACS Nano, 2009. **3**(2): p. 418-24.
- 17. Demers, L.M., et al., A fluorescence-based method for determining the surface coverage and hybridization efficiency of thiol-capped oligonucleotides bound to gold thin films and nanoparticles. Analytical Chemistry, 2000. **72**(22): p. 5535-5541.
- 18. Bartczak, D. and A.G. Kanaras, *Preparation of Peptide-Functionalized Gold Nanoparticles Using One Pot EDC/Sulfo-NHS Coupling*. Langmuir, 2011. **27**(16): p. 10119-10123.
- 19. Pirrung, M.C., The Synthetic Organic Chemist's Companion. 2007: Wiley.
- 20. Hummers, W.S. and R.E. Offeman, *Preparation of Graphitic Oxide*. Journal of the American Chemical Society, 1958. **80**(6): p. 1339-1339.
- 21. Dreyer, D.R., et al., *The chemistry of graphene oxide*. Chemical Society Reviews, 2010. **39**(1): p. 228-240.
- 22. Seferos, D.S., et al., *Nano-flares: Probes for transfection and mRNA detection in living cells.* J Am Chem Soc, 2007. **129**(50): p. 15477-15479.
- 23. Zheng, D., et al., *Aptamer Nano-flares for Molecular Detection in Living Cells*.

 Nano Letters, 2009. **9**(9): p. 3258-3261.
- 24. Prigodich, A.E., et al., *Nano-flares for mRNA Regulation and Detection*. ACS Nano, 2009. **3**(8): p. 2147-2152.

- 25. Prigodich, A.E., et al., *Multiplexed nanoflares: mRNA detection in live cells*.

 Anal Chem, 2012. **84**(4): p. 2062-6.
- 26. Altschul, S.F., et al., *Basic local alignment search tool*. Journal of Molecular Biology, 1990. **215**(3): p. 403-410.
- 27. Li, N., et al., A Multicolor Nanoprobe for Detection and Imaging of Tumor-Related mRNAs in Living Cells. Angewandte Chemie-International Edition, 2012. **51**(30): p. 7426-7430.
- 28. Pan, W., et al., Multiplexed Detection and Imaging of Intracellular mRNAs

 Using a Four-Color Nanoprobe. Analytical Chemistry, 2013. **85**(21): p. 1058110588.
- 29. Li, N., et al., *A tumour mRNA-triggered nanocarrier for multimodal cancer cell imaging and therapy*. Chemical Communications, 2014. **50**(56): p. 7473-7476.
- 30. Mohan, P. and N. Rapoport, Doxorubicin as a molecular nanotheranostic agent: effect of doxorubicin encapsulation in micelles or nanoemulsions on the ultrasound-mediated intracellular delivery and nuclear trafficking. Mol Pharm, 2010. **7**(6): p. 1959-73.
- 31. Heuer-Jungemann, A., et al., Copper-free click chemistry as an emerging tool for the programmed ligation of DNA-functionalised gold nanoparticles.

 Nanoscale, 2013. 5(16): p. 7209-7212.
- 32. Mirkin, C.A., et al., A DNA-based method for rationally assembling nanoparticles into macroscopic materials. Nature, 1996. **382**(6592): p. 607-609.
- 33. Taton, T.A., Scanometric DNA Array Detection with Nanoparticle Probes. Science, 2000. **289**(5485): p. 1757-1760.
- 34. Cao, Y.C., R. Jin, and C.A. Mirkin, *Nanoparticles with Raman spectroscopic fingerprints for DNA and RNA detection*. Science, 2002. **297**(5586): p. 1536-40.

- 35. Kanaras, A.G., et al., *Enzymatic disassembly of DNA-gold nanostructures*. Small, 2007. **3**(4): p. 590-4.
- 36. Kanaras, A.G., et al., Site-specific ligation of DNA-modified gold nanoparticles activated by the restriction enzyme Styl. Small, 2007. **3**(1): p. 67-70.
- 37. Wang, Z.H., et al., *Polyvalent DNA-graphene nanosheets "click" conjugates*. Nanoscale, 2012. **4**(2): p. 394-399.
- 38. Lee, P.Y., et al., Agarose gel electrophoresis for the separation of DNA fragments. J Vis Exp, 2012(62).
- Warr, G.W., J.D. Karam, and L. Chao, Methods in Nucleic Acids Research.1990: Taylor & Francis.
- 40. Blake, R.D. and S.G. Delcourt, *Thermodynamic Effects of Formamide on DNA Stability*. Nucleic Acids Research, 1996. **24**(11): p. 2095-2103.
- 41. Haiss, W., et al., *Determination of size and concentration of gold nanoparticles* from UV-Vis spectra. Analytical Chemistry, 2007. **79**(11): p. 4215-4221.
- 42. Crothers, D.M. and B.H. Zimm, *Theory of the melting transition of synthetic polynucleotides: Evaluation of the stacking free energy.* Journal of Molecular Biology, 1964. **9**(1): p. 1-9.
- 43. DeVoe, H. and I. Tinoco Jr, *The stability of helical polynucleotides: Base contributions*. Journal of Molecular Biology, 1962. **4**(6): p. 500-517.
- 44. Bonilla, J.V. and G.S. Srivatsa, *Handbook of Analysis of Oligonucleotides and Related Products*. 2011: Taylor & Francis.
- 45. Cho, E.C., et al., Understanding the Role of Surface Charges in Cellular Adsorption versus Internalization by Selectively Removing Gold Nanoparticles on the Cell Surface with a I-2/KI Etchant. Nano Letters, 2009. **9**(3): p. 1080-1084.

- 46. Mie, G., Beiträge zur Optik trüber Medien, speziell Kolloidaler Metallösungen.
 Annalen der Physik, 1908. **25**(4): p. 377-445.
- 47. Prigodich, A.E., A.H. Alhasan, and C.A. Mirkin, *Selective Enhancement of Nucleases by Polyvalent DNA-Functionalized Gold Nanoparticles*. Journal of the American Chemical Society, 2011. **133**(7): p. 2120-2123.
- 48. Wu, X.C.A., et al., *Intracellular Fate of Spherical Nucleic Acid Nanoparticle Conjugates*. Journal of the American Chemical Society, 2014. **136**(21): p. 7726-7733.
- 49. Strober, W., *Trypan Blue Exclusion Test of Cell Viability*, in *Current Protocols in Immunology*. 2001, John Wiley & Sons, Inc.
- 50. Bozzola, J.J. and L.D. Russell, *Electron Microscopy: Principles and Techniques* for Biologists. 1999: Jones and Bartlett.
- 51. Reynolds, E.S., *The use of lead citrate at high pH as an electron-opaque stain in electron microscopy.* J Cell Biol, 1963. **17**: p. 208-12.

CHAPTER 4

-Results and discussion on synthesis and surface functionalization of nanomaterials-

The ability to synthesise a variety of different nanoparticles with high control over shape and size, good stability and ease of surface modifications is highly important for designing functional nanomaterials.

In the following chapters different nanomaterials were utilized with a view of ultimately being applied in biomedical applications (**chapters 5 and 6**). For this it is crucial that nanomaterials display excellent solubility in aqueous media, as well as great stability, function and biocompatibility. These characteristics can be achieved by means of surface modifications with steric or highly charged molecules, such as oligonucleotides (see **chapter 2** for background information).

This chapter discusses the synthesis of two different sizes of gold nanoparticles (13 nm in section 4.1.1 and 5 nm in section 4.1.2) following well-established literature procedures (see chapter 2 for background information and chapter 3 for experimental procedures). Furthermore, the conjugation of oligonucleotides to different types of nanomaterials (gold nanoparticles of different sizes (section 4.2.1 and 4.2.2), Cu_{2-x}Se NPs (section 4.2.3), Fe₃O₄ nanocubes (NCs) (section 4.2.3)) and graphene oxide (GO) (section 4.2.4) is discussed.

4.1 Spherical gold nanoparticles.

4.1.1 Gold nanospheres (13 \pm 1 nm).

Gold nanospheres of 13 nm size were synthesised by the Turkevich method (optimised by Frens) based on the citrate reduction of Au (III) salts [1-5] (background information on the reaction mechanisms and experimental procedures can be found in **sections 2.1** and **3.1**). Citrate-coated particles are generally susceptible to irreversible aggregation, due to insufficiently strong electrostatic stabilisation of the nanoparticle core by citrate [6, 7]. The colloidal stability was improved by a ligand exchange reaction with the charged, bulky phosphine ligand BSPP [8] (see **chapter 2** for

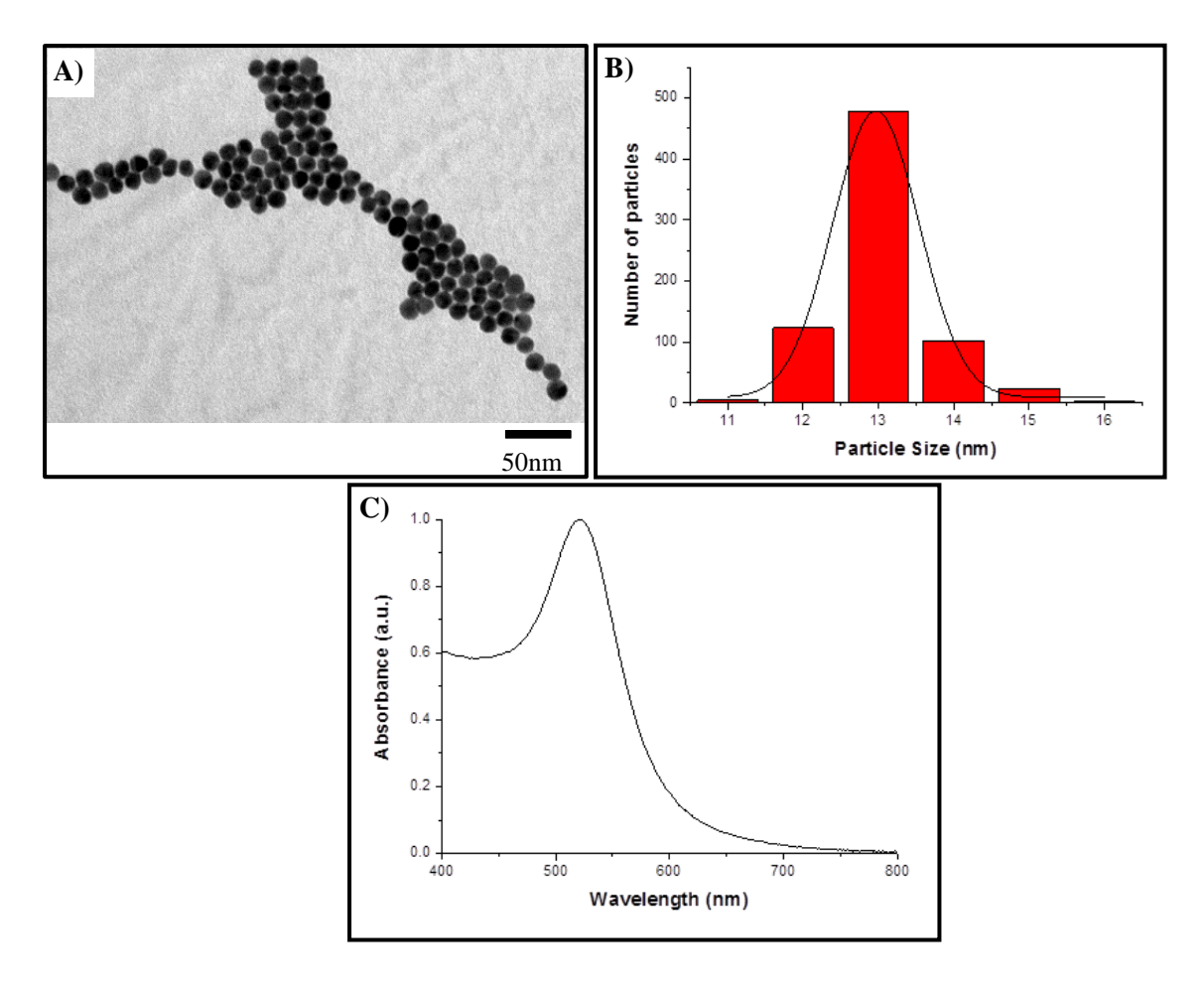


Figure 4.1 Transmission electron micrograph **A**), corresponding size distribution histogram **B**) and normalized UV-vis spectrum **C**) of 13 nm AuNPs.

93

background information) as previously reported by Alivisatos *et al.*[9]. **Figure 4.1A** shows a representative TEM image of the obtained particles. A corresponding size distribution histogram was obtained by analysis of at least 500 particles from at least three independent syntheses (**Figure 4.1B**). The estimated average particle size was 13 \pm 1 nm.

Due to the optical properties of gold nanoparticles UV-vis spectroscopy poses an excellent tool to monitor their stability and monodispersity. The corresponding UV-vis spectrum displayed a narrow LSPR peak at 523 nm, characteristic for monodisperse 13 nm AuNPs (**Figure 4.1C**) [3, 10].

4.1.2 Gold nanospheres (5 \pm 2 nm).

Spherical AuNPs of 5 nm were synthesised according to a recently reported literature protocol [11] (see section 3.1 for experimental procedure). For the synthesis of AuNPs with a diameter of less than 10 nm, the citrate reduction method is no longer suitable as the size distribution of the synthesised particles broadens significantly [12]. Commonly stronger reduction agents active at lower temperatures are required in order to slow down reaction kinetics and hence nucleation and growth processes (see section 2.1 for background information). Here the strong reducing agent NaBH₄ was employed at low temperature to achieve the synthesis of small AuNPs [11]. BSPP was utilized to coat the nanoparticles for increased colloidal stability [8, 9]. A representative TEM image is depicted in Figure 4.2A. By analysing more than 500 particles from at least three different syntheses, a corresponding size distribution histogram was generated (Fig. 4.2B). The average size of the nanoparticles was estimated to be 5 ± 2 nm. Furthermore Figure 4.2 C shows a sharp, narrow peak in the UV-vis spectrum with a

maximum extinction at 520 nm – characteristic of small and robust spherical AuNPs [3, 11, 13].

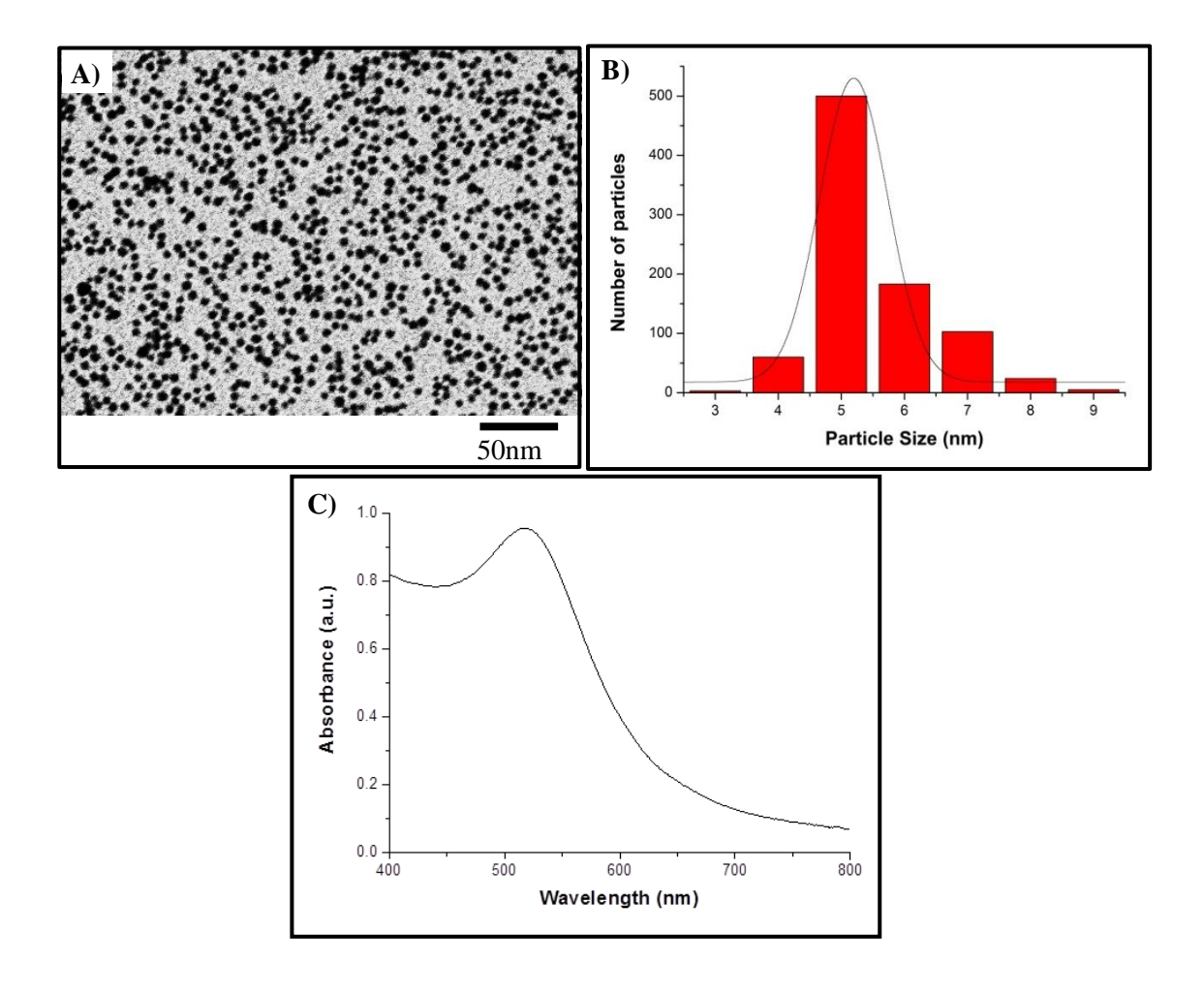


Figure 4.2 Transmission electron micrograph **A**) and corresponding size distribution histogram **B**) as well as a normalized UV-vis spectrum **C**) of 5 nm AuNPs.

4.2 Surface modification of nanomaterials with oligonucleotides.

Different nanomaterials namely AuNPs of 5 and 13 nm, Cu_{2-x}Se NPs and Fe₃O₄ NCs (Cu_{2-x}Se NPs and Fe₃O₄ NCs were obtained from Prof. Liberato Manna and Dr Teresa Pellegrino at the Istituto Italiano di Tecnologia, see **Appendix II** for synthetic protocols) and graphene oxide (obtained from Dr Emmanuel Stratakis and Dr Emmanuel Kymakis, ITE-FORTH, Greece, see **Appendix II**) were functionalized with

different oligonucleotides. Gold nanoparticles utilized for biomedical applications such as live cell mRNA detection and targeted drug delivery were coated with different target-specific oligonucleotides (see **chapter 5**). Nanomaterials used for self-assembly applications were modified with oligonucleotide strands **S1** and **S2** for click ligation [14] (see **chapter 6**).

4.2.1 Mono-functionalization of 5 nm AuNPs.

AuNPs (5 ± 2 nm) conjugated to one, two or three DNA strands were prepared according to modified literature procedures [15] (see section 3.2.1 for experimental details). The DNA modification endows the nanoparticle with functional properties, such as accurate addressability and high target specificity [14-17] (e.g. for highly specific biosensing or for the controlled formation of assemblies cf. chapters 5 and 6). In order to obtain greater control in a self-assembly process, it is desirable to obtain nanoparticles with a discrete number of oligonucleotides attached. Thiolated oligonucleotides were attached to the gold surface by means of well-established sulfurgold chemistry [18-20]. The strength of the covalent bonding between sulfur and gold is similar to that of a gold-gold bond [21, 22] and thus the use of thiolated molecules to stabilize and functionalize gold nanostructures is one of the most common and widely used to date [7, 8, 23-26].

One of the key challenges of obtaining nanoparticles conjugated to a defined number of DNA strands is the separation of mono-, di- or triconjugates (one, two or three DNA strands per particle) [16, 27-29]. Currently, two efficient methods exist. The first strategy involves the employment of chromatography, such as AE-HPLC to separate nanoparticles conjugated to one, two or three DNA strands [27]. In this case it is imperative for the particles to have a minimum charge to facilitate the pathway

through the column. This is typically achieved by the passivation of the nanoparticle surface with methoxy-PEG [27]. Due to the increase in negative charge from mono-, to di- to triconjugates, different retention times can be achieved, resulting in efficient separation. However, a disadvantage of this method is the need for costly reagents and equipment (mPEG and HPLC). Another more cost efficient and more widely used method for the separation of nanoparticles bearing a small number of oligonucleotides is agarose gel electrophoresis, where molecules are separated according to their size and charge [28, 30, 31]. However, this method equally has a significant disadvantage: for efficient separation of particles without DNA strands on their surface from mono-, di- or triconjugates, the size distribution of colloidal particles must be narrow and the DNA length to particle size ratio must be around 1:10 [30]. It was found that lower ratios resulted in less efficient separation, with no separation at all being seen for ratios below 1:4. In this case the addition of one DNA strand does not cause a change in size and charge significant enough to affect the electrophoretic mobility of conjugates [30].

In this study 5 nm AuNPs were chosen and functionalised with 27 or 29 mer thiolated oligonucleotides bearing either azide (S2) or alkyne (S1) functional groups (for synthetic protocols see section 3.2.1, for applications see chapter 6). Figure 4.3 shows a typical gel of AuNPs post DNA conjugation. Due to the ratio of AuNP size to DNA length being less than 1:10, the separation of non-functionalised AuNPs, monoand diconjugates was not ideal, yet individual bands were distinguishable. Monoconjugates were employed in programmed assembly studies (see chapter 6).

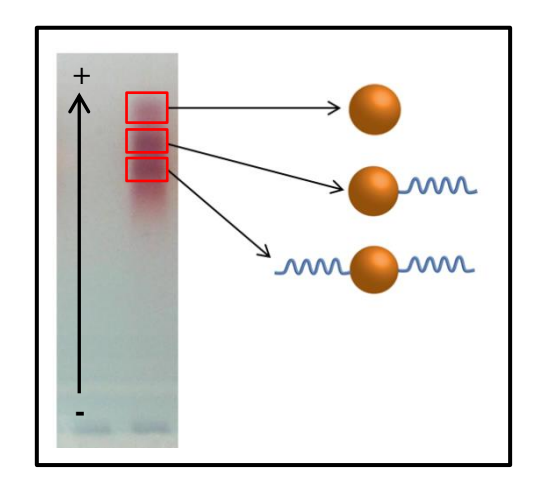


Figure 4.3 Agarose gel for the separation of 5nm AuNP mono- and diconjugates.

4.2.2 AuNPs coated with a dense shell of oligonucleotides.

13 ± 1 nm AuNPs (see **section 4.1.2**) were modified with a dense shell of oligonucleotides following two different literature procedures [32, 33]. In order to achieve a high surface loading, it is imperative to screen the repulsive charges between the gold nanoparticle surface and the negatively charged phosphate backbone on the DNA as well as the charges between individual DNA strands [34]. Therefore both methods employed in this study involved a 'salt ageing' process in which the concentration of sodium ion was gradually raised over time. The final oligonucleotide surface-loading can be finely tuned by means of adjusting the final sodium ion concentration [33, 35] (see **sections 2.4** and **3.2** for background information and experimental procedures).

Although on the one hand the coating of nanoparticles with many DNA strands is timeconsuming, on the other hand it does not require further purification steps such as gel electrophoresis as for the case of separating mono- and diconjugates.

 ζ - potential measurements, UV visible spectroscopy and gel electrophoresis were employed to qualitatively realise the conjugation of oligonucleotides to

nanoparticles in the form of a thick shell. **Figure 4.4** shows complementary results derived from the different techniques. UV-visible spectroscopy reveals a sharp plasmon peak with a maximum extinction at around 525 nm for DNA-coated AuNPs, suggesting a stable colloidal solution (**Figure 4.4 A**). The small red-shift in the plasmon peak (523 nm for BSPP-AuNPs to 525 nm for DNA-AuNPs) can be attributed to an increased refractive index of the immediate environment surrounding the nanoparticle core, caused by the thick DNA corona [23, 36]. Furthermore, no visible peak broadening accompanying the red-shift of the LSPR that would suggest particle aggregation was observed [23, 36, 37].

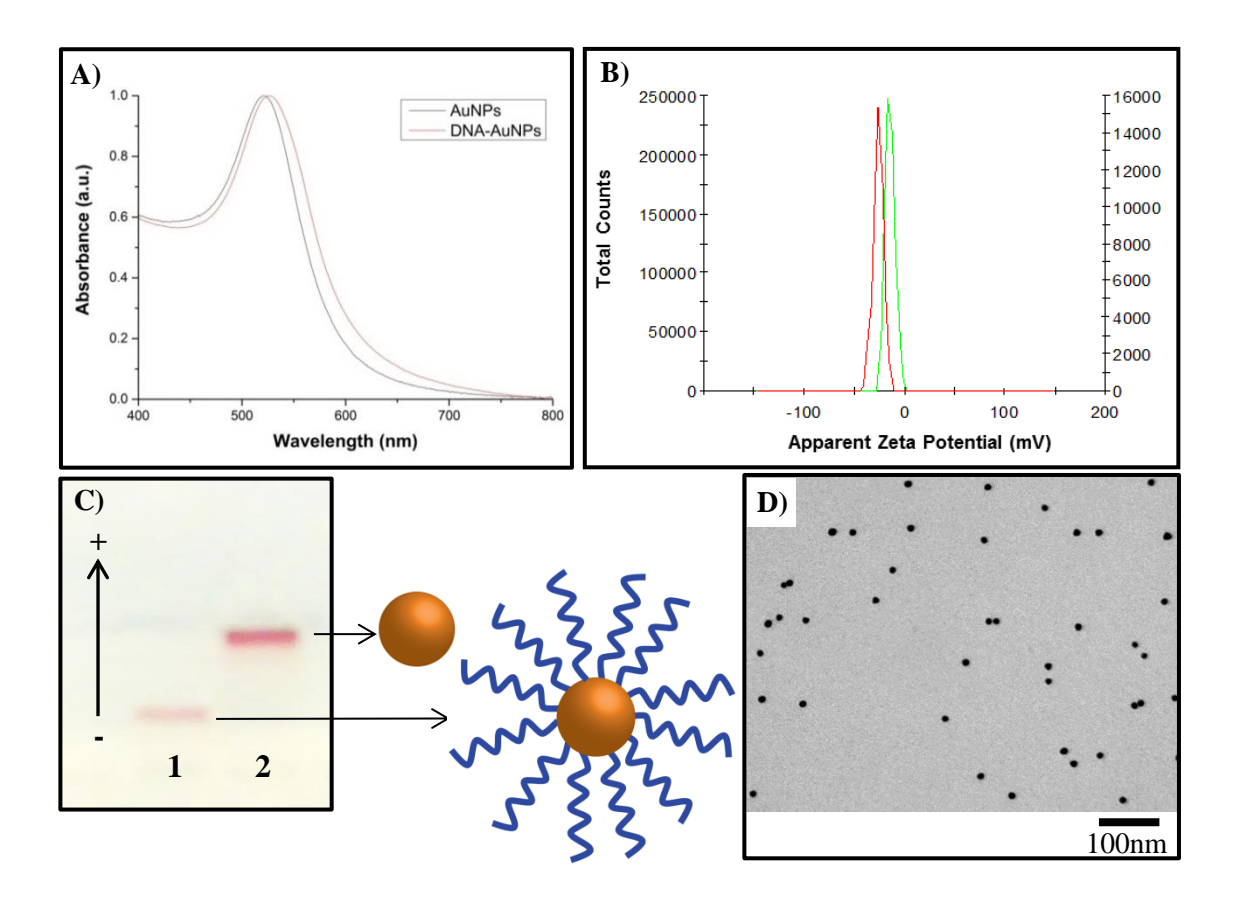


Figure 4.4 A) Normalized UV-vis spectra of BSPP- (black) and DNA-coated (red) AuNPs. **B)** Corresponding ζ-potential measurements of BSPP-coated AuNPs (green) and DNA-AuNPs (red). **C)** Agarose gel of BSPP-coated AuNPs (lane 2) and DNA-AuNPs (lane 1). **D)** TEM micrograph of DNA-AuNPs.

The depicted agarose gel (**Figure 4.4 C**), where particles and molecules are separated according to their volume and charge [30], shows DNA-coated particles exhibiting a lower electrophoretic mobility with respect to unmodified AuNPs. This can be rationalized due to the increased size arising from the thick DNA shell.

Although a decrease in charge from -7.25 ± 0.17 mV for BSPP-AuNPs to -22.87 ± 1.63 mV for DNA-AuNPs was determined by ζ -potential measurements (**Fig. 4.4 B**), the increased size of the conjugates is the most influential factor affecting electrophoretic mobility in this case [38]. Nevertheless, Gracheva *et al.* reported in their studies a maximum voltage recorded for free single-stranded DNA of -30 mV [39]. As the charge of the conjugate is mostly determined by the DNA corona, this result is in good agreement with the obtained results and thus further suggested successful DNA conjugation [40].

For many applications, especially in bio-sensing, it is imperative to determine the exact oligonucleotide loading on a nanoparticle [41-44]. This can be achieved by different methods. Attached DNA can be released from the gold surface by the small thiolated molecule dithiothreitol (DTT) [45-48]. If the recovered oligonucleotides are functionalized with a fluorescent dye, they can then be quantified *via* fluorescence spectroscopy [41]. A second method involves the etching of the gold core using a KI/I₂ solution [49]. The RedOx reaction resulting in the dissolution of the core is outlined below:

$$I_{2} + \Gamma \rightarrow I_{3}^{-}$$

$$I_{3}^{-} + 2e^{-} \rightarrow 3\Gamma$$

$$2\Gamma + Au \rightarrow AuI_{2} + 2e^{-}$$

Scheme 4.1 RedOx reactions leading to the dissolution of gold.

Removal of remaining gold salts by ion exchange chromatography (e.g. using a NAP10 column) then allows for analysis of the liberated oligonucleotides by UV-vis spectroscopy. Following the described procedure, oligonucleotide loadings were determined to be 160 ± 4 DNA or 120 ± 2 DNA strands per particle, depending on the conjugation method and final salt concentration (see **Appendix II** for results from 4 independent measurements per method and corresponding calculations).

Conjugates were employed for biomedical sensing (see **chapter 5**) or as building blocks for the programmed assembly of advanced nanostructures (see **chapter 6**).

4.2.3 DNA attachment to $\text{Cu}_{2\text{-x}}\text{Se NPs}$ and Fe_3O_4 nanocubes \emph{via} EDC coupling.

In the case of oligonucleotide conjugation to Cu_{2-x}Se NPs and Fe₃O₄ nanocubes a different approach was employed. Both nanoparticle types were functionalized with dense PEG-COOH shells for particle stabilisation (see **Appendix II** for synthetic protocols and functionalization procedures). The conjugation protocol was therefore altered accordingly, utilizing EDC/sulfo-NHS coupling [50] with amine-terminated oligonucleotides **AmS1** and **AmS2** (oligonucleotide sequences can be found in **table** 3.1. Also see **section 3.2.3** for experimental procedures). These oligonucleotides were similar to **S1** and **S2** in sequence design and were equally intended for self-assembly purposes (see **chapter 6**).

TEM micrographs of Cu_{2-x}Se NPs (**Fig. 4.5 D and E**) and Fe₃O₄ nanocubes (**Fig. 4.5 A and B**) show that both particle types were stable and the inorganic core was not affected by the DNA conjugation procedure.

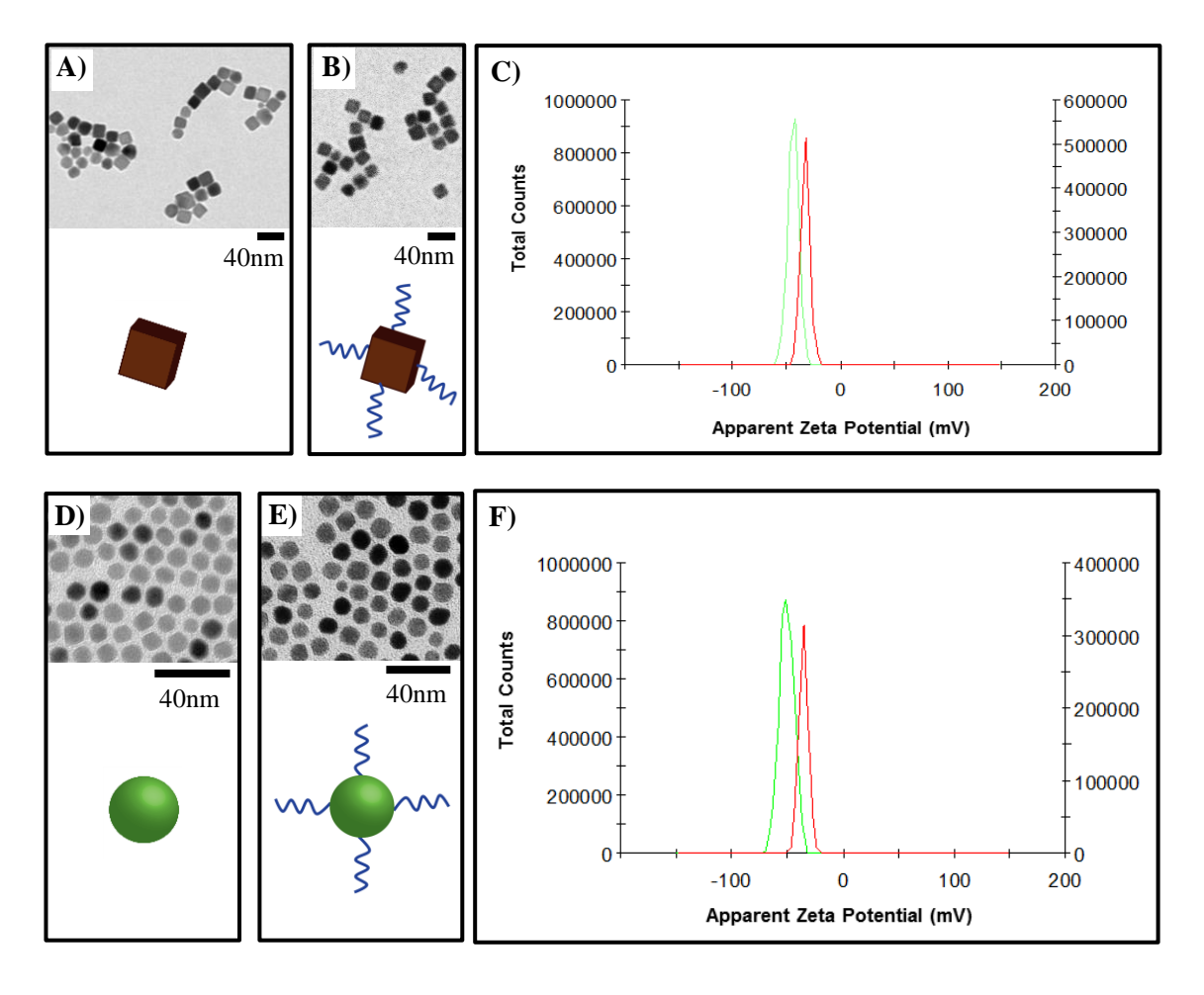


Figure 4.5 TEM micrographs of Fe_2O_3 nanocubes **A**) and Cu2-xSe NPs **D**) before and after DNA conjugation **B**) and **E**). Corresoponding ζ -potential measurements of Fe_3O_4 nanocubes **C**) and Cu2-xSe NPs **F**). before (red) and after DNA conjugation (green).

 ζ -potential measurements were used to give insight into whether DNA conjugation was successful. **Figures 4.5 C and F** show the results for both particle types. Both Cu_{2-x}Se NPs and Fe₃O₄ NCs showed negative ζ -potentials of -35.1 \pm 1.1 mV and -33.3 \pm 0.5 mV respectively before DNA conjugation (**Figure 4.5 C** and **F** red curves). Afterwards the apparent ζ -potentials were decreased for both particle types to -51.1 \pm 1.8 mV (Cu_{2-x}Se@DNA) and -41.4 \pm 1.6 mV (Fe₃O₄@DNA) respectively. This observation was attributed to the added charge inferred by the DNA phosphate backbone as discussed previously (**section 4.2.2**). It is worth noting here that other techniques such as agarose

gel electrophoresis failed to give conclusive results in the characterization of these conjugates to date, but are the subject of future work.

Cu_{2-x}Se@DNA and Fe₃O₄@DNA were further utilized as building blocks for the programmed assembly of advanced nanostructures for potential biomedical applications (see **chapter 6**).

4.2.4 DNA Attachment to graphene oxide via EDC coupling.

Graphene oxide sheets were functionalized with oligonucleotides in a similar fashion to Cu_{2-x}Se NPs and Fe₃O₄ NCs (see **section 4.2.3**). A variety of oxygen containing surface functional groups endow graphene oxide not only with excellent water dispersity but also the possibility of further surface functionalization [51]. Making use of the abundance of free carboxylic groups, EDC/sulfo-NHS coupling was employed to attach amine-terminated DNA **AmS2** covalently to GO [50] (see **table 3.1** for oligonucleotide sequence).

Recent studies have shown the non-covalent interactions of DNA and GO [52, 53]. These studies found that ssDNA readily physibsorbs onto GO by means of π -stacking interactions, whilst dsDNA does not - a finding that allowed for the fabrication of a plethora of DNA sensors [54-57]. It was further found, that the purine bases Adenine (A) and Guanine (G), show stronger interactions with GO's large delocalized π -electron system compared to the pyrimidine bases, resulting in strong non-covalent interactions [58, 59]. The increased interactions of purines with GO arise most likely from their extended delocalised π -electron system. To rule out non-specific interactions of oligonucleotide with GO sheets, great care in the oligonucleotide design was taken to minimize the A/G content.

The conjugation of DNA to GO sheets was realized by UV-vis spectroscopy making use of the distinct absorption characteristics of GO [55]. **Figure 4.6** depicts the relevant spectra. The spectrum of GO exhibits a maximum peak at 230nm, owing to $\pi \rightarrow \pi^*$ transitions (C=C bonds) as well as a shoulder from 290-350nm attributed to $n \rightarrow \pi^*$ transitions (C=O bonds) [60]. A slight red-shift as well as a slight broadening of the shoulder could be observed when GO was reacted with EDC and sulfo-NHS only (red graph **Fig. 4.6 A**.

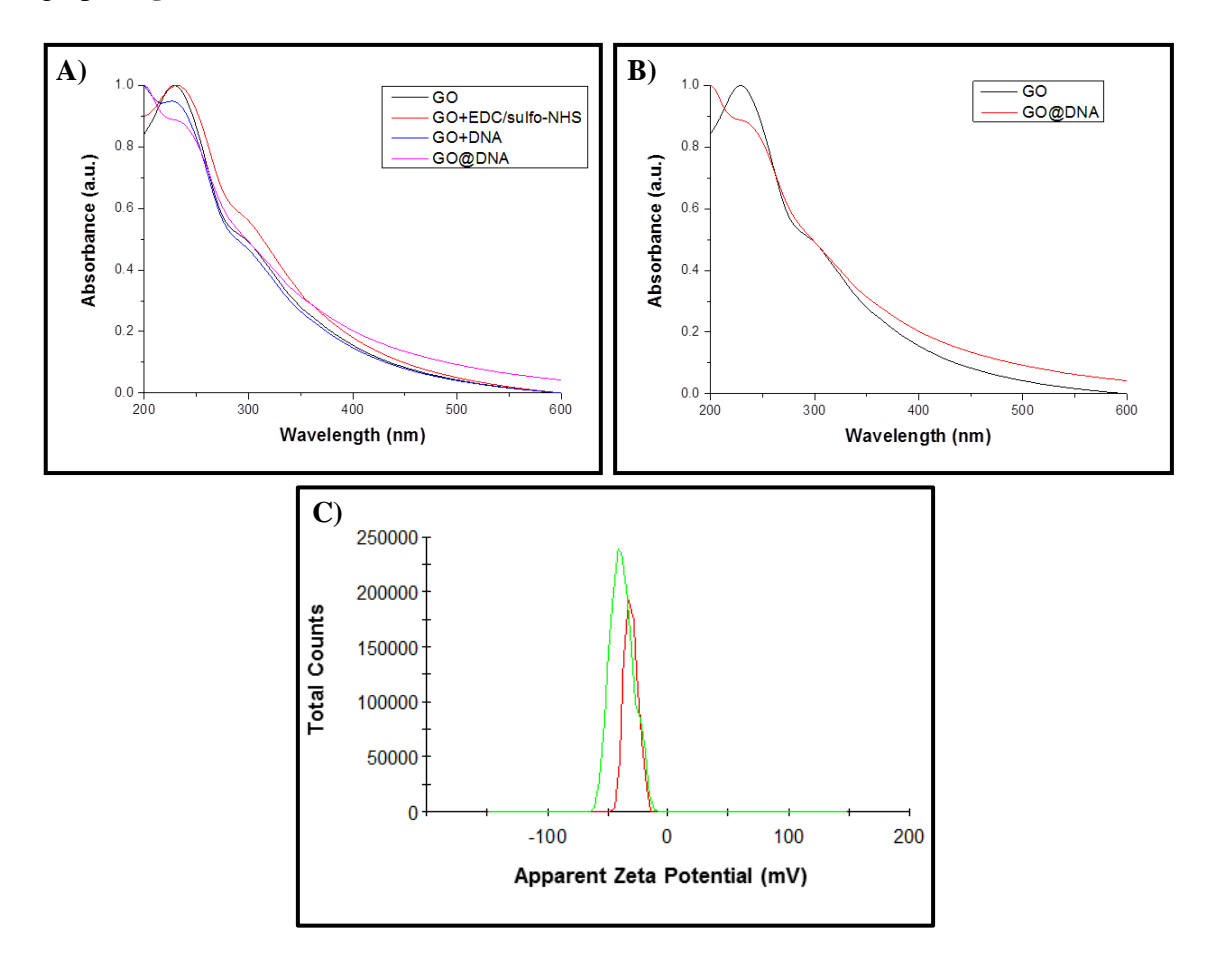


Figure 4.6 A) Normalized UV-visible spectra of graphene oxide (**black**), graphene oxide and EDC/sulfo-NHS (**red**), graphene oxide mixed with DNA (non-covalent) (**blue**) and graphene oxide with covalently attached DNA after EDC coupling (**pink**). **B)** UV-vis spectra of GO (**black**) and GO@DNA (**red**). **C)** ζ-potential graphs of GO (**red**) and GO@DNA (**green**).

This can be attributed to a slight decrease in $n\rightarrow\pi^*$ transitions [60, 61] due to the activation of carboxylic groups with EDC and sulfo-NHS. When GO was simply mixed with DNA, a slight decrease of the shoulder was observed (blue graph, **Fig. 4.6 A**). A potential cause for this could be that few DNA molecules adsorbed onto the GO surface and were not completely removed by purification through centrifugation. However, non-covalent adsorption of DNA onto GO surface is purely based on π -stacking interactions [62-64] and is hence not sufficiently strong to withstand purification procedures without significant DNA desorption. Following EDC/sulfo-NHS coupling and subsequent purification steps, a red-shift of from 230 nm to 235 nm was observed as well as the disappearance of the shoulder at 280-350 nm (pink graph **Fig. 4.6 A** and red graph **Fig. 4.6 B**).

DNA conjugation alters the electronic ground state of GO resulting in the spectral changes observed. In accordance with previous literature reports, this suggested that DNA was conjugated to the GO surface [55]. Furthermore ζ -potential measurements showed a decrease in charge from -25.2 \pm 0.4 mV to -40.1 \pm 1.4 mV after DNA conjugation (**Figure 4.6 B**). As previously discussed (see **sections 4.2.2** and **4.2.3**) this can be attributed to the increased charge inferred by the DNA phosphate backbone. Nevertheless, these obtained results do not confirm for certain that covalent attachment was successful. Further evidence for this will be shown in **chapter 6**, **Figures 6.11** and **6.14**.

GO@DNA conjugates were further employed for the controlled assembly of hybrid GO/AuNP nanostructures (see **chapter 6**).

4.3 References.

- 1. Turkevich, J., P.C. Stevenson, and J. Hillier, A study of the nucleation and growth processes in the synthesis of colloidal gold. Discussions of the Faraday Society, 1951. **11**(0): p. 55-75.
- Frens, G., Controlled Nucleation for Regulation of Particle-Size in Monodisperse Gold Suspensions. Nature-Physical Science, 1973. 241(105): p. 20-22.
- 3. Kreibig, U.V., M., *Optical Properties of Metal Clusters*. Vol. 25. 1995: Springer: Berlin.
- 4. Kimling, J., et al., *Turkevich method for gold nanoparticle synthesis revisited*. Journal of Physical Chemistry B, 2006. **110**(32): p. 15700-15707.
- Turkevich, J., P.C. Stevenson, and J. Hillier, *The Formation of Colloidal Gold*.
 The Journal of Physical Chemistry, 1953. 57(7): p. 670-673.
- 6. Mohr, F. and H. Schmidbaur, *Gold Chemistry: Applications and Future Directions in the Life Sciences*. 2009: John Wiley & Sons.
- 7. Rurack, K. and R. Martinez-Manez, *The Supramolecular Chemistry of Organic-Inorganic Hybrid Materials*. 2010: Wiley.
- 8. Schmid, G. and A. Lehnert, *The Complexation of Gold Colloids*. Angewandte Chemie-International Edition in English, 1989. **28**(6): p. 780-781.
- 9. Loweth, C.J., et al., *DNA-based assembly of gold nanocrystals*. Angewandte Chemie-International Edition, 1999. **38**(12): p. 1808-1812.
- Mie, G., Beiträge zur Optik trüber Medien, speziell Kolloidaler Metallösungen.
 Annalen der Physik, 1908. 25(4): p. 377-445.
- 11. Zhang, T., et al., A new strategy improves assembly efficiency of DNA monomodified gold nanoparticles. Chem Commun (Camb), 2011. **47**(20): p. 5774-6.

- 12. Li, X., P. Jiang, and G. Ge, Synthesis of small water-soluble gold nanoparticles and their chemical modification into hollow structures and luminescent nanoclusters. Colloids and Surfaces A: Physicochemical and Engineering Aspects, 2011. **384**(1–3): p. 62-67.
- Mie, G., Beiträge zur Optik trüber Medien, speziell kolloidaler Metallösungen.
 Annalen der Physik, 1908. 330(3): p. 377-445.
- 14. Heuer-Jungemann, A., et al., Copper-free click chemistry as an emerging tool for the programmed ligation of DNA-functionalised gold nanoparticles.

 Nanoscale, 2013. 5(16): p. 7209-7212.
- 15. Claridge, S.A., et al., Enzymatic ligation creates discrete multinanoparticle building blocks for self-assembly. J Am Chem Soc, 2008. **130**(29): p. 9598-9605.
- 16. Kim, J.W., J.H. Kim, and R. Deaton, *DNA-linked nanoparticle building blocks* for programmable matter. Angew Chem Int Ed Engl, 2011. **50**(39): p. 9185-90.
- 17. Tan, S.J., Campolongo, M. J., Luo, D., Cheng, W., *Building plasmonic nanostructures with DNA*. Nature Nanotechnology, 2011. **6**: p. 268 276.
- 18. Mirkin, C.A., et al., A DNA-based method for rationally assembling nanoparticles into macroscopic materials. Nature, 1996. **382**(6592): p. 607-609.
- Herne, T.M. and M.J. Tarlov, Characterization of DNA probes immobilized on gold surfaces. Journal of the American Chemical Society, 1997. 119(38): p. 8916-8920.
- 20. Laibinis, P.E., et al., COMPARISON OF THE STRUCTURES AND WETTING PROPERTIES OF SELF-ASSEMBLED MONOLAYERS OF NORMAL-ALKANETHIOLS ON THE COINAGE METAL-SURFACES, CU, AG, AU. Journal of the American Chemical Society, 1991. 113(19): p. 7152-7167.

- 21. Hakkinen, H., *The gold-sulfur interface at the nanoscale*. Nat Chem, 2012. **4**(6): p. 443-455.
- 22. Pakiari, A.H. and Z. Jamshidi, *Nature and Strength of M-S Bonds (M = Au, Ag, and Cu) in Binary Alloy Gold Clusters*. The Journal of Physical Chemistry A, 2010. **114**(34): p. 9212-9221.
- 23. Murphy, C.J., et al., *Chemical sensing and imaging with metallic nanorods*. Chemical Communications, 2008(5): p. 544-557.
- 24. Daniel, M.-C. and D. Astruc, *Gold Nanoparticles: Assembly, Supramolecular Chemistry, Quantum-Size-Related Properties, and Applications toward Biology, Catalysis, and Nanotechnology.* Chemical Reviews, 2003. **104**(1): p. 293-346.
- 25. Sardar, R., et al., Gold Nanoparticles: Past, Present, and Future†. Langmuir, 2009. 25(24): p. 13840-13851.
- Jin, R., Quantum sized, thiolate-protected gold nanoclusters. Nanoscale, 2010.2(3): p. 343-362.
- 27. Claridge, S.A., et al., *Isolation of discrete nanoparticle DNA conjugates for plasmonic applications*. Nano Letters, 2008. **8**(4): p. 1202-1206.
- 28. Parak, W.J., et al., Conformation of oligonucleotides attached to gold nanocrystals probed by gel electrophoresis. Nano Letters, 2003. **3**(1): p. 33-36.
- Yan, W.J., et al., Self-Assembly of Chiral Nanoparticle Pyramids with Strong
 R/S Optical Activity. Journal of the American Chemical Society, 2012. 134(36):
 p. 15114-15121.
- 30. Zanchet, D., et al., *Electrophoretic isolation of discrete Au nanocrystal/DNA conjugates*. Nano Letters, 2001. **1**(1): p. 32-35.

- 31. Qin, W.J. and L.Y.L. Yung, Nanoparticle-DNA conjugates bearing a specific number of short DNA strands by enzymatic manipulation of nanoparticle-bound DNA. Langmuir, 2005. **21**(24): p. 11330-11334.
- 32. Kanaras, A.G., et al., *Towards multistep nanostructure synthesis: Programmed enzymatic self-assembly of DNA/gold systems*. Angewandte Chemie-International Edition, 2003. **42**(2): p. 191-194.
- 33. Rosi, N.L., et al., Oligonucleotide-modified gold nanoparticles for intracellular gene regulation. Science, 2006. **312**(5776): p. 1027-1030.
- 34. Demers, L.M., et al., A fluorescence-based method for determining the surface coverage and hybridization efficiency of thiol-capped oligonucleotides bound to gold thin films and nanoparticles. Analytical Chemistry, 2000. **72**(22): p. 5535-5541.
- 35. Hill, H.D., et al., *The role radius of curvature plays in thiolated oligonucleotide loading on gold nanoparticles*. ACS Nano, 2009. **3**(2): p. 418-24.
- 36. Li, X., et al., Localized surface plasmon resonance (LSPR) of polyelectrolyte-functionalized gold-nanoparticles for bio-sensing. Colloids and Surfaces a-Physicochemical and Engineering Aspects, 2009. **332**(2-3): p. 172-179.
- 37. Sonnichsen, C., et al., A molecular ruler based on plasmon coupling of single gold and silver nanoparticles. Nat Biotechnol, 2005. **23**(6): p. 741-5.
- 38. Pellegrino, T., et al., *Gel electrophoresis of gold-DNA nanoconjugates*. Journal of Biomedicine and Biotechnology, 2007.
- 39. Gracheva, M.E., A. Aksimentiev, and J.P. Leburton, *Electrical signatures of single-stranded DNA with single base mutations in a nanopore capacitor*.

 Nanotechnology, 2006. **17**(13): p. 3160-3165.

- 40. Giljohann, D.A., et al., Oligonucleotide loading determines cellular uptake of DNA-modified gold nanoparticles. Nano Letters, 2007. **7**(12): p. 3818-3821.
- 41. Li, N., et al., A Multicolor Nanoprobe for Detection and Imaging of Tumor-Related mRNAs in Living Cells. Angewandte Chemie-International Edition, 2012. **51**(30): p. 7426-7430.
- 42. Seferos, D.S., et al., *Nano-flares: Probes for transfection and mRNA detection in living cells.* J Am Chem Soc, 2007. **129**(50): p. 15477-15479.
- 43. Zheng, D., et al., *Aptamer Nano-flares for Molecular Detection in Living Cells*.

 Nano Letters, 2009. **9**(9): p. 3258-3261.
- 44. Prigodich, A.E., et al., *Nano-flares for mRNA Regulation and Detection*. ACS Nano, 2009. **3**(8): p. 2147-2152.
- 45. Li, F., et al., *Thermal Stability of DNA Functionalized Gold Nanoparticles*. Bioconjugate Chemistry, 2013. **24**(11): p. 1790-1797.
- 46. Letsinger, R.L., et al., *Use of a steroid cyclic disulfide anchor in constructing gold nanoparticle-oligonucleotide conjugates.* Bioconjugate Chemistry, 2000. **11**(2): p. 289-291.
- 47. Dougan, J.A., et al., Enhanced oligonucleotide-nanoparticle conjugate stability using thioctic acid modified oligonucleotides. Nucleic Acids Research, 2007. **35**(11): p. 3668-3675.
- Mei, B.C., et al., Effects of Ligand Coordination Number and Surface Curvature on the Stability of Gold Nanoparticles in Aqueous Solutions. Langmuir, 2009.
 25(18): p. 10604-10611.
- 49. Cho, E.C., et al., Understanding the Role of Surface Charges in Cellular Adsorption versus Internalization by Selectively Removing Gold Nanoparticles

- on the Cell Surface with a I-2/KI Etchant. Nano Letters, 2009. **9**(3): p. 1080-1084.
- 50. Bartczak, D. and A.G. Kanaras, *Preparation of Peptide-Functionalized Gold Nanoparticles Using One Pot EDC/Sulfo-NHS Coupling*. Langmuir, 2011. **27**(16): p. 10119-10123.
- 51. Wang, Z.H., et al., *Polyvalent DNA-graphene nanosheets "click" conjugates*.

 Nanoscale, 2012. **4**(2): p. 394-399.
- 52. Lu, C.H., et al., *A Graphene Platform for Sensing Biomolecules*. Angewandte Chemie-International Edition, 2009. **48**(26): p. 4785-4787.
- 53. Jang, H., et al., *A Graphene-Based Platform for the Assay by Helicase*.

 Angewandte Chemie-International Edition, 2010. **49**(33): p. 5703-5707.
- 54. Zhang, F., et al., *Graphene Covalently Modified by DNA G-Base*. Journal of Physical Chemistry C, 2013. **117**(7): p. 3513-3519.
- 55. Liu, F., J.Y. Choi, and T.S. Seo, *Graphene oxide arrays for detecting specific DNA hybridization by fluorescence resonance energy transfer.* Biosensors & Bioelectronics, 2010. **25**(10): p. 2361-2365.
- 56. Tang, L.A.L., J.Z. Wang, and K.P. Loh, *Graphene-Based SELDI Probe with Ultrahigh Extraction and Sensitivity for DNA Oligomer*. Journal of the American Chemical Society, 2010. **132**(32): p. 10976-10977.
- 57. Tang, Z.W., et al., Constraint of DNA on Functionalized Graphene Improves its

 Biostability and Specificity. Small, 2010. 6(11): p. 1205-1209.
- 58. Premkumar, T. and K.E. Geckeler, *Graphene-DNA hybrid materials: Assembly, applications, and prospects.* Progress in Polymer Science, 2012. **37**(4): p. 515-529.

- 59. Varghese, N., et al., Binding of DNA Nucleobases and Nucleosides with Graphene. Chemphyschem, 2009. **10**(1): p. 206-210.
- 60. Yang, Q., et al., Covalent Functionalization of Graphene with Polysaccharides.

 Industrial & Engineering Chemistry Research, 2011. **51**(1): p. 310-317.
- 61. Bustos-Ramirez, K., et al., Covalently Bonded Chitosan on Graphene Oxide via Redox Reaction. Materials, 2013. **6**(3): p. 911-926.
- 62. Tang, L.H., et al., DNA-Directed Self-Assembly of Graphene Oxide with Applications to Ultrasensitive Oligonucleotide Assay. Acs Nano, 2011. **5**(5): p. 3817-3822.
- 63. Tao, Y., et al., Self-assembled, functionalized graphene and DNA as a universal platform for colorimetric assays. Biomaterials, 2013. **34**(20): p. 4810-4817.
- 64. Cui, L., et al., *Graphene Oxide Protected Nucleic Acid Probes for Bioanalysis* and *Biomedicine*. Chemistry-a European Journal, 2013. **19**(32): p. 10442-10451.

CHAPTER 5

-Results and discussion for biomedical applications of DNA-gold nanoparticle conjugates-

Gold nanoparticle (13 nm)-DNA conjugates were employed for both live cell mRNA detection and targeted drug delivery. The urgent requirements for faster disease diagnosis and targeted treatment were discussed in **chapter 2**. In order to meet these requirements, nano-probes to address both challenges were designed.

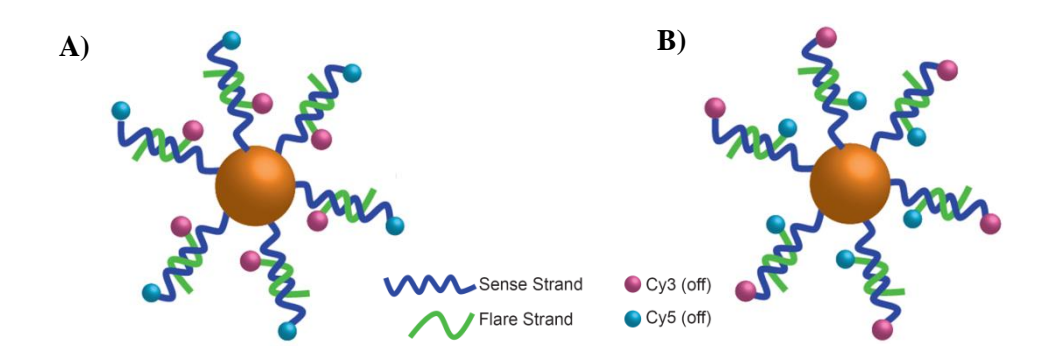
In the following chapter the synthesis, physicochemical characterisation, stability and specificity assays of nano-probes for live cell mRNA detection [1-5] and targeted drug delivery will be described (sections 5.1 and 5.3), followed by their interactions with cell culture (section 5.2 and 5.4).

5.1 Formation, physicochemical characterisation, stability and specificity tests of nano-probes.

In the following sections, the formation and physicochemical characterisations of nano-probes will be discussed (**section 5.1.1**). In order for nano-probes to find applications as live cell mRNA sensors, they are required to display excellent stability towards conditions met within a biological environment. Various factors affecting stability were thus investigated. These include DNA displacement by glutathione (**section 5.1.2.1**), probe degradation by nuclease enzymes (**section 5.1.2.2**) and stability in various cell culture media (**section 5.1.2.3**). Finally their specificity towards designed mRNA targets will be discussed (**section 5.1.3**).

5.1.1 Formation and physicochemical characterisation of nano-probes.

AuNPs were modified with a dense shell of thiolated sense oligonucleotide strands for the detection of total mRNA, Desmocollin, Vimentin and Cytokeratin 8 following established literature protocols [6] (see sections 3.2 and 3.3 for experimental procedure and table 3.2 for oligonucleotide sequences. Also see chapter 4 for results on the attachment of DNA strands on nanoparticles). Subsequently, corresponding dyemodified named here "flare" strands (Cy5 for total mRNA and Cy3 for Desmocollin and Cyotkeratin 8) were hybridised to the sense strand to yield the final probes (see scheme 5.1, also see sections 2.5 and 3.3 for background information and experimental procedures).



Scheme 5.1 Schematic illustration of the nano-probes. **A)** Desmocollin and Cytokeratin 8 nano-probes display Cy3-modified flare strands and Cy5-modified sense strands. **B)** Vimentin and total mRNA nano-probes display Cy5-modified flare strands and Cy3-modified sense strands.

The successful hybridisation of the flare strand was monitored by DNA fluorescence melting. When the flare is hybridised on the sense strand fluorescence of the flare strand is quenched due to the close proximity to the gold nanoparticle core [2, 3, 7, 8]. Upon melting of the DNA duplex, the flare strand diffuses away from the

particle core and its fluorescence is restored [3]. **Figure 5.1** shows fluorescence melting curves for all nano-probes used in this study.

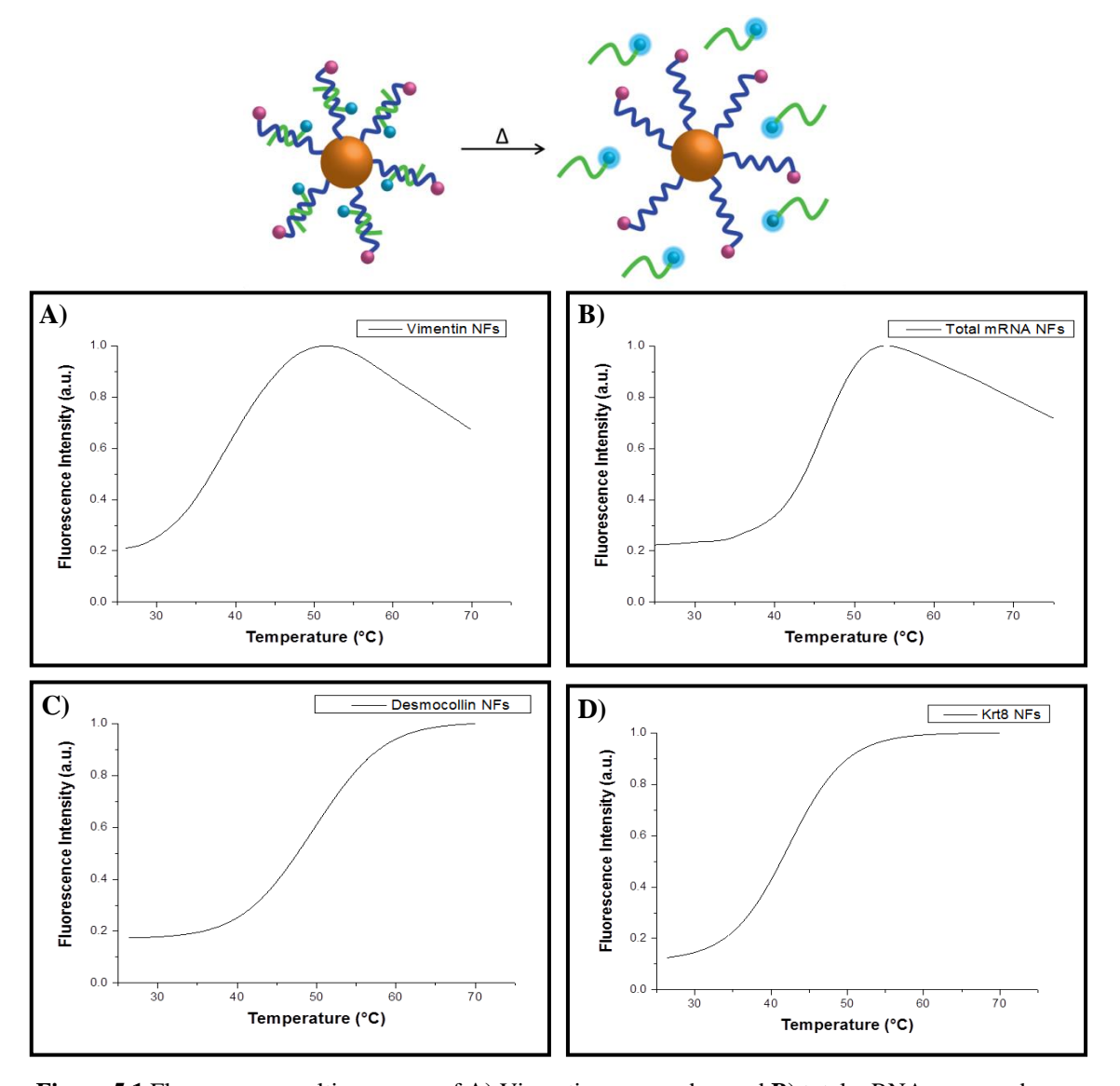


Figure 5.1 Fluorescence melting curves of **A**) Vimentin nano-probes and **B**) total mRNA nano-probes (both modified with Cy5) and **C**) Desmocollin nano-probes and **D**) Krt8 nano-probes (both modified with Cy3).

The fluorescence melting curves for all probes showed a characteristic sigmoidal melting curve shape (see **section 6.1** for extended discussion on melting curves), suggesting successful flare hybridisation and release [9]. Furthermore melting curves allowed for the determination of the DNA melting temperature (Tm), defined as the temperature at which half of the duplex is denatured [10, 11]. As typical human cell

culture conditions require a constant temperature of 37 °C, it was imperative for nanoprobes to display melting temperatures > 37 °C in order to avoid flare strand release through duplex melting. As can be seen from **Figure 5.1**, all probes displayed a melting temperature of > 37 °C. A decrease in fluorescence intensity at higher temperatures was observed for Cy5-modified flare strands (total mRNA and Vimentin probes). This was attributed to the temperature dependent fluorescence of Cy5, which decreases with increasing temperatures [12].

5.1.2 Stability of nano-probes.

5.1.2.1 Glutathione assay.

Glutathione (GSH), a biomolecule present in all human cells, serves as a sulfhydryl buffer as well as an antioxidant [13]. Due to its free thiol group in the form of a cysteine residue (see **Figure 3.3** for chemical structure), it is possible for GSH to cause DNA release *via* ligand replacement. To test the resistance of nano-probes to DNA strand displacement, probes were treated with high concentrations of GSH (5 mM, typical intracellular concentrations vary from 0.5 to 5 mM [14]). The fluorescence of Cy3 on the sense strand was closely monitored for 24 h (see **Figure 5.2**).

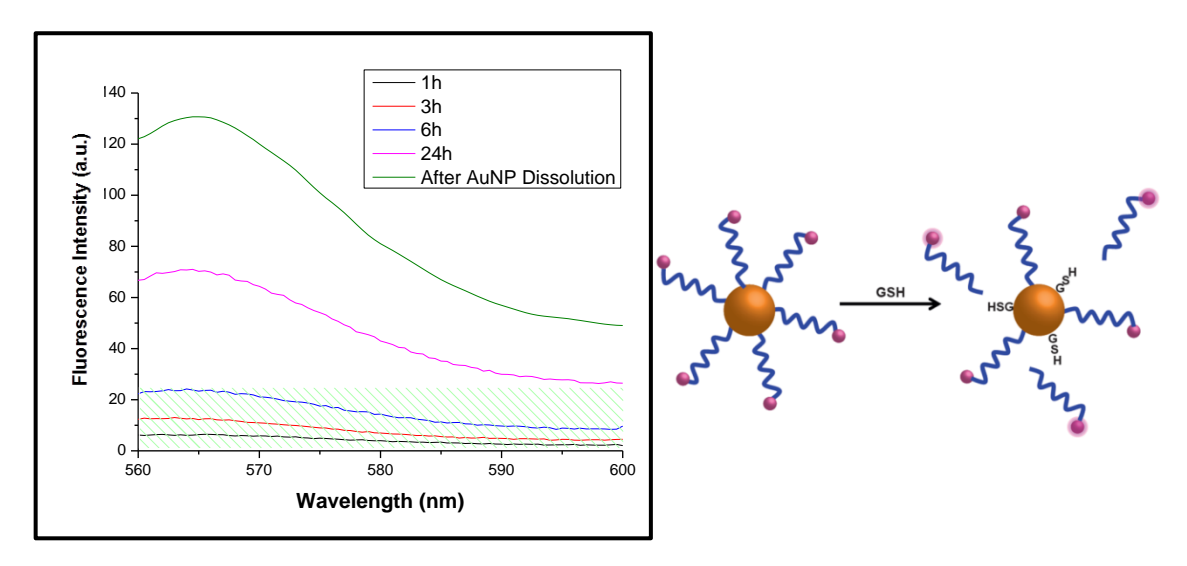


Figure 5.2 Fluorescence spectra of total mRNA detecting nano-probes incubated with GSH and free Cy3-DNA after particle dissolution.

The spectra demonstrate that even at high levels of GSH, more than 50 % of the oligonucleotides remained conjugated to the gold nanoparticle surface after 24 h (**Fig. 5.2** pink graph) compared to oligonucleotide fluorescence after AuNP dissolution (**Fig. 5.2** green graph). This suggested good stability towards DNA displacement by GSH. [15].

5.1.2.2 Nuclease assays.

An inherent complication with oligonucleotide-based intracellular probes is their susceptibility to degradation by nuclease enzymes. However, studies have suggested that probes based on DNA-AuNP conjugates show an increased stability towards nuclease digestion, especially by DNAse I [16, 17]. DNAse I is an endonuclease present within the cytoplasm of all cells and thus presents a great challenge to be overcome.

In order to determine the stability of our nano-probes with respect to enzymatic degradation, probes were incubated with DNAse I enzyme at 37 °C and the fluorescence of both the sense and the flare strand was monitored for 40 h (see **section** 3.5 for experimental procedures). The corresponding data is depicted in **Figure 5.3.**

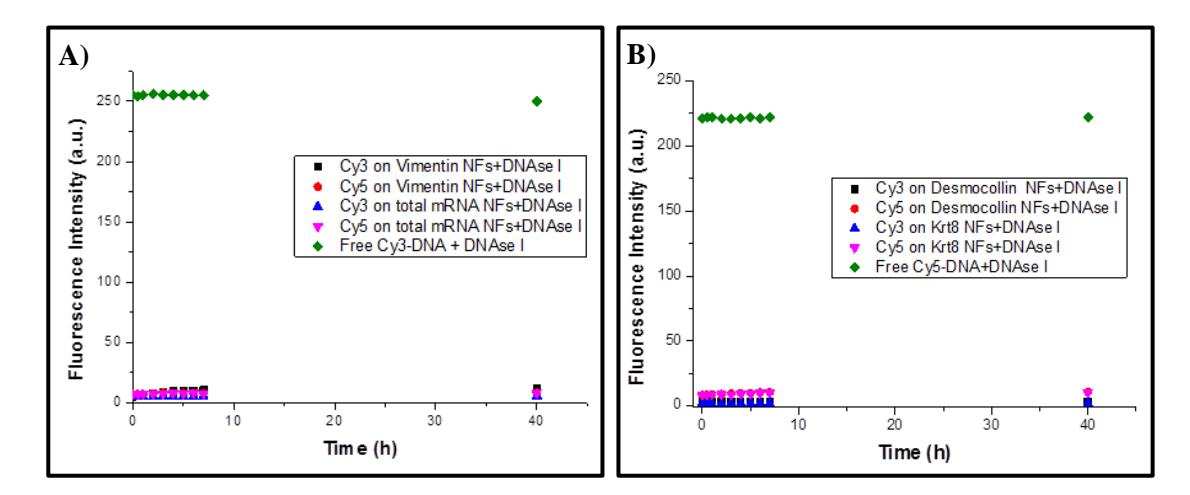
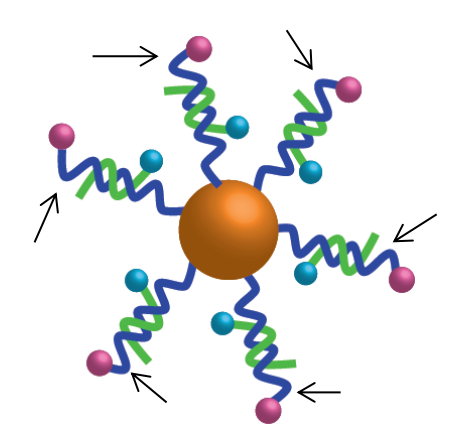


Figure 5.3 Graphs showing the fluorescence of the sense and flare strands for **A**) Vimentin and total mRNA NFs (Sense: Cy3, Flare: Cy5) and **B**) Desmocollin and Cytokeratin 8 NFs (Sense: Cy5, Flare: Cy3). For comparison the fluorescence of free sense DNA after particle dissolution (at constant probe concentrations) is shown in green.

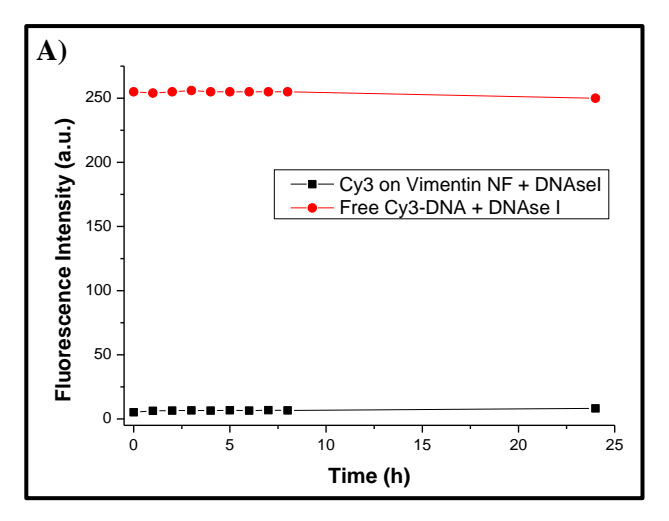
In comparison to 'free' sense or flare strands (obtained by particle dissolution), no significant increase of fluorescence in either the flare or the sense strands could be observed for the DNAs attached to the particles. This suggested that, nano-probes displayed no significant susceptibility to degradation by DNAse I [4]. The reason for this increased stability is still under intense investigation to date and several factors have to be considered, which will be discussed hereafter.

Studies have shown that the enzyme shows high preference for dsDNA compared to ssDNA [18]. Examining the structure of the nano-probes, one can see that the accessible outermost parts of the conjugated oligonucleotides are single-stranded (see **Scheme 5.2**). This could result in an increased stability towards DNAse I.



Scheme 5.2 Schematic illustration of the nano-probe. Arrows indicate outermost parts of oligonucleotides, accessible by DNAse I.

In order to investigate if dsDNA-AuNP conjugates were more susceptible to DNAse I degradation, Vimentin nano-probes were hybridised with their perfect target sequence (see **table 3.1** for oligonucleotide sequences) in order to achieve full length duplexes. The probes were subsequently incubated with DNAse I as before and fluorescence of the sense strand was monitored for 24 h. The result of this assay is depicted in **Figure 5.4** A.



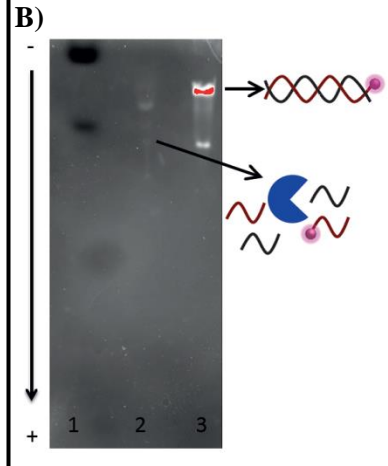


Figure 5.4 A) Spectrum showing the fluorescence of the Vimentin sense strand (black) and for comparison the fluorescence of free sense DNA after particle dissolution (red). **B)** Native polyacrylamide gel displaying a reference dye in lane 1, the degradation of a 'free' DNA duplex (Vimentin dsDNA) in lane 2, and the still intact duplex in lane 3.

As before, no significant increase in Cy3 fluorescence could be observed, suggesting that preference of DNAse I for dsDNA may not be the cause for the increased resistance of the nano-probes towards nuclease degradation. For comparison, a free duplex of DNA was incubated with DNAse I under the same conditions. Polyacrylamide gel electrophoresis was then utilized to visualise the result (**Figure 5.4 B**). Lane 1 shows a reference dye, whilst lanes 2 and 3 show the DNA duplex with (lane 2) and without DNAse I treatment (lane 3). Only very faint bands were observed in lane 2, suggesting that most of the duplex had been degraded by the enzyme, as expected.

Mirkin and co-workers hypothesised that the increased stability of DNA-AuNP conjugates to DNAse I was due to a high concentration of sodium ions being trapped between DNA strands on the nanoparticle surface [19, 20]. The activity of DNAse I has been found to be highly reduced in the presence of high concentrations (> 0.1 M) of monovalent cations [21]. In order to investigate this further, fully assembled Vimentin nano-probes were washed three times with a CaCl₂ solution (0.075 M) before incubation with DNAse I in order to displace monovalent sodium ions by divalent

calcium ions, which enhance the enzymes' activity. The relevant results of this study are shown in **Figure 5.5**.

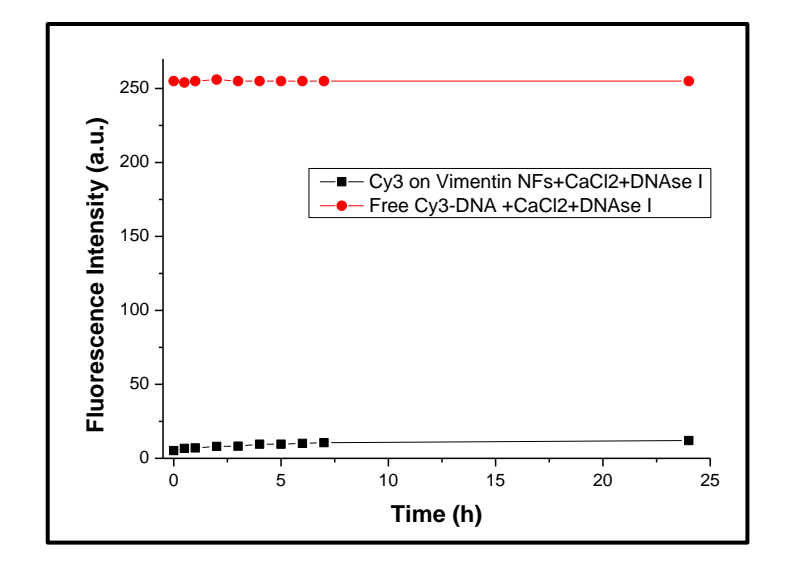


Figure 5.5 Fluorescence monitoring of Vimentin probe sense strand fluorescence (Cy3) after washing with CaCl₂ and treatment with DNAse I.

The results show that as before, no significant fluorescence increase could be observed. Therefore, the high sodium ion concentration around the nano-probe is not likely the major cause of the increased nuclease resistance of these probes towards DNAse I. A possible explanation could be that oligonucleotides assembled on the nanoparticle surface adopt a slightly altered conformation compared to their natural form as suggested by Pellegrino *et al.* [22]. As DNAse I is a minor groove binder and very sensitive to the conformation of the minor groove [23], a small change in conformation due to dense packing of the DNA on the particle surface could therefore result in inefficient binding [20]. However, this hypothesis requires evidence, which could be possibly achieved using extensive computer modelling.

Recently Mirkin and co-workers suggested that DNA-AuNP conjugates, although displaying increased resistance towards digestion by DNAse I, could be

degraded by DNAse II [17]. This endonuclease exhibits optimal activity at acidic pH, as it is mostly located in lysosomes [24]. Unlike DNAse I, whose function is dependent on the presence of divalent cations, DNAse II requires the absence of these for optimal activity [24]. The mechanism of action of DNAse II is based on hydrolysis of the DNA phosphodiester backbone [25, 26]. Due to its lysosomal location, studies suggest that its main function is the degradation of exogenous DNA [24, 27].

In order to test the stability of the nano-probes used in this study with respect to degradation by DNAse II, fully assembled probes were incubated with the enzyme at pH 4.5. The fluorescence of both the sense and the flare strand were monitored for 24 h. The results of this assay are outlined in **Figure 5.6.**

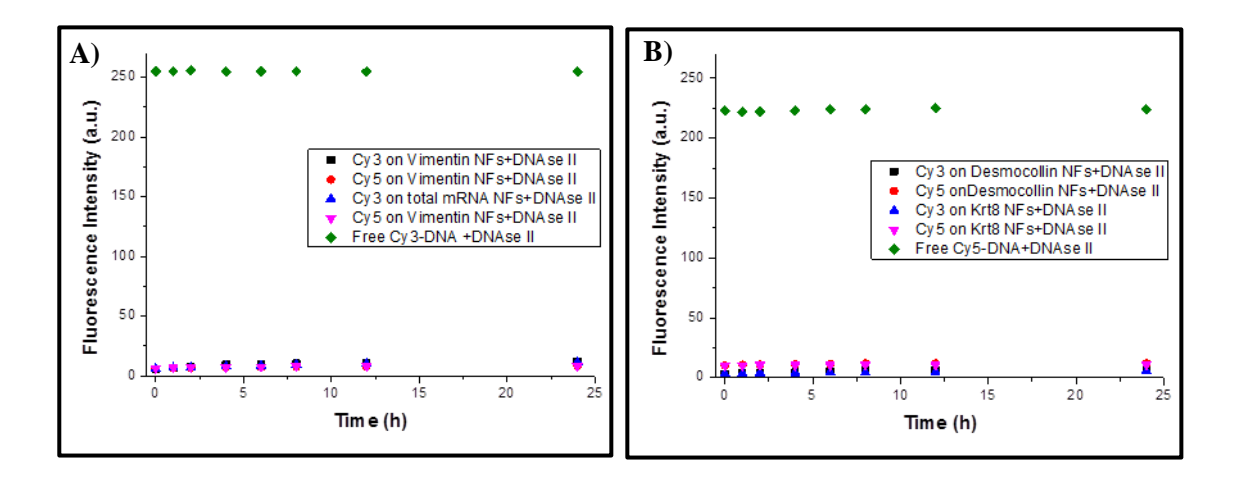


Figure 5.6 Fluorescence monitoring of **A**) Vimentin and total mRNA nano-probes (Sense strand: Cy3, Flare strand: Cy5) incubated with DNAse II and **B**) Desmocollin and Krt8 nano-probes (Sense strand: Cy5, Flare strand: Cy3) incubated with DNAse II.

One can observe that neither the fluorescence of the flare nor the sense strand increased significantly (see data in green for 'free' oligonucleotides at similar concentrations). Thus it appeared that nano-probes were stable with respect to degradation by DNAse II. This result was found to be contradictory to the findings reported by Mirkin *et al*. They showed that after 4 h, ~60 % of the initial oligonucleotides loaded onto the AuNP

surface had been degraded by DNAse II [17]. However, in their studies the reported oligonucleotide-loading was 80 ± 5 strands/particle, while for the nano-probes tested here, the loading was found to be 120 ± 2 strands/particle (see **Appendix II**). This increased density of DNA strands on the nanoparticle surface could result in reduced accessibility of the enzyme leading to the increased resistance towards degradation by DNAse II. Further studies utilizing varying oligonucleotide loadings are required for confirmation and will be the subject of future work.

Similar to DNAse I, DNAse II shows a preference for dsDNA [24]. Thus a dsDNA-AuNP conjugate utilizing the Vimentin nano-probe as before was incubated with the enzyme. The fluorescence of the sense strand was monitored for 24 h. The relevant data is shown in **Figure 5.7**.

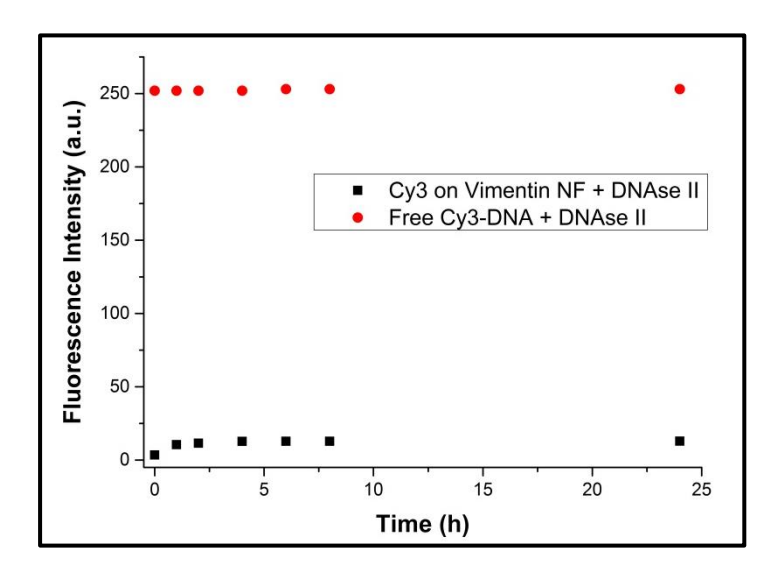


Figure 5.7 Data showing the fluorescence of the Vimentin sense strand (black) upon incubation with DNAse II and for comparison the fluorescence of free sense DNA after particle dissolution (red).

The data suggest that degradation of dsDNA-AuNP conjugates by DNAse II is negligible. As previously discussed the reason for this increased resistance towards degradation by nuclease enzymes is unknown at this time, but will be the subject of future work.

5.1.2.3 Cell culture media stability assays

Many reports have investigated the interactions of nanoparticles with full serum cell culture media. Different components such as salts and proteins found within these media can interact with the nanoparticles and alter their biological identity [28-30]. In order to test the functionality of the nano-probes upon incubation in cell culture media, probes were incubated with three commonly used culture media (MEM, DMEM and RPMI, see **Appendix I** for chemical composition). The fluorescence of sense and flare strand was monitored for up to 18 h (see **section 3.5** for experimental procedures). UV-vis spectroscopy was further employed to investigate nanoparticle stability. Corresponding results are depicted in **Figure 5.8**.

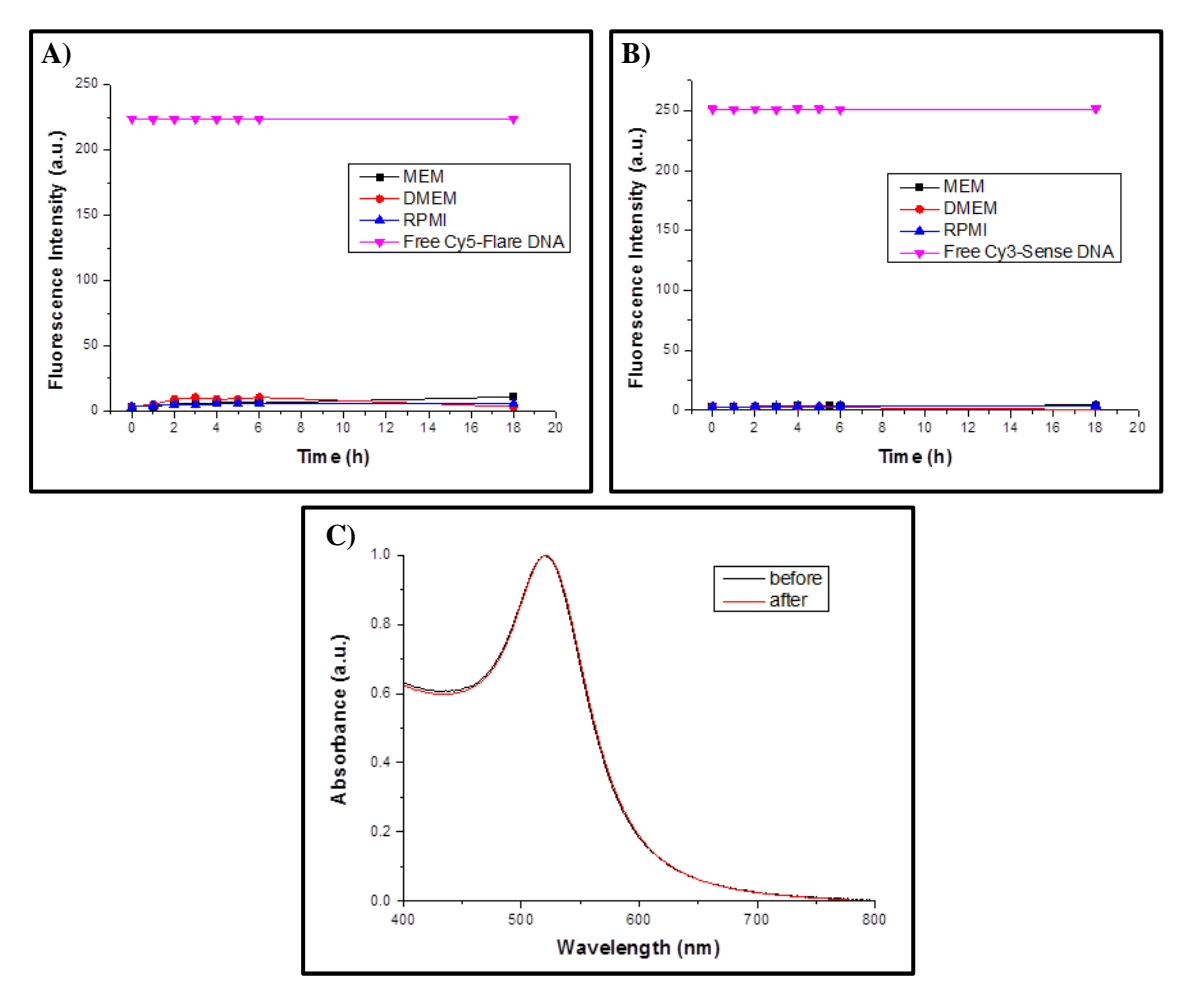


Figure 5.8 Fluorescence spectra of total mRNA nano-probes (**A**) flare strand Cy5 and **B**) sense strand Cy3 fluorescence) incubated in different cell culture media. **C**) UV-vis spectrum of nano-probes before (black) and after (red) incubation with cell culture media.

The data shown, suggested that the probe stability was not affected by incubation with cell culture media. Oligonucleotides remained attached to the nanoparticle surface evident from a constant fluorescence emission of both the flare and the sense strands. Furthermore no signs of nanoparticle aggregation could be observed, determined by the sharp, unchanged plasmon peak [31] shown by a representative UV-vis spectrum in **Figure 5.8 C**.

5.1.3 Specificity assay.

In order to test for response rates, fully assembled nano-probes were incubated with artificial mRNA targets (see **table 3.2** for oligonucleotide sequences).

Flare strand fluorescence was measured over a period of 160 min. Relevant representative fluorescence spectra are shown in **Figure 5.9.**

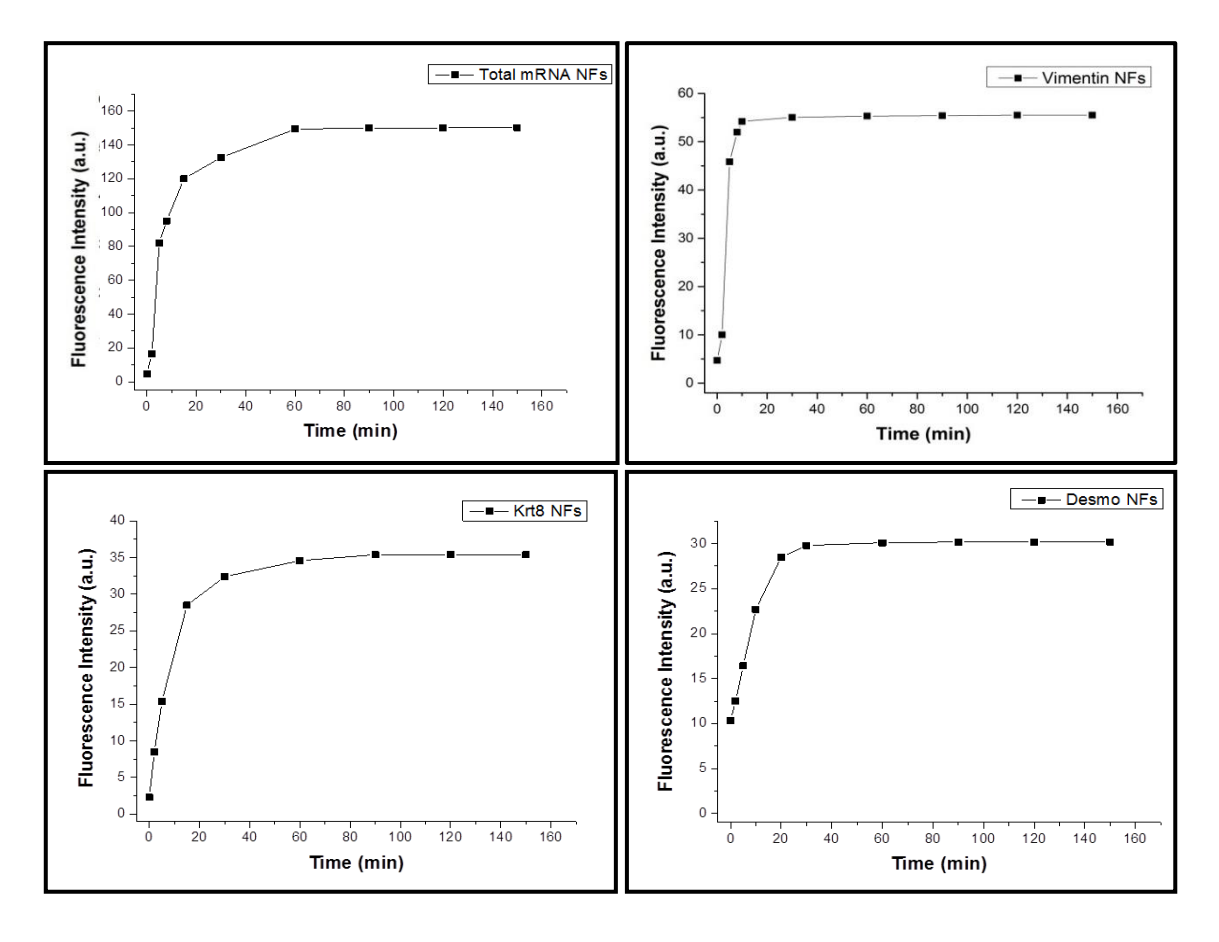


Figure 5.9 Fluorescence spectra of nano-probes incubated with their respective mRNA targets.

From the data shown in **Figure 5.9** one can see that all probes displayed a very fast response rate. Already after a few minutes the fluorescence intensity of the flares strand was increased around twofold. For all probes a plateau was reached after around 60 min, suggesting that all flare strands had been released at this time.

Further studies were then conducted to test for probe specificity. Fully assembled nano-probes were incubated with artificial mRNA targets containing one or two mismatches (see **chapter 3** for oligonucleotide sequences). The flare strand fluorescence was then measured after incubation for 1 h. Resulting spectra are depicted in **Figure 5.10**.

The spectra show that incubation with mismatched targets (blue and pink graphs) induced only minimal fluorescence increase compared to the perfect target and thus suggested high target specificity.

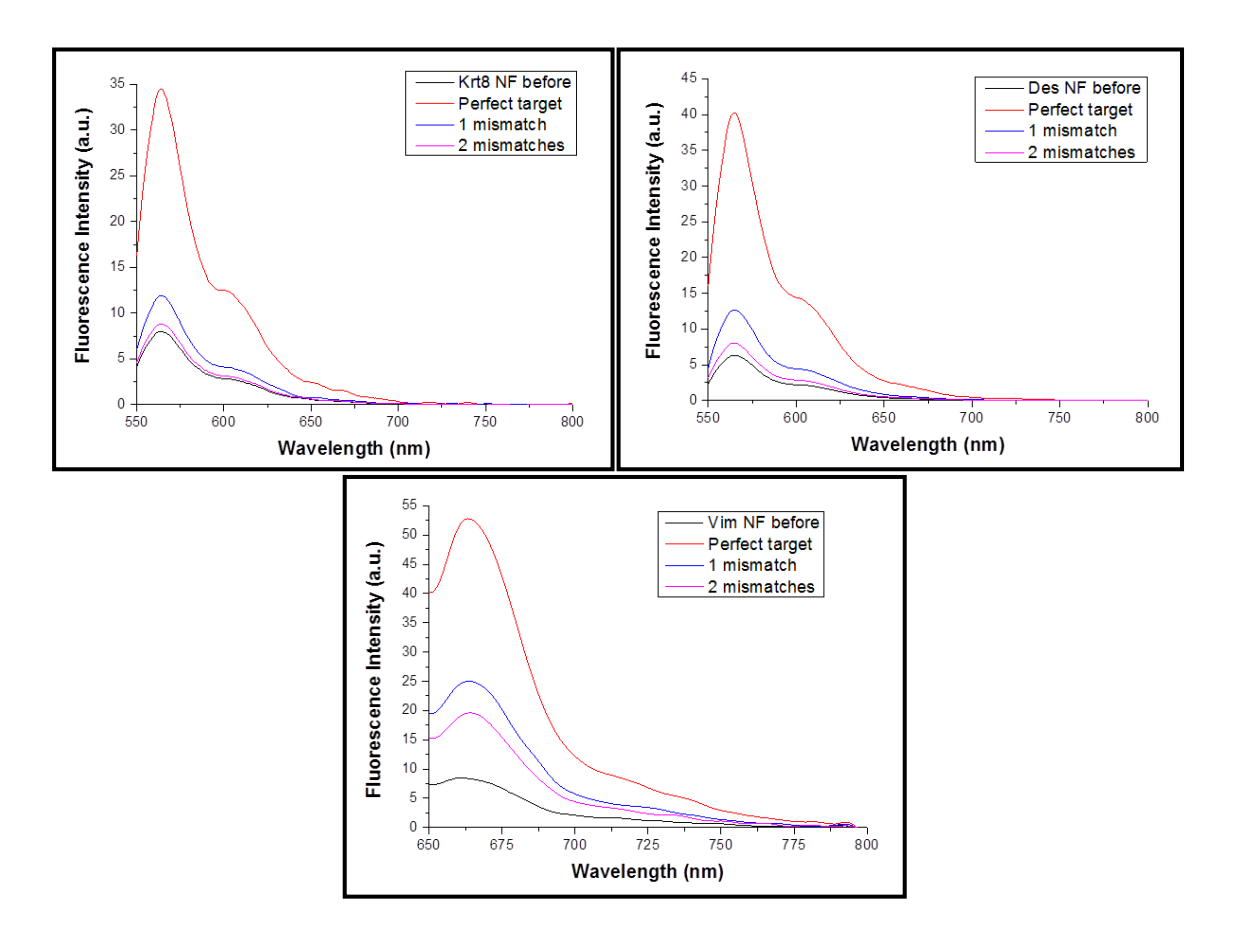


Figure 5.10 Fluorescence spectra of nano-probes incubated with matched and mismatched targets.

The detection limit of each nano-probe was determined by incubation with increasing amounts of perfect target. Fluorescence of the corresponding flare strand was measured after incubation for 1h. Resulting data is shown in **Figure 5.11**.

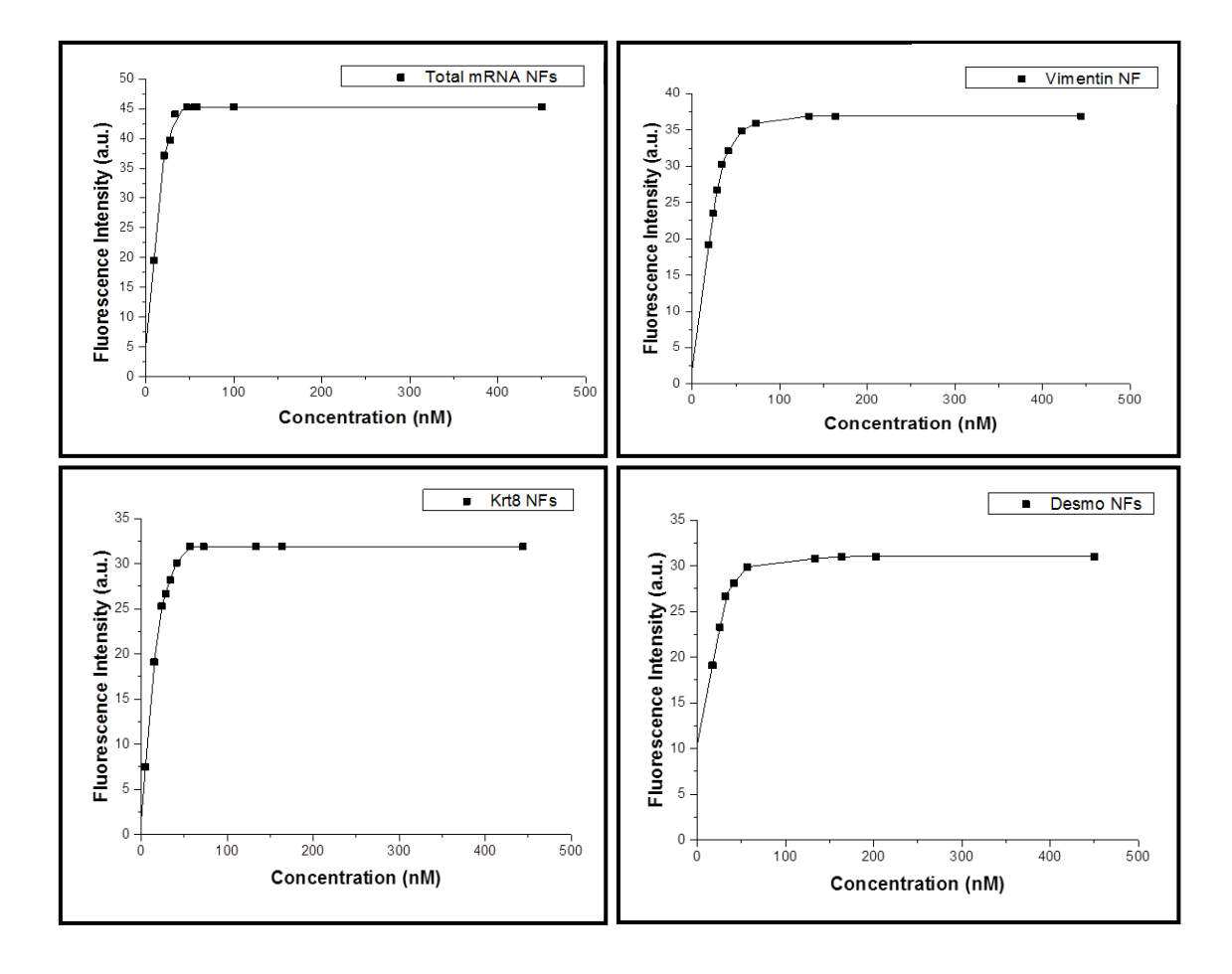


Figure 5.11 Fluorescence emissions of flare strands in response to increasing target concentrations.

The data depicted in **Figure 5.11** shows that all nano-probes show an increase in flare strand fluorescence in response to target concentrations in the nanomolar range in accordance with previous literature reports [4].

5.2 Interactions of nano-probes with cell culture.

Following physicochemical characterisation, stability assays and target specificity determination (see **section 5.1**), nano-probes were incubated *in vitro* with

human lung epithelial cells (16HBE) and fetal lung fibroblasts (MRC-5). These two cell types play very different roles within the human body and thus also display very different characteristics. Whilst epithelial cells form a stationary layer, fibroblasts are highly motile and individual. However, during tumour progression, epithelial cells begin to display fibroblast-specific cell characteristics such as expression of Vimentin and down-regulation of Desmocollin and Cytokeratin 8 [32] (see section 2.6 for theoretical background). These three different epithelial or fibroblast-specific mRNAs were chosen as targets (see section 2.6).

Initially, the expression of Vimentin, Desmocollin and Cytokeratin 8 proteins were visualised using immunofluorescent labelling (section 5.2.1).

5.2.1 Immunofluroescent labelling of cells.

In order to test for expression of Vimentin, Desmocollin and Cytokeratin 8 proteins, cells were fixed and labelled with the corresponding primary antibody and subsequently the fluorophore-labelled (AlexaFluor 546, Invitrogen) secondary antibody for visualisation by confocal microscopy (see **section 3.7** for experimental procedure). Corresponding images are depicted in **Figure 5.12**.

Confocal images show that only fibroblasts display Vimentin expression (**Fig. 5.12 A**). Being an intermediate filament protein, Vimentin can be found all throughout the cytoplasm of mesenchymal cells (e.g. fibroblasts) [33]. Contrastingly, Desmocollin expression was only observed in epithelial cells (**Fig. 5.12 B**). Desmocollin is a protein of the cadherin cell adhesion molecule family, involved in formation of desmosomes for cell-cell interactions [34]. Therefore it can be found only in the cell membrane, as can be seen in **Figure 5.12 B**₂. Cytokeratin 8, another member of the intermediate protein family equally shows expression in epithelial cells only (**Fig. 5.12 C**).

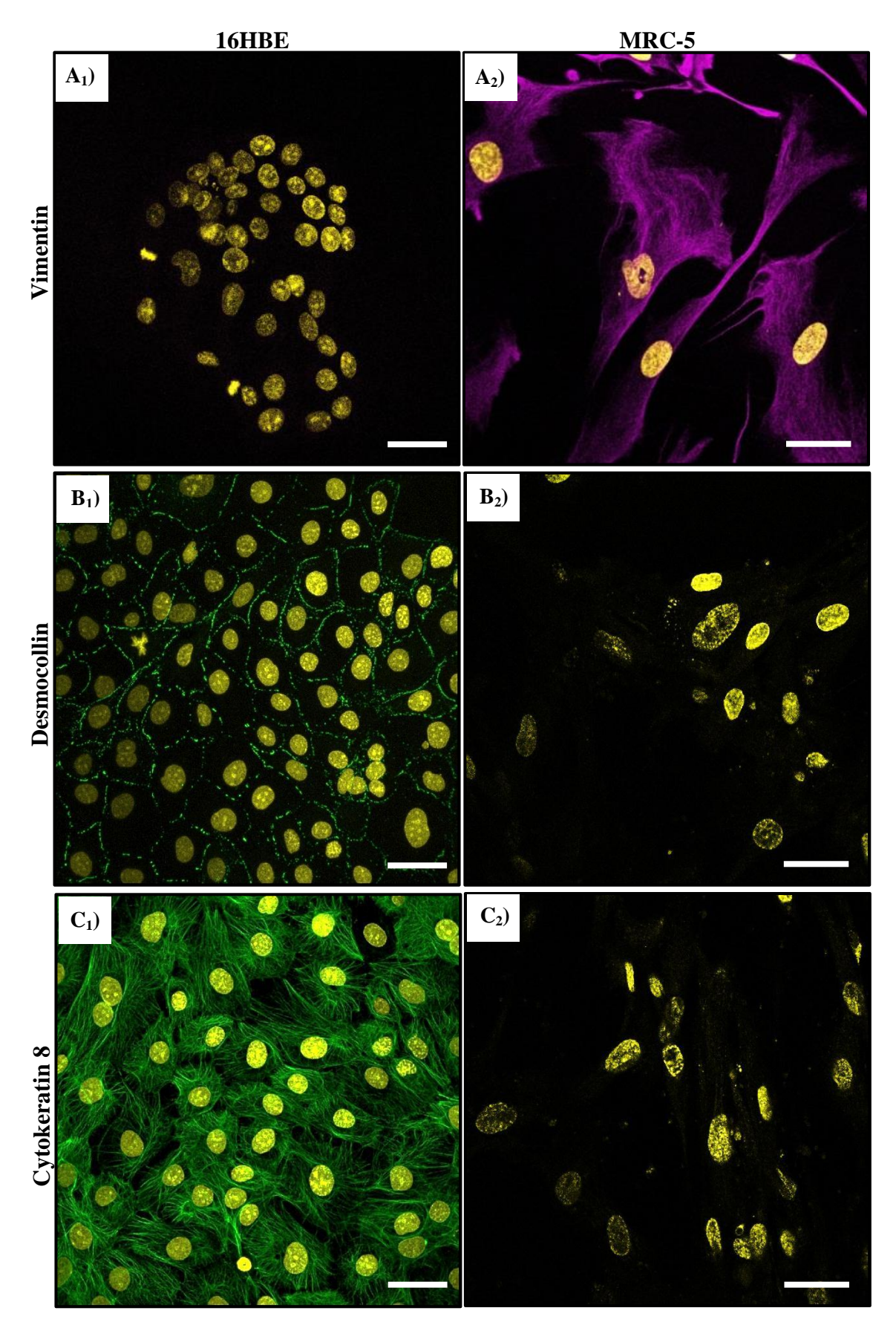


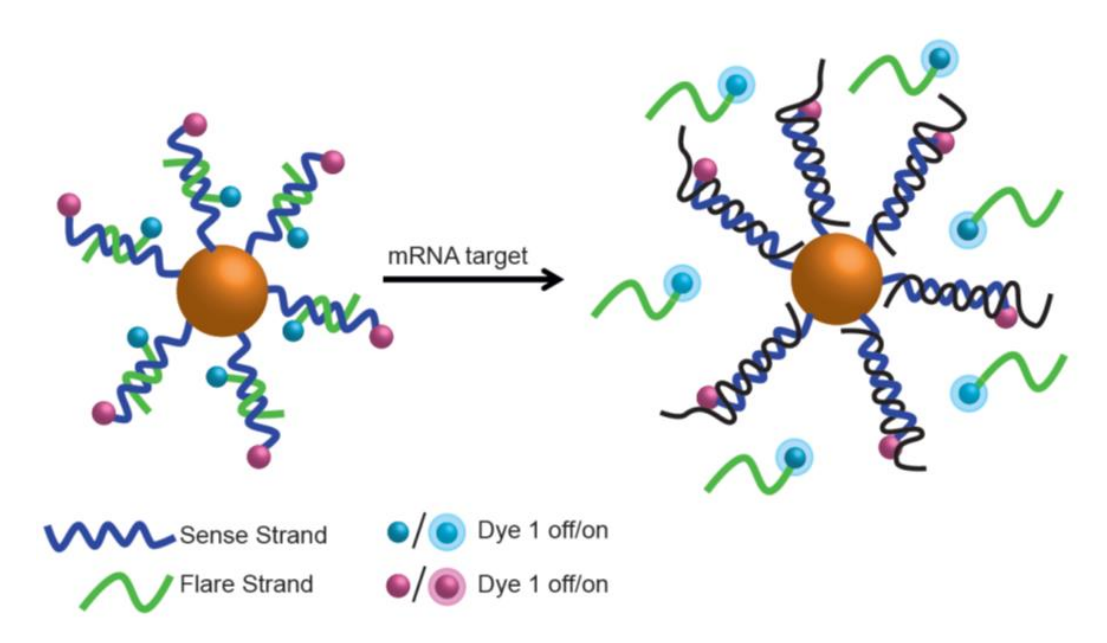
Figure 5.12 Immunofluorescent labelling of 16HBE (1) and fibroblasts (2) with Vimentin **A**), Desmocollin **B**) and Cytokeratin 8 **C**). Nuclei are stained with DAPI. Scale bars are 30 μm.

Similar to Vimentin, expression can be seen in the intracytoplasmic cytoskeleton [35, 36].

5.2.2 Live cell mRNA detection.

Various groups have explored the uptake mechanism of functionalised gold nanoparticles. Many studies have investigated the effects of size, shape and charge of nanoparticles on cellular uptake [8, 37-51]. As such, it is widely known that positively charged species enter cells much more readily than negatively charged ones, due to their electrostatic interactions with the negatively charged lipid membranes [52]. Thus, in many studies, in order to introduce nucleic acid-based systems into cells, complexation with positively charged co-carriers was carried out [53-55]. However, it has been shown that DNA-AuNP conjugates, although highly negatively charged, are taken up by cells in large numbers [40] without the aid of a co-carrier [40, 52].

In order to determine the uptake of nano-probes as well as their target detection capabilities, cells were incubated with different nano-probes. The basic concept of these probes is outlined in **scheme 5.3**



Scheme 5.3 Schematic illustration of the nano-probe for live cell mRNA detection based on DNA-AuNP conjugates.

In the first instance, as a proof of concept, nano-probes for the detection of total mRNA were tested (see **chapters 2** and **3** for theoretical background and experimental procedure). By displaying a sense sequence consisting of polyT, these probes were designed to detect all mature mRNAs *via* their characteristic polyA tail [56]. Confocal microscopy was used to visualise cells (**Figure 5.13**).

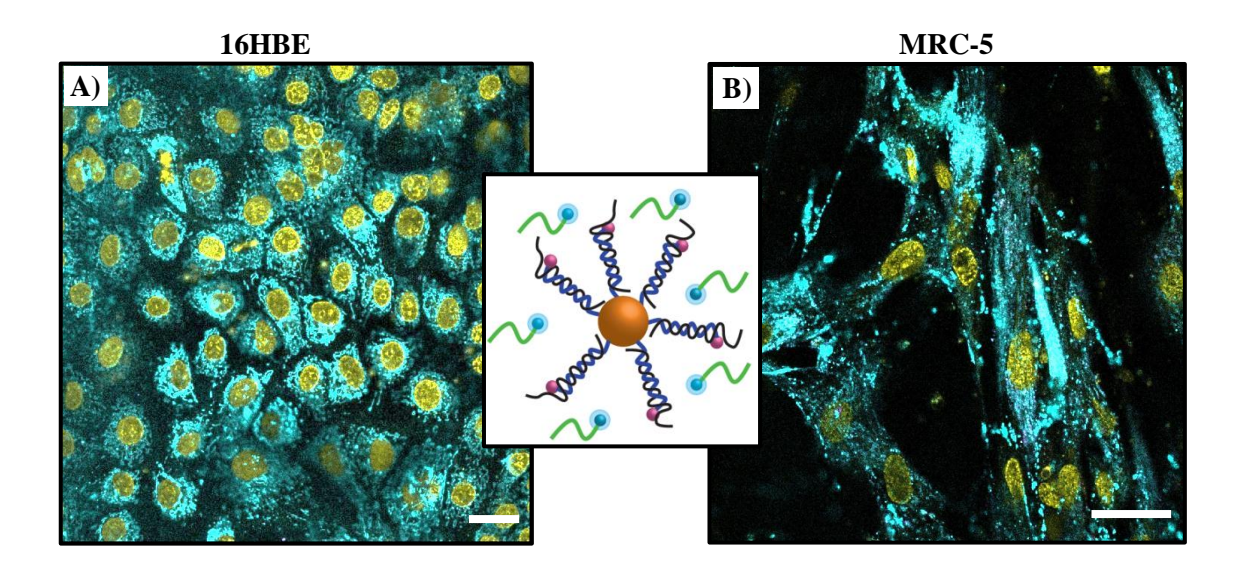


Figure 5.13 Confocal microscopy images showing the successful detection of total mRNA in **A**) epithelial cells (16HBE) and **B**) fibroblasts (MRC-5). Nuclei are stained with Hoechst 33342 (Invitrogen). Scale bars are 30 μ m.

Confocal images revealed no Cy3 fluorescence (pink) from the sense strands in either sample, indicating that the DNA on the nanoprobes was not subject to degradation. Furthermore a bright fluorescence signal of the flare strand (Cy5, blue) could be observed throughout the cytoplasm of epithelial cells **A**) as well as fibroblasts **B**). This suggested that mRNA detection was possible.

Following successful initial live cell experiments, probes were tested for specificity. Accordingly, Vimentin, Desmocollin and Cytokeratin 8 nano-probes were incubated with both 16HBE and MRC5 cell lines as before. Confocal microscopy was used to visualise cells (**Figure 5.14**).

As before no fluorescence from the respective sense strands could be observed, indicating that sense DNA on the nanoparticle remained attached and was not subject to degradation. As can be seen from **Figure 5.14 A**₂, probes for the detection of Vimentin mRNA displayed fluorescence in the fibroblasts only. Our observations were in agreement with the previously conducted immunofluorescent studies (see **section 5.2.1**), as epithelial cells do not express Vimentin [57]. On the other hand, the probes that detect Desmocollin and Cytokeratin 8 mRNAs displayed activity in epithelial cells only (**Fig. 5.14 B**₂ and **C**₂).

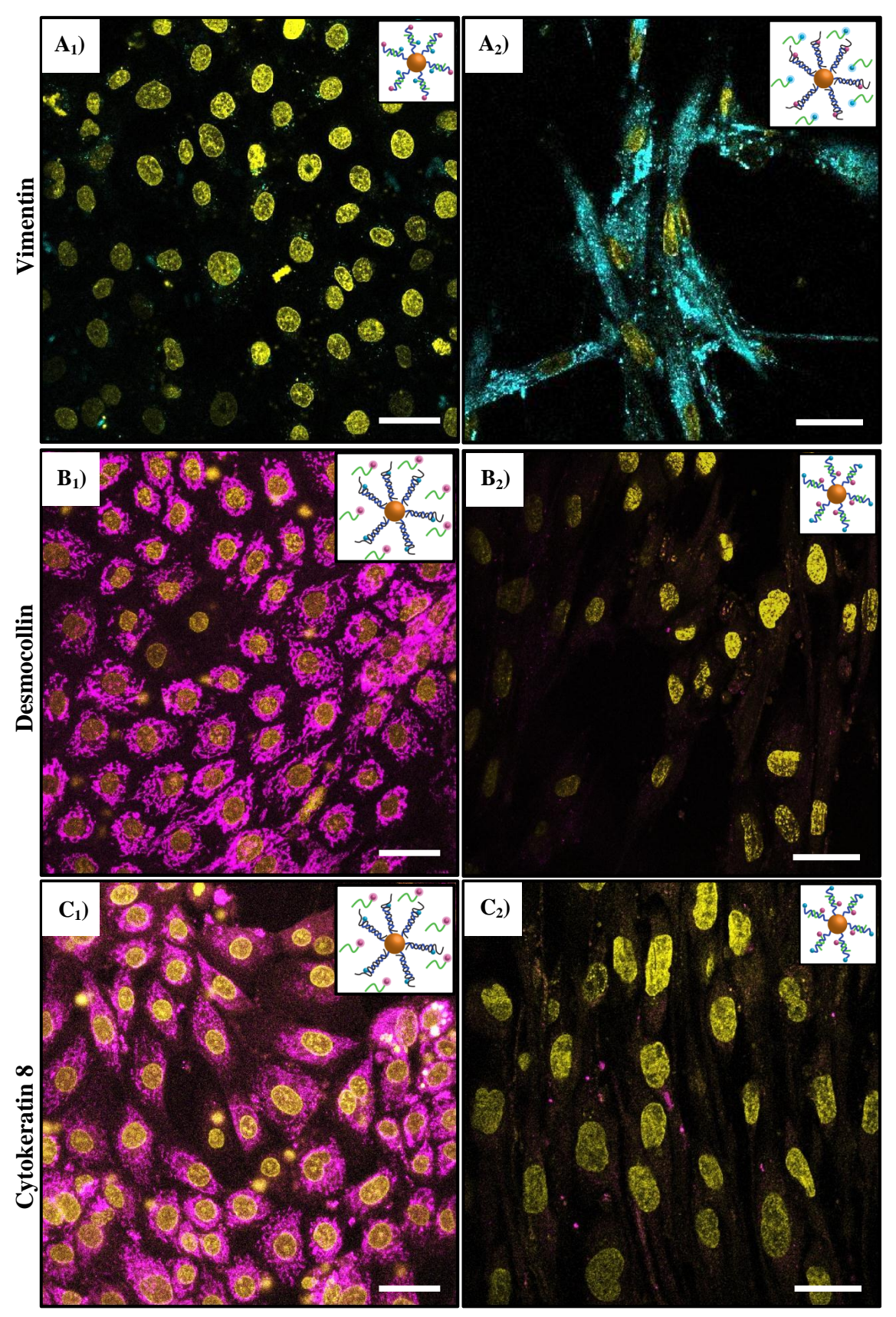


Figure 5.14 Confocal microscopy images of live cells (1) 16HBE epithelial cells, 2) MRC-5 fibroblasts) incubated with mRNA detection probes. A) Vimentin detection Cy5, blue, B) Desmocollin detection, Cy3, pink and C) Cytokeratin 8 detection, Cy3, pink. Nuclei are stained with Hoechst 33342 (Invitrogen). Scale bars are 30 μ m.

A confocal cross-sectional image displayed in **Figure 5.15** confirmed that fluorescence was indeed localized within the cytoplasm of the cells, rather than the cell membrane.

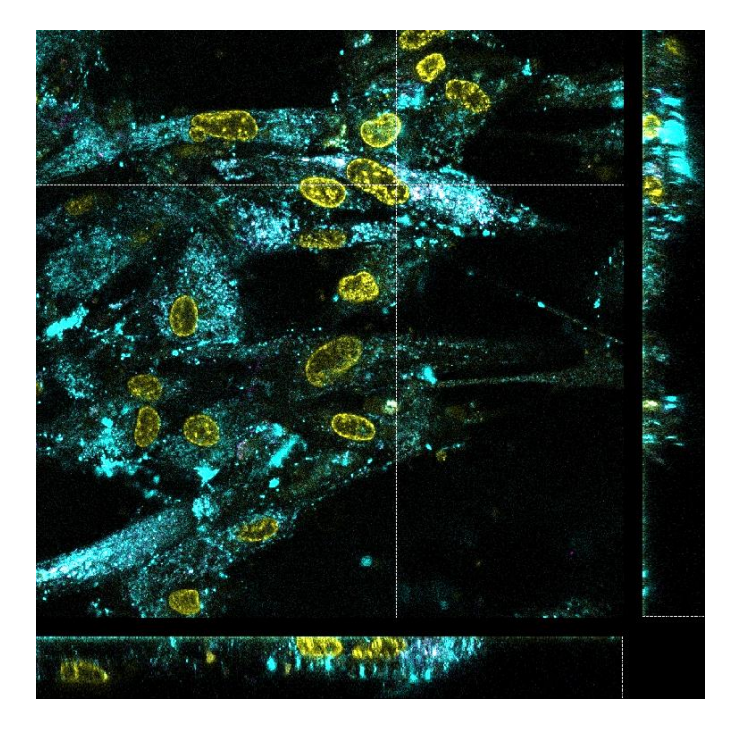


Figure 5.15 Confocal cross-section image of Vimentin nano-probes in MRC-5. The cross-hairs mark the point of interest; X and Y sections are shown on the right hand side and the bottom of the image. Nuclei are stained with Hoechst 33342 (Invitrogen).

An unexpected observation was the appearance of distinct localization of the fluorescence signal in epithelial cells. Both **Fig.5.13 A** and **5.14 B**₁/C₁ showed fluorescence with distinct localization, potentially corresponding to association with mitochondria [58] or the endoplasmatic reticulum [59] (see **Appendix II** for additional images at higher magnification). A study by Bao *et al.* showed that 2'-deoxy and 2'-O-methyl oligonucleotides labelled with Cy dyes displayed fluorescence signal colocalization with mitochondria [60]. They suggested that mitochondrial membrane potential mediates this accumulation which is furthermore dependent on the dye. While both Cy3 and Cy5-labelled oligonucleotides displayed mitochondrial co-localization,

oligonucleotides functionalized with anionic dyes such as the Alexa Flour dyes displayed perinuclear localization [60]. It is therefore likely that Cy dye-labelled flare strands, after release from the particle are trapped in the inner mitochondrial membrane, resulting in the observed fluorescence signal localization.

In order to investigate the optimum incubation time for maximum fluorescence, epithelial cells were incubated with Desmocollin nano-probes and subsequently imaged for 18 h by fluorescence microscopy (see **chapter 3** for experimental protocol). Representative images are depicted in **Figure 5.16**.

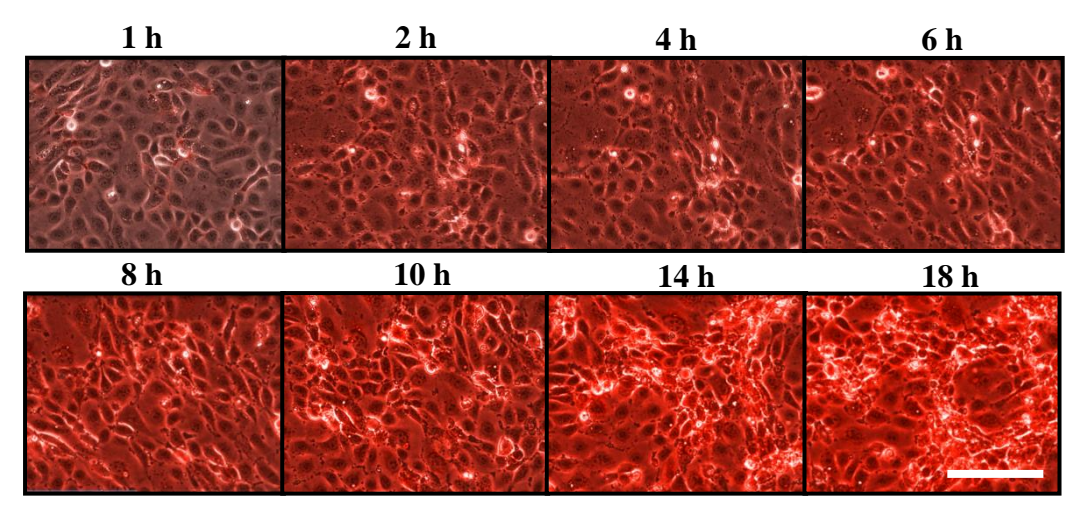


Figure 5.16 Fluorescence time-lapse study on epithelial cells incubated with Desmocollin nano-probes (Cy3 fluorescence). Scale bar is 100 µm.

From the time-lapse images one can see that the maximum fluorescence signal was achieved after 14 to 18 h of incubation. Therefore an incubation time of 18 h was chosen for all cell culture-nano-probe studies.

5.2.3 Transmission electron microscopy of cells incubated with nanoprobes.

To visualise the intracellular location of nano-probes, cells were incubated with total mRNA detection probes for 2, 4, 6 and 18 h and subsequently processed for TEM

thin sectioning (see **section 3.7** for experimental procedure). Representative TEM micrographs are depicted in **Figure 5.17**.

The depicted images show that 2 h after incubation, particles were mostly localized on the cell periphery or being endocytosed (Fig. 5.17 A_1). However, few particles were found in the cytosol (indicated by a red arrow, Fig. 5.17 A₂). The mechanism by which particles are able to escape endosomal compartmentalisation is still under intensive investigation by various research groups to date [17] and will also with respect to this project be the subject of future work. After 4 h most particles were found to be encapsulated within endosomes and late endosomes/ multivesicular bodies (MVB) [61] (Fig. 5.17 B₂). However, as before some particles were found in the cytosol, not encapsulated in a cellular vesicle (Figure 5.17 B₁). After 6 h and 18 h particles were found almost exclusively in cellular vesicles such as endosomes or MVBs. Interestingly, particles were never found inside lysosomes, in accordance with previous literature findings [17]. The reason for this remains so far unknown. As can be seen from the TEM images, the maximum number of particles appeared to be located intracellularly after 18 h (Fig.5.17 D) [62]. However, as only very thin sections of cells were visualised here, it was not possible to quantify uptake with a high degree of accuracy. For this, inductively-coupled plasma mass spectrometry or atom emission spectrometry will be utilized in future work.

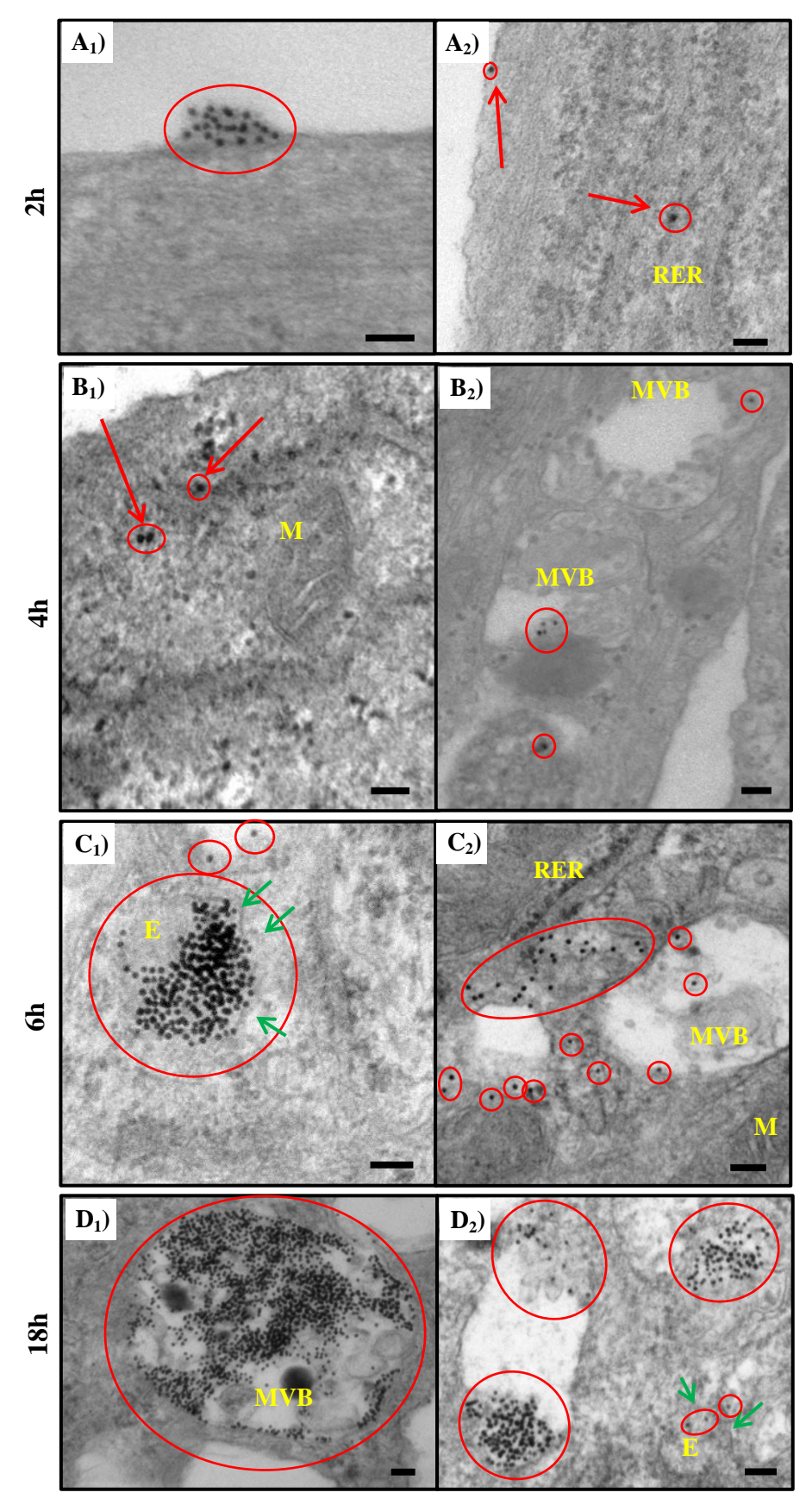


Figure 5.17 Transmission electron micrographs of cells incubation with nano-probes. Scale bars are 100 nm. Red arrows indicate NPs in the cytosol. Green arrows indicate endosomal barriers. RER = rough endoplasmatic reticulum; MVB = multivesicular body; E = endosome, M = mitochondrion.

5.2.4 Viability assays for cells incubated with nano-probes.

The excellent biocompatibility of DNA-gold nanospheres presents one of the reasons for their extensive use in biomedical studies [1-3, 6, 40, 44, 49, 63-68]. Several studies showed that gold nanoparticles functionalized with oligonucleotides are not cytotoxic [2-4, 6, 16, 65]. Accordingly, Mirkin *et al.* did not observe any toxicity of their nano-flares in cell antisense experiments [6]. In another study, Tang *et al.* conducted MTT assays [69] to assess the cell viability with their multiplexed nanoflares [4]. The authors reported that within concentrations of around 5 nM and an incubation time of up to 48 h, the cell viability was always greater than 85 %. Likewise, an MTT assay carried out by Gu and co-workers revealed that the viability of MCF-5 and C6 mouse glioma cell lines was not affected by the treatment with their nano-sensor [70]. The cytotoxicity of the nano-probes utilized in this study with respect to the two different cell types used was hence investigated utilizing a trypan blue dye-exclusion assay [71] (see section 3.7 for experimental procedure). Cells were incubated with different nano-probes for 18 h and the cell viability was subsequently determined. The results for the dye-exclusion assays are shown in Figure 5.18.

It can be observed that within the employed conditions (concentration of nano-probes: 1.5 nM, incubation time 18 h, (~1.4 pmol of probes per 100.000 cells, see **section 3.5**) the cell viability was not affected in accordance with previous findings [1-4, 16, 65, 70]. Further studies involving higher concentrations and varying incubation times in order to develop a cytotoxicity profile will be the subject of future work.

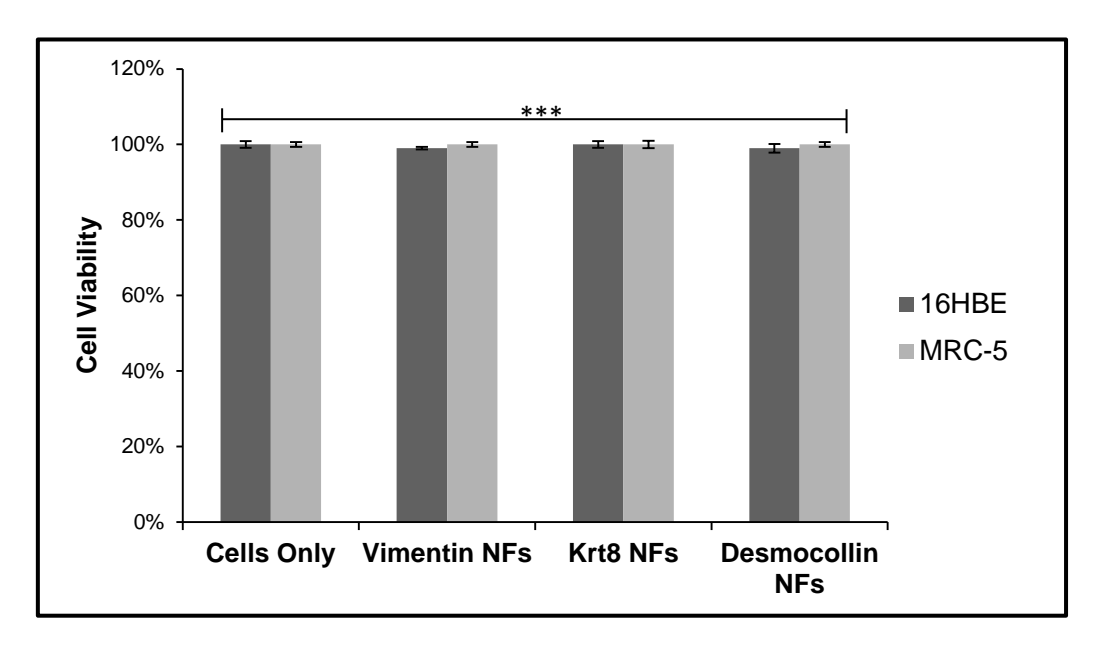


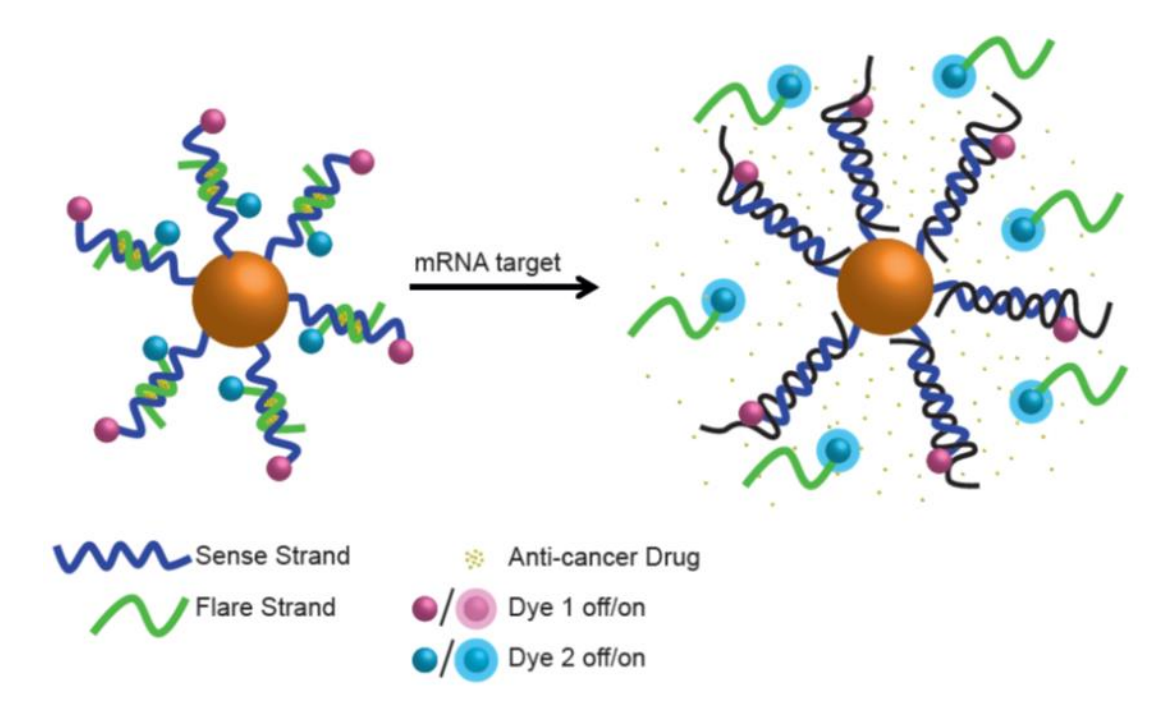
Figure 5.18 Viability assay for cells incubated with different nano-probes. (n=3, ***p < 0.01 for a one-tailed t test).

The high target specificity, good biocompatibility and bio-stability of nanoprobes discussed in **section 5.1** and **5.2** display their excellent capabilities of live cell mRNA detection agents. The potential to further develop these probes into multiplexed theranostic agents will thus be discussed in the following sections.

5.3 Nano-probes for targeted drug delivery.

Various studies have recently shown that gold nanoparticles with varying surface capping can act as efficient drug delivery vehicles [72-75]. For example, AuNPs conjugated to cytotoxic platinum anti-cancer compounds showed promising properties as chemotherapeutic agents [76-78]. Furthermore gold nanospheres and rods have been shown to effectively deliver anthracycline drugs for chemotherapeutic applications [79-82]. Taking advantage of the high target specificity of the nano-probes described in section 5.1 and 5.2, an extension of their applicability towards a 'theranostic' probe was

investigated. The DNA intercalating, fluorescent anti-cancer drug Doxorubicin (DOX) was utilized (see **scheme 5.4**. Also see **Figure 2.3** for chemical structure of DOX).



Scheme 5.4 Illustration of the multi-functional nano-probe capable of mRNA detection and simultaneous targeted drug delivery.

In the following sections, the formation and physicochemical characterisations of DOX-loaded Vimentin nano-probes will be discussed (**section 5.3.1**). Furthermore their interactions with cell cultures as well as targeted drug release capabilities will be shown (**section 5.3.2**).

5.3.1 Physicochemical characterisation and stability assays of drug-loaded Vimentin nano-probes.

Vimentin nano-probes were loaded with doxorubicin according to the experimental procedure described in **section 3.3**. In order to visualize the success of doxorubicin intercalation, fluorescence melting curves were obtained (**Fig. 5.19**).

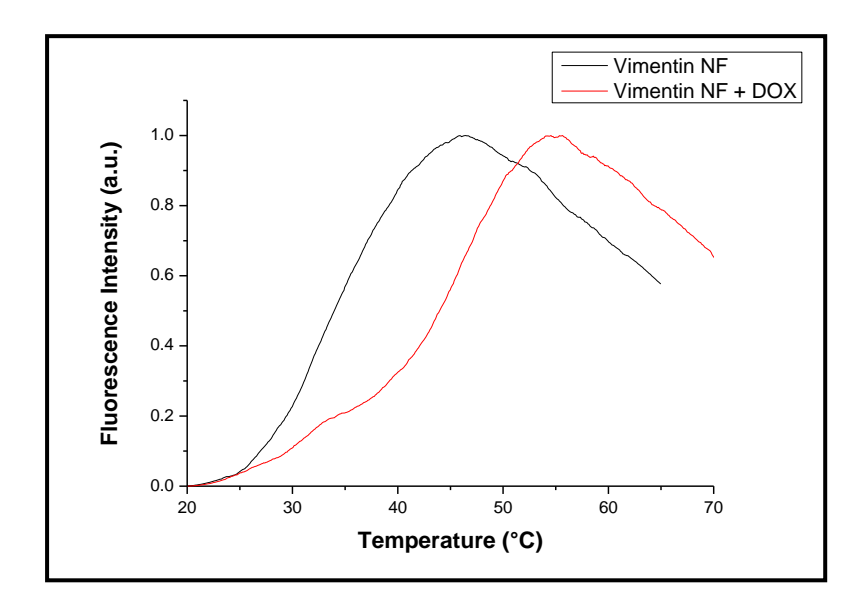


Figure 5.19 Fluorescence melting curves of Vimentin nano-flares and Doxorubicin-loaded Vimentin nano-flares.

Drug intercalation results in a stabilization of the DNA duplex. Crystal structures revealed that the cationic daunosamine sugar unit of DOX locates in the minor groove of a DNA duplex. This results in decreased electrostatic repulsion between DNA strands in the duplex. The aromatic chromophore aglycone unit of the drug interacts with the aromatic DNA bases via increased van der Waals interactions [79, 83]. These stabilization interactions can be assessed via the DNAs melting profile. Figure 5.19 shows a clear shift of $\sim +10$ °C in the melting profile of Vimentin nanoprobes after drug incorporation (red graph). As previously shown by Drabowiak and coworkers, the increased melting temperature gave a good indication of successful incorporation of doxorubicin [79].

Having established that DOX can be successfully intercalated into Vimentin nano-probes, a subsequent step was to study their stability with respect to drug retention.

Studies have shown that the fluorescence of DOX can be quenched by intercalation into a DNA duplex [84] as well as by being located in close proximity to a gold nanoparticle [85]. This property was utilized to investigate the stability of DOX-loaded probes. Doxorubicin fluorescence in the supernatant of drug-loaded Vimentin nano-probes was monitored for 24 h at 37 °C. **Figure 5.20** shows the results of this study.

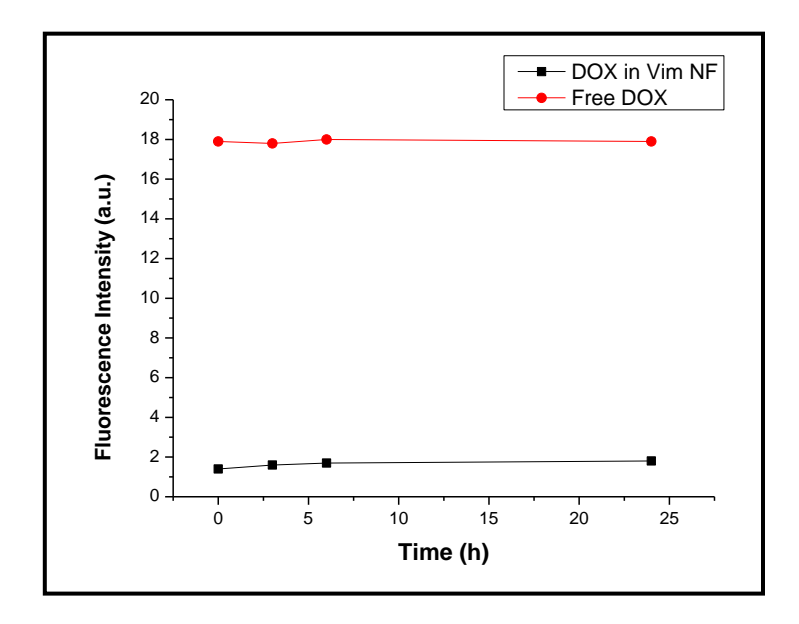


Figure 5.20 Fluorescence time-course measuring the potential leaking of doxorubicin from the Vimentin nano-flares (black graph). For comparison, fully released doxorubicin at the same concentration was measured also (red graph).

The obtained fluorescent data (black line) was compared to the fluorescence of doxorubicin after liberation from the nano-probe (achieved *via* DNA melting. Concentrations of nano-probes and DOX loading was ensured to be constant). As can be seen from the data, no significant increase in fluorescence occurred after 24 h, suggesting that there was no leaking of DOX from the nano-probes.

In order to be considered as therapeutic drug delivery agents, the loading capacity of the probes must be tunable, depending on individual requirements. As DOX

intercalates into dsDNA, varying the number of duplexes formed on the nanoparticle surface should enable controlled drug-loading (see **Appendix II**).

Making once again use of the inherent fluorescent properties of DOX, drug-loading as a function of varying duplex numbers was investigated by fluorescence spectroscopy (see **section 3.5** for experimental details). **Figure 5.21 A** shows a calibration curve for concentration-dependent DOX fluorescence. Fluorescence spectra of DOX after liberation from nano-probes are shown in **Figure 5.21 B**.

From these data it was possible to determine that the number of DOX molecules per nano-probe could be finely tuned by varying the number of duplexes on the nano-probe (39 \pm 3 for 40x duplex, 57 \pm 4 for 60x duplex and 73 \pm 2 for 80x duplex. See **Appendix II** for calculations).

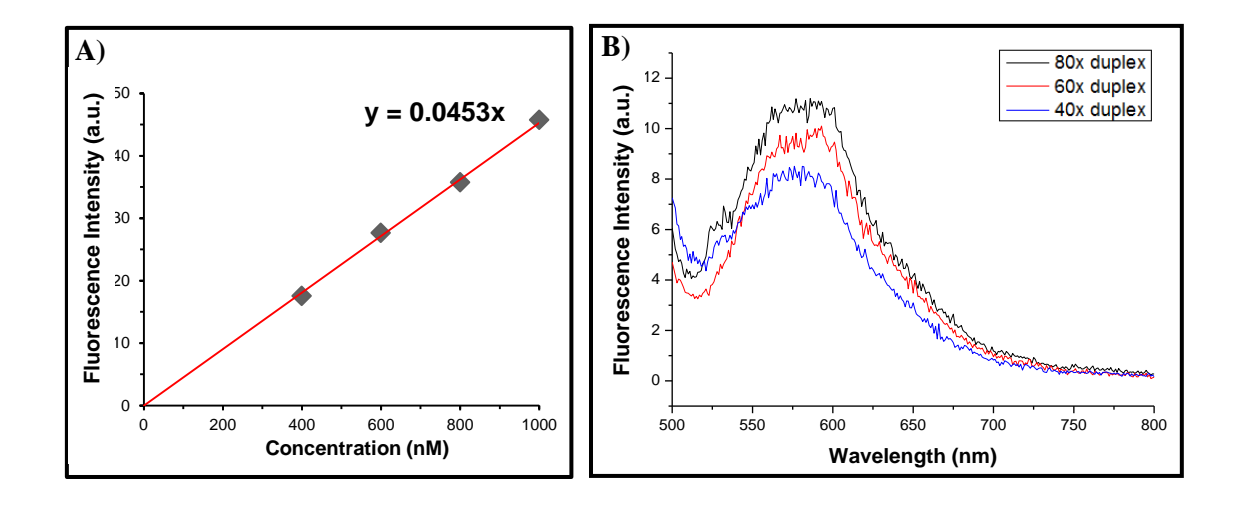


Figure 5.21 A) Fluorescence calibration curve for concentration-dependent doxorubicin fluorescence. **B)** Varying DOX fluorescence (concentration) with varying flare strand amounts.

5.3.2 Interactions of drug-loaded Vimentin nano-probes with cell culture.

Following physicochemical characterization (see **section 5.3.1**), the interactions of drug-loaded Vimentin nano-probes with 16HBE and MRC-5 cells were explored. In **section 5.2** it was shown that Vimentin nano-probes exhibit activity exclusively in the

Vimentin-expressing fibroblast cell line. In order to investigate if drug-loaded probes retained target binding capabilities and target specificity *in vitro*, they were incubated with both 16HBE and MRC-5 cells (see **section 3.7** for experimental details). Confocal microscopy was utilized to visualise nano-probe cell interactions (see **Figure 5.22**).

The confocal images revealed no obvious fluorescence corresponding to DOX or the flare strand in the epithelial cell line (**Fig. 5.22 A**). This suggested that nanoprobes remained 'silent' with doxorubicin being held within the probes. As epithelial

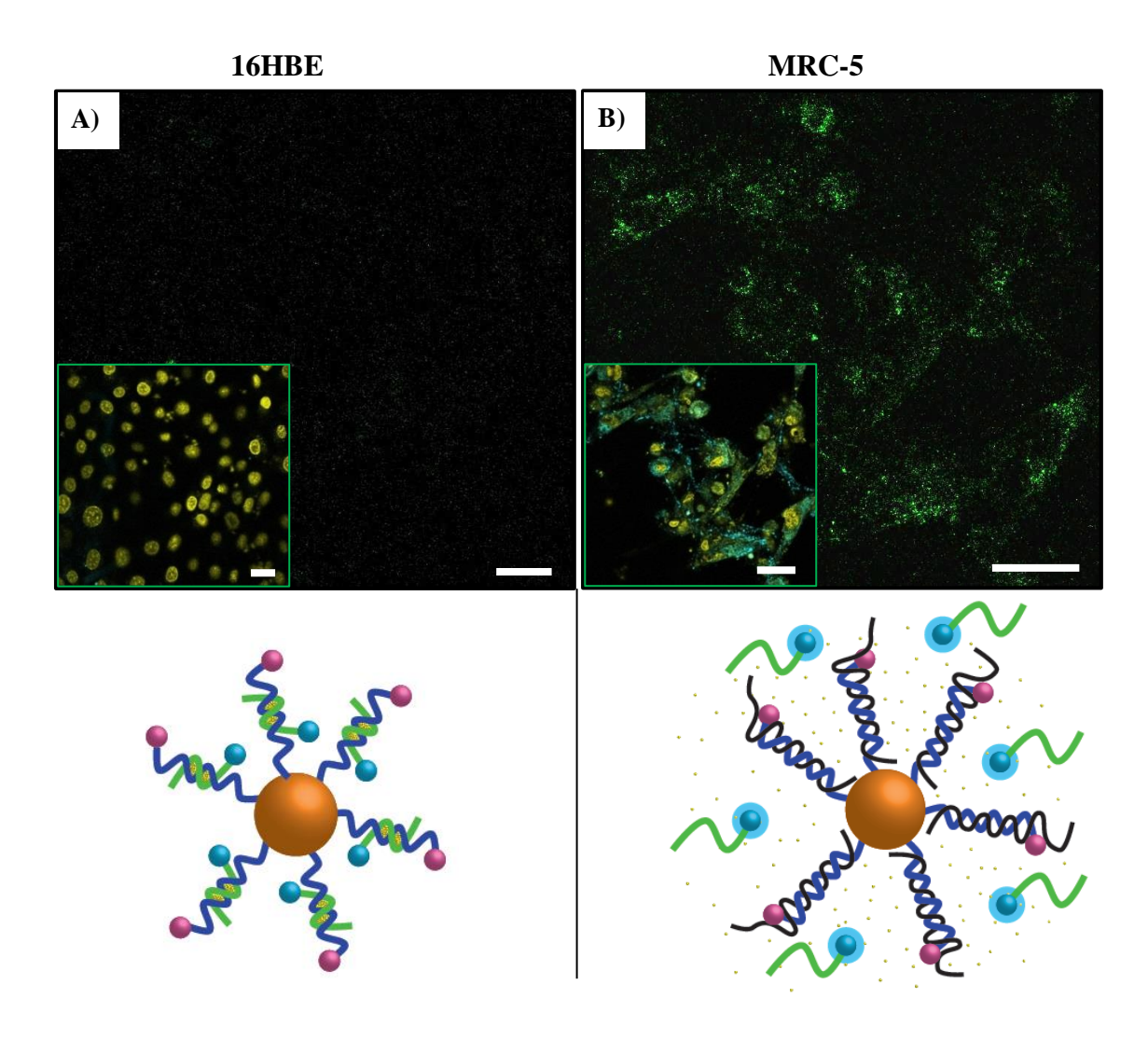


Figure 5.22 Confocal microscopy images of **A**) 16HBE epithelial cells and **B**) fetal lung fibroblasts (MRC-5) after 18h incubation with doxorubicin-loaded Vimentin nano-flares. The large images show doxorubicin fluorescence only (green) while the small inset images show the full image with stained nuclei (yellow) and flare fluorescence (cyan), see **Appendix II** for larger images. Nuclei were stained with Hoechst 33342 (Invitrogen). Scale bars are 30 μm.

cells do not express the target mRNA (Vimentin), this result implies that nano-probes had retained their target specificity. Contrastingly, a distinct DOX fluorescence signal as well as flare strand fluorescence was observed in MRC-5 fibroblasts (**Fig. 5.22 B**). This implies that despite their increased stability, drug-loaded Vimentin nano-probes not only retained their target binding capability and specificity, but also delivered the drug in a target-specific manner. This finding was in accordance with recently published results by Tang *et al.* utilizing drug-loaded molecular beacon-AuNP probes for tumour targeting [82].

As can be seen from **Figure 5.22**, DOX fluorescence is visible throughout the cells' cytoplasm, but not the nucleus. Within a cell, DNA is mainly arranged into chromosomes and localized almost exclusively to the nucleus (with exceptions of mitochondrial DNA) [86]. As discussed previously, upon DNA intercalation, DOX fluorescence is quenched [83, 84, 87]. Thus, any DOX localized in the nucleus or the mitochondria would be invisible by confocal microscopy.

5.3.2.1 Viability assay of cells incubated with drug-loaded Vimentin nanoprobes.

A trypan blue dye-exclusion assay was utilized to give insight into whether DOX delivered *via* the Vimentin nano-probes induced cytotoxicity in the tested cell lines. Both 16HBE epithelial cells and MRC-5 fibroblasts were incubated with drugloaded Vimentin nano-probes containing varying amounts of DOX (at a steady NP concentration, see **section 3.7** for experimental procedures). After 18 h, cells were harvested and visualised using the trypan blue live/dead assay [71]. Representative results for both cell types are shown in **Figure 5.23**.

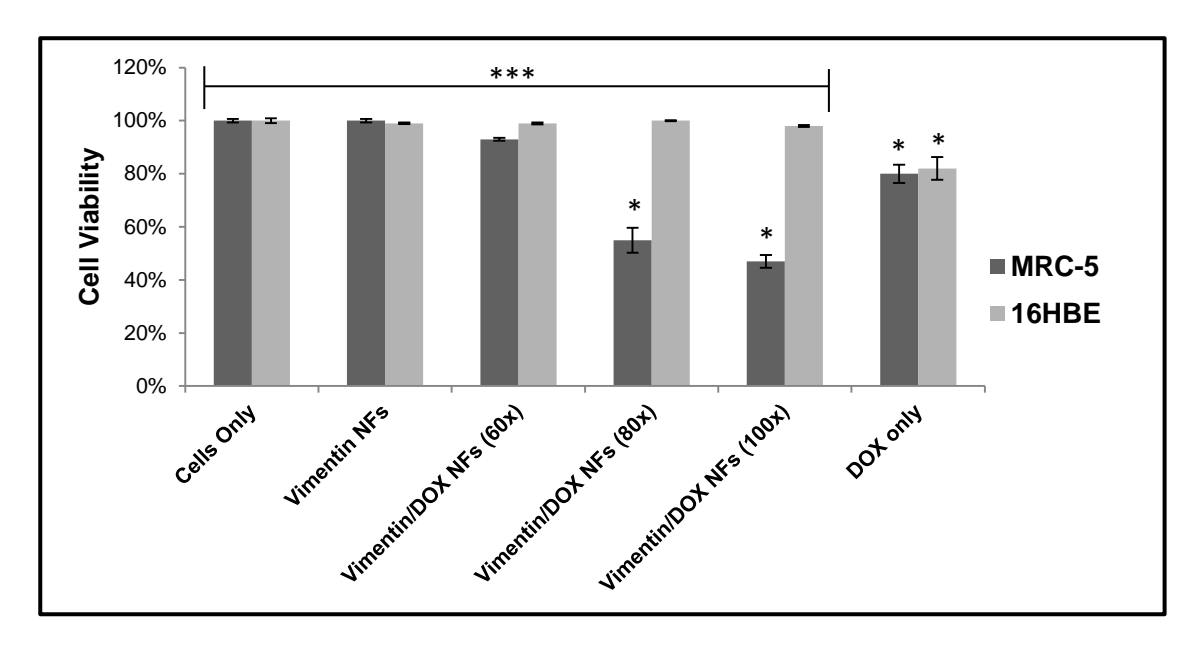


Figure 5.23 Viability assay of 16HBE and MRC-5 cells incubated with Doxorubicin only (400 pmol) as well as Vimentin nano-probes (1 pmol) with varying amounts of drug-loading. Mean SEM, n=3, ***p < 0.001, ** p < 0.01, * p < 0.1 for a one-tailed t test.

The assay results imply that while Vimentin nano-probes on their own displayed no significant cytotoxicity in either cell line, drug-loaded probes exhibited increasing cytotoxicity with increasing drug-loading for MRC-5 fibroblasts only.

Furthermore, doxorubicin delivered on its own at a dose $3.3 \times$ higher than that found in the highest nano-probe loading (400 pmol vs. 120 pmol), exhibited a two-fold lower cytotoxicity. Dabrowiak and co-workers suggested in their study that DOX concentrations of more than 5 μ M were required to achieve a cytotoxicity greater than 50% [88]. Here the 50% cytotoxicity is achieved with 120 pmol of DOX (assuming that all DOX was released from the probes), suggesting a vast increase in delivery efficiency. This thus suggested that the nano-probes employed here possess a great potential for future applications in targeted drug delivery to minimize toxic side-effects.

In order to meet the demands in biomedicine, even more advanced multi-role nano-probes will have to be developed. To answer these requirements, potential novel probes based on nanoparticle assemblies will be introduced in **chapter 6**.

5.4 References

- 1. Prigodich, A.E., et al., *Multiplexed nanoflares: mRNA detection in live cells*.

 Anal Chem, 2012. **84**(4): p. 2062-6.
- 2. Prigodich, A.E., et al., *Nano-flares for mRNA Regulation and Detection*. ACS Nano, 2009. **3**(8): p. 2147-2152.
- 3. Seferos, D.S., et al., *Nano-flares: Probes for transfection and mRNA detection in living cells.* J Am Chem Soc, 2007. **129**(50): p. 15477-15479.
- 4. Li, N., et al., A Multicolor Nanoprobe for Detection and Imaging of Tumor-Related mRNAs in Living Cells. Angewandte Chemie-International Edition, 2012. **51**(30): p. 7426-7430.
- 5. Heuer-Jungemann, A., et al., Gold nanoparticles and fluorescently-labelled DNA as a platform for biological sensing. Nanoscale, 2013. **5**(20): p. 9503-9510.
- 6. Rosi, N.L., et al., Oligonucleotide-modified gold nanoparticles for intracellular gene regulation. Science, 2006. **312**(5776): p. 1027-1030.
- 7. Kang, K.A., et al., Fluorescence Manipulation by Gold Nanoparticles: From Complete Quenching to Extensive Enhancement. Journal of Nanobiotechnology, 2011. 9.
- 8. Wu, Z.S., et al., Optical detection of DNA hybridization based on fluorescence quenching of tagged oligonucleotide probes by gold nanoparticles. Analytical Biochemistry, 2006. **353**(1): p. 22-29.
- 9. Huang, Q., et al., Multiplex Fluorescence Melting Curve Analysis for Mutation

 Detection with Dual-Labeled, Self-Quenched Probes. Plos One, 2011. 6(4).

- Azbel, M.Y., DNA SEQUENCING AND MELTING CURVE. Proceedings of the National Academy of Sciences of the United States of America, 1979. 76(1): p. 101-105.
- 11. Bonilla, J.V. and G.S. Srivatsa, *Handbook of Analysis of Oligonucleotides and Related Products*. 2011: Taylor & Francis.
- 12. Didenko, V.V., Fluorescent Energy Transfer Nucleic Acid Probes: Designs and Protocols. 2006: Humana Press.
- 13. Meister, A. and M.E. Anderson, *Glutathione*. Annual Review of Biochemistry, 1983. **52**: p. 711-760.
- 14. Lushchak, V.I., Glutathione Homeostasis and Functions: Potential Targets for Medical Interventions. Journal of Amino Acids, 2012. **2012**: p. 26.
- Li, Z., et al., Multiple thiol-anchor capped DNA-gold nanoparticle conjugates.
 Nucleic Acids Research, 2002. 30(7): p. 1558-1562.
- 16. Pan, W., et al., Multiplexed Detection and Imaging of Intracellular mRNAs

 Using a Four-Color Nanoprobe. Analytical Chemistry, 2013. 85(21): p. 10581
 10588.
- 17. Wu, X.C.A., et al., *Intracellular Fate of Spherical Nucleic Acid Nanoparticle Conjugates*. Journal of the American Chemical Society, 2014. **136**(21): p. 7726-7733.
- Suck, D., *DNA recognition by DNase I*. Journal of Molecular Recognition, 1994.7(2): p. 65-70.
- 19. Kewalramani, S., et al., Counterion Distribution Surrounding Spherical Nucleic Acid-Au Nanoparticle Conjugates Probed by Small-Angle X-ray Scattering. Acs Nano, 2013. **7**(12): p. 11301-11309.

- Zwanikken, J.W., et al., Local Ionic Environment around Polyvalent Nucleic Acid-Functionalized Nanoparticles. The Journal of Physical Chemistry C, 2011.
 115(33): p. 16368-16373.
- 21. Melgar, E. and D.A. Goldthwait, *ENZ DNA NUCLEASES II THE EFFECTS OF METALS ON THE MECHANISM OF ACTION OF ENZ DNASE I ESCHERICHIA-COLI*. Journal of Biological Chemistry, 1968. **243**(17): p. 4409-4416.
- 22. Pellegrino, T., et al., *Gel electrophoresis of gold-DNA nanoconjugates*. Journal of Biomedicine and Biotechnology, 2007.
- 23. Suck, D. and C. Oefner, Structure of DNase I at 2.0 [angst] resolution suggests a mechanism for binding to and cutting DNA. Nature, 1986. **321**(6070): p. 620-625.
- 24. Evans, C.J. and R.J. Aguilera, *DNase II: genes, enzymes and function*. Gene, 2003. **322**(0): p. 1-15.
- 25. Ehrlich, S.D., G. Torti, and G. Bernardi, *Acid deoxyribonuclease. IX. 5'-Hydroxy-terminal and penultimate nucleotides of oligonucleotides obtained from calf thymus deoxyribonucleic acid.* Biochemistry, 1971. **10**(11): p. 2000-2009.
- 26. Townend, R. and G. Bernardi, *STUDIES ON ACID DEOXYRIBONUCLEASE*.10. MOLECULAR WEIGHT IN DENATURING SOLVENTS. Archives of Biochemistry and Biophysics, 1971. **147**(2): p. 728-&.
- 27. Pinto-Gonzalez Howell, D., et al., *Deoxyribonuclease II is a Lysosomal Barrier to Transfection*. Mol Ther, 2003. **8**(6): p. 957-963.
- 28. Albanese, A., et al., Secreted Biomolecules Alter the Biological Identity and Cellular Interactions of Nanoparticles. ACS Nano, 2014. **8**(6): p. 5515-5526.

- 29. Chanana, M., et al., Physicochemical Properties of Protein-Coated Gold Nanoparticles in Biological Fluids and Cells before and after Proteolytic Digestion. Angewandte Chemie-International Edition, 2013. 52(15): p. 4179-4183.
- 30. Huhn, D., et al., Polymer-Coated Nanoparticles Interacting with Proteins and Cells: Focusing on the Sign of the Net Charge. Acs Nano, 2013. **7**(4): p. 3253-3263.
- 31. Mie, G., *Beiträge zur Optik trüber Medien, speziell Kolloidaler Metallösungen.*Annalen der Physik, 1908. **25**(4): p. 377-445.
- 32. Lee, J.M., et al., *The epithelial–mesenchymal transition: new insights in signaling, development, and disease.* The Journal of Cell Biology, 2006. **172**(7): p. 973-981.
- 33. Katsumoto, T., A. Mitsushima, and T. Kurimura, *The role of the vimentin intermediate filaments in rat 3Y1 cells elucidated by immunoelectron microscopy and computer-graphic reconstruction*. Biology of the Cell, 1990. **68**(2): p. 139-146.
- 34. Mechanic, S., et al., *Desmocollins Form a Distinct Subset of the Cadherin Family of Cell-Adhesion Molecules*. Proceedings of the National Academy of Sciences of the United States of America, 1991. **88**(10): p. 4476-4480.
- 35. Barak, V., et al., *Clinical utility of cytokeratins as tumor markers*. Clinical Biochemistry, 2004. **37**(7): p. 529-540.
- 36. Buccheri, G. and D. Ferrigno, *Lung tumor markers of cytokeratin origin: an overview*. Lung Cancer, 2001. **34, Supplement 2**(0): p. S65-S69.
- 37. Mahmoudi, M., et al., *Interaction of stable colloidal nanoparticles with cellular membranes*. Biotechnology Advances, 2014. **32**(4): p. 679-692.

- 38. Bartczak, D., et al., Interactions of Human Endothelial Cells with Gold Nanoparticles of Different Morphologies. Small, 2012. 8(1): p. 122-130.
- 39. Chithrani, B.D. and W.C.W. Chan, *Elucidating the mechanism of cellular* uptake and removal of protein-coated gold nanoparticles of different sizes and shapes. Nano Letters, 2007. **7**(6): p. 1542-1550.
- 40. Giljohann, D.A., et al., Oligonucleotide loading determines cellular uptake of DNA-modified gold nanoparticles. Nano Letters, 2007. **7**(12): p. 3818-3821.
- 41. Bartczak, D., et al., Receptor-Mediated Interactions between Colloidal Gold Nanoparticles and Human Umbilical Vein Endothelial Cells. Small, 2011. **7**(3): p. 388-394.
- 42. Kang, B., M.A. Mackey, and M.A. El-Sayed, *Nuclear Targeting of Gold Nanoparticles in Cancer Cells Induces DNA Damage, Causing Cytokinesis Arrest and Apoptosis*. J Am Chem Soc, 2010. **132**(5): p. 1517-+.
- 43. Albanese, A., P.S. Tang, and W.C.W. Chan, *The Effect of Nanoparticle Size, Shape, and Surface Chemistry on Biological Systems*. Annual Review of Biomedical Engineering, Vol 14, 2012. **14**: p. 1-16.
- 44. Nativo, P., I.A. Prior, and M. Brust, *Uptake and intracellular fate of surface-modified gold nanoparticles*. ACS Nano, 2008. **2**(8): p. 1639-1644.
- 45. Saha, K., et al., Surface Functionality of Nanoparticles Determines Cellular Uptake Mechanisms in Mammalian Cells. Small, 2013. **9**(2): p. 300-305.
- 46. Tu, Y.Q., et al., Fluorescence quenching of gold nanoparticles integrating with a conformation-switched hairpin oligonucleotide probe for microRNA detection.

 Chemical Communications, 2012. **48**(87): p. 10718-10720.

- 47. Zhu, Z.J., et al., The Interplay of Monolayer Structure and Serum Protein Interactions on the Cellular Uptake of Gold Nanoparticles. Small, 2012. 8(17): p. 2659-2663.
- 48. Chen, H.J., et al., *Plasmon-molecule interactions*. Nano Today, 2010. **5**(5): p. 494-505.
- 49. Connor, E.E., et al., Gold nanoparticles are taken up by human cells but do not cause acute cytotoxicity. Small, 2005. **1**(3): p. 325-327.
- 50. Brandenberger, C., et al., Quantitative Evaluation of Cellular Uptake and Trafficking of Plain and Polyethylene Glycol-Coated Gold Nanoparticles.

 Small, 2010. 6(15): p. 1669-1678.
- 51. Van Hoecke, K., et al., *Ecotoxicity and uptake of polymer coated gold nanoparticles*. Nanotoxicology, 2013. **7**(1): p. 37-47.
- 52. Giljohann, D.A., et al., *Gold nanoparticles for biology and medicine*. Angew Chem Int Ed Engl, 2010. **49**(19): p. 3280-94.
- 53. Boussif, O., et al., A Versatile Vector for Gene and Oligonucleotide Transfer into Cells in Culture and in-Vivo Polyethylenimine. Proceedings of the National Academy of Sciences of the United States of America, 1995. **92**(16): p. 7297-7301.
- 54. Haensler, J. and F.C. Szoka, *Polyamidoamine Cascade Polymers Mediate Efficient Transfection of Cells in Culture*. Bioconjug Chem, 1993. **4**(5): p. 372-379.
- 55. Lv, H.T., et al., *Toxicity of cationic lipids and cationic polymers in gene delivery*. Journal of Controlled Release, 2006. **114**(1): p. 100-109.
- 56. Meijer, H. and C. de Moor, *Fractionation of mRNA Based on the Length of the Poly(A) Tail*, in *RNA*, H. Nielsen, Editor. 2011, Humana Press. p. 123-135.

- 57. Ivaska, J., et al., *Novel functions of vimentin in cell adhesion, migration, and signaling.* Experimental Cell Research, 2007. **313**(10): p. 2050-2062.
- 58. Rizzuto, R., et al., Double labelling of subcellular structures with organelle-targeted GFP mutants in vivo. Current Biology, 1996. **6**(2): p. 183-188.
- 59. Shu, X., et al., A Genetically Encoded Tag for Correlated Light and Electron

 Microscopy of Intact Cells, Tissues, and Organisms. Plos Biology, 2011. 9(4).
- 60. Rhee, W.J. and G. Bao, Slow non-specific accumulation of 2'-deoxy and 2'-O-methyl oligonucleotide probes at mitochondria in live cells. Nucleic Acids Research, 2010. **38**(9).
- 61. Alberts, B., *Molecular Biology of the Cell: Reference edition*. 2008: Garland Science.
- 62. Kim, J.A., et al., Role of cell cycle on the cellular uptake and dilution of nanoparticles in a cell population. Nature Nanotechnology, 2012. **7**(1): p. 62-68.
- 63. Yang, H., et al., Effects of nanoparticle size and gestational age on maternal biodistribution and toxicity of gold nanoparticles in pregnant mice. Toxicology letters, 2014. **230**(1): p. 10-8.
- 64. Giljohann, D.A., et al., Gene Regulation with Polyvalent siRNA-Nanoparticle

 Conjugates. J Am Chem Soc, 2009. **131**(6): p. 2072-+.
- 65. Zheng, D., et al., *Aptamer Nano-flares for Molecular Detection in Living Cells*.

 Nano Letters, 2009. **9**(9): p. 3258-3261.
- 66. Massich, M.D., et al., Cellular Response of Polyvalent Oligonucleotide-Gold Nanoparticle Conjugates. ACS Nano, 2010. **4**(10): p. 5641-5646.
- 67. Hao, L., et al., Nucleic acid-gold nanoparticle conjugates as mimics of microRNA. Small, 2011. **7**(22): p. 3158-62.

- 68. Jennings, T. and G. Strouse, *Past, present, and future of gold nanoparticles*. Bio-Applications of Nanoparticles, 2007. **620**: p. 34-47.
- 69. Gerlier, D. and N. Thomasset, *Use of MTT colorimetric assay to measure cell activation*. Journal of Immunological Methods, 1986. **94**(1–2): p. 57-63.
- 70. Xue, J.P., et al., Visual detection of STAT5B gene expression in living cell using the hairpin DNA modified gold nanoparticle beacon. Biosensors & Bioelectronics, 2013. **41**: p. 71-77.
- 71. Strober, W., *Trypan Blue Exclusion Test of Cell Viability*, in *Current Protocols in Immunology*. 2001, John Wiley & Sons, Inc.
- 72. Latorre, A., et al., DNA and aptamer stabilized gold nanoparticles for targeted delivery of anticancer therapeutics. Nanoscale, 2014. **6**(13): p. 7436-7442.
- 73. Ma, P. and R.J. Mumper, Anthracycline nano-delivery systems to overcome multiple drug resistance: A comprehensive review. Nano Today, 2013. **8**(3): p. 313-331.
- 74. Webb, J.A. and R. Bardhan, *Emerging advances in nanomedicine with engineered gold nanostructures*. Nanoscale, 2014. **6**(5): p. 2502-2530.
- 75. Tonga, G.Y., et al., *Inorganic nanoparticles for therapeutic delivery: Trials, tribulations and promise.* Current Opinion in Colloid & Interface Science, 2014. **19**(2): p. 49-55.
- 76. Dhar, S., et al., *Polyvalent Oligonucleotide Gold Nanoparticle Conjugates as*Delivery Vehicles for Platinum(IV) Warheads. Journal of the American

 Chemical Society, 2009. **131**(41): p. 14652-14653.
- 77. Kumar, A., et al., Neuropilin-1-Targeted Gold Nanoparticles Enhance

 Therapeutic Efficacy of Platinum(IV) Drug for Prostate Cancer Treatment. ACS

 Nano, 2014. 8(5): p. 4205-4220.

- 78. Brown, S.D., et al., Gold Nanoparticles for the Improved Anticancer Drug

 Delivery of the Active Component of Oxaliplatin. Journal of the American

 Chemical Society, 2010. **132**(13): p. 4678-4684.
- 79. Alexander, C.M., M.M. Maye, and J.C. Dabrowiak, *DNA-capped nanoparticles designed for doxorubicin drug delivery*. Chemical Communications, 2011. **47**(12): p. 3418-3420.
- 80. Alexander, C.M., J.C. Dabrowiak, and M.M. Maye, Investigation of the Drug Binding Properties and Cytotoxicity of DNA-Capped Nanoparticles Designed as Delivery Vehicles for the Anticancer Agents Doxorubicin and Actinomycin D. Bioconjugate Chemistry, 2012. 23(10): p. 2061-2070.
- 81. Xiao, Z., et al., DNA Self-Assembly of Targeted Near-Infrared-Responsive Gold Nanoparticles for Cancer Thermo-Chemotherapy. Angewandte Chemie International Edition, 2012. **51**(47): p. 11853-11857.
- 82. Li, N., et al., A tumour mRNA-triggered nanocarrier for multimodal cancer cell imaging and therapy. Chemical Communications, 2014. **50**(56): p. 7473-7476.
- 83. Frederick, C.A., et al., *Structural comparison of anticancer drug-DNA complexes: adriamycin and daunomycin.* Biochemistry, 1990. **29**(10): p. 2538-2549.
- 84. Bagalkot, V., et al., *An Aptamer–Doxorubicin Physical Conjugate as a Novel Targeted Drug-Delivery Platform.* Angewandte Chemie, 2006. **118**(48): p. 8329-8332.
- 85. Kim, D., Y.Y. Jeong, and S. Jon, A Drug-Loaded Aptamer—Gold Nanoparticle Bioconjugate for Combined CT Imaging and Therapy of Prostate Cancer. ACS Nano, 2010. **4**(7): p. 3689-3696.
- 86. Berg, J.M.T., J.L.; Streyer, L., Biochemistry. 7 ed. 2011: W.H. Freeman.

- 87. Thorn, C.F., et al., *Doxorubicin pathways: pharmacodynamics and adverse effects*. Pharmacogenetics and Genomics, 2011. **21**(7): p. 440-446.
- 88. Alexander, C.M., et al., *Multifunctional DNA-Gold Nanoparticles for Targeted Doxorubicin Delivery*. Bioconjugate Chemistry, 2014. **25**(7): p. 1261-1271.

CHAPTER 6

-Results and discussion on programmed ligation of

DNA-functionalized nanomaterials-

Chapter 5 discussed the great potential of DNA-AuNP conjugates as biomedical probes. However, the requirements for novel, more advanced probes are ever growing. Recently assemblies of nanoparticles have emerged as potential candidates [1, 2]. For example, the flexibility in bringing together two independent nanoparticles to create a stable nanoparticle dimer allows one to envisage the formation of a dimer between two single nanoparticle mRNA probes. This dimeric probe is inherently superior to a single nanoparticle probe because the nanoparticle dimers will act synergistically in the local microenvironment, a function that will be drastically less efficient when single nanoparticle probes are employed.

In order to create a library of assemblies for potential applications as advanced biomedical probes, different types of nanomaterials (AuNPs (13 nm and 5 nm), Cu_{2-x}Se NPs, Fe₃O₄ NCs and graphene oxide) were conjugated to azide (**S1**) or alkyne (**S2**) modified oligonucleotides (see **chapter 4**). These were subsequently assembled into homo- and heterostructures using DNA 'click' ligation [3] (see **section 2.6** for background information on heterostructures and their applications in biomedicine). As initial proof of concepts, only simple assemblies (dimers and trimers) were formed.

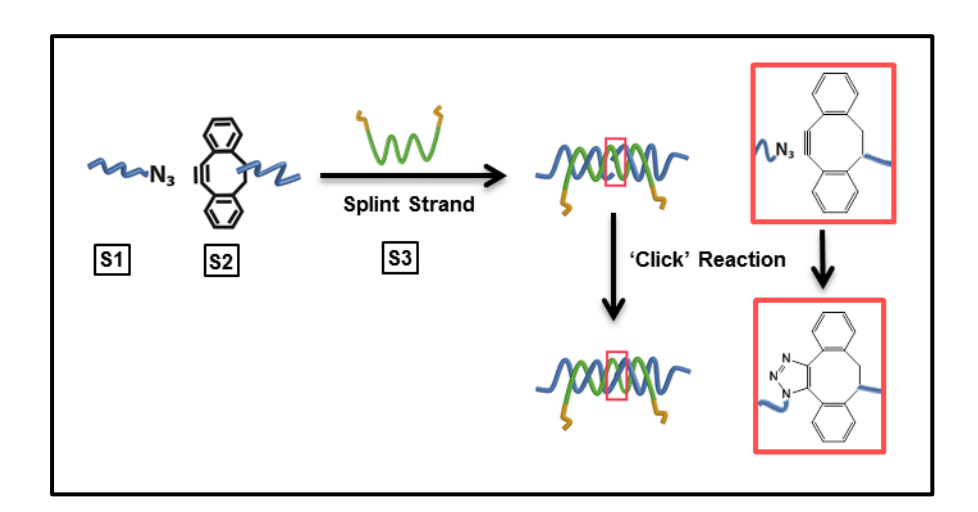
The analysis of the employed oligonucleotide strands will be outlined in **section 6.1**, whilst assembly formation of homo- and hetero-nanostructures is elucidated in **section 6.2**). The main aim of this study is the development of novel and robust advanced nano-probes. Therefore preliminary results on the stability of gold

nanoparticle dimers with respect to various conditions met within a biological environment are shown in **section 6.3.**

Parts of this chapter were published in: <u>Heuer-Jungemann</u>, <u>A</u>.; Kirkwood, R.; El-Sagheer, A.; Brown, T.; Kanaras, A. G. "Copper-free Click Chemistry as an Emerging Tool for the Programmed Ligation of DNA-functionalised Gold Nanoparticles", *Nanoscale*, **2013**, 5 (16), 7209-7212.

6.1 Analysis of oligonucleotides.

Prior to conjugation to different nanomaterials, oligonucleotides employed in this study (see **table 3.1** for oligonucleotide sequences) were analyzed for duplex formation and click ligation [4-6] by UV melting (see **section 6.1.1**) and denaturing polyacrylamide gel electrophoresis (see **section 6.1.2**). To program nanoparticle assembly it is imperative that only the desired oligonucleotide sequences hybridize and subsequently ligate to form a continuous DNA strand (see **scheme 6.1**).



Scheme 6.1 Illustration of the DNA click ligation process. Azide (**S1**) and alkyne (**S2**) oligonucleotides are brought together *via* a complementary splint strand (**S3**). The click reaction then takes place resulting in a ligated strand.

6.1.1 Oligonucleotide UV melting.

The distinct absorption characteristics of single-stranded (ss) and double-stranded (ds) oligonucleotides allow for duplex formation to be monitored by UV-visible spectroscopy [7]. dsDNA characteristically displays a lower absorption than ssDNA. Hydrogen bonding in the duplex results in decreased resonance in the DNA bases, which in turn causes reduced absorbance of UV light (hypochromic effect) [8]. As the duplex is denatured (chemically or thermally) into two single strands, π - π stacking interactions are broken. Due to this, π -electrons in the purine and pyrimidine bases display and increased interaction with light, giving rise to a stronger absorption. These characteristics give rise to the distinct sigmoidal shape (hyperchromic shift), characteristic of a DNA melting curve [9]. **Figure 6.1** depicts the corresponding spectra for melting curves of the relevant oligonucleotides (**S1**, **S2** and **S3**, see **table 3.1** for sequences), recorded at the characteristic absorption maximum for DNA (260 nm) [7] at temperature ranging from 15-85 °C (see **section 3.5** for experimental procedure).

Only combinations of oligonucleotides involving S3 (Fig. 6.2 B-D) displayed the characteristic DNA melting curves, arising from the different interaction of ssDNA and dsDNA with light, as previously discussed. Figure 6.1 A displayed no sigmoidal curve, suggesting that no duplexes were formed between S1 and S2 (see scheme 6.1).

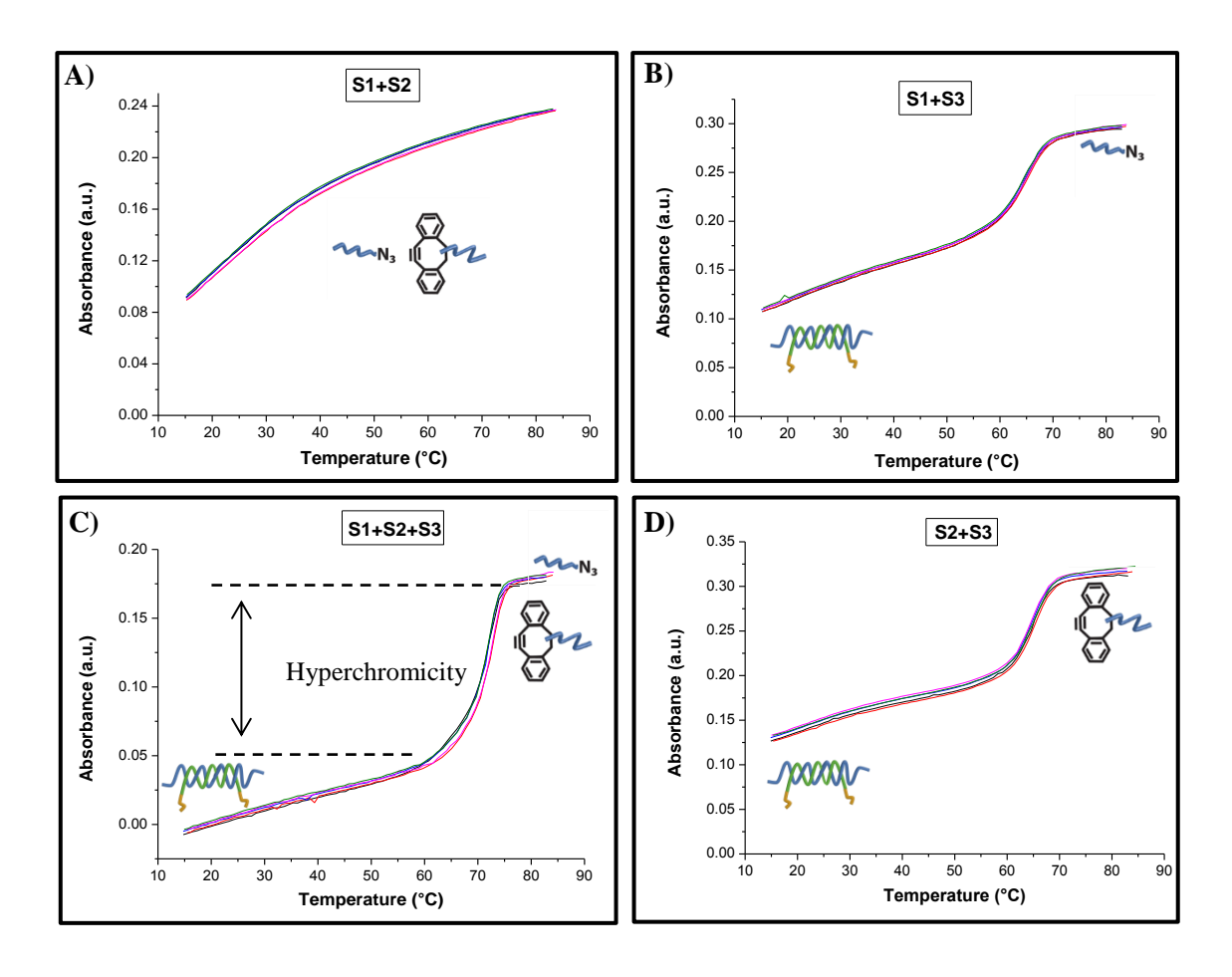


Figure 6.1 A) UV melting curve of S1 + S2. No duplex is formed due to a lack of complementarity. B) Melting curve for S1+S3 showing duplex melting. C) Melting curve for S1 + S2 +S3 showing duplex melting between all three strands. D) Melting curve for S2+S3 showing duplex melting.

6.1.2 Denaturing polyacrylamide gel electrophoresis.

Ligation of the click reaction was confirmed by denaturing polyacrylamide gel electrophoresis. In this method DNA is denatured chemically by formamide and strands are subsequently separated according to their size, conformation and charge in a polymer gel matrix (see **section 3.5** for experimental procedures). **Figure 6.2** shows a representative gel.

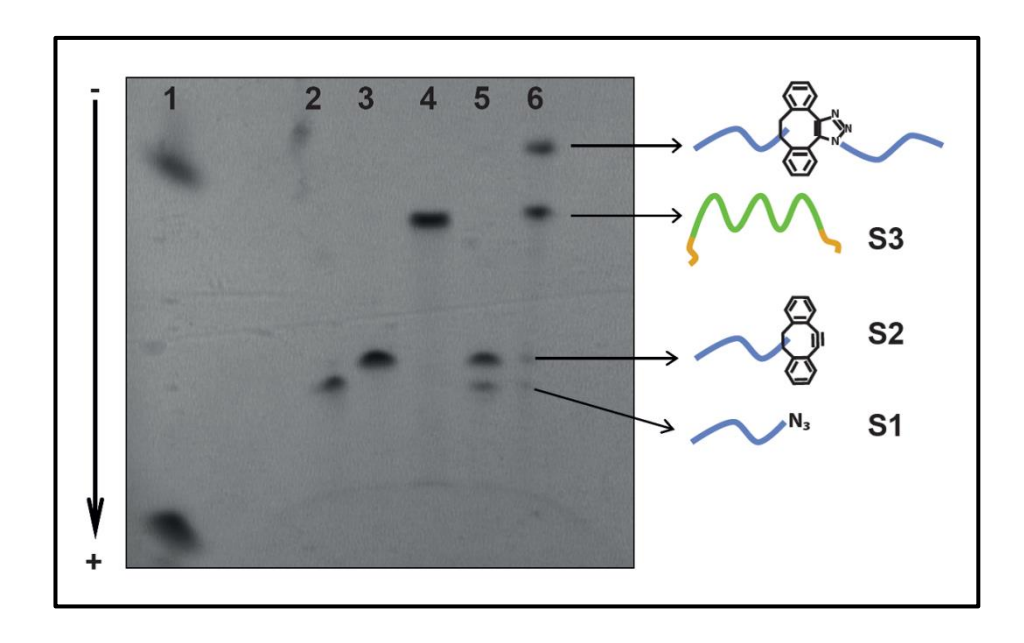
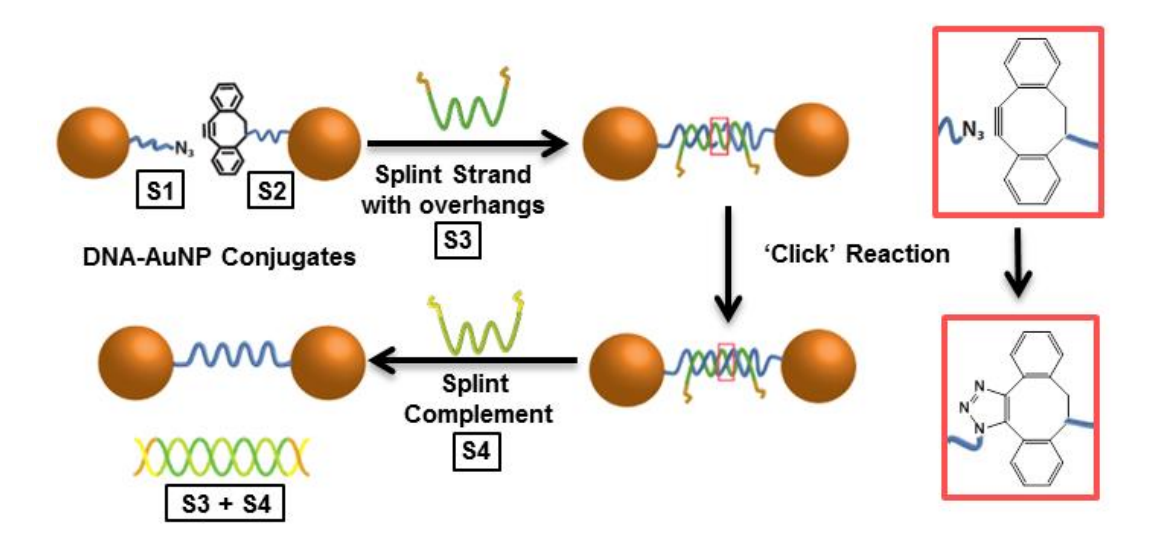


Figure 6.2 Denaturing polyacrylamide gel of free DNA. Lane 1: Reference dye, Lane 2: **S1** (27mer), Lane 3: **S2** (31mer), Lane 4: **S3** (52mer), Lane 5: **S1**+**S2**; Lane 6: Clicked DNA (58mer).

Lane 1 contains a reference dye. Lanes 2-4 resemble each individual strand S1, S2 and S3, respectively. Lane 5 displays a mixture of S1 and S2, while lane 6 shows the result from the click ligation post hybridisation (see scheme 6.1 for schematic illustration). Two distinct bands were visible in lane 5, corresponding to S1 and S2. This suggested that duplex formation and subsequent clicking were not possible in the absence of the templating splint strand S3 under current conditions. This was also observed from the melting studies (section 6.1.1). On the other hand, lane 6 displayed a strong band with low electrophoretic mobility as well as a band corresponding to S3. This suggested that a new product was formed from S1, S2 and S3. Thus successful clicking of the two desired strands S1 and S2 (brought together *via* S3) was confirmed in accordance with previous literature reports [6].

6.2 Programmed ligation of DNA-nanomaterials

DNA-coated nanomaterials were assembled into homostructures (5 nm AuNP dimers see section 6.2.1, 13 nm AuNP dimers and trimers see section 6.2.2, Fe₃O₄ NC dimers see section 6.2.3) and heterostructures (Cu_{2-x}Se-Au and Fe₃O₄-Au heterodimers see section 6.2.4 and GO-AuNP hybrid structures see section 6.2.5). The general concept behind the assembly process is outlined in scheme 6.2.



Scheme 6.2 Illustration of dimer formation using the method of DNA- click chemistry. 3'-azide (S1) and 5'-alkyne (S2) DNA-AuNP conjugates are brought into close proximity through a templating splint strand (S3) with non-complementary overhangs (*orange*). 'Clicking' occurs immediately after hybridisation. Addition of a single DNA strand (S4), fully complementary to S3, results in the removal of S3 through competitive hybridisation, leaving a nanoparticle dimer system connected via a single continuous DNA strand.

The resulting assemblies are covalently linked. This should result in increased stability towards conditions met within a biological environment and reduce the possibility of intracellular disassembly.

6.2.1 Formation of 5 nm AuNP dimers

5 nm AuNP-DNA monoconjugates of **S1** and **S2** were incubated in equimolar quantities with **S3** to form dimers (see **section 3.4** for experimental procedures. Also see **scheme 6.2**). Dimerization was visualized by agarose gel electrophoresis (**Figure 6.3**). Two strong bands with different electrophoretic mobilities were observed. One band with comparably higher mobility corresponded to non-hybridised monoconjugates, whilst the second, more retarded band represented hybridised dimers.

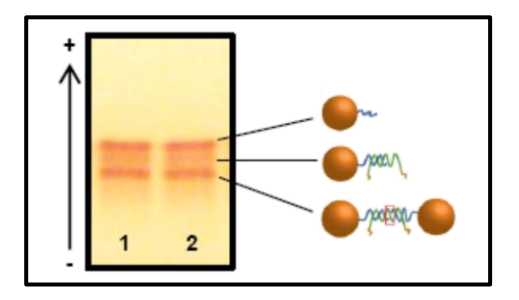


Figure 6.3 Agarose gel electrophoresis showing distinct bands for unreacted monoconjugates and dimers dimer systems. A faint band in the middle corresponds to monoconjugates hybridized to **S3** without having formed dimers.

A third faint band with medium electrophoretic mobility was also observed. This was accounted for by monoconjugates hybridized to S3 only, not forming dimers [10]. After recovery of dimers from the gel (see section 3.5), purification by agarose gel electrophoresis as well as analysis by transmission electron microscopy were employed to confirm that the click reaction had taken place. The corresponding agarose gel is displayed in Figure 6.4.

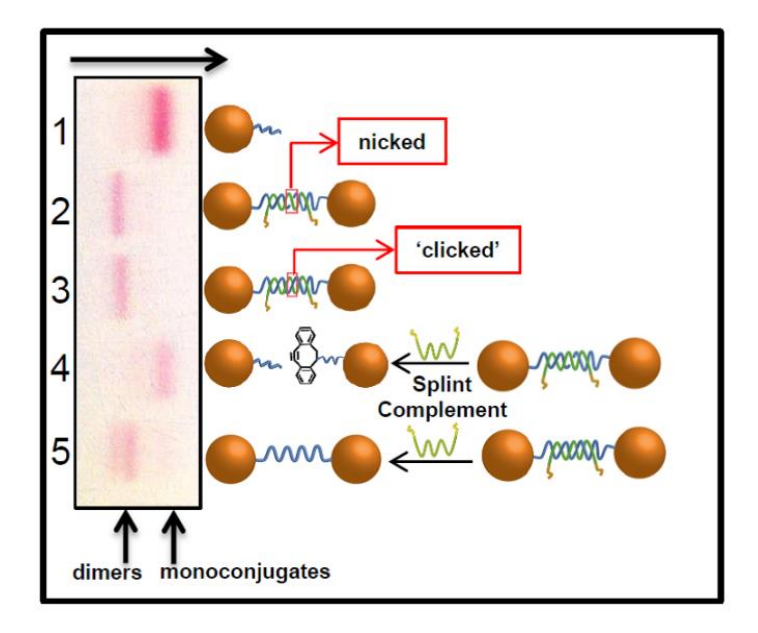
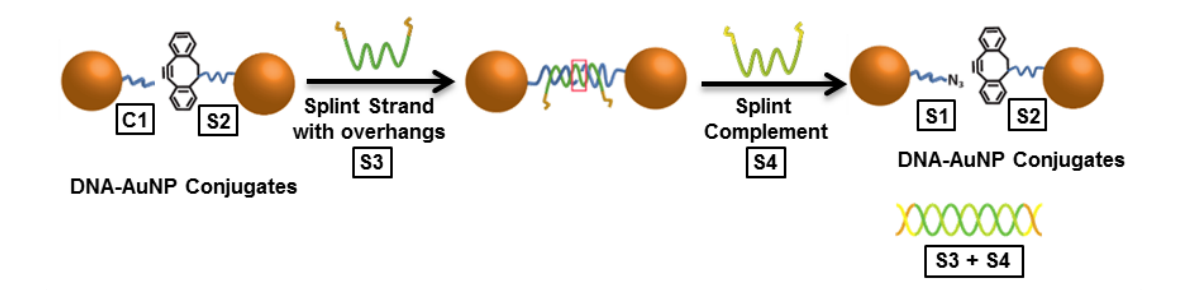


Figure 6.4 Agarose gel electrophoresis demonstrates the success of the 'click' reaction. Lane 1: Monoconjugate as reference; Lane 2: 'nicked' dimers, connected via splint strand S3; Lane 3: 'clicked' dimers, hybridized to S3; Lane 4: 'nicked' dimers treated with splint complement S4; Lane 5: 'clicked' dimers treated with S4.

Lanes 1, 2 and 4 show control experiments, while lanes 3 and 5 show the ligated products. As the most representative control experiment, **S1** was synthesised without the azide functional group (**C1**), so that particles modified with this particular strand could click to alkyne modified particles (see **scheme 6.3** for schematic illustration).



Scheme 6.3 Schematic representation of the gold nanoparticle assembly using 'nicked' DNA. Due to the lack of an azide group on **C1**, dimer formation is only possible in the presence of the splint strand **S3.** Upon treatment with **S4** the system breaks apart into mono-conjugates as the DNA strands were unable to undergo the click reaction

These dimers displayed similar mobility in the gel compared to the ligated dimers (lanes 2 and 3). However, after the removal of the splint strand S3 through competitive hybridisation with S4 (see section 3.4 for experimental procedures), the difference in mobility became very clear (lanes 4 and 5). The non-ligated particles dehybridised and ran as monomers while the ligated particles remained dimeric [3]. Dimers in lane 5, connected via a single strand of ssDNA presented minor changes in mobility, possibly due to the extra flexibility allowed by the non-rigid single strand. Using the software image J to compare optical densities for monoconjugates and dimers, it was possible to estimate that the reaction was completed to 92 % (see Appendix II). This yield was significantly higher than the yields reported for the ligation of particles when enzymes were used (ranging from 50 % - 72 %) [11-15].

Transmission electron microscopy was employed to visualize the assembled structures. **Figure 6.5 A** depicts the representative images and according grouping chart, created from statistical analysis of more than 500 NPs from at least three different experiments. The TEM micrographs show that the majority of particles were assembled into dimers. Variations of inter-particle distances could be observed, which possibly derive from the flexibility of the ssDNA. However, as expected the maximum distance between two particles never exceeded the maximum length of the ligated DNA strand (19.7nm). **Figure 6.5 B** shows TEM images of the control reaction and a corresponding grouping chart, created from statistical analysis of more than 500 NPs from at least three different experiments. The images and representative grouping chart show that after treatment with **S4** only monoconjugates were visible (single particles), which is in agreement with the gel electrophoresis results (see **Fig. 6.4**) and suggest that assemblies only stay connected if covalently linked through the click ligation. (Further TEM micrographs can be found in the corresponding publication [3] or **Appendix II**).

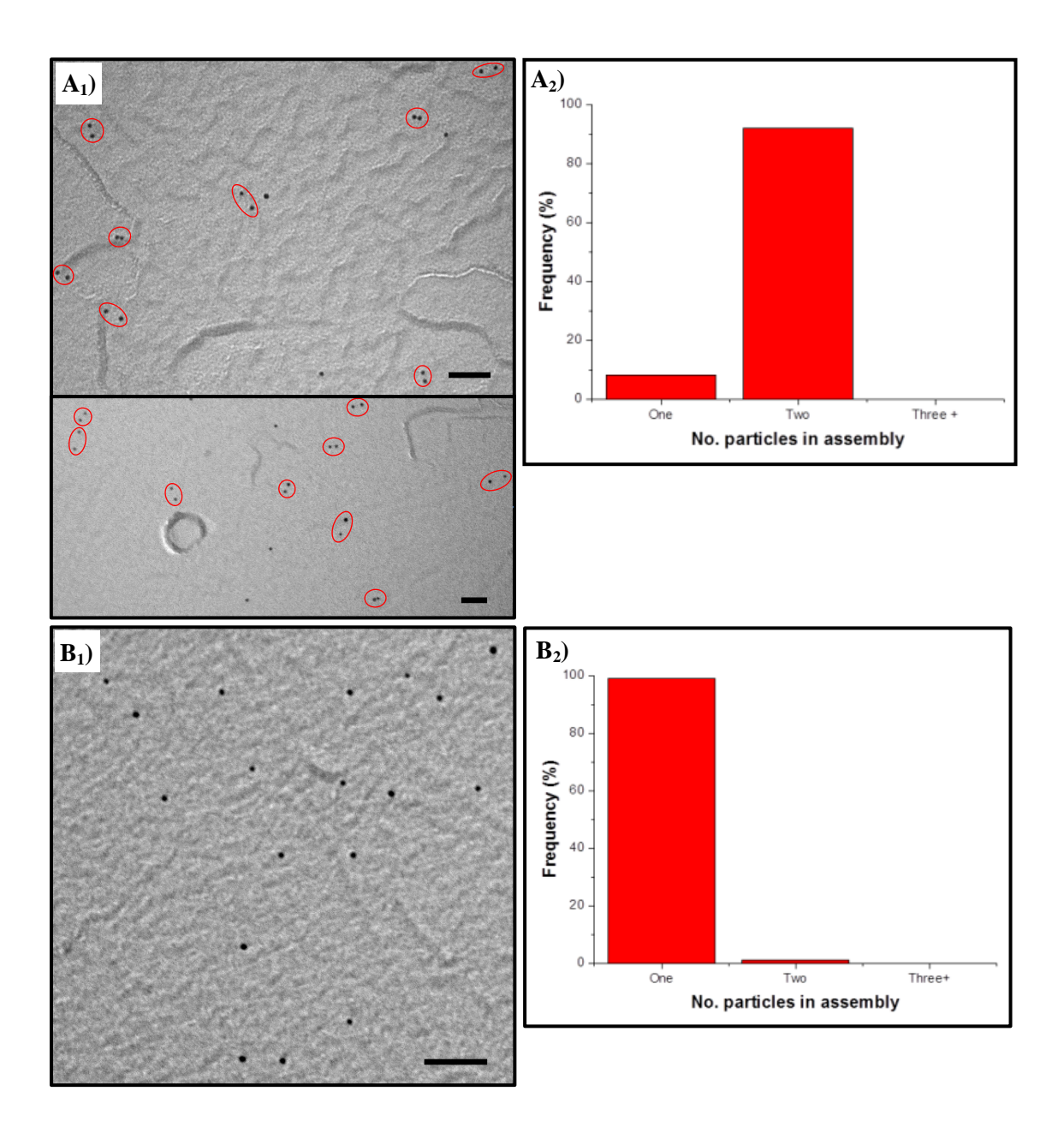
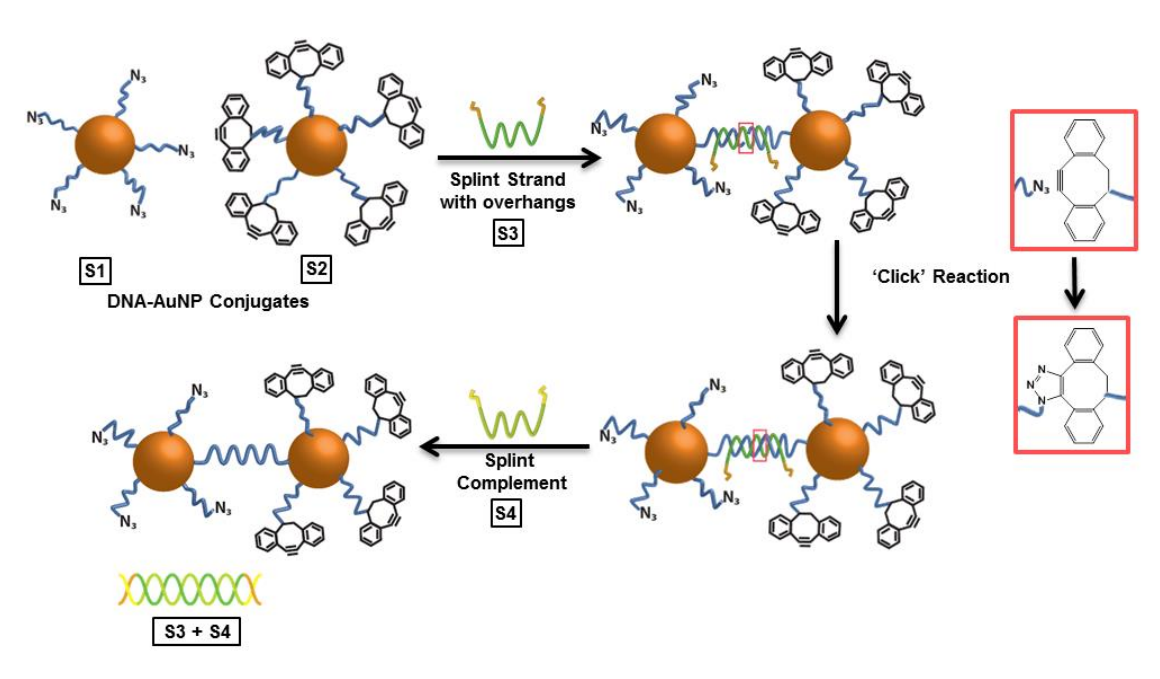


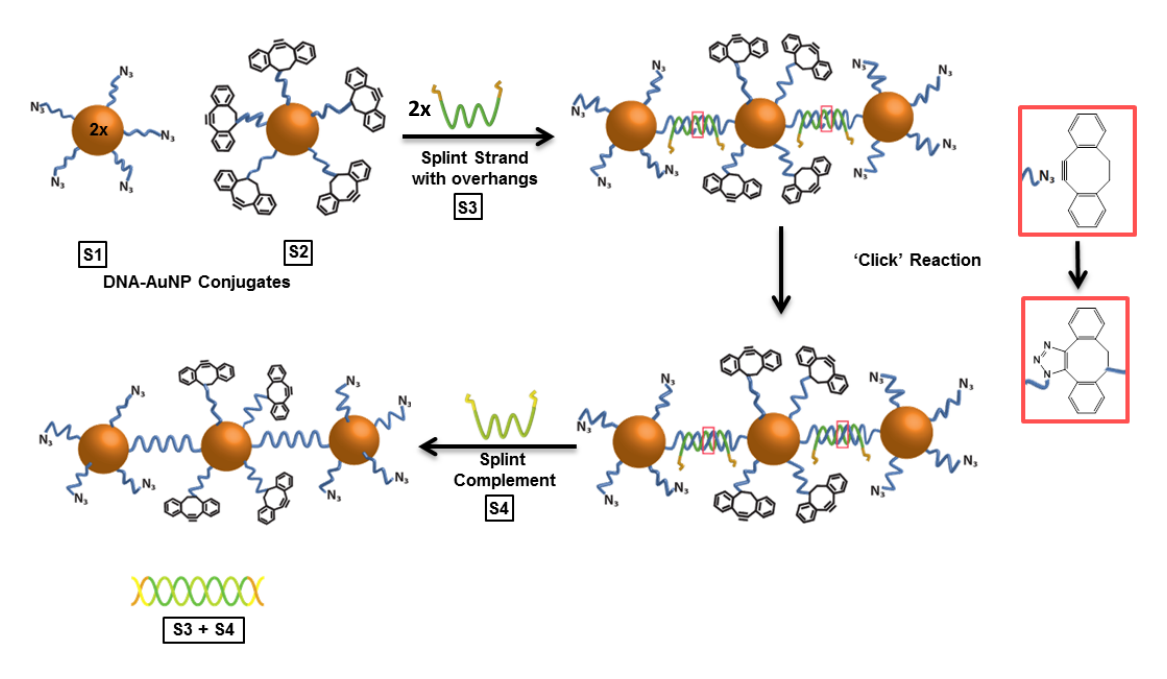
Figure 6.5 TEM images of **A**) clicked 5 nm AuNP dimers connected via a continuous single strand of ssDNA **B**) TEM images of the control experiment. As DNA cannot click, the dimer breaks apart and mostly monoconjugates can be found. Scale bars are 50 nm.

6.2.2 Formation of 13 nm AuNP dimers and trimers.

 13 ± 1 nm AuNPs, functionalized with a dense shell of oligonucleotides **S1** or **S2** [15] (see **table 3.1** for oligonucleotide sequences and **sections 3.2** and **3.4** for experimental procedures) were assembled to form dimers and trimers (see **schemes 6.4** and **6.5**).



Scheme 6.4 Schematic illustration of the formation of 13 nm AuNP dimers using DNA click ligation.



Scheme 6.5 Schematic illustration of the formation of 13 nm AuNP trimers using DNA click ligation.

The formation of 5 nm AuNP dimers could be controlled well, due to the employment of monoconjugates (see **section 6.2.1**). However, the control of the assembly process in the case of 13 nm AuNPs presented a greater challenge. Dimers or trimers of particles were formed by carefully controlling the ratio of **S1**-AuNPs to **S2**-AuNPs to **S3** (1:1:1 ratio for dimers, 1:2:2 ratio for trimers) to avoid the formation of larger assemblies [16]. Agarose gel electrophoresis was employed to separate dimers from trimers and single DNA-AuNPs (**Figure 6.6**).

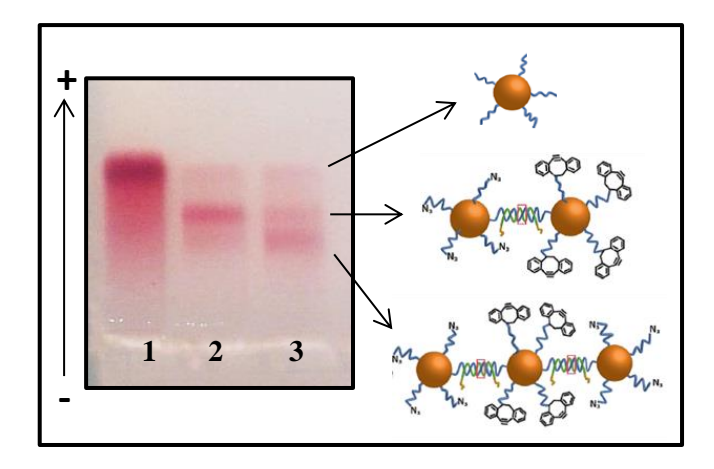


Figure 6.6 Agarose gel showing the different mobilities of AuNPs, dimers and trimers.

DNA-AuNPs are represented as a control in lane 1, whilst dimers and trimers are shown in lanes 3 and 2 respectively. The gel shows that dimers as well as trimers were formed within the same reaction – due to the nature of this process this could not be avoided. However, one can see that by varying the ratios of **S1-**AuNPs to **S2-**AuNPs to **S3**, the formation of one over the other is favoured. Moreover the separation of these two assemblies can easily be achieved via agarose gel electrophoresis. After recovery of assemblies from the gel, **S4** could then be employed to remove the splint strand **S3** *via* competitive hybridization [3, 12] (see **section 3.4** for experimental procedures).

Transmission electron microscopy images depict the assembled nanostructures (see **Figure 6.7**).

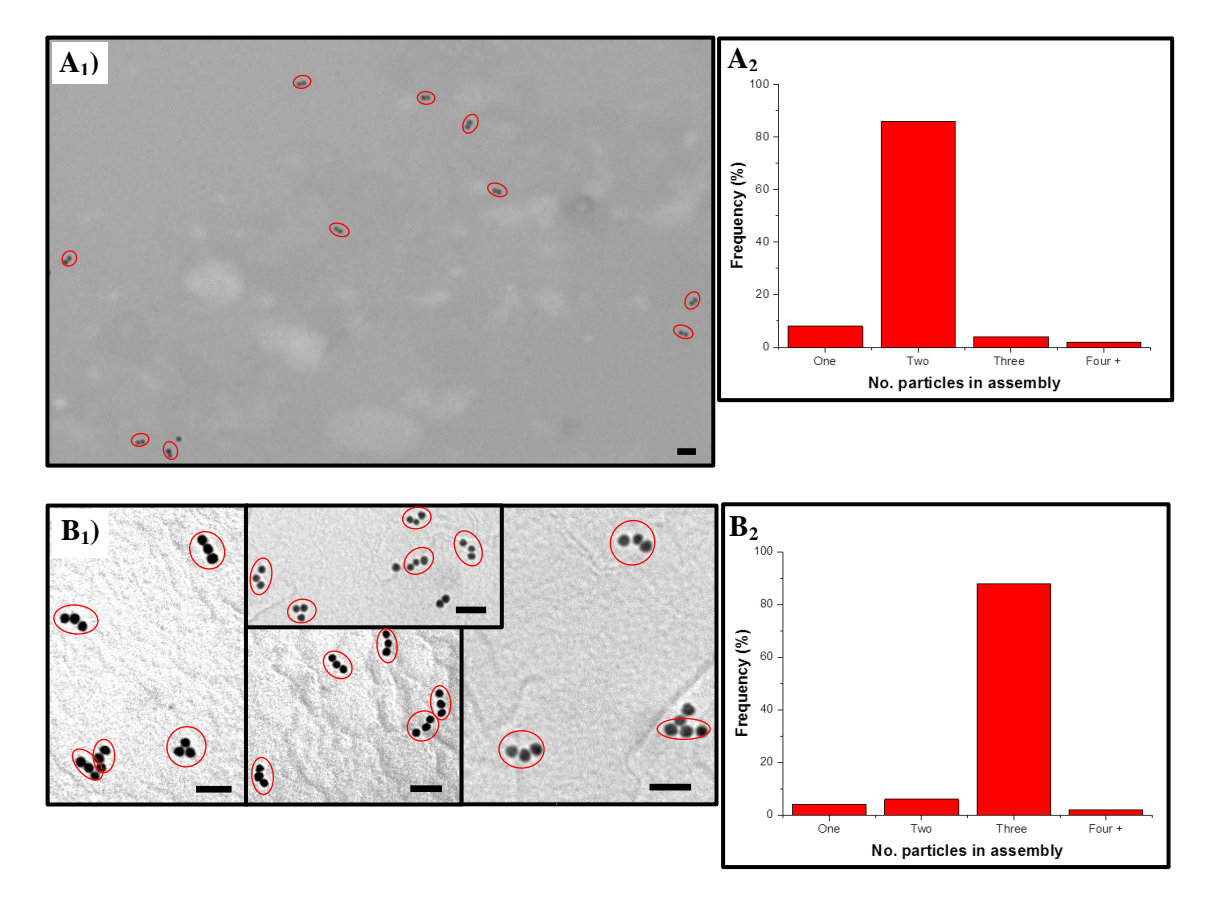


Figure 6.7 TEM micrographs and corresponding grouping charts of **A**) 13 nm AuNP dimers and **B**) trimers. Scale bars are 50 nm. For statistical analyses more than 200 particles from at least three different experiments were counted.

It is evident from the TEM images as well as the corresponding grouping charts that the purity of each structure is high (> 80 % for both types) and importantly, assembled structures stayed connected even after the removal of the splint strand, suggesting successful clicking as discussed previously (see **section 6.2.1**). For additional TEM micrographs please see **Appendix II**.

To explore their potential as novel advanced nano-probes, 13 nm dimers were further employed in cell culture studies (see **section 6.3**).

6.2.3 Formation of Fe₃O₄ NC dimers

PEG-COOH coated Fe₃O₄ NCs were obtained from Prof. Liberato Manna and Dr. Teresa Pellegrino at the Istituto Italiano di Tecnologia, see **Appendix II**. Fe₃O₄ NCs have been used extensively in biomedical applications such as magnetic hyperthermia and magnetic resonance imaging [17, 18]. Therefore they present a suitable building block for implementation into novel biomedical probes.

Particles were conjugated to oligonucleotides (AmS1 and AmS2) via EDC coupling (see section 3.2 for synthetic protocols). The resulting conjugates were then assembled into dimers (see section 3.4 for experimental procedure). Due to the nature of the EDC coupling process [19], it was difficult to conjugate only one DNA strand to each particle. It was therefore crucial to have equal ratios between AmS1-NPs to AmS2-NPs in order to prevent the formation of larger aggregates. Transmission electron microscopy was utilized to visualize assemblies (Figure 6.8). A representative grouping chart was created by statistical analysis of at least 200 particles from two different experiments.

The TEM image and corresponding grouping chart suggest that dimer formation was successful, with more than 50 % of particles having formed dimers. Optimisation procedures and investigations into possible purification methods are the subject of future work.

Assemblies are currently being investigated for their use as MRI contrast agents at the Istituto Italiano di Tecnologia.

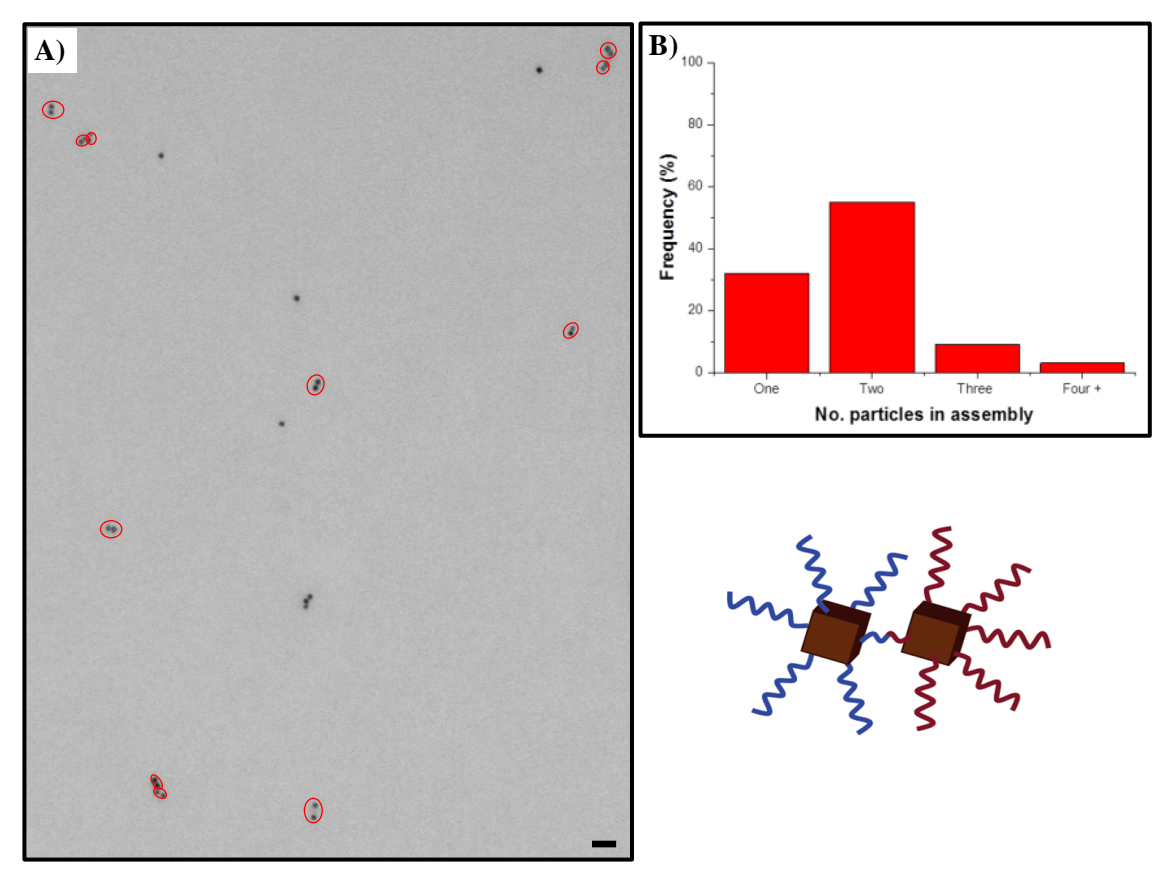


Figure 6.8 TEM micrograph and corresponding grouping chart of Fe₃O₄ NC dimers. Scale bar is 100 nm.

6.2.4 Formation of heterodimers.

The combination of two or more different nanoparticles within one functional nano-probe will result in highly interesting, multi-role agents (see **section 2.6** for background information). Nanoparticle heterostructures to date have been synthesised by methods including non-covalent interactions [20-23], direct growth [24-26] or by enclosure within a coating [27]. Only a few reports have discussed the formation of covalently linked heterostructures [28-30]. However, downfalls of reported methods include low stability towards conditions met within a biological environment or limited applicability. The following section shows the results of the formation of covalently ligated heterodimeric structures of Cu_{2-x}Se NP-AuNP and Fe₃O₄NC-AuNP by applying the protocol of programmed click ligation [3] as previously discussed for AuNP

dimer/trimers (see **section 6.1**). Cu_{2-X}Se nanoparticles display a plasmon band in the NIR [31] and has shown potential for photothermal therapy applications [32]. Therefore they show good potential as building blocks for biomedical probes based on nanoparticle assemblies.

AmS2-Fe₃O₄ NCs and AmS2-Cu_{2-x}SeNP were mixed with 5nm S1-AuNP monoconjugates and splint strand S3 and subsequently assembled into heterodimeric structures (see section 2.6 for background information). Similarly to the cases of dimer formation of 13nm AuNPs and Fe₃O₄ NCs (see section 2 6.2.2 and 6.2.3), it was vital to ensure a 1:1:1 ratio of AmS1-NPs to S2-AuNP to S3 in order to prevent the formation of larger aggregates.

Transmission electron microscopy was utilized to visualize resulting assemblies. **Figure 6.9** displays micrographs of Fe₃O₄-Au heterodimers and a corresponding grouping chart. **Figure 6.10** shows micrographs of Cu_{2-X}Se-Au heterodimers and a corresponding grouping chart. Representative grouping charts were created by statistical analysis of at least 200 particles from at least two different experiments.

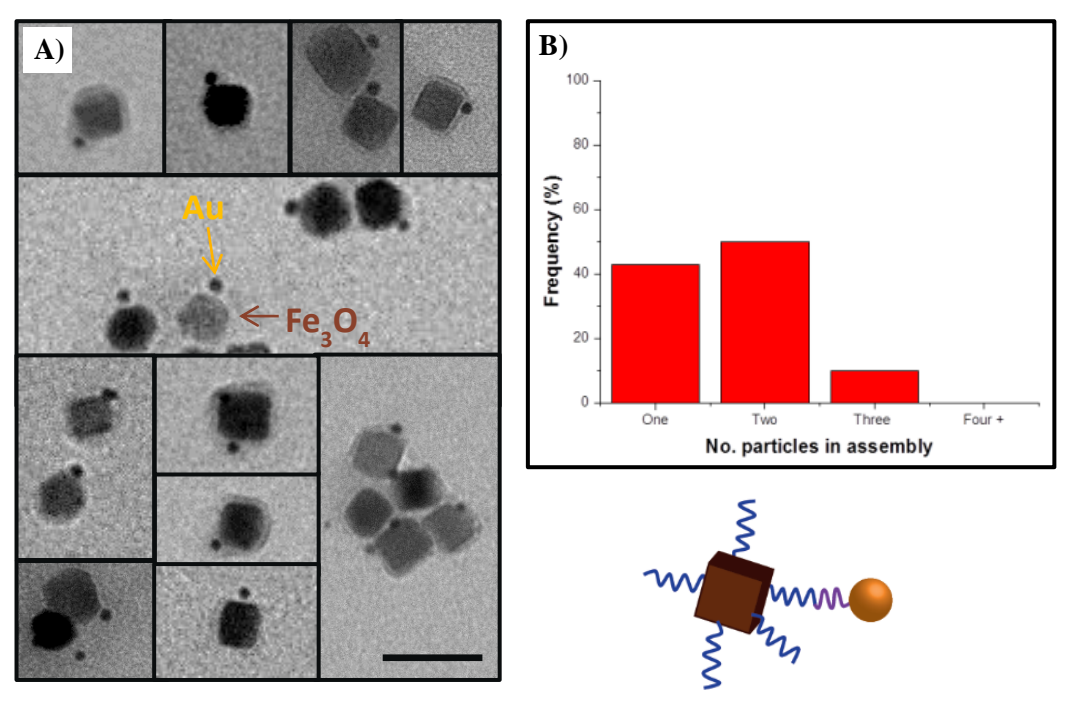


Figure 6.9 A) TEM micrographs of Fe₃O₄-Au heterodimers and **B)** corresponding grouping chart. Scale bar is 50 nm.

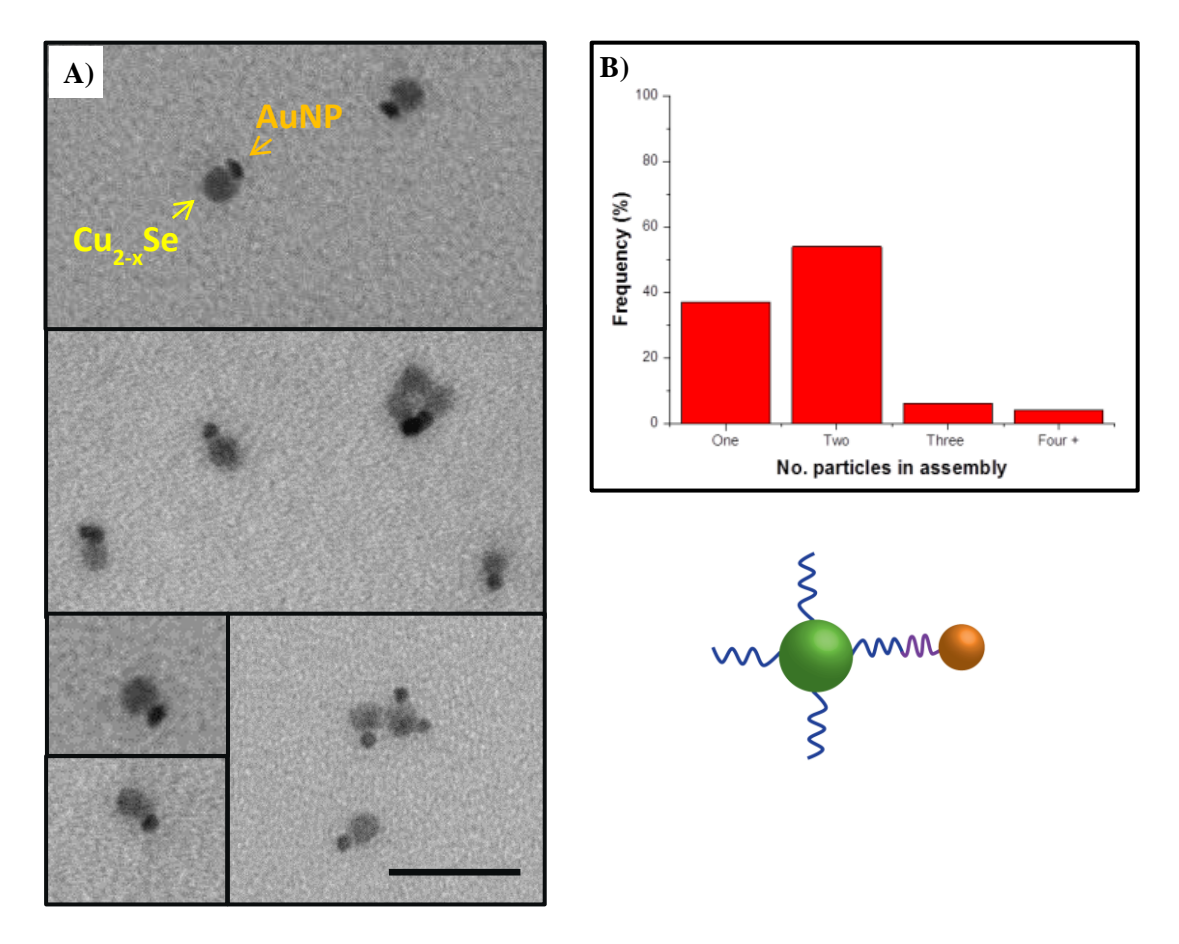


Figure 6.10 A) TEM micrographs of $Cu_{2-x}Se$ -Au heterodimers and **B)** corresponding grouping chart. Scale bar is 50 nm.

Figures 6.9 and **6.10** showed that the formation of heterodimeric structures was successful. In both cases more than 50 % of particles had formed heterodimers and few had formed heterotrimers. However, similar to the case of Fe₃O₄ homodimers (see section **6.2.3**) around 40 % of particles were found to have remained individual/unreacted. At this stage no conclusive explanation for this observation can be given. A variety of factors must be considered, such as potential low EDC coupling yield resulting in incomplete DNA conjugation or low hybridisation yields caused by increased repulsive forces between particles. Optimisation procedures and investigations into possible purification methods are the subject of future work.

It is envisaged that heterostructures will be investigated for novel optical properties and biomedical applications in the near future (see section 7.1).

6.2.5 Formation of GO/AuNP hybrid structures.

In order to build robust hybrid GO/nanoparticle structures, that are stable within conditions met in biological environments or organic solvents, a strong covalent link between GO and the nanoparticles is required [33]. The following section discusses the results of the formation of hybrid GO/AuNP nanostructures by programmed ligation [3].

Graphene oxide sheets (obtained from the Institute for Electronic Structure and Laser – FORTH, Crete see **Appendix II**) were conjugated to **AmS2** oligonucleotides (see **section 3.2** and **table 3.1** for experimental procedures and oligonucleotide sequences). DNA-GO conjugates were subsequently hybridised and ligated with an excess of **S1-**AuNP using **S3** to template the reaction (see **section 3.4** for experimental procedure).

The purification of GO/AuNP hybrid assemblies from excess AuNPs was achieved by agarose gel electrophoresis (several runs were performed in order to ensure that all non-ligated AuNPs were removed). A representative gel is depicted in **Figure 6.11**.

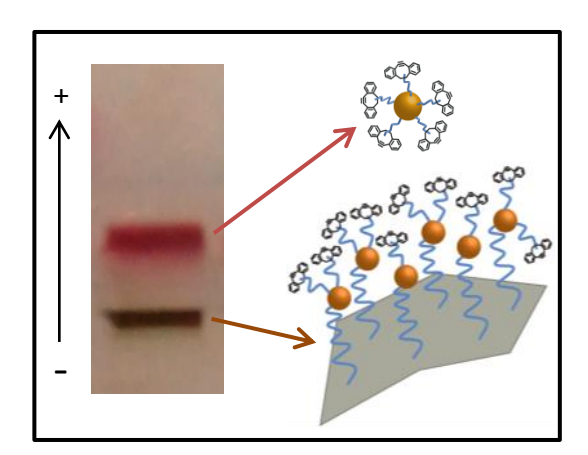


Figure 6.11 Purification of unconjugated AuNPs from GO/AuNP hybrid structures *via* agarose gel electrophoresis.

Figure 6.11 shows a distinct red band, corresponding to DNA-AuNPs. The small pore size of the agarose gel matrix allowed only the comparatively small nonconjugated DNA-AuNPs to enter the gel, whilst large GO/AuNP assemblies remained in the wells (brown band) in accordance with previous literature reports [33].

The unique optical properties of GO [34] and AuNPs [35] allowed for the characterisation of hybrid assemblies, after recovery from the gel, using UV-visible spectroscopy. Corresponding spectra are depicted in **Figure 6.12**.

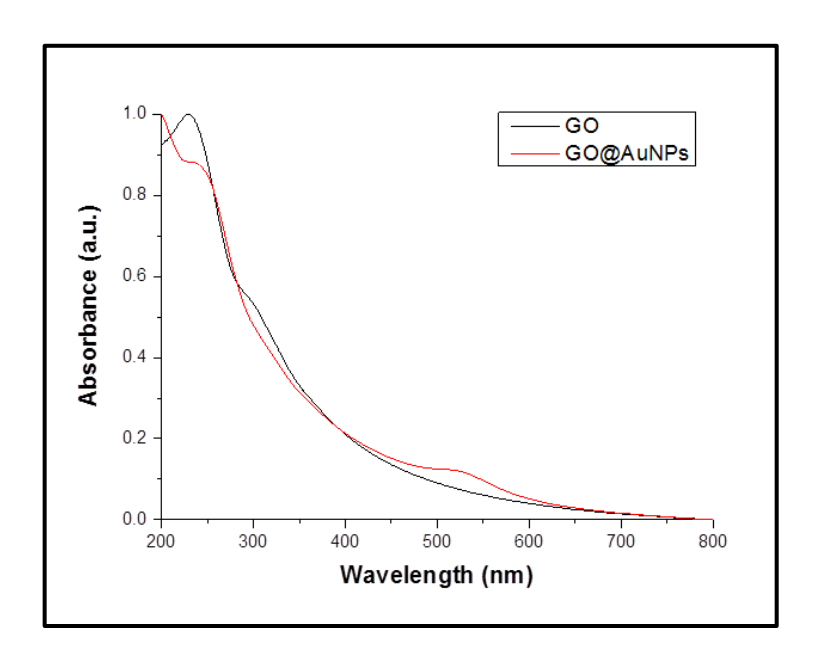


Figure 6.12 Normalized UV-vis spectra of GO (red) and GO/AuNP hybrid assemblies (black).

A red-shift in the peak maximum of GO from 230 nm to 235 nm, was attributed to an alteration in the electronic ground state of GO induced by DNA conjugation [36] as previously discussed in **section 4.2**. The distinct plasmon peak at 520 nm in the spectrum of GO/AuNP assemblies suggested that AuNPs were successfully conjugated to the GO surface (**Fig. 6.12**, red graph) as reported in previous work [36].

Visualisation of GO/AuNP hybrid assemblies was achieved by transmission electron microscopy. Corresponding micrographs, shown in **Figure 6.13** depict sheets

of graphene oxide, decorated with gold nanoparticles and thus further suggested the successful formation of GO/AuNP hybrid assemblies.

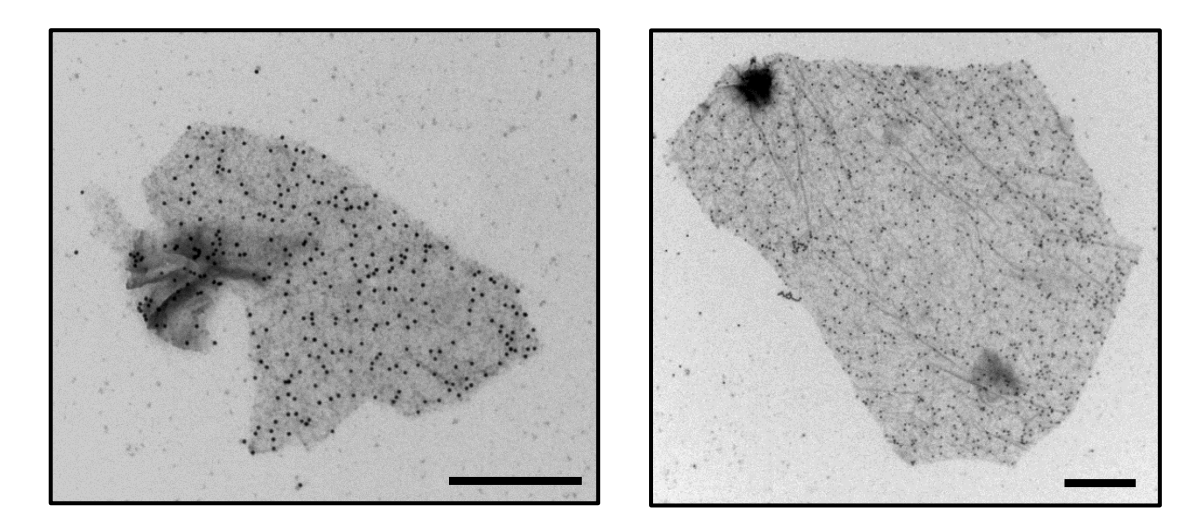
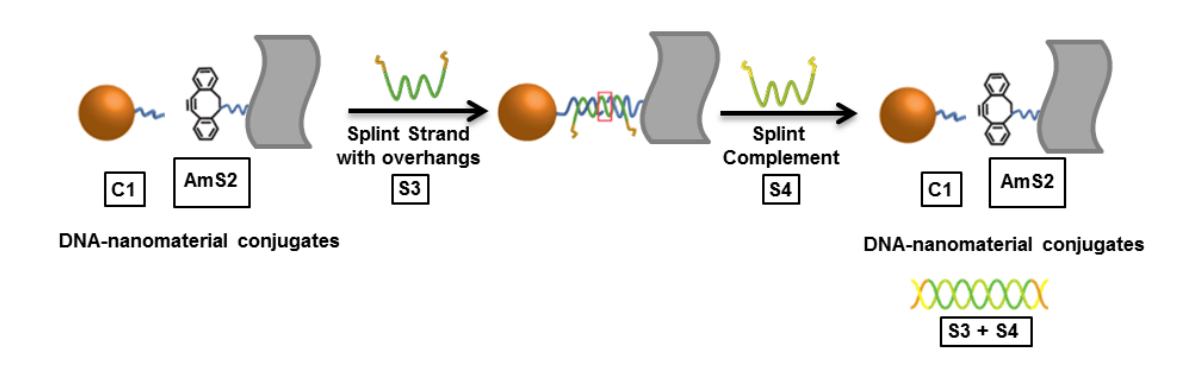


Figure 6.13 Representative TEM images for GO/AuNP hybrid assemblies. Scale bars are 500 nm.

In order to confirm that AuNPs and GO sheets were ligated, assemblies were incubated with the splint complement S4. This resulted in the removal of S3 by competitive hybridisation [3]. As a representative control experiment, assemblies were formed as before, but with AuNP-DNA conjugates lacking the alkyne functional group (see scheme 6.6 and table 3.1 for oligonucleotide sequence of C1). In this case



Scheme 6.6 Schematic illustration of the control experiment. **C1** modified AuNPs and **AmS2**-modified GO are brought together *via* **S3**. Upon treatment with **S4**, assemblies dissociate as they were not able to ligate. N.B.: Only one DNA strand is shown per material for ease of visualisation. However, in the reality both materials are modified with a number of DNA strands.

assemblies would still form in the presence of the splint strand **S3**, however after removal of **S3**, the assemblies should disassemble. Both types of assemblies (ligated and hybridised) were run in an agarose gel matrix. **Figure 6.14** shows the relevant gel.

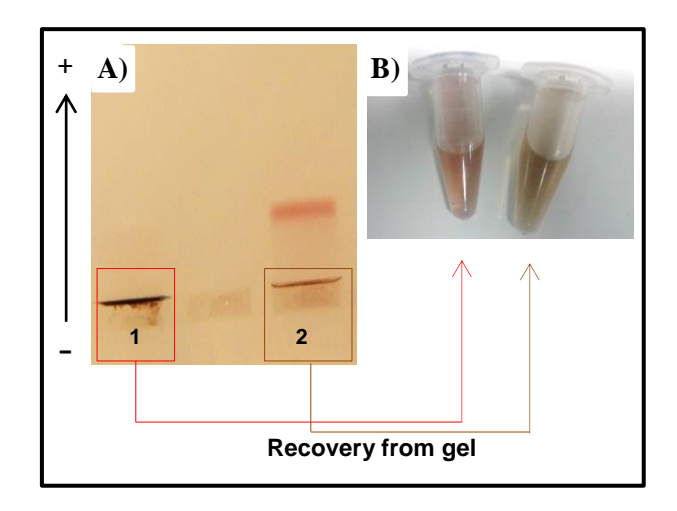


Figure 6.14 A) Agarose gel purification of covalently linked GO-AuNP assemblies (lane 1) and assemblies formed simply by DNA hybridisation (lane 2) after treatment with **S4**. **B)** The corresponding, recovered products of lanes **1** and **2**.

Lane 2 shows the control experiment. A red band, representing unbound DNA-AuNPs, was visible in the gel. On the other hand, no red band could be seen for ligated assemblies (lane 1). This suggested that the click ligation was successful and assemblies remained intact after the removal of **S3** unlike assemblies formed solely by DNA hybridisation. This was further observed by the differences in colour of either product after recovery from the gel. While ligated assemblies displayed a pale red colour, which was attributed to conjugated AuNPs, 'control' assemblies displayed a pale brown colour, characteristic of GO [33].

Products recovered from the agarose gel were further investigated by UV-vis spectroscopy. Representative spectra are shown in **Figure 6.15.**

The red graph, resembling ligated assemblies, displayed the characteristic gold nanoparticle plasmon peak at 520nm [35], whilst the UV-vis spectrum of 'control'

assemblies (black curve) displayed only the characteristic peak of GO conjugated to DNA [36] (see **chapter 4**).

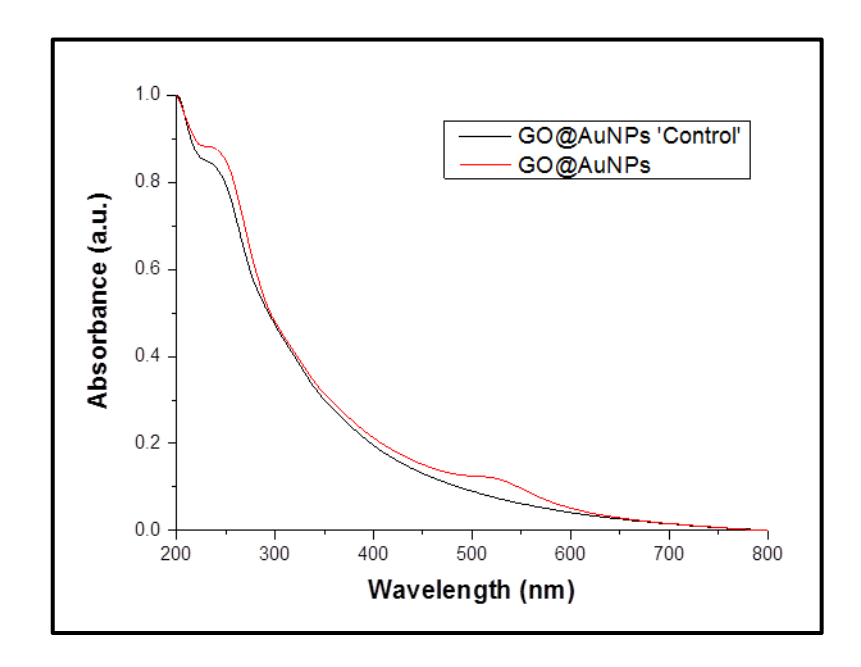


Figure 6.15 Normalized UV-vis spectra of clicked GO/AuNP hybrid assemblies and 'control' assemblies after treatment with **S4** and agarose gel purification.

Transmission electron microscopy further confirmed the obtained results (Figure 6.16).

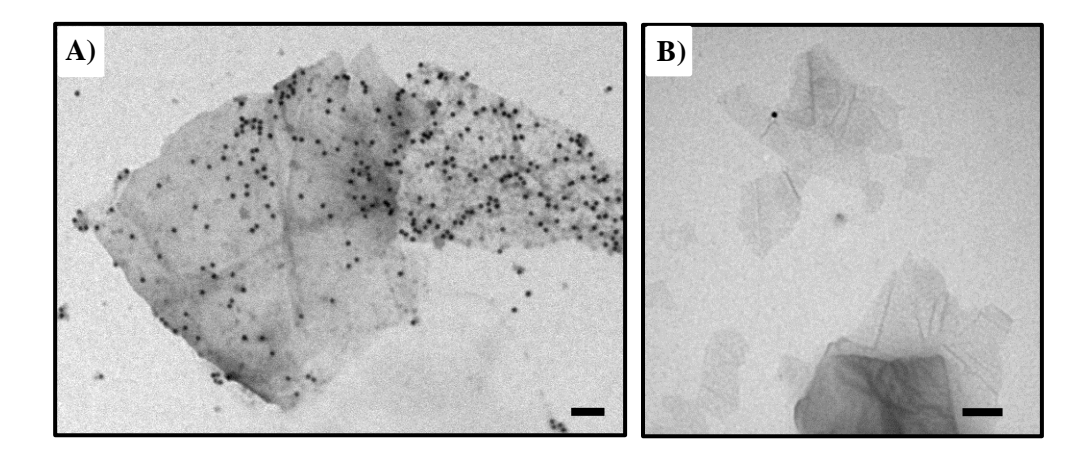


Figure 6.16 TEM micrographs of ligated (**A**) and control AuNP/GO assemblies after treatment with **S4**. Scale bars are 100 nm.

Ligated assemblies showed GO sheets decorated with AuNPs (**Fig. 6.16 A**). However, assemblies formed by hybridisation only, showed mostly bare GO sheets (**Fig. 6.16 B**). This suggested that 'control' assemblies had dissociated, as discussed before. The TEM images complementary to the agarose gel and UV-vis results, suggested that ligated GO/AuNP hybrid assemblies were firmly connected and displayed good stability.

GO/AuNP hybrid assemblies will be investigated for applications as biosensors in the future. They are furthermore being investigated for implementation into solar cells by Dr. Emmanuel Stratakis at the IESL-FORTH, Crete.

6.3 Gold nanoparticle dimers for intracellular applications.

The potential of using gold nanoparticle assemblies for biomedical applications has recently been reported [1, 2]. For such applications it is highly important that assemblies are stable within the intra- and extracellular environment. As discussed in section 2.5, results by Chan and co-workers showed the intracellular disassembly of nanostructures. The assemblies produced in this chapter are covalently linked. Thus their stability towards conditions met with in a biological environment should be increased. In order to investigate this, the simplest assemblies, dimers of AuNPs formed by DNA click ligation were tested for stability in serum-containing cell culture medium. Additionally their susceptibility towards degradation by nuclease enzymes was elucidated (section 6.4.1). Finally the interactions of AuNP dimers with cells were investigated (section 6.4.2).

6.3.1 Stability assays of dimers.

6.3.1.1 Cell culture media stability assays of dimers.

Initially the stability of AuNP dimers in serum containing cell culture medium (MEM + 10 % FBS, see **Appendix I** for formulation) was investigated. After incubation at 37 °C for 24 h, dimer integrity was visualised using agarose gel electrophoresis. A corresponding gel is depicted in **Figure 6.17.**

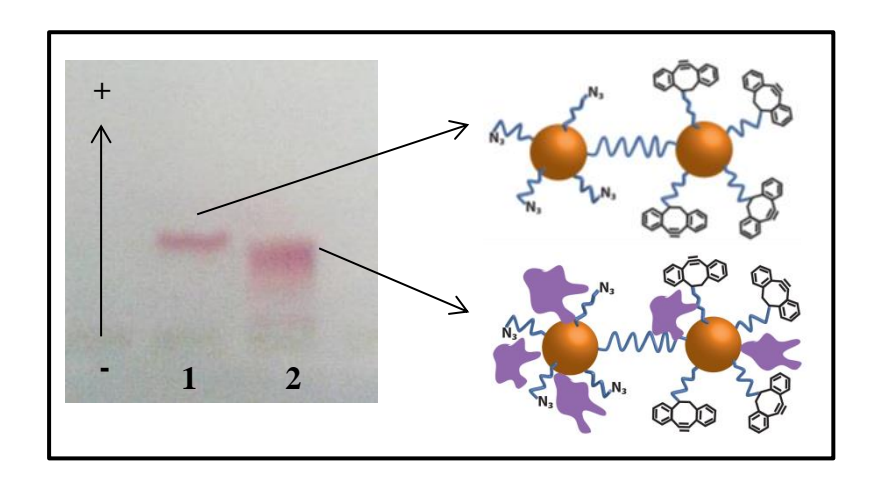


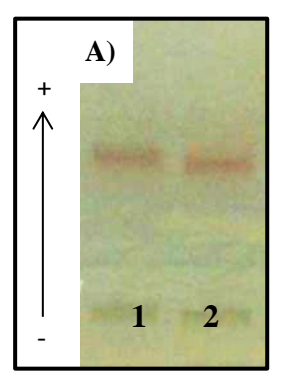
Figure 6.17 Agarose gel electrophoresis of AuNP dimers after incubation in cell culture medium (lane 2). Lane 1: dimers as reference.

The agarose gel depicted in **Fig. 6.17** shows dimers as a reference in lane 1, whilst lane 2 represents dimers after incubation in cell culture medium. One can see that dimers in lane 2 display a broader band with slightly decreased electrophoretic mobility. This can be attributed to interactions with serum proteins [37]. Importantly, no dimer dissociation could be observed, implying that assemblies were stable in MEM cell culture medium.

6.3.1.2 Nuclease assay of dimers.

Another important factor, which must be considered, is stability of DNA-nanoparticle dimers with respect to nuclease degradation. Although individual DNA-AuNPs exhibit increased resistance towards digestion by nucleases [38] as previously discussed (see **section 5.1.2.2**), assemblies might dissociate as a result of DNA degradation.

In order to investigate the effect of nucleases on dimer stability, dimers were incubated with DNAse I or DNAse II in appropriately buffered solutions at 37 °C for 18 h (cf. section 5.1.2.2.). The results of this assay were visualised by agarose gel electrophoresis (Figure 6.18).



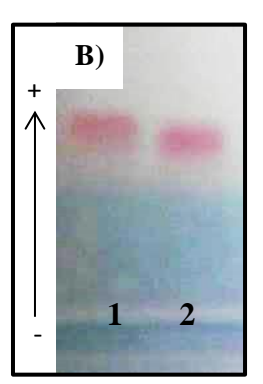


Figure 6.18 Agarose gel electrophoresis of AuNP dimers after incubation with **A**) DNAse I and **B**) DNAse II.

Lane 1 represents untreated dimers as a reference, whilst lane 2 shows dimers after incubation with either DNAse I (**Fig. 6.18 A**) or DNAse II (**Fig. 6.18 B**).

Both agarose gels showed no significant change in lane 2 compared to reference in lane 1. Slight decreases in electrophoretic mobility could be observed in both cases. This was attributed to interactions with the respective nuclease enzyme or BSA, present in the solution. Furthermore, no additional bands suggesting dimer disassembly could be observed after the nuclease assays. This implied that AuNP dimers, analogous to

individual DNA-AuNP conjugates, displayed increased resistance towards degradation by both DNAse I and DNAse II nucleases.

Further confirmations of stability such as analysis by transmission electron microscopy after stability assays will be carried out in the future.

6.3.2 Interactions of dimers with cell culture.

Dimers were investigated for their biocompatibility (section 6.3.2.1) and intracellular stability (6.3.2.2).

6.4.2.1 Viability assays of cells incubated with dimers.

As shown in **section 5.2.4**, DNA-AuNP conjugates were found to exhibit no significant cytotoxicity. However, various studies have shown that nanoparticles of different shapes, sizes and surface modifications can display different toxicity profiles [39, 40]. As interactions of dimeric gold nanoparticle assemblies with cell culture have not been studied to date, it is imperative to determine their cytotoxicity. Dimers were incubated with 16HBE and MRC-5 cells for 18 h (~1.4 pmol of AuNPs per 100.000 cells). Cell viability was subsequently assessed using a trypan bule dye-exclusion assay [41] (see **section 3.7** for experimental procedures). The corresponding results are depicted in **Figure 6.19.** The viability assay shows that, analogous to individual AuNP-DNA conjugates, dimers exhibited no significant cytotoxicity within the conditions tested. A broader range of conditions will be investigated in order to create a detailed cytotoxicity profile in the future.

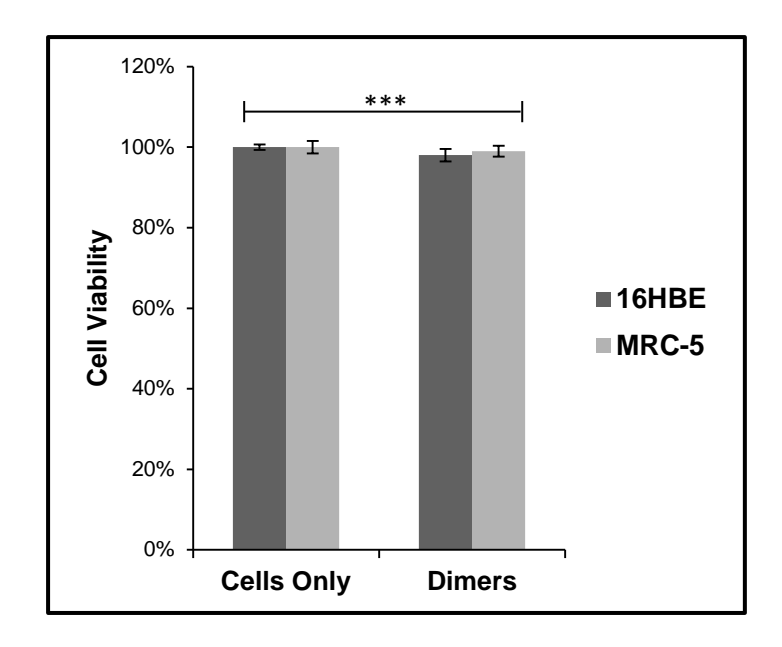


Figure 6.19 Viability assay of MRC-5 fibroblasts incubated with AuNP dimers. Mean SEM, n=3, *** p < 0.01 for a one-tailed t-test.

6.3.2.2 Transmission electron microscopy of cells incubated with dimers.

In order to visualise the intracellular localization of dimers and to qualitatively assess their stability within biological structures, dimers were incubated with fibroblasts or epithelial cells for 18 h and subsequently processed for thin sectioning (see section 3.7 for experimental procedures). Transmission electron microscopy was employed to visualise cell sections (Figure 6.20).

TEM micrographs reveal that assemblies appear to retain their dimeric structure when internalized by cells. After 18 h assemblies were mostly located within cellular vesicles as a result of being endocytosed. This is in accordance with earlier findings for AuNP-DNA conjugates (see **Figure 5.16**). However, **Fig. 6.20 B** showed interestingly the apparent formation of exosomes (indicated by the label EX). These small cellular vesicles are formed by the inward budding of the endosomal membrane during the evolution of endosomes into multivesicular bodies. Exosomes, carrying exogenous miRNA or mRNA are then secreted and subsequently taken up by another cell [42].

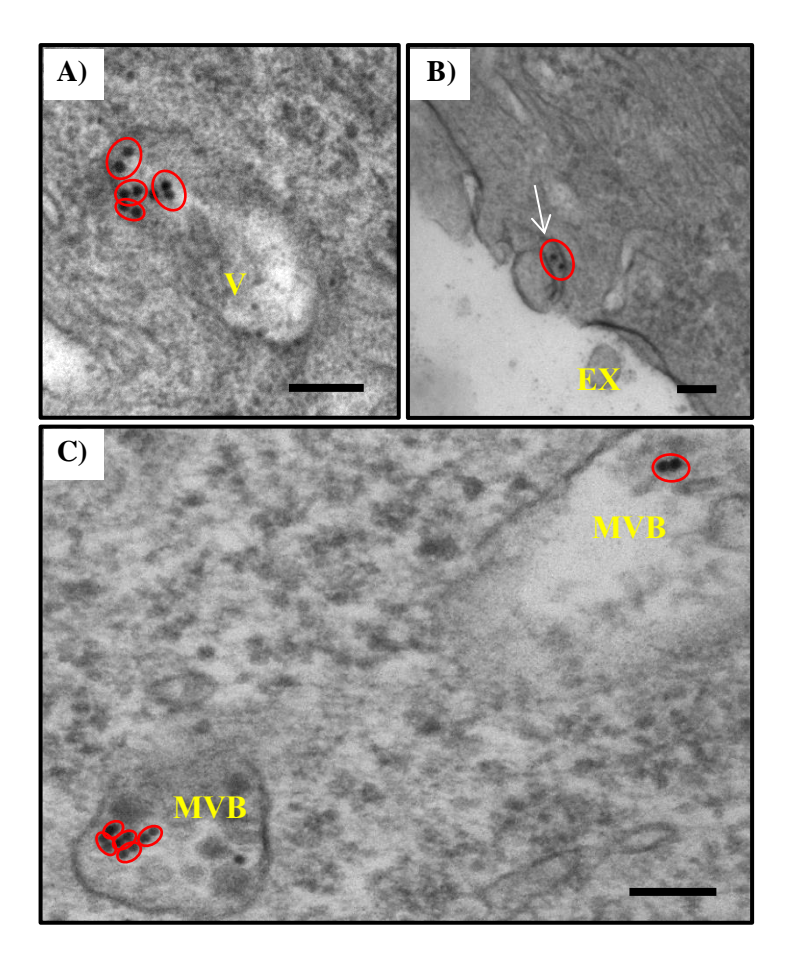
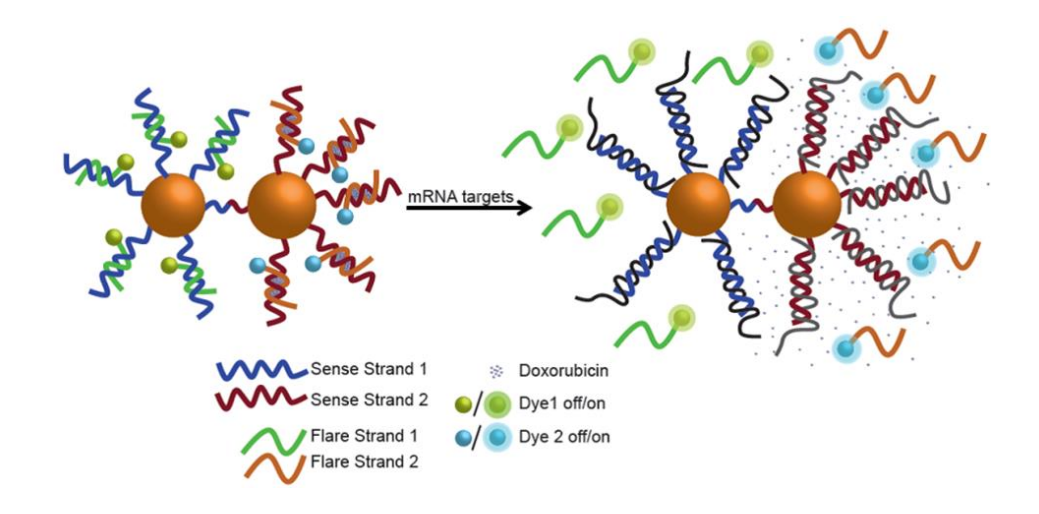


Figure 6.20 TEM micrographs of cells incubated with AuNP dimers. Scale bars are 100 nm. V= vesicle, EX = exosome, MVB = multivesicular body.

Their potential use as delivery vehicles for nanomaterials has recently been discussed by Mirkin *et al.* [43]. They showed that a small percentage (< 1 %) of DNA-AuNP conjugates was sorted into exosomes, after incubation with different cell cultures. Similarly, it is hypothesized that the dimer indicated by the white arrow in **Figure 6.20 B** could have been sorted into an exosome. This finding will be further investigated in future work and potential advantages of exosome encapsulation will be explored.

Following these initial promising findings, it is envisaged that AuNP dimers will be further developed into multiplexed theranostic nano-probes in the future (see **scheme 6.6**).



Scheme 6.7 Schematic illustration of a multiplexed nano-probe based on a dimer of gold nanoparticles.

6.4 References

- Chou, L.Y.T., K. Zagorovsky, and W.C.W. Chan, DNA assembly of nanoparticle superstructures for controlled biological delivery and elimination. Nature Nanotechnology, 2014. 9(2): p. 148-155.
- Xu, L.G., et al., Regiospecific Plasmonic Assemblies for in Situ Raman Spectroscopy in Live Cells. Journal of the American Chemical Society, 2012.
 134(3): p. 1699-1709.
- 3. Heuer-Jungemann, A., et al., Copper-free click chemistry as an emerging tool for the programmed ligation of DNA-functionalised gold nanoparticles.

 Nanoscale, 2013. 5(16): p. 7209-7212.
- 4. Haque, M. and X. Peng, *DNA-associated click chemistry*. Science China Chemistry, 2014. **57**(2): p. 215-231.
- 5. Jawalekar, A.M., et al., Oligonucleotide Tagging for Copper-Free Click Conjugation. Molecules, 2013. **18**(7): p. 7346-7363.

- 6. Shelbourne, M., et al., Fast copper-free click DNA ligation by the ring-strain promoted alkyne-azide cycloaddition reaction. Chemical Communications, 2011. 47(22): p. 6257-6259.
- 7. Azbel, M.Y., *DNA SEQUENCING AND MELTING CURVE*. Proceedings of the National Academy of Sciences of the United States of America, 1979. **76**(1): p. 101-105.
- 8. Gray, B.J., Basic biochemical methods: By RR Alexander, JM Griffiths and ML Wilkinson. pp. 241. John Wiley & Sons, Chichester. 1985. £31.60 ISBN 0-471-88027-2. Biochemical Education, 1985. **13**(4): p. 186-186.
- Blackburn, G.M., Nucleic Acids in Chemistry and Biology. 2006, Cambridge:
 Royal Society of Chemistry.
- Ackerson, C.J., M.T. Sykes, and R.D. Kornberg, *Defined DNA/nanoparticle conjugates*. Proceedings of the National Academy of Sciences of the United States of America, 2005. 102(38): p. 13383-13385.
- 11. Keller, S. and A. Marx, *The use of enzymes for construction of DNA-based objects and assemblies.* Chemical Society Reviews, 2011. **40**(12): p. 5690-5697.
- 12. Claridge, S.A., et al., Enzymatic ligation creates discrete multinanoparticle building blocks for self-assembly. J Am Chem Soc, 2008. **130**(29): p. 9598-9605.
- 13. Kanaras, A.G., et al., Enzymatic disassembly of DNA-gold nanostructures. Small, 2007. **3**(4): p. 590-4.
- 14. Kanaras, A.G., et al., Site-specific ligation of DNA-modified gold nanoparticles activated by the restriction enzyme Styl. Small, 2007. **3**(1): p. 67-70.

- 15. Kanaras, A.G., et al., *Towards multistep nanostructure synthesis: Programmed enzymatic self-assembly of DNA/gold systems*. Angewandte Chemie-International Edition, 2003. **42**(2): p. 191-+.
- 16. Xu, X., et al., Asymmetric Functionalization of Gold Nanoparticles with Oligonucleotides. Journal of the American Chemical Society, 2006. **128**(29): p. 9286-9287.
- 17. Kolosnjaj-Tabi, J., et al., *Heat-Generating Iron Oxide Nanocubes: Subtle* "Destructurators" of the Tumoral Microenvironment. ACS Nano, 2014. **8**(5): p. 4268-4283.
- 18. Lee, N., et al., Water-Dispersible Ferrimagnetic Iron Oxide Nanocubes with Extremely High r2 Relaxivity for Highly Sensitive in Vivo MRI of Tumors. Nano Letters, 2012. **12**(6): p. 3127-3131.
- Bartczak, D. and A.G. Kanaras, Preparation of Peptide-Functionalized Gold Nanoparticles Using One Pot EDC/Sulfo-NHS Coupling. Langmuir, 2011.
 27(16): p. 10119-10123.
- 20. Gschneidtner, T.A., et al., A Versatile Self-Assembly Strategy for the Synthesis of Shape-Selected Colloidal Noble Metal Nanoparticle Heterodimers. Langmuir, 2014. **30**(11): p. 3041-3050.
- 21. Zhao, Y., et al., Shell-Engineered Chiroplasmonic Assemblies of Nanoparticles for Zeptomolar DNA Detection. Nano Letters, 2014. **14**(7): p. 3908-3913.
- 22. Maye, M.M., O. Gang, and M. Cotlet, *Photoluminescence enhancement in CdSe/ZnS-DNA linked-Au nanoparticle heterodimers probed by single molecule spectroscopy*. Chemical Communications, 2010. **46**(33): p. 6111-6113.

- 23. Yugang, Z., et al., A general strategy for the DNA-mediated self-assembly of functional nanoparticles into heterogeneous systems. Nature Nanotechnology, 2013. **8**(11): p. 865-72.
- 24. Lee, J.-H., G.-H. Kim, and J.-M. Nam, *Directional Synthesis and Assembly of Bimetallic Nanosnowmen with DNA*. Journal of the American Chemical Society, 2012. **134**(12): p. 5456-5459.
- 25. Sun, Y., et al., Interfaced Metal Heterodimers in the Quantum Size Regime.

 Nano Letters, 2013. **13**(8): p. 3958-3964.
- 26. Read, C.G., A.J. Biacchi, and R.E. Schaak, *Au–Ge and Ag–Ge Heterodimers* with Tunable Domain Sizes: A Supersaturation-Precipitation Route to Colloidal Hybrid Nanoparticles. Chemistry of Materials, 2013. **25**(21): p. 4304-4311.
- 27. Yi, D.K., et al., Silica-Coated Nanocomposites of Magnetic Nanoparticles and Quantum Dots. Journal of the American Chemical Society, 2005. **127**(14): p. 4990-4991.
- 28. Wang, M., et al., *Cross-linked Heterogeneous Nanoparticles as Bifunctional Probe.* Chemistry of Materials, 2012. **24**(13): p. 2423-2425.
- 29. Truby, R.L., S.Y. Emelianov, and K.A. Homan, *Ligand-Mediated Self-Assembly of Hybrid Plasmonic and Superparamagnetic Nanostructures*. Langmuir, 2013. **29**(8): p. 2465-2470.
- 30. Peng, E., et al., Multifunctional PEGylated nanoclusters for biomedical applications. Nanoscale, 2013. **5**(13): p. 5994-6005.
- 31. Liu, Y., et al., *Synthesis of Cu2–xSe Nanocrystals by Tuning the Reactivity of Se.*The Journal of Physical Chemistry C, 2011. **115**(20): p. 9909-9916.
- 32. Liu, X., et al., Cu2-xSe@mSiO2-PEG core-shell nanoparticles: a low-toxic and efficient difunctional nanoplatform for chemo-photothermal therapy under near

- infrared light radiation with a safe power density. Nanoscale, 2014. **6**(8): p. 4361-4370.
- 33. Wang, Z.H., et al., *Polyvalent DNA-graphene nanosheets "click" conjugates*. Nanoscale, 2012. **4**(2): p. 394-399.
- 34. Loh, K.P., et al., *Graphene oxide as a chemically tunable platform for optical applications*. Nat Chem, 2010. **2**(12): p. 1015-1024.
- 35. Mie, G., Beiträge zur Optik trüber Medien, speziell Kolloidaler Metallösungen.

 Annalen der Physik, 1908. **25**(4): p. 377-445.
- 36. Liu, F., J.Y. Choi, and T.S. Seo, *Graphene oxide arrays for detecting specific DNA hybridization by fluorescence resonance energy transfer*. Biosensors & Bioelectronics, 2010. **25**(10): p. 2361-2365.
- 37. Albanese, A., et al., Secreted Biomolecules Alter the Biological Identity and Cellular Interactions of Nanoparticles. Acs Nano, 2014. **8**(6): p. 5515-5526.
- 38. Wu, X.C.A., et al., *Intracellular Fate of Spherical Nucleic Acid Nanoparticle Conjugates*. Journal of the American Chemical Society, 2014. **136**(21): p. 7726-7733.
- 39. Tarantola, M., et al., Toxicity of gold-nanoparticles: Synergistic effects of shape and surface functionalization on micromotility of epithelial cells.

 Nanotoxicology, 2011. **5**(2): p. 254-268.
- 40. Shang, L., K. Nienhaus, and G. Nienhaus, *Engineered nanoparticles interacting* with cells: size matters. Journal of Nanobiotechnology, 2014. **12**(1): p. 5.
- 41. Strober, W., *Trypan Blue Exclusion Test of Cell Viability*, in *Current Protocols in Immunology*. 2001, John Wiley & Sons, Inc.
- 42. Thery, C., L. Zitvogel, and S. Amigorena, *Exosomes: Composition, biogenesis and function.* Nature Reviews Immunology, 2002. **2**(8): p. 569-579.

43. Alhasan, A.H., et al., Exosome Encased Spherical Nucleic Acid Gold Nanoparticle Conjugates as Potent MicroRNA Regulation Agents. Small, 2014.

10(1): p. 186-192.

CHAPTER 7

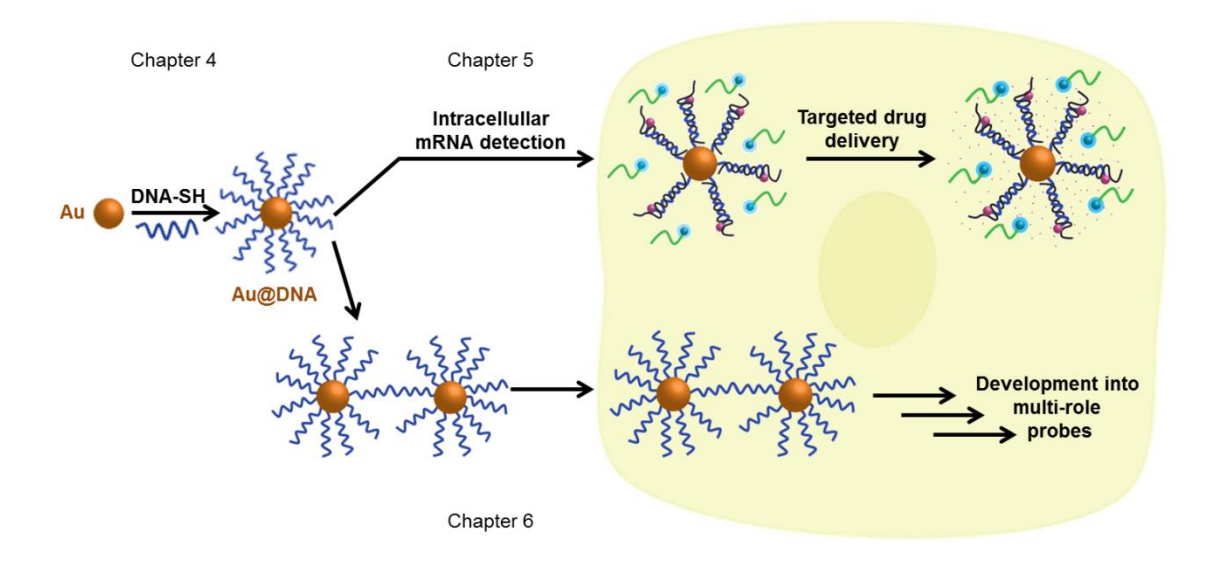
-Summary and Outlook-

The last decades have seen a rapid development in the field of bionanotechnology. The library of functional nanomaterials available has expanded tremendously with new discoveries constantly emerging. In particular the development of DNA-modified nanomaterial systems has come to maturity with demands for implementation in biosensing, metamaterials and far beyond.

In this project DNA-nanomaterial conjugates were investigated for their potential applications in biomedicine. A summary of obtained results and an outlook to future work are outlined below.

7.1 Summary of results.

Gold nanoparticles were conjugated to oligonucleotides (**chapter 4**). The conjugation to oligonucleotides endows nanomaterials with additional functionality. This functionality is inherent of the DNA ligand and infers stability, biocompatibility and the ability to bind to a specific target. Consequently, DNA-gold nanoparticle conjugates were explored for their use in biomedical applications (**chapter 5**). **Scheme 7.1** shows a summarizing illustration. Probes capable of intracellular detection of mRNAs in live cells were demonstrated. These probes consist of gold nanoparticles conjugated to fluorophore-tagged oligonucleotides. The sequence of these oligonucleotides was designed to detect different pre-chosen mRNAs. By careful BLAST searching, oligonucleotides for the sensing of Vimentin, Desmocollin, Cytokeratin 8 and total mRNA were designed. The former three targets were chosen due to their significance in epithelial cell-based cancer [1-6]. Initial experiments indicated

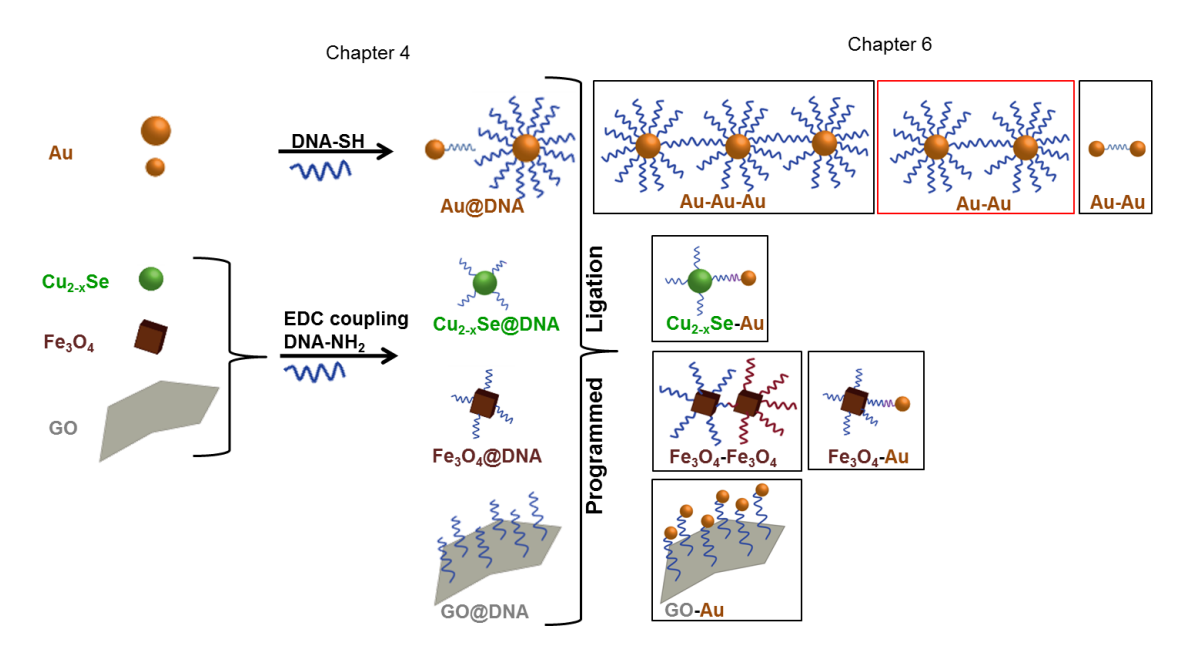


Scheme 7.1 Schematic illustration of the different applications of DNA-AuNP conjugates. Single conjugates were developed into live cell mRNA detection probes and drug delivery vehicles. Interactions of AuNP dimers with cells were investigated.

that both epithelial and fibroblast cell lines showed good uptake of total mRNA detecting nano-probes without significant cytotoxicity. Furthermore confocal microscopy revealed a high fluorescent signal, arising from the detection of total mRNA. The employment of Vimentin, Desmocollin and Cytokeration 8 detection nano-probes showed that selective sensing of each mRNA was possible. The sensing of mRNA targets involved in tumerogenesis could allow for early detection of cancer and aid in the determination of tumour progression.

As a further development, the chemotherapeutic drug doxorubicin was incorporated into the probe design. Confocal microscopy showed that highly selective drug release in conjunction with mRNA detection was possible. The activity of the drug delivered by the nano-probes was found to be significantly higher than that of the free drug. It is envisaged that the obtained results will be useful for the universal design of nanoplatforms that can act as a 'Trojan horse' - bringing important biomolecules and drugs into cells, including DNA.

As discussed above, the detection of mRNA targets involved in tumerogenesis is highly important for the determination of tumour progression. However, researchers have shown that often at least two different mRNA targets should be monitored [7]. For this, two different detection probes could be used. However, it would be difficult to ensure their localization within the same local microenvironment. Therefore we proposed the use of a probe consisting of two covalently linked gold nanoparticles. This dimer consists of two different mRNA detection probes. Due to the covalent connection between each probe, detection within the same local microenvironment would be made possible. Moreover, assemblies of nanoparticles have recently been reported as potent agents for biomedical applications [8, 9]. Exploring this further, a new strategy to prepare highly stable assemblies of nanomaterials was developed (**chapter 6**). In order to create a library of functional building blocks, different nanomaterials (Cu_{2-x}Se, Fe₃O₄, GO) were conjugated to DNA. Especially for Cu_{2-x}Se this had not been demonstrated before. DNA-nanomaterial conjugates were organized into pre-defined structures by



Scheme 7.2 Schematic illustration of the surface modifications of different nanomaterials with oligonucleotides in order to create building blocks for self-assembly. Assembled structures shown are AuNP dimers (13 nm and 5 nm) and trimers (13 nm), Cu_{2-x}Se-AuNP heterodimers, Fe₃O₄-AuNP heterodimers, Fe₃O₄ dimers, GO-AuNP hybrid assemblies.

programmed DNA hybridisation. Both homo- and heterogeneous assemblies were formed (see scheme 7.2). Furthermore, copper-free click chemistry was introduced as a novel tool to ligate assembled structures. This method enables the facile fabrication of nano-sized assemblies, connected by single-stranded DNA. It presents an easy way for multistep synthesis of highly advanced nanostructures. An advantage of this method is the retained ability of the linking DNA to hybridise to complementary targets [10]. Another advantage is the increased stability of assemblies owing to the covalent bond linking individual building blocks.

The universal applicability of the demonstrated approach was validated by the formation of gold nanoparticle/graphene oxide hybrid materials. Commonly these types of hybrids are formed *via* non-covalent interactions. These have proven to be unsuitable for many biological applications [11]. Here it was shown that the employment of click ligation resulted in highly stable, covalently linked AuNP/GO hybrid materials that could find applications in many fields ranging from implementation into photovoltaics to biomedicine.

As an extension to the current developments, preliminary results on the interactions of gold nanoparticle dimers with cells were presented (cf. scheme 7.1). These dimers were prepared by the programmed ligation approach. Dimers showed good stability with respect to conditions met within a biological environment. Moreover, transmission electron micrographs of cell thin sections suggested that dimers appeared to stay assembled after cellular uptake. It is expected that gold nanoparticle dimers have the potential of being developed into multi-role probes (see section 7.2).

7.2 Outlook to future work.

Using ligated gold nanoparticle dimers (see **chapter 6**), it is envisaged to create a multiplexed probe, capable of detecting simultaneously more than one mRNA target and furthermore releasing one or two chemotherapeutic drugs. In this dimeric probe, the nanoparticles forming the dimer will act synergistically in a local microenvironment. This function would be drastically less efficient if single nanoparticle probes were employed.

Furthermore the results of this project show that DNA-AuNP conjugates show great potential as theranostic agents. However, some fundamental issues still remain unsolved. One of the most important ones is the question of 'How do nano-probes escape the endosomes'? Both confocal and TEM images suggest that some nanoparticles are localized in the cytosol. Furthermore, as discussed in **chapter 5**, fluorescence of the flare strands often displays co-localization with mitochondria. This strongly suggests that mRNA detection occurs inside the cytosol. Therefore a study should be conducted involving the simultaneous imaging and tracking of the nanoparticle core as well as the flare strand fluorescence. In conjunction with organelle-labelling, this should shed light on the potential endosomal escape mechanism. This study should be conducted for both single particle nano-probes as well as for assemblies.

Moreover the applications of heterogeneous assembly systems will be tested *in vitro*. For example, an Au-Cu_{2-X}Se dimer could show great potential as a theranostic probe. Cu_{2-X}Se nanoparticles display a plasmon band in the NIR [12]. This property can be used for laser hyperthermia applications *in vivo*, as the so-called 'biological windows' occur between 650-950 and 1000-1350 nm [13]. In these ranges, maximum tissue penetration by laser light can be achieved. Thus Cu_{2-X}Se nanoparticles have shown great potential for photothermal therapy [14]. Making use of the properties of both particles,

one could envisage a Au- Cu_{2-x}Se heterodimer as a multi-functional biosensor for combined target detection in conjunction with chemo- and photothermal therapy. The combination of chemo- and photothermal therapy allows the use of lower laser powers and hence results in lower tissue damage. On the other hand, a heterodimer made up of an optical (e.g. Au) and a magnetic nanomaterial could find exciting applications for combined target detection in conjunction with chemotherapy and magnetic hyperthermia. Furthermore one could envisage applications for water treatment. Whilst the optical nanoparticle could be used to detect and bind to specific pathogens in drinking water (using DNA), the magnetic properties of the second nanoparticle could allow for the removal of these pathogens by simply applying a magnetic field.

Thus by expanding the library of DNA-nanomaterials available for assembly formation, the possibilities of creating different probes with varying properties on demand are seemingly endless.

A further very important step will then be the applications *in vivo*. Many studies have aimed to understand the distribution and clearance of metal nanoparticles from the body [9, 15-19]. However, fully conclusive results have not yet been reached. Therefore it would be highly interesting and of benefit to the scientific community to study the potential delivery routes, biodistribution and activity of DNA-AuNP detection agents *in vivo*. Recently it was shown that peptide-coated AuNPs are capable of penetrating through skin [20]. The possibility of transdermal delivery of the nano-probes would be highly attractive and should be investigated.

All in all, this field is still in its infancy and great discoveries should be expected.

After addressing some fundamental issues, the applications of nanomaterials for biomedicine should take this field to the next level.

The author of this thesis was awarded a one year fellowship ('Doctoral Prize') by the EPSRC. The proposed project for this fellowship will be based on the use of AuNP dimers for biomedical applications as discussed above.

7.3 References.

- 1. Cui, T., et al., *Diagnostic and prognostic impact of desmocollins in human lung* cancer. Journal of Clinical Pathology, 2012. **65**(12): p. 1100-1106.
- 2. Satelli, A. and S. Li, *Vimentin in cancer and its potential as a molecular target for cancer therapy*. Cellular and Molecular Life Sciences, 2011. **68**(18): p. 3033-3046.
- 3. Dauphin, M., et al., Vimentin expression predicts the occurrence of metastases in non small cell lung carcinomas. Lung Cancer, 2013. **81**(1): p. 117-122.
- 4. Buccheri, G. and D. Ferrigno, *Lung tumor markers of cytokeratin origin: an overview*. Lung Cancer, 2001. **34, Supplement 2**(0): p. S65-S69.
- 5. Fukunaga, Y., et al., Expression of cytokeratin 8 in lung cancer cell lines and measurement of serum cytokeratin 8 in lung cancer patients. Lung Cancer, 2002.

 38(1): p. 31-38.
- 6. Barak, V., et al., *Clinical utility of cytokeratins as tumor markers*. Clinical Biochemistry, 2004. **37**(7): p. 529-540.
- 7. Pan, W., et al., Multiplexed Detection and Imaging of Intracellular mRNAs

 Using a Four-Color Nanoprobe. Analytical Chemistry, 2013. 85(21): p. 10581
 10588.
- 8. Xu, L.G., et al., Regiospecific Plasmonic Assemblies for in Situ Raman Spectroscopy in Live Cells. Journal of the American Chemical Society, 2012. 134(3): p. 1699-1709.

- 9. Chou, L.Y.T., K. Zagorovsky, and W.C.W. Chan, *DNA assembly of nanoparticle superstructures for controlled biological delivery and elimination*.

 Nature Nanotechnology, 2014. **9**(2): p. 148-155.
- 10. Claridge, S.A., et al., Enzymatic ligation creates discrete multinanoparticle building blocks for self-assembly. J Am Chem Soc, 2008. **130**(29): p. 9598-9605.
- 11. Wang, Z.H., et al., *Polyvalent DNA-graphene nanosheets "click" conjugates*.

 Nanoscale, 2012. **4**(2): p. 394-399.
- 12. Liu, Y., et al., *Synthesis of Cu2–xSe Nanocrystals by Tuning the Reactivity of Se.*The Journal of Physical Chemistry C, 2011. **115**(20): p. 9909-9916.
- 13. Tsai, M.-F., et al., Au Nanorod Design as Light-Absorber in the First and Second Biological Near-Infrared Windows for in Vivo Photothermal Therapy.

 ACS Nano, 2013. 7(6): p. 5330-5342.
- 14. Liu, X., et al., Cu2-xSe@mSiO2-PEG core-shell nanoparticles: a low-toxic and efficient difunctional nanoplatform for chemo-photothermal therapy under near infrared light radiation with a safe power density. Nanoscale, 2014. **6**(8): p. 4361-4370.
- 15. Marchesano, V., et al., *Imaging Inward and Outward Trafficking of Gold Nanoparticles in Whole Animals*. Acs Nano, 2013. **7**(3): p. 2431-2442.
- 16. Simpson, C.A., et al., *In vivo toxicity, biodistribution, and clearance of glutathione-coated gold nanoparticles.* Nanomedicine: Nanotechnology, Biology and Medicine, 2013. **9**(2): p. 257-263.
- 17. Goel, R., et al., *Biodistribution of TNF-alpha-coated gold nanoparticles in an in vivo model system.* Nanomedicine, 2009. **4**(4): p. 401-410.
- 18. Almeida, J.P.M., et al., *In vivo biodistribution of nanoparticles*. Nanomedicine, 2011. **6**(5): p. 815-835.

CHAPTER 7 - Summary and Outlook

- 19. Khlebtsov, N. and L. Dykman, *Biodistribution and toxicity of engineered gold nanoparticles: a review of in vitro and in vivo studies.* Chemical Society Reviews, 2011. **40**(3): p. 1647-1671.
- 20. Fernandes, R., et al., *Interactions of Skin with Gold Nanoparticles of Different Surface Charge, Shape, and Functionality*. Small, 2014: p. n/a-n/a.

APPENDIX I

-List of reagents and suppliers-

AI.1 List of reagent suppliers.

Sigma Aldrich: Sodium tetrachloroaurate (III) dihydrate, trisodium citrate,

sodium phosphate monobasic, sodium phosphate dibasic, Bis(p-sulfonatophenyl)phenyl

phosphine dihydrate dipotassium salt (BSPP), sodium borohydride, glutathione, DNASe

I, DNAse II Tris base, EDTA, agarose, bovine serum albumin (BSA), sodium dodecyl

sulfate (SDS), fetal bovine (FBS), trypsin, trypan blue, 1-(3serum

(dimethylamino)propyl)-3-ethyl-carbodiimidemethiodide (EDC), phosphate buffered

silane (PBS tablets), N,N,N',N'-tetramethylethylenediamine, ammonium persulfate,

Ficoll, Urea, doxorubicin hydrochloride, Hank's Balanced Salt Solution (HBSS),

Mowiol.

Fisher Scientific: Potassium carbonate, N-hydroxysulfosuccinimide (sulfo-

NHS), Calcium carbonate, Potassium iodide, Iodine, boric acid, sodium hydroxide,

acrylamide:bis acrylamide 40%, ethanol, acetonitrile.

Agar Scientific: osmium tetroxide, uranyl acetate, lead nitrate, Spurr resin,

glutaraldehyde, formaldehyde, piperazine-1,4-bis(2-ethanesulfonic acid) (PIPES buffer),

200 mesh copper/nickel grid.

SPI: Carbon film 400 mesh copper grid.

i

Gibco: Minimum Essential Medium (MEM), Dulbecco's Modified Essential Medium (DMEM), RPMI medium, Pen/Strep, L-glutamine, nystatin.

lifetechnologies (**Invitrogen**): Antibodies for Vimentin, Desmocollin and Cytokeratin 8 (mouse monoclonal AB), Alexa Flour 568 Goat Anti-mouse IgG, 4',6-diamidino-2-phenylindole (DAPI), Hoechst 33342.

AI.2 Formulations of cell culture media.

All formulations were taken from www.lifetechnologies.com.

Table AI.1 Formulation of Minimum Essential Medium.

Components	Molecular Weight	Concentration (mg/L)	mM	
	Amino Aci			
L-Arginine hydrochloride	211	126	0.597	
L-Cystine	240	24	0.1	
L-Glutamine	146	292	2	
L-Histidine hydrochloride- H2O	210	42	0.2	
L-Isoleucine	131	52	0.397	
L-Leucine	131	52	0.397	
L-Lysine hydrochloride	183	73	0.399	
L-Methionine	149	15	0.101	
L-Phenylalanine	165	32	0.194	
L-Threonine	119	48	0.403	
L-Tryptophan	204	10	0.049	
L-Tyrosine	181	36	0.199	
L-Valine	117	46	0.393	
	Vitaming	3		
Choline chloride	140	1	0.00714	
D-Calcium pantothenate	477	1	0.0021	
Folic Acid	441	1	0.00227	
Niacinamide	122	1	0.0082	
Pyridoxal hydrochloride	204	1	0.0049	
Riboflavin	376	0.1	0.000266	
Thiamine hydrochloride	337	1	0.00297	
i-Inositol	180	2	0.0111	
	Inorganic S	alts		
Calcium Chloride (CaCl2-2H2O)	147	264	1.8	
Magnesium Sulfate (MgSO4-7H2O)	246	200	0.813	

Potassium Chloride (KCl)	75	400	5.33					
Sodium Bicarbonate	84	2200	26.19					
(NaHCO3)								
Sodium Chloride (NaCl)	58	6800	117.24					
Sodium Phosphate monobasic	156	158	1.01					
(NaH2PO4-2H2O)								
Other Components								
D-Glucose (Dextrose)	180	1000	5.56					
Phenol Red	376.4	10	0.0266					

 Table AI.2 Formulations of Dulbecco's Modified Essential Medium (DMEM).

Components	Molecular Weight	Concentration (mg/L)	mM
A	mino Acids	(g/22)	
Glycine	75	30	0.4
L-Arginine hydrochloride	211	84	0.398
L-Cystine 2HCl	313	63	0.201
L-Glutamine L-Glutamine	146	580	3.97
L-Histidine hydrochloride-H2O	210	42	0.2
L-Isoleucine	131	105	0.802
L-Leucine	131	105	0.802
L-Lysine hydrochloride	183	146	0.798
L-Methionine	149	30	0.201
L-Phenylalanine	165	66	0.4
L-Serine L-Serine	105	42	0.4
L-Threonine	119	95	0.798
L-Tryptophan	204	16	0.0784
L-Tyrosine	181	72	0.398
L-Valine	117	94	0.803
	Vitamins		
Choline chloride	140	4	0.0286
D-Calcium pantothenate	477	4	0.00839
Folic Acid	441	4	0.00907
Niacinamide	122	4	0.0328
Pyridoxine hydrochloride	204	4	0.0196
Riboflavin	376	0.4	0.00106
Thiamine hydrochloride	337	4	0.0119
i-Inositol	180	7.2	0.04
Ind	rganic Salts		
Calcium Chloride (CaCl2-2H2O)	147	264	1.8
Ferric Nitrate (Fe(NO3)3"9H2O)	404	0.1	0.000248
Magnesium Sulfate (MgSO4-7H2O)	246	200	0.813
Potassium Chloride (KCl)	75	400	5.33
Sodium Bicarbonate (NaHCO3)	84	3700	44.05
Sodium Chloride (NaCl)	58	6400	110.34
Sodium Phosphate monobasic (NaH2PO4-2H2O)	154	141	0.916

Other Components								
D-Glucose (Dextrose) 180 4500 25								
Phenol Red 376.4 15 0.0399								

 Table AI.3 Formulation of Roswell Park Memorial Medium (RPMI).

Components	Molecular	Concentration	mM						
_	Weight	(mg/L)							
	Amino Acids								
Glycine	75	10	0.133						
L-Arginine hydrochloride	211	240	1.14						
L-Asparagine	132	50	0.379						
L-Aspartic acid	133	20	0.15						
L-Cystine	240	50	0.208						
L-Glutamic Acid	147	20	0.136						
L-Glutamine	146	300	2.05						
L-Histidine	155	15	0.0968						
L-Hydroxyproline	131	20	0.153						
L-Isoleucine	131	50	0.382						
L-Leucine	131	50	0.382						
L-Lysine hydrochloride	183	40	0.219						
L-Methionine	149	15	0.101						
L-Phenylalanine	165	15	0.0909						
L-Proline	115	20	0.174						
L-Serine	105	30	0.286						
L-Threonine	119	20	0.168						
L-Tryptophan	204	5	0.0245						
L-Tyrosine	181	20	0.11						
L-Valine L-Valine	117	20	0.171						
	Vitamins	•							
Biotin	244	0.2	0.00082						
Choline chloride	140	3	0.0214						
D-Calcium pantothenate	477	0.25	0.000524						
Folic Acid	441	1	0.00227						
Niacinamide	122	1	0.0082						
Para-Aminobenzoic Acid	137	1	0.0073						
Pyridoxine hydrochloride	206	1	0.00485						
Riboflavin	376	0.2	0.000532						
Thiamine hydrochloride	337	1	0.00297						
Vitamin B12	1355	0.005	0.0000037						
i-Inositol	180	35	0.194						
Inorganic Salts									
Calcium nitrate (Ca(NO3)2 4H2O)	236	100	0.424						
Magnesium Sulfate (MgSO4-7H2O)	246	100	0.407						
Potassium Chloride (KCl)	75	400	5.33						

APPENDIX I - List of reagents and suppliers

Sodium Bicarbonate (NaHCO3)	84	2000	23.81				
Sodium Chloride (NaCl)	58	6000	103.45				
Sodium Phosphate dibasic	142	800	5.63				
(Na2HPO4) anhydrous							
Other Components							
Otl	ner Components						
D-Glucose (Dextrose)	ner Components 180	2000	11.11				
	1	2000	11.11 0.00326				

APPENDIX II

- Supplementary information-

AII.1 Sample calculation for the determination of the concentration of a colloidal gold solution.

Concentrations of colloidal gold solutions were determined from the corresponding absorption spectrum at the peak maximum (~520 nm for 13 nm gold nanospheres) using the Beer-Lambert Law (see **chapter 3**) and the appropriate molar extinction co-efficient. ε (13 nm AuNPs) = 2.27×10^8 L mol⁻¹cm⁻¹, ε (5 nm AuNPs) = 9.969×10^6 L mol⁻¹cm⁻¹ [1]. For an optical density of 0.3 and a dilution factor of 10, the concentration can be calculated as follows:

$$c = \frac{AD}{\varepsilon l}$$

$$c = \frac{0.3 \times 10}{1 \text{ cm} \times 2.27 \times 10^8 \text{ L mol}^{-1} \text{cm}^{-1}}$$

$$c = 13.2 \text{ nM}$$

Equation AII.1 Sample calculation for the determination of the concentration of a gold nanoparticle solution.

AII.2 Synthesis of oligonucleotides.

All oligonucleotides were synthesised by Dr. Afaf El-Sagheer at the University of Oxford (formerly at the University of Southampton). The general synthetic procedure is outlined in the following section: Standard DNA phosphoramidites, solid supports, and additional reagents were purchased from Link Technologies and Applied Biosystems Ltd. All oligonucleotides were synthesized on an Applied Biosystems 394

automated DNA/RNA synthesizer using a standard 1.0 µmole phosphoramidite cycle of acid-catalyzed detritylation, coupling, capping, and iodine oxidation. Stepwise coupling efficiencies and overall yields were determined by the automated trityl cation conductivity monitoring facility and in all cases were > 98.0%. All β-cyanoethyl phosphoramidite monomers were dissolved in anhydrous acetonitrile to a concentration of 0.1 M immediately prior to use. The coupling time for normal A, G, C, and T monomers was 35 s, and the coupling time for the modified phosphoramidite monomers (C6-disulfide and aminolink C6, (Link Technologies)) was extended to 360 s. Aminolink C7 columns (Link Technologies) were used for the introduction of the 3'aminohexyl moiety into oligonucleotides. Cleavage of the oligonucleotides from the solid support and deprotection was achieved by exposure to concentrated aqueous ammonia solution for 60 min at room temperature followed by heating in a sealed tube for 5 h at 55 °C. The oligonucleotides were purified by reversed-phase HPLC on a Gilson system using an XBridgeTM BEH300 Prep C18 10 µM 10 x 250 mm column (Waters) with a gradient of acetonitrile in ammonium acetate (0 % to 50 % buffer B over 30 min, flow rate 4 mL/min), buffer A: 0.1 M ammonium acetate, pH 7.0, buffer B: 0.1 M ammonium acetate, pH 7.0, with 50 % acetonitrile. Elution was monitored by UV absorption at 300 nm. After HPLC purification, oligonucleotides were desalted using NAP-10 Sephadex columns (GE Healthcare) and analysed by gel electrophoresis. All oligonucleotides were characterised by electrospray mass spectrometry and capillary electrophoresis (CE). Mass spectra of oligonucleotides were recorded in ES- mode, and in all cases confirmed the integrity of the sequences.

AII.3 Synthesis and water transfer of Cu_{2-x}Se NPs.

AII.3.1 Synthesis of Cu_{2-x}Se NPs.

Cu_{2-x}Se NPs were synthesised and characterized at the Istituto Italiano di Tecnologia by Mr Francesco de Donato according to the following protocol [2]:

Anhydrous CuCl (0.099 g, 1 mmol, Strem Chemicals) was added to a mixture of 5 mL of oleylamine (5 mL, Sigma Aldrich) and 1-octadecene (ODE) (5 mL, Sigma Aldrich). After evacuation of the reaction flask for 1 h at 80 °C using standard Schlenk line technique, the reaction mixture was exposed to a constant flow of nitrogen. The temperature was then set to 300 °C. A solution of Se (0.039 g, 0.5 mmol) in oleylamine (3 mL) was prepared and heated to 150 °C under vacuum for 1 h using standard Schlenk line technique followed by switching to a nitrogen flow and heating to 230 °C for 1 h to fully dissolve the selenium. This solution was then cooled to 100 °C. The solution was kept at this temperature and transferred into a glass syringe equipped with a large needle (12 gauge external diameter) and injected quickly into the flask. After injection, the temperature of the reaction mixture dropped to 280 °C, and it was allowed to recover to the pre-injection value. The overall reaction time after injection was 15 min, after which the flask was rapidly cooled to room temperature. Once at room temperature, toluene (5 mL) was added to the reaction mixture. The resulting solution was then transferred into a vial under a blanket of nitrogen, and stored inside a glovebox. This solution was then washed by precipitation (via addition of ethanol) and redissolution in toluene. After the washing step, the Cu_{2-x} Se nanocrystals were dissolved in 3 mL of toluene.

Concentration by ICP: [Cu] = 1.284 g/L; [Se] = 1.0445 g/L

AII.3.2 Water transfer of Cu_{2-x}Se NPs.

 $Cu_{2-X}Se$ NPs were synthesised in organic solvents according to the protocol outlined in **sections AII.3.1**. Transfer to the aqueous phase was carried out by a ligand exchange reaction performed by Dr. Andreas Riedinger.

In a typical procedure, 200 μL of Cu_{2-x}Se NCs (ca. 2g/L Cu) in toluene were mixed with a solution of HS-PEG-COOH (HS-C₂H₄-CONH-PEG-C₃H₆COOH, Rapp Polymere, 3000 kDa, 20 mg in 1 mL toluene) and triethylamine (50 μl) in an 8 mL glass vial. After vortexing for several seconds, milliQ water (2 mL) was added and the mixture was emulsified by gentle shaking. The phases were allowed to separate by letting the vial stand for some minutes and the aqueous phase (lower phase) containing the NCs (green color) was collected with a syringe. This step (addition of water to the org. phase, emulsification, phase separation, sample collection) was repeated until no NCs are left in the org. phase (usually after 3 times, all NCs were in the aqueous phase, indication by the green color of the NCs). The combined aqueous phases were given in a round bottom flask at residual org. solvents and triethylamine were removed under reduced pressure at 40 °C on a rotavapor system (step-wise reduction of pressure until 70 mbar was reached). The sample was cleaned from excess HS-PEG-COOH either by dialysis (in 50 kDa MWCO acetyl acetate tubes against milliQ water) or repeated centrifugal filtration in Amicon tubes (MQCO 100 kDa, 3000 rpm, 5 min).

AII.4 Synthesis and water transfer of Fe₃O₄ NCs.

AII.4.1 Synthesis of Fe₃O₄ NCs.

Fe₃O₄ NCs were synthesised by Mr. Giammarino Pugliese according at the Istituto Italiano di Tecnologia according to the following protocol [3]:

All experiments were carried out in 50 mL (14/23) three-neck round bottom flasks equipped with a water cooled Allhin-condenser connected to a standard Schlenk

line. Briefly, in a 50 mL three neck flask, of iron(III) acetylacetonate (0.353 g, 1 mmol), decanoic acid (0.69 g, 4 mmol) and dibenzyl ether (DBE) (9 mL) were dissolved in squalane (16 mL). After degassing for 120 minutes at 65 °C, the mixture was heated up to 200 °C (3 °C min⁻¹) and kept at this value for 2.5 h (a shorter "ageing time" at 200 °C led to lower reproducibility as well as to broadening of the size and shape distributions of the final particles). The temperature was then increased at a heating rate of 7 °C min⁻¹ up to 310 °C or reflux temperature and maintained at this value for 1 h. After cooling down to room temperature, acetone (60 mL) was added and the solution was centrifuged at 8500 rpm. The supernatant was then discarded and the black precipitate was dispersed in chloroform (2-3 mL): this washing procedure was repeated at least two more times. Finally, the collected particles were dispersed in chloroform (15 mL).

Concentration by ICP: [Fe] = 1.659 g/L

AII.4.2 Water transfer of Fe₃O₄ NCs.

Fe₃O₄ NCs were synthesised in organic solvents according to the protocol outlined in **section AII4.1**. Transfer to the aqueous phase was carried out by a ligand exchange reaction performed by Dr. Andreas Riedinger [3].

Briefly, after reducing the temperature of the reaction mixture from 310 to 70 °C, GA-PEG solution (0.1 M, 15 mL in chloroform containing triethylamine (1 mL)) was injected and the resulting mixture was stirred overnight at constant temperature. Then the mixture was allowed to cool to room temperature and was transferred to a separating funnel. De-ionized water (10 mL) was then added, which led to the formation of two phases. After emulsification by means of shaking, the phases were allowed to separate and the aqueous phase containing the IONP bearing GA-PEG was collected. This step was repeated until all nanocubes were transferred into water. After the solution was

concentrated under reduced pressure at 40 °C to a final volume of about 50 mL, the excess of GA-PEG was removed by dialysis versus de-ionized water (5 L), using cellulose membrane tubing with a pore size of 50 kDa. The sample was left in dialysis overnight at room temperature. This step was repeated 5 times. Finally, the nanocube solution was concentrated by centrifugation in a centrifuge filter (molecular cut-off point 100 kDa).

AII.5 Synthesis of graphene oxide.

Graphene oxide was synthesised by Stratakis and Kymakis research groups at IESL, Greece. GO was prepared from graphite powder (Alfa Aesar. ~200 mesh) according to a modified Hummers' method [4]. In more detail, graphite powder (0.5 g) was placed into a mixture of H₂SO₄ (40 mL, 98%) and NaNO₃ (0.375 g). The mixture was then stirred and cooled in an ice bath. While maintaining vigorous stirring, KMnO₄ (3.0 g) was then added in portions over a period of 2 h. The reaction mixture was left for 4 h in order to reach room temperature before being heated to 35 °C for 30 min. It was then poured into a flask containing deionized water (50 mL) and further heated to 70 °C for 15 min. The mixture was then decanted into 250 mL of deionized water and the unreacted KMnO₄ was removed by adding 3% H₂O₂. The reaction mixture was then allowed to settle and decanted. The graphite oxide obtained was then purified by repeated centrifugation and redispersed in deionized water until neutralized pH was achieved. Finally, the resulting GO was dried at 60 °C in a vacuum oven for 48 h before use.

AII.6 Determination of DNA-loading on a gold nanoparticle.

The average number of DNA strands per AuNP (13nm), prepared by two different methods, were quantified after dissolution of the gold core (see **chapter 3** for experimental procedures). The following table (**table AII.1**) shows the summarized results from four different measurements.

Table AII.1 Determination of DNA-loading on AuNPs.

Measurement	Estimated strands per AuNP for Method 1 [5]	Estimated strands per AuNP for Method 2 [6]
1	154	118
2	153	125
3	165	121
4	160	116
Average	160	120
Std. Error	4	2

DNA-loading for method 1: 160 ± 4 strands per particle.

DNA-loading for method 2: 120 ± 2 strands per particle.

AII.7 Quantification of duplexes on nano-probes.

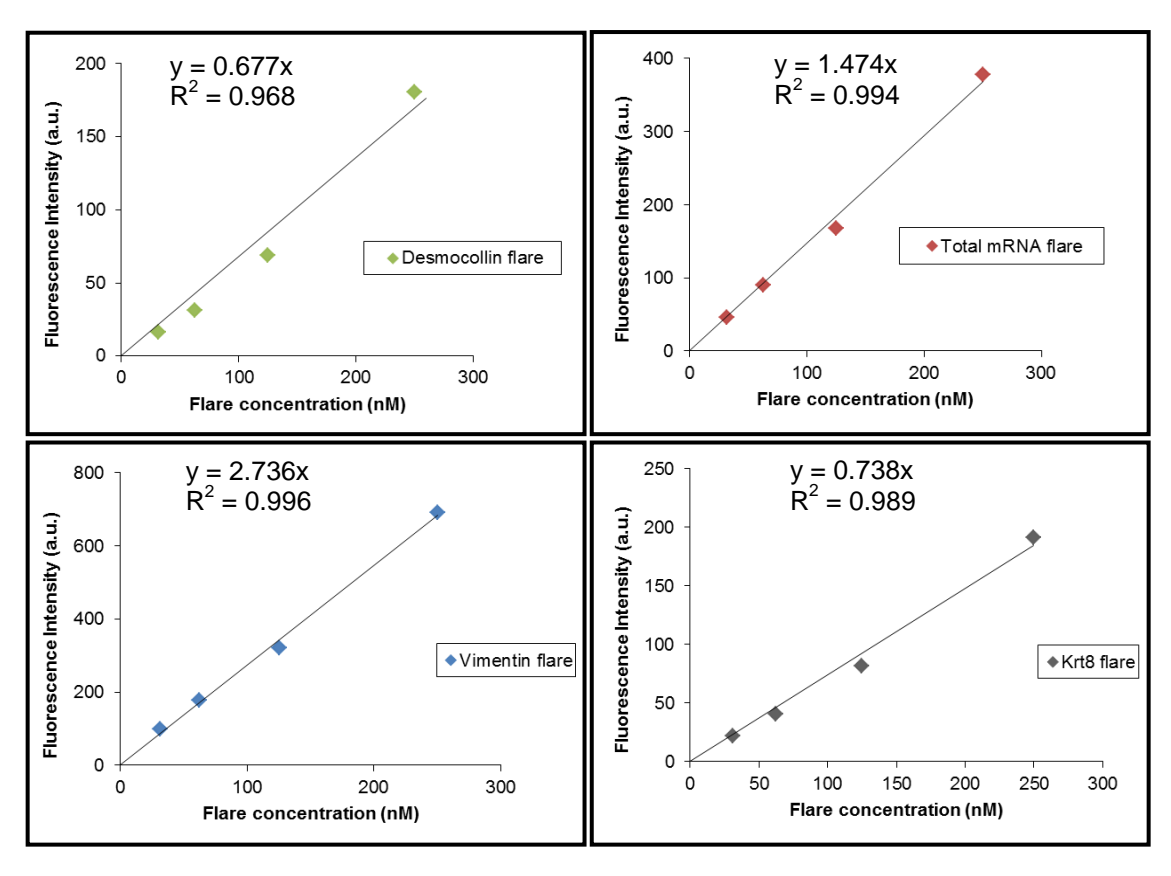


Figure AII.1 Calibration curves of the relative fluorescence of Desmocollin, Cytokeratin 8, Vimentin and total mRNA flare strands.

From these calibration curves the numbers of duplexes (sense-flare) per AuNP were determined. Results are shown in **table AII.2**.

Table AII.2 Quantification of sense-flare duplexes on AuNPs.

Estimated no. of duplexes per AuNP (total mRNA)									
Measurement 40x 60x 80x 100x									
1	37	53	74	90					
2	35	58	72	95					
3	46	65	85	108					
Average	39	59	77	98	*:				
Std. Error	3	3	4	5					

Estimated no. of duplexes per AuNP (Vimentin)							
Measurement	40x	60x	80x	100x			
1	42	61	86	98			
2	45	60	74	92			
3	31	52	79	102			
Average	39	58	80	97			
Std. Error	4	3	3	3			

Estimated no. of duplexes per AuNP (Cytokeratin 8)							
Measurement	40x	60x	80x	100x			
1	34	51	74	92			
2	42	59	72	98			
3	45	67	85	105			
Average	40	59	77	98			
Std. Error	3	5	4	4			

Estimated no. of duplexes per AuNP (Desmocollin)							
Measurement	40x	60x	80x	100x			
1	40	58	81	107			
2	35	62	83	94			
3	44	65	77	97			
Average	40	62	80	99	*		
Std. Error	3	2	2	4			

(Mean SEM, n=3, *** p < 0.001, ** p < 0.01, * p < 0.1)

AII.8 Additional confocal microscopy images for chapter 5.

The following confocal microscopy images at higher magnification give a better view of the co-localization of the fluorescence signal of the flare strand and mitochondria.

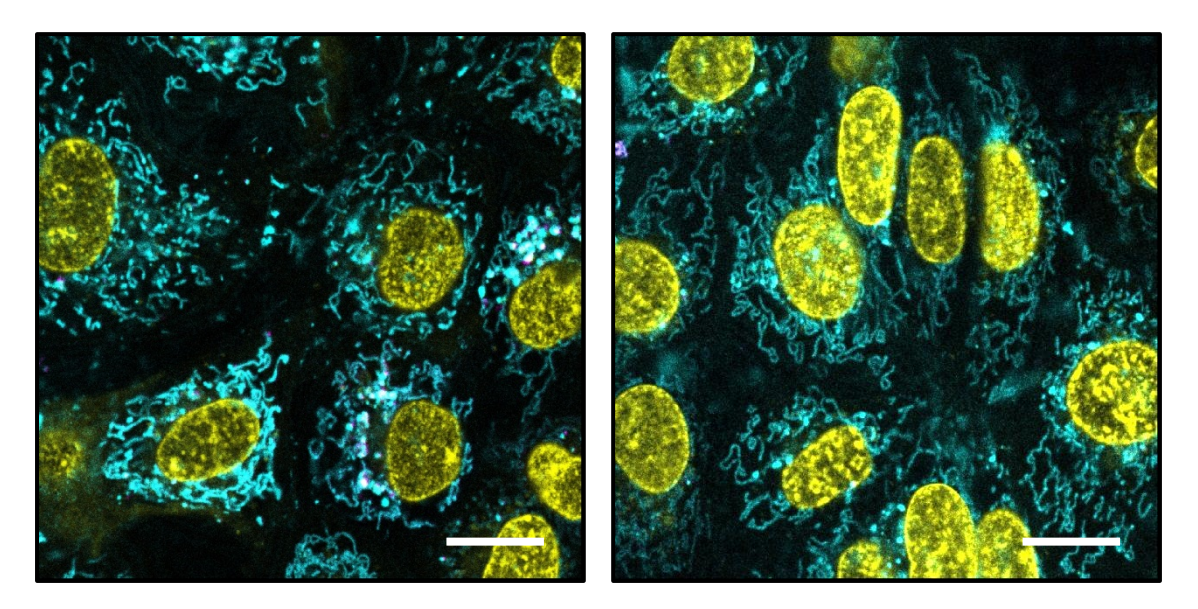


Figure AII.2 Additional magnified confocal microscopy images of epithelial cells incubated with total mRNA detection nano-probes. Mitochondrial association of flare strands can be clearly observed. Scale bars are 15 μ m.

AII.9 Determination of Doxorubicin loading.

Vimentin nano-probes were loaded with varying amounts of Doxorubicin by means of creating varying amounts of duplexes (see **chapter 3** for experimental details). The fluorescence of Doxorubicin upon duplex melting was measured and related to the calibration curve displayed in **Figure 5.20.** Results from three independent measurements are summarized in **table AII.3**.

Table AII.3 Determination of Doxorubicin loading.

		40x				60x				80x		
Measurement	Abs. (a.u.)	Conc. (nM)	No. of moles (pmol)	Equiv.	Abs. (a.u.)	Conc. (nM)	No. of moles (pmol)	Equiv.	Abs. (a.u.)	Conc. (nM)	No. of moles (pmol)	Equiv.
1	4.21	92.73	13.91	37.09	5.89	129.74	19.46	51.89	8.15	179.52	26.93	71.81
2	5.17	113.88	17.08	45.55	7.48	164.76	24.71	65.90	8.83	194.49	29.17	77.80
3	4.13	90.97	13.65	36.39	6.22	137.00	20.55	54.80	7.92	174.45	26.17	69.78
Std. Error	0.33	7.36	1.10	2.94	0.48	10.67	1.60	4.27	0.27	6.02	0.90	2.41
Average	4.50	99.19	14.88	39.68	6.53	143.83	21.57	57.53	8.30	182.82	27.42	73.13

Doxorubicin-loading for $40 \times (40 \text{ duplexes}) = 39 \pm 3 \text{ per AuNP ***}$ Doxorubicin-loading for $60 \times (60 \text{ duplexes}) = 57 \pm 4 \text{ per AuNP ***}$ Doxorubicin-loading for $80 \times (80 \text{ duplexes}) = 73 \pm 2 \text{ per AuNP ***}$

(Mean SEM, n=3, *** p < 0.001, ** p < 0.01, * p < 0.1)

AII.10 Additional TEM images for chapter 6.

AII.10.1 5 nm AuNP dimers.

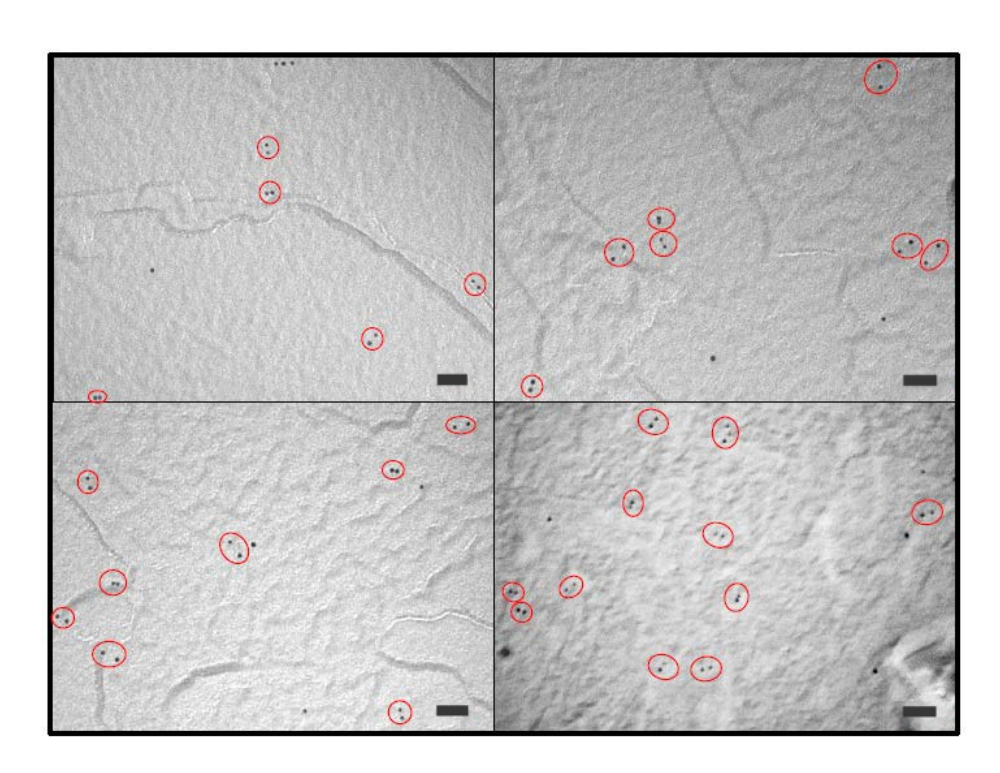


Figure AII.3 Additional TEM images for 5 nm AuNP dimers connected via single strand of clicked ssDNA. (Scale bars are 40 nm).

AII.10.2 13 nm AuNP dimers and trimers.

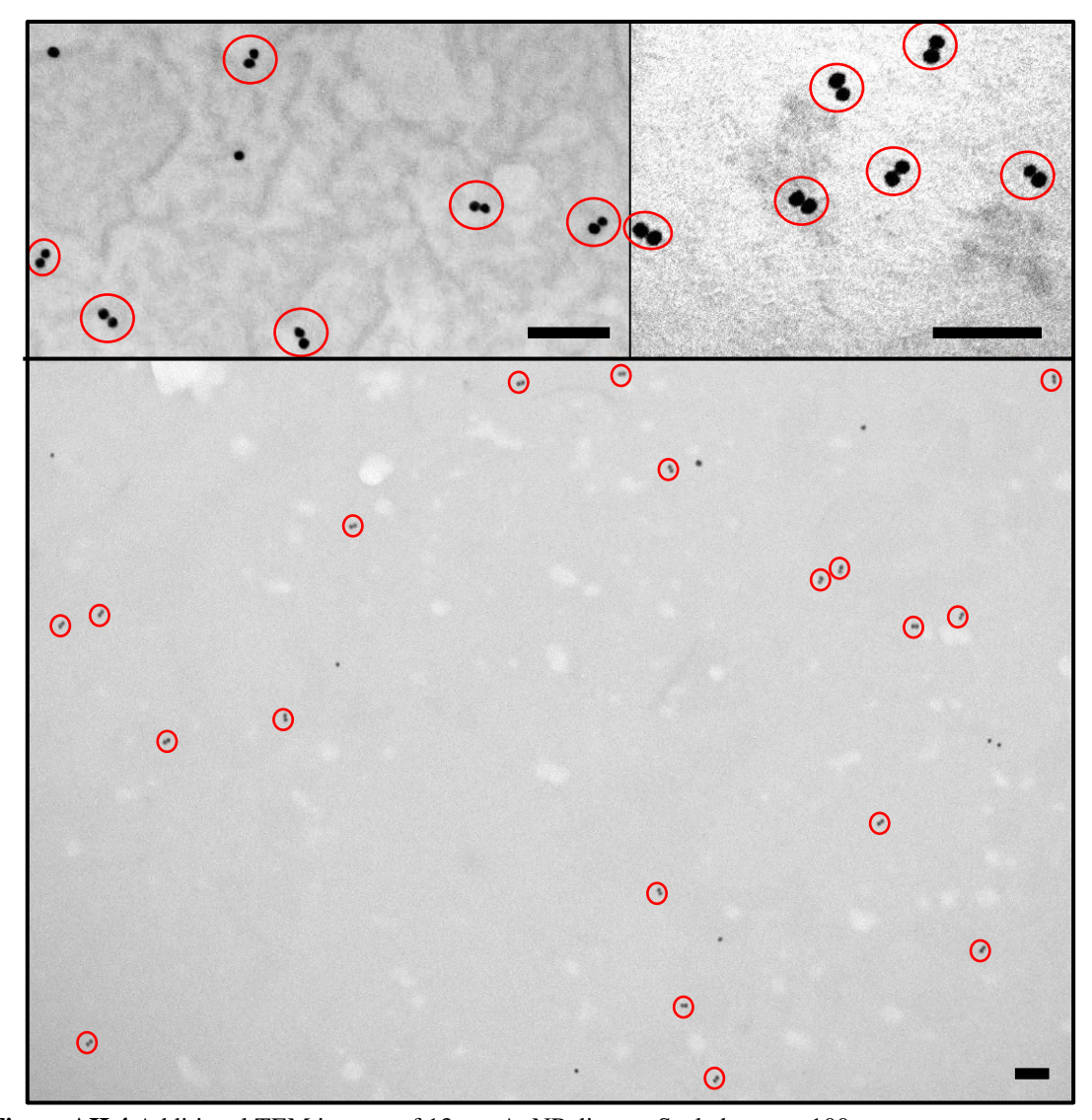


Figure AII.4 Additional TEM images of 13 nm AuNP dimers. Scale bars are 100 nm.

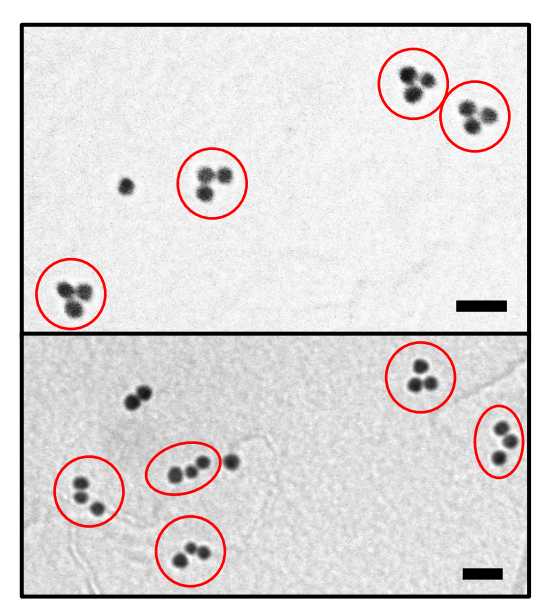


Figure AII.5 Additional TEM images of 13 nm AuNP trimers. Scale bars are 40 nm.

AII.11.3 GO/AuNP hybrid assemblies.

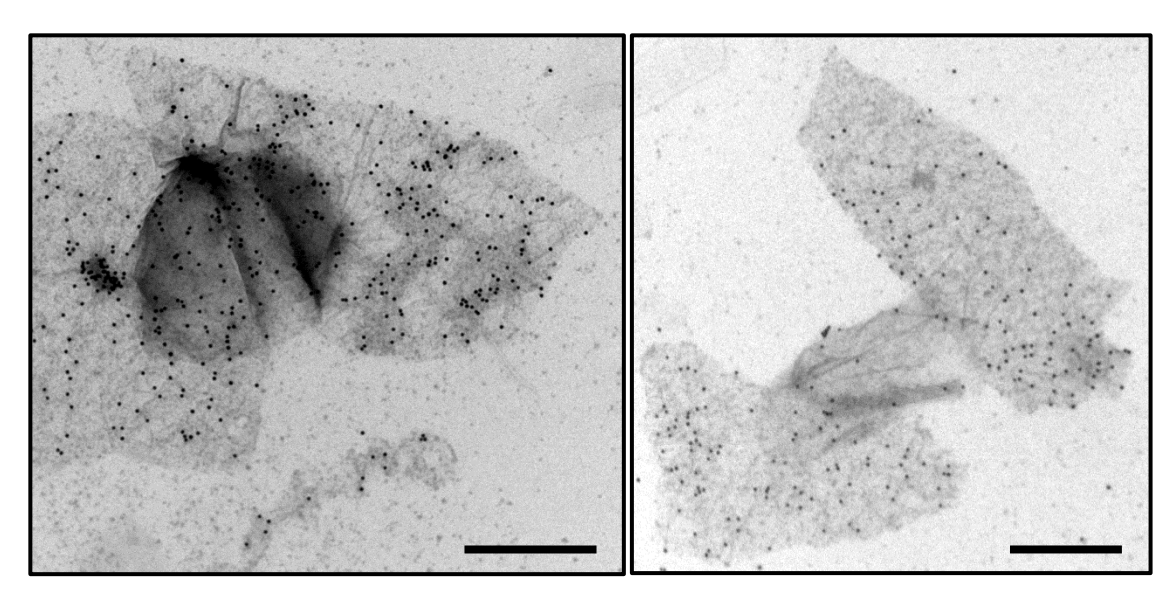


Figure AII.6 TEM images of AuNP/GO hybrid assemblies. Scale bars are 500 nm.

AII.12 Gel analysis using ImageJ.

The agarose gel depicted in **Figure AII.7** was analysed using image J. The resulting graphs are shown next to the gel. The gel analysis tool was utilized to determine relative electrophoretic positions and intensities.

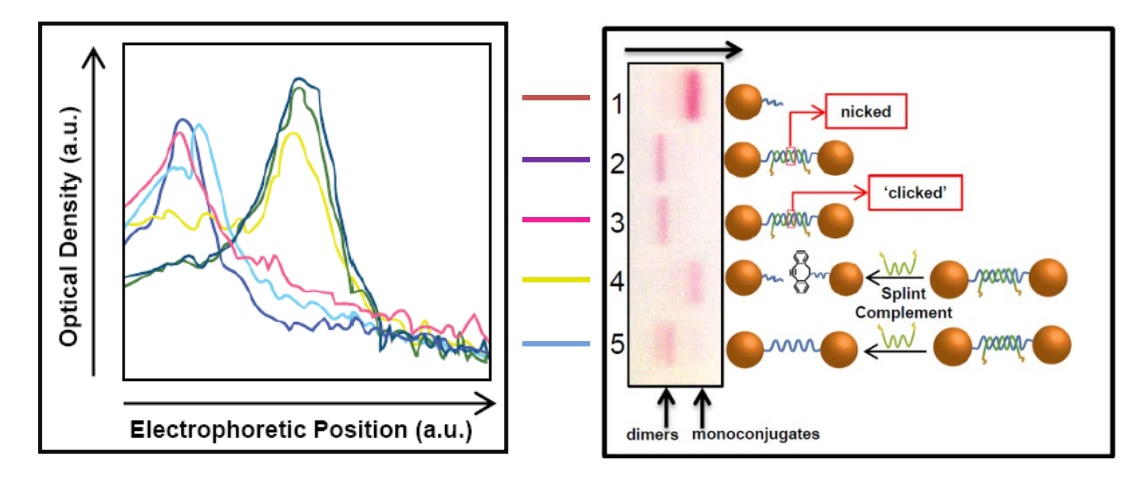


Figure AII.7 ImageJ analysis of the agarose gel depicting the success of the 'click' reaction (cf. **Figure 6.4**).

AII.13 References

- 1. Haiss, W., et al., *Determination of size and concentration of gold nanoparticles*from UV-Vis spectra. Analytical Chemistry, 2007. **79**(11): p. 4215-4221.
- 2. Dorfs, D., et al., Reversible Tunability of the Near-Infrared Valence Band Plasmon Resonance in Cu2-xSe Nanocrystals. Journal of the American Chemical Society, 2011. **133**(29): p. 11175-11180.
- 3. Guardia, P., et al., One pot synthesis of monodisperse water soluble iron oxide nanocrystals with high values of the specific absorption rate. Journal of Materials Chemistry B, 2014. **2**(28): p. 4426-4434.
- 4. Hummers, W.S.O., R.E., *Preparation of Graphitic Oxide*. J. Am. Chem. Soc., 1958. **80**.
- 5. Kanaras, A.G., et al., *Towards multistep nanostructure synthesis: Programmed enzymatic self-assembly of DNA/gold systems*. Angewandte Chemie-International Edition, 2003. **42**(2): p. 191-194.
- 6. Rosi, N.L., et al., Oligonucleotide-modified gold nanoparticles for intracellular gene regulation. Science, 2006. **312**(5776): p. 1027-1030.